# Affinity Maturation in the Immune System

Dagmar Iber

A dissertation submitted to the University of Oxford
in candidature for the degree of
MRes in Applied and Computational Mathematics

Wadham College
Oxford

Mathematical Institute
Centre of Mathematical Biology
Oxford

# Abstract

The affinity of antibody[1] for antigen increases during an immune response. This is achieved by mutation of the genes encoding for the antibody and subsequent selection of the best binder. The process takes place in a special microenvironment, the germinal centre.

In this dissertation, a mathematical model is presented, which reproduces experimental data on the kinetics of this process and on the affinity maturation observed during the reaction. It further allows predictions to be made about parameters such as the selection rate of centrocytes and the recycling probability of selected centrocytes. Additionally it is shown that termination of somatic hypermutation several days before the end of the germinal centre reaction is beneficial for affinity maturation as is a start of memory cell formation well after the onset of somatic hypermutation.

Selection of B cells during the germinal centre reaction is based on antigen recognition and is believed to involve interaction of B cells with membrane bound antigen. It has been shown that such encounter of membrane bound antigen leads to a re-organisation of proteins and lipids such that raft lipids are accumulating in the contact zone. In a second project possible driving forces for such a lipid re-organisation are investigated and the analysis shows that the accumulation of a special lipid sort in the contact zone can be understood by their high affinity for proteins engaged in the contact zone. Interaction between lipids themselves has no positive impact on the accumulation of lipids in the contact zone and strong interactions between lipids may even prohibit the domain formation in the contact zone by the trapping of lipids in patches elsewhere on the cell surface.

[1]Technical terms are defined in the Glossary in Appendix A

# Declaration

The work outlined in this dissertation was carried out at the Mathematical Institute, Centre of Mathematical Biology, Oxford over the period from October 2000 to August 2001. All models and simulations described are the result of my own work. This work has not been submitted whole or in parts to any other university.

Dagmar Iber
Oxford
September 2001

# Contents

**Abstract** i

**Declaration** iii

**Acknowledgements** xv

**Part I: A Model of Affinity Maturation** xvii

**1 Introduction to the Humoral Immune Response** 1
- 1.1 Biological Background . . . 1
  - 1.1.1 Principles of Innate and Adaptive Immunity . . . 1
  - 1.1.2 The Humoral Immune Response . . . 2
- 1.2 Mathematical Model of the Germinal Center Kinetics . . . 8
- 1.3 Scope of the Study . . . 12

**2 Model of Affinity Maturation** 15
- 2.1 Introduction . . . 15
- 2.2 Model of the Germinal Center Kinetics . . . 18
- 2.3 Affinity and Antigen Density Dependence . . . 26
- 2.4 Modelling Affinity Maturation . . . 31
  - 2.4.1 Analytical Analysis of the Model . . . 32
  - 2.4.2 Numerical Simulation of the Model . . . 43

**3 Conclusion** 49
- 3.1 Summary of Results and Discussion . . . 49
- 3.2 Further Work . . . 50

**Part II: Simulation of Biological Membranes** i

**4 Introduction to Biological Membranes** 53
- 4.1 Membrane architecture . . . 55
- 4.2 Model of Lipid Distribution on Membranes . . . 56
  - 4.2.1 Analytic solution for spherical cells . . . 57
- 4.3 Scope of the study . . . 60

**5 Methods** **61**
5.1 General Setup . . . 61
5.2 Monte Carlo Method . . . 62
5.3 The Algorithm . . . 63
5.3.1 Algorithm for Simulation of Cylinder Cells . . . 63
5.3.2 Algorithm for Simulation of Spherical Cells . . . 66

**6 Results of the Membrane Simulation** **71**
6.1 Results for cells of cylinder shape . . . 71
6.1.1 Diffusion of lipids in the membrane . . . 71
6.1.2 Equilibrium cell shape . . . 72
6.1.3 Domain Formation and Phase Transition . . . 75
6.2 Results for Cells of Sperical Shape . . . 78

**7 Conclusion from the Membrane Studies** **81**
7.1 Summary of Results and Discussion . . . 81
7.2 Further Work . . . 81

**A Glossary** **89**

**B Extension of 1.2 to Affinity Maturation** **93**
B.1 Density Dependent Centroblast-Centrocyte Conversion . . . 94
B.2 Time Dependent Centroblast-Centrocyte Conversion . . . 97
B.2.1 Kinetics of GC reaction . . . 98
B.2.2 Affinity maturation . . . 99
B.3 Generation dependent Centroblast-Centrocyte Conversion . . . 103
B.3.1 Model . . . 103
B.3.2 Results . . . 110
B.4 Conclusion . . . 112

**C Program Codes for Chapter 2** **117**
C.1 Program to the Numerical Solutions of the Model in 2.2 . . . 117
C.2 Program to the Numerical Solutions of the Model in 2.4 . . . 125

**D Numerical Solution used in Chapter 4** **141**
D.1 Numerical solution of equation 4.4 . . . 141

**E Program Codes for Simulations presented in Chapter 6** **145**
E.1 Programs for the Simulation of Cylinder Cells . . . 145
E.1.1 C Program for the Simulation of Cylinder Cells . . . 145
E.1.2 Matlab Programs for Visualisation of the Results . . . 145
E.2 C Program for the Simulations of Spherical Cells . . . 150

**F Explicit Calculations and Program Codes for Appendix B** **183**
F.1 Explicit Calculations and Programs for the Model in B.1 . . . 183
F.1.1 Calculation of the Steady state values for the model in B.1 183
F.1.2 Program to the Numerical Solutions of the Model in B.1 . 184
F.2 Programs to the Numerical Solutions of the Model in B.2 . . . 187

F.2.1 Program for the model in Chapter B.2.1 . . . . . 187
F.2.2 Program for the model in Chapter B.2.2 . . . . . 189
F.3 Programs to the numerical solutions of the model in B.3 . . . . . 193

# List of Figures


1.1 The lymphoid organs in humans[2] . . . . . 4
1.2 Illustration of a simple model of the processes in the germinal centre (GC) . . . . . 7
1.3 Germinal centre dynamics as used in the model of Kesmir and deBoer . . . . . 9
1.4 Kinetic results of the model of Kesmir and de Boer [26] . . . . . 12
1.5 GC dissolution by day 5 if centrocytes cannot recycle back to replenish the centroblast pool. . . . . 13
1.6 GC kinetics measured by Liu et al. (1991) [32] . . . . . 14

2.1 Scheme of the model for the primed primary immune response. Abbreviations are explained in Table 2.2. . . . . 18
2.2 Stability analysis of the minimal model for the primed primary immune response . . . . . 22
2.3 GC kinetics of the primed primary immune response in the minimal model . . . . . 24
2.4 GC kinetics of the primed primary immune response if somatic hypermutation terminates at day 16 . . . . . 26
2.5 GC kinetics of the primed primary immune response where the selection factor and the recycling probability depend nonlinearly on antigen density and somatic hypermutation terminates on day 16 of the response . . . . . 29
2.6 Parameter Space for which the system 2.29-2.34 attains a non-trivial equilibrium state for different values of $\mathbf{M}_{11}$ . . . . . 33
2.7 Analysis of the stability of steady states for the system 2.29-2.34 with $0.74 < \mathbf{M}_{11} < 1$ . . . . . 35
2.8 Analysis of the stability of steady states for the system 2.29-2.34 with $0.9 < \mathbf{M}_{11} < 1$) . . . . . 36
2.9 Consecutive application of the mutation matrix $\mathbf{M}$ . . . . . 41
2.10 GC kinetics and affinity maturation of the primed primary immune response in the 1 generation model. . . . . 46
2.11 GC kinetics and affinity maturation of the primed primary immune response in the 2 generation model. . . . . 47


[2]The image was taken from the web page of Nick Holmes at the University of Cambridge http://immserv1.path.cam.ac.uk/immuno/part1.html

4.1 Concentration of GM1 in the contact zone of two cells . . . . . 54
4.2 Schematic figure of a biological membrane . . . . . 55
4.3 Solution of equation 4.4 for h . . . . . 59

5.1 The cell becomes flattened upon interaction with a second cell. . 61
5.2 Replacement of the second cell by application of an affinity field on the flattened part of the cell. . . . . 62
5.3 Calculation of the interaction energy in case of cylinder cells . . . 64
5.4 Notation for the calculation of the geometric properties of the deformed cylinder . . . . . 65

6.1 Diffusion of lipids on the cylinder cell surface. . . . . 72
6.2 Inner energy and concentration of lipid A in the contact zone. . . 73
6.3 Distribution of lipids in equilibrium . . . . . 73
6.4 Cell height in dependence of sticker density $n$ and binding energy $\frac{U}{T}$ . . . . . 74
6.5 Cell height in dependence of sticker density $n$ and binding energy $\frac{U}{T}$ . . . . . 74
6.6 The correlation function for the cylinder cells fitted with a modified Bessel function. . . . . 76
6.7 The correlation function for the cylinder cells for $J \neq 0$. . . . . 76
6.8 The correlation function for the cylinder cells for $J = 0$. . . . . 77
6.9 The correlation function for the cylinder cells for different affinity fields $B$ . . . . . 78
6.10 Initial lipid distribution on spherical cells . . . . . 79
6.11 Contact zone of spherical cell . . . . . 79
6.12 Contact zone of spherical cell . . . . . 79

B.1 Germinal centre dynamics with density dependent centroblast-centrocyte conversion for $K_b = 10^3$ . . . . . 96
B.2 GC kinetics modelled with density dependent conversion by Oprea and Perelson (1997)[44] . . . . . 97
B.3 Germinal centre dynamics with time dependent centroblast-centrocyte conversion . . . . . 99
B.4 Distribution of values in a row in the mutation matrix . . . . . 101
B.5 Affinity development of centrocytes without density dependent selection. . . . . 102
B.6 Affinity development of centrocytes with density dependent selection, $\theta = 33$. . . . . 103
B.7 Germinal centers dissolve within 3.5 days if recycling is inhibited ($p_r = 0$) . . . . . 106
B.8 Threshold curve . . . . . 109
B.9 Kinetics of generation dependent model . . . . . 111
B.10 Affinity maturation in generation dependent model . . . . . 112
B.11 Kinetics of generation dependent model . . . . . 114
B.12 Affinity maturation in generation dependent model . . . . . 115
B.13 GC kinetics as measured by Liu et al. [32] with all rats included 116

B.14 GC kinetics as measured by Liu et al. [32] with 1 rat at day 10 excluded116

# List of Tables

1.1 GC kinetics in the primed primary immune response . . . . . 5
1.2 Parameters for the GC kinetic model of Kesmir and de Boer [26] 10
1.3 Initial values for the GC kinetic model of Kesmir and de Boer [26] 11

2.1 GC kinetics in the primed primary immune response . . . . . 17
2.2 Parameters for the minimal model . . . . . 19

B.1 GC kinetics of the true primary immune response . . . . . 98
B.2 Symbols used in the mutation matrix with discrete affinty shifts . 107

# Acknowledgements

During the course of my work I have received a great deal of help from members of the Mathematical Institute, the Computing Laboratory and elsewhere. In particular, I would like to thank my supervisor, Philip Maini, for his help, encouragement and criticism throughout the course of the project and especially for giving a trained biochemist the chance of undertaking mathematical research in his group. I am indebted to Hillary Ockendon for her encouragement and support when embarking on this - given my background - unusual carrier.

I am grateful to Ian C. MacLennan, from the MRC Manchester, who helped with details on the germinal centre reaction and with unpublished data.

The second part of the project was entirely supervised by Reinhard Lipowsky and Thomas Gruhn from the Max Planck Institute for colloids and interfaces in Golm, Germany. I wish to thank for their interest in the project and their support despite the unfavorable geographical distance. I am also grateful to Mark Sansom and Tony Watts - both at the biochemistry department of the University of Oxford - for discussing membranes with me.

I am especially thankful to David Gavaghan for many valuable discussions and for critically reading the manuscript. The manuscript was also improved by comments of Philip Maini and Jonathan Whiteley whom I also wish to thank.

Finally I would like to thank for financial support through the Studienstiftung des deutschen Volkes and an EPSRC scholarship.

# Part I: A Model of Affinity Maturation

# Chapter 1

# Introduction to the Humoral Immune Response

## 1.1 Biological Background

### 1.1.1 Principles of Innate and Adaptive Immunity

Higher organisms face continuous infection by all sorts of pathogenic microorganisms. In order to successfully fight these aggressive invaders, the body needs to distinguish self from non-self and to eliminate the non-self. This task is carried out by the immune system[1].

The immune system follows two different strategies to identify non-self. One part, the innate immune system, relies on the quick recognition of common surface patterns of microorganisms while the other part, the adaptive immune system, takes care of all the other invaders and produces specifically adapted weapons against their special surface structures. The latter approach is much more specific and much more efficient once the weapons have been manufactured. It nevertheless would be hard for an organism to survive without the innate immune system, since the onset of a proper adaptive immune response can take up to 21 days after infection and invaders such as bacteria divide quickly. The innate immune system works in that time as a first line of defense against most invaders but leaves the complete clearance of the invader to the adaptive immune system. Effectors of the innate immune system are phagocytes which can eliminate the invader by eating it and the complement system which leads to the lysis (disintegration) of invader cells.

Microorganisms are able to frequently change their surface molecules and can therefore escape recognition by the innate immune system which is only triggered by a small set of specific signals. In this case, recognition and activation of the immune response can only happen through the adaptive immune system. One distinguishes two different sorts of adaptive immune responses: the humoral and the cellular immune response. Which immune response is triggered depends on the infection.

If the infection actually enters cells (as in the cases of viruses and some

[1] A suitable reference textbook for immunology is that of Janeway & Travers [22].

bacteria), it is hidden from most monitoring which only considers extracellular parts of the body. Specialised cells, termed T cells, can nevertheless identify the infected cells and kill them in order to prohibit spreading of the infection. This response is called the cellular immune response.

Invaders which reside outside cells, e.g. are swimming in the blood or in the lymph, can be recognised by either components of the innate immune system or by those of the humoral immune response. As already mentioned, the innate immune response can only react against a subset of invaders while the effector cells of the humoral immune response (B lymphocytes) are capable of raising an immune response against almost every foreign compound. The main players of the humoral immune response are the so called B cells which produce antibodies. Antibodies are proteins that can firmly and specifically bind to the invader. Binding of the antibody prevents the invader from interacting with other body structures, a process called neutralisation. Further on, antibodies mark the object which they are binding to for destruction by either phagocytes or the complement system. In order to only attack the invader and not body cells themselves, it is indispensable that antibodies bind very specifically. In addition, they need to bind very firmly since rash detachment would not allow the destruction of the invader. How B cells manufacture these highly specific proteins with the extraordinary affinity for its target is the subject of this dissertation.

### 1.1.2 The Humoral Immune Response

B cells are produced in the bone marrow and every B cell expresses one sort of antibody which can bind to a small group of possible antigens[2]. During the humoral immune response, B cells which express an antibody that binds the antigen at least weakly, need to be selected, and the binding characteristics of the antibody for the target need then to be improved. This is believed to be achieved by several rounds of mutation and selection [35].

The whole process can be divided into three phases. In phase one antigen is concentrated in secondary lymphoid organs such as the lymph nodes and the spleen. In the second phase, naive B cells from the bone marrow meet antigen in these secondary lymphoid organs and are activated to run through a cycle of mutation and selection which is meant to improve the binding characteristics of the antibodies, which they are expressing. In the third phase, B cells again leave these organs and either secrete highly specific, high affinity antibodies that fight the invader or they become memory cells that remember the invader as a protection against a second infection.

#### Concentration of Antigen

Concentration of antigen is important since every B cell expresses only one sort of antibody which recognises a small subset of all possible antigens and therefore almost every B cell must have been in contact with the antigen within a short

[2]Formally antigen is defined as a molecule that reacts with antibodies. In our description invaders are possible antigens.

time in order to guarantee a successful immune response. Antigens can however enter the body at every part of the body's boundary and every B cell can only travel limited distances within a few days. Without concentration of antigen at central points the probability that a specific B cell interacts with the antigen would be extremely small [13]. Concentration of antigen at central points such as the lymph nodes and the spleen (see Figure 1.1 for illustration) is achieved continuously by filtering blood and lymph and upon inflammatory signals by specific cells, the dendritic cells, that wait for the invader at strategic points such as under the skin and capture the antigen upon stimulation. Subsequently the antigen is then delivered to the lymph nodes by such dendritic cells. In the follicles of these lymph organs, B cells can interact with the presented antigen [13]. Upon recognition via their specific receptors, B cells are induced to stay in the organ and to migrate to the T cell zone where they interact with T helper cells [14, 19, 32]. If they fail to find the right antigen they leave after 10-20 hours and travel to the next lymph node [56].

In order to successfully interact with T cells in the T cell zone B cells need to internalise the recognized antigen and to express parts of it on their surface. B cells that have recognized antigen but fail to interact with a specific T cell die [15, 52]. This is a protection against auto-immunity since T cells which are recognising self are eliminated early in their development and are therefore not available in the T cell zone of secondary lymphoid organs to interact with B cells that have recognised self-antigen. The interaction with T cells is therefore a double-check so that only immune responses against foreign compounds are raised [7]. We will meet this approach again in the germinal centre reaction.

Once B cells have successfully interacted with antigen and T cells they start to proliferate [32]. The emerging B cells can take two different routes. Presumably the clones with lower affinity for the antigen form extrafollicular foci where they mature and become early plasma cells [10]. Plasma cells are antibody secreting cells. Given that these B cells have not run through any sort of improvement, the antibodies they produce will only bind with low affinity to the invader. They are, nevertheless, indispensable as a first defense against the invader until the immune response is fully working. The second route is to enter follicles and to form germinal centers (GCs) where the antibody production is improved [20, 35]. The germinal centre reaction will be explained in much greater detail since all mathematical analysis in this dissertation focusses on this process.

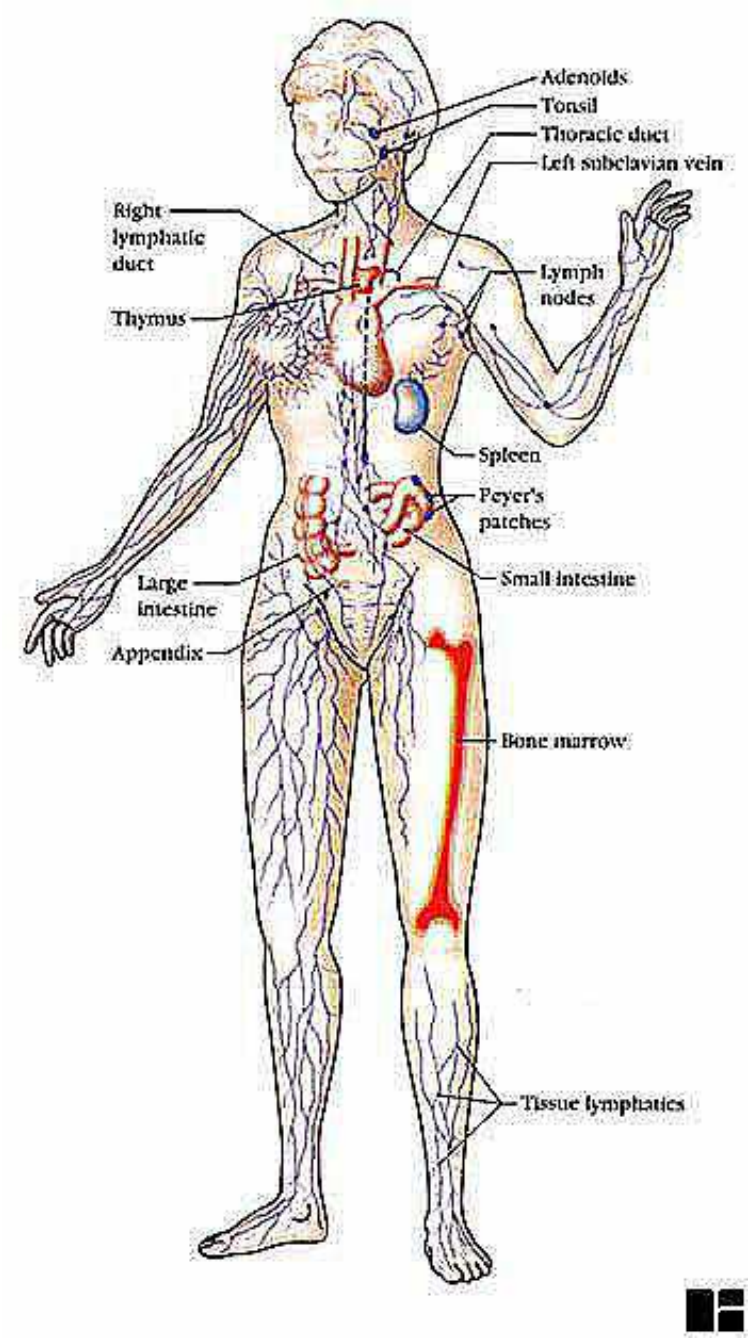



Figure 1.1: The lymphoid organs in humans

### The Germinal Center Reaction

During the germinal centre (GC) reaction low affinity B cell clones are multiplied and the genes coding for the antibodies are mutated. The mutation of these genes leads to a change in the binding characteristics of the antibody. These changes can either improve the binding characteristics or make them worse. In the worst case these antibodies can even recognise their body components which could lead to an autoimmune response. Selection of the beneficial clones and extinguishing of the others is therefore clearly needed. Selected B cells can then either leave the germinal centers as plasma cells, which produce antibodies to fight the invader or as memory cells that protect the body from re-infection. There is accumulating evidence that there exists also a third route for selected centrocytes, namely to recycle and to run through further rounds of multiplication, mutation and selection [10, 15, 32]. Mathematical analysis shows that recycling increases the efficiency of affinity maturation [25] so that after several rounds of mutations and selection, high affinity clones can emerge.

The germinal centre reaction can be divided into three phases. In the first phase which takes about three days the B cell clones only multiply. In the second phase the real germinal centre structures develop, and in the third phase the germinal centre is dissolved. The exact kinetics of these phases depend on whether the body is infected by the antigen for the first time (*primary response*) or has been infected by the same antigen before (*secondary response*). A further experimental scenario is to first prime the animal with a carrier protein and to then immunise the animal again with a compound, termed hapten, bound to the carrier protein. The priming leads to the expansion of specific T cells so that the immune response against the hapten is faster and stronger. The experimental advantage of investigating primed immune responses is better control over the setup. Given that the processes occurring under these three conditions are believed to be similar except for the timing and given further that the most detailed data are available for the primed primary immune response, the GC reaction will be explained by taking this response as an example. Figure 1.2 and Table 1.1 should help on GC organisation and timing.

Table 1.1: GC kinetics in the primed primary immune response

| days | Action | References |
|---|---|---|
| 1 | immunisation | |
| first 3 | B blast proliferation with 1 division within 6-7 hours | [32] |
| 3 | first apoptosis (no memory cells yet) | [34] |
| 3 - 4 | differentiation of B blasts into centroblasts, | [32] |
| | onset of somatic hypermutation | |
| | (at 96 hours already two generations of mutations) | [34] |
| 4 | GC formation: centroblast (dark zone) and centrocytes (light zone) | [19], [20], [32] |
| | GC biggest now | |
| 5 | mutated plasma cells can be found (maybe appeared already earlier) | [34] |
| 21 | GC reaction finishes | [19], [20], [32] |

Calculations based on the kinetics of the emergence of antigen specific B cells led to the suggestion that follicles are seeded during the first hours of infection (immunisation in experiments) and that each follicle soon becomes

dominated by five or less clones [19, 27, 32]. The clones in the follicle enter the blast state and go through rapid cell cycles, increasing some 4000-fold in three days, filling the spaces between the network of follicular dendritic cells (FDC) [35, 36].

After this period of exponential growth, the proliferating B blasts differentiate to centroblasts. Centroblasts are fast proliferating B cells (1 cell division per 6-7 hours [32]) which no longer display any antibodies on their surface. The area which is occupied by centroblasts in the germinal centers is called dark zone and this dark zone is mainly found adjacent to the outer T cell zone [35]. Centroblasts mutate the antibody genes. The onset of the mutation has long been under discussion and varies from organ to organ. While somatic hypermutation is already found by day 3 or 4 after immunisation in the lymph nodes [34] it is not measured in the spleen before day 7 or 8 after immunisation [19]. At this stage the germinal centre is fully developed.

At about the same time as the dark zone appears, the FDC network begins to fill with small irregularly shaped cells which are not dividing but displaying antibodies [36]. These cells are termed centrocytes and are the progeny of centroblasts. The area occupied by the centocytes is known as the light zone of the germinal centre. In that area the network of FDCs is thickest. It is generally believed that the selection of B cells takes place at this stage. Centrocytes express antibody receptors on their surface and these receptors are interacting with the antigen that is displayed on the surface of FDCs. The dendritic structure of FDCs allows them to intersperse between the germinal centre cells and provides therefore a large interaction surface. For selection, centrocytes need to bind antigen, extract it and display fragments of it to T cells that are located in the periphery of the germinal centre. Selection is believed to depend on the quality of the B cell receptor (BCR), which is described in terms of affinity for its target, the antigen. Strength of antibody:antigen binding does clearly not only depend on affinity but also on avidity[3]. We need to keep this in mind but will nevertheless use the term affinity throughout the study.

Centrocytes which fail on one of these steps start to undergo apoptosis after about 12 hours [36]. Selected B cells probably take either of three different routes. Either they differentiate back and replenish the centroblast pool or they differentiate to either plasma cells or memory cells [35]. It is still unclear which signals govern these differentiations but it is suggested that the relative quality of the receptor is decisive. By going through multiple rounds of mutation and selection the binding characteristics of the antibodies are optimised. Optimal antibodies are created by the introduction of about 8 mutations and somatic hypermutation leads to about one mutation per cell per generation. We can therefore expect it to take at least eight generations to obtain high affinity antibodies. About three weeks after immunisation the germinal centers dissolve and the process described above stops [32].

[3]Avidity is the sum total of the strength of binding of two molecules or cells to one another at multiple sites. It is distinct from affinity, which is the strength of binding of one site on a molecule to its ligand [22].

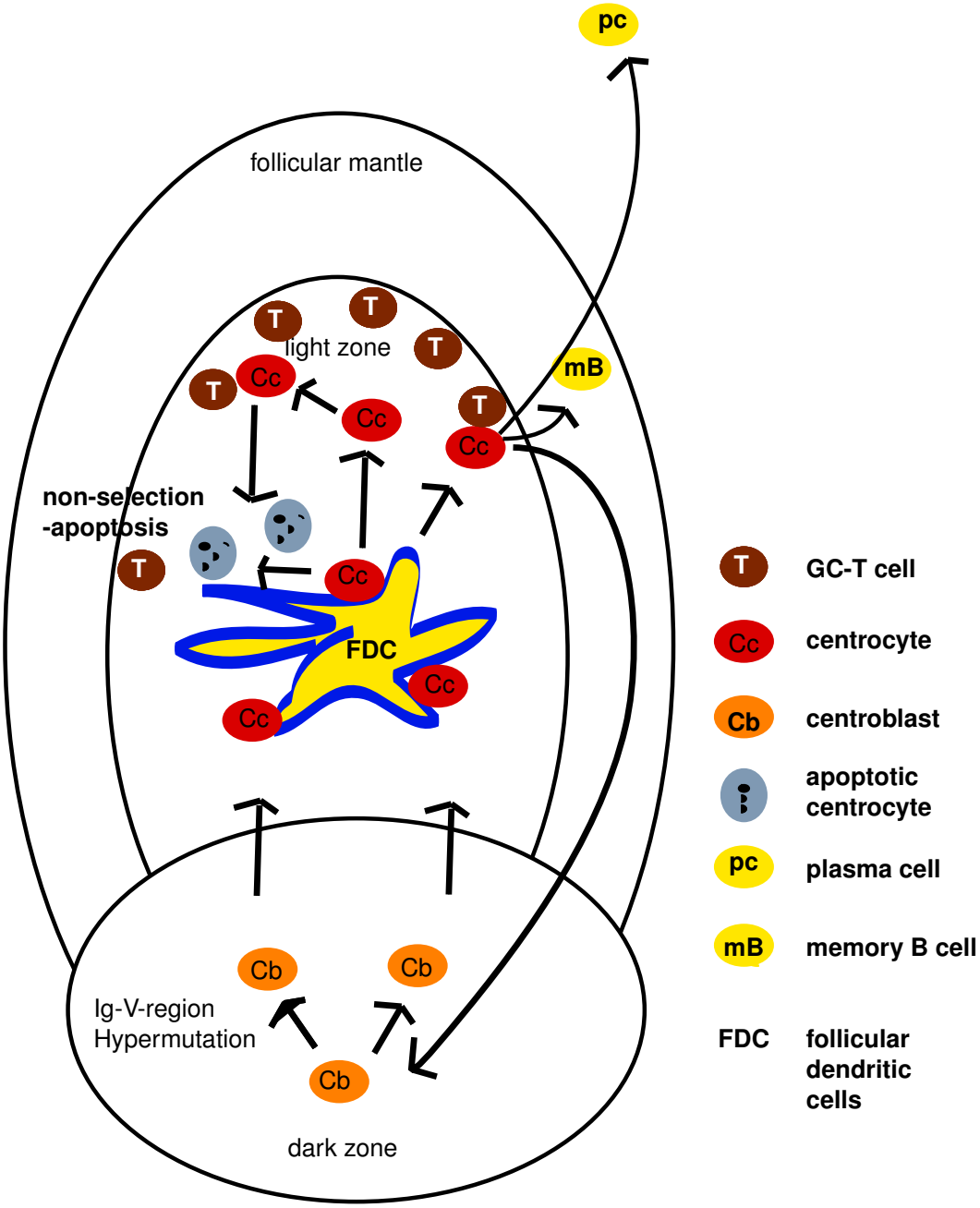



Figure 1.1 Simple model of the processes in the germinal centre (GC) [after MacLennan et al. (2000)]

Figure 1.2: Germinal centre dynamics.

## 1.2 Mathematical Model of the Germinal Center Kinetics

Kesmir and de Boer [26] developed a model of the GC reaction with the aim of capturing the main behaviour without having to consider to many details, since many of them are still unknown. Before this model there was none in which GC termination could be obtained without unreasonable biological assumptions. This model reproduces data of both unprimed and primed primary immune response reasonably well with some inaccuracies which will be discussed later.

In their model, the authors make three key assumptions. The first concerns the signal that leads to the differentiation of centroblasts into centrocytes. This problem has not yet been fully resolved experimentally and Kesmir and de Boer assume that centroblasts remember the number of divisions they have gone through since their existence as centroblasts and differentiate into centrocytes after a fixed number of cell divisions. Their model reproduces the measured germinal centre kinetics if centroblasts go through somewhere between 4 and 10 cell divisions before conversion except for the relative size of centrocyte to centroblast pool. Experimentalists observe that centrocytes outnumber centroblasts during the main GC reaction [36] while in this model both populations are of about the same size. As we will see later this is due to the number of centroblast generations used in the model and the model given in Chapter 2 will fix this problem by presenting an alternative description of the process that allows to reproduce the overall kinetics with only one centroblast generation.

The second assumption is made in order to understand the termination of the germinal centre reaction - a feature that had not been incorporated in earlier models. In this model germinal centre termination is achieved by antigen depletion. Experimentalists however still find large amounts of antigen in the follicles even after GC termination. This mechanism cannot therefore be correct and an alternative based on antigen density dependent selection will be presented in the model studied in this dissertation (Chapter 2).

The third assumption concerns the T cell dynamics. In this model T cells influence B cell kinetics only by supporting centrocyte selection in the light zone. This assumption seems to capture reality quite well since simulations of different immune responses where mainly the T cell influence differs (true and primed primary immune response) reproduce the measured kinetics quite well. The main conclusion to be drawn from this model is therefore that T cell kinetics could cause the different B cell kinetics in true primary or primed primary immune response. It will be interesting to also use the proposed T cell dynamics when modelling memory and plasma cell formation which seem to strongly depend on signals received from T cells.

The germinal centre reaction has already been described in detail in the introduction of the immune response. Figure 1.3 highlights the processes that have been incorporated in the model and the set of differential equations is derived by transferring the arrows into mathematical equations. The variables and parameters are defined in Table 1.2.

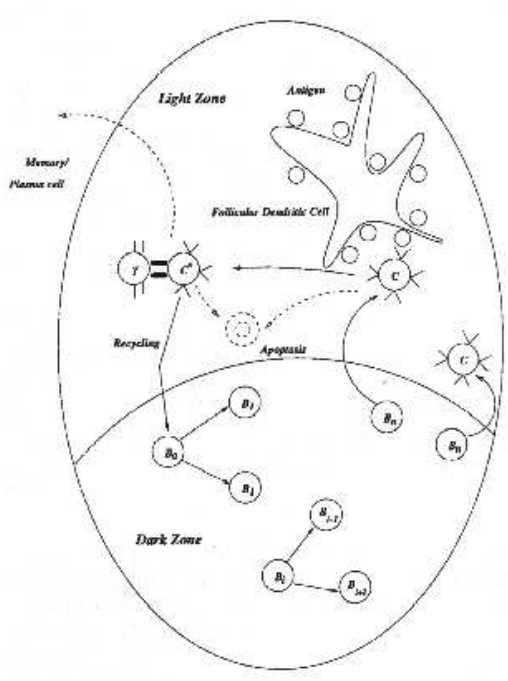



Figure 1.3: Germinal centre dynamics as used in the model of Kesmir and deBoer

$$\frac{dB_0}{dt} = p_r \mu C_T^* - \rho B_0 - \delta_b B_0 \tag{1.1}$$

$$\frac{dB_i}{dt} = \rho(1+\alpha_b)B_{i-1} - \rho B_i - \delta_b B_i \qquad \text{for i = 1,2, ..., n} \tag{1.2}$$

$$\frac{dC}{dt} = d\rho B_n - \mu C \tag{1.3}$$

$$\frac{dC^*}{dt} = \mu(C_A - C^*) \tag{1.4}$$

$$\frac{dM}{dt} = (1-p_r)\mu C_T^* \tag{1.5}$$

$$\frac{dA}{dt} = -zA - uC_A \tag{1.6}$$

$$\frac{dT}{dt} = \sigma + p\alpha_t C_T^* - \delta_t T \tag{1.7}$$

$$C_A = \frac{CA}{s_A + A} \qquad C_T^* = \frac{C^* T}{s_T + C^*} \tag{1.8}$$

$$\alpha_b = \frac{K_b}{K_b + \sum_{i=0}^{n} B_i} \qquad \alpha_t = \frac{K_t}{K_t + T} \tag{1.9}$$

The different $i$'s label the different centroblast generations through which centroblasts go before differentiation into centrocytes. $n$ lies between 4 and 10. In the numerical solutions below $n = 10$ was used.

Table 1.2: Parameters for the GC kinetic model of Kesmir and de Boer [26]

| | | |
|---|---|---|
| $n$ | number of cycles before centrocyte conversion | |
| $B_i$ | number of centroblasts after i divisions | |
| $C$ | number of centrocytes | |
| $C^*$ | number of centrocytes that are presenting antigen on their surface | |
| $C_T^*$ | number of centrocytes that have been selected by T cells | |
| $M$ | number of memory cells | |
| $Ag$ | initial number of immune complexes on FDCs | |
| $T$ | number of T helper cells | |
| $p_r = 0.15$ | probability of recycling | |
| $K_b = 10^4$ or $10^9$ | density dependent centroblast proliferation | |
| $K_t = 100$ | Constant for density dependent T cell proliferation | |
| $\rho = 4$ | maximum proliferation rate of centroblast ($d^{-1}$) | [32] |
| $p = 2$ | maximum proliferation rate of GC T cells ($d^{-1}$) | [23] |
| $\delta_b = 0.8$ | Death rate of centroblasts ($d^{-1}$) | [3] |
| $\delta_t = 0.8$ | Death rate of T helper cells ($d^{-1}$) | [23] |
| $d = 2$ | Maximum rate of centrocyte $\rightarrow$ centrocytes diff. ($d^-1$) | [32] |
| $\mu = 3$ | maximum apoptosis rate for centrocytes ($d^{-1}$) | [8] |
| $s_A = 500$ | saturation constant for B cells binding FDCs | |
| $s_T = 50$ | saturation constant for centrocyte-T cell interaction | |
| $u = 0.15$ | antigen consumption per centrocyte-FDC complex | |
| $\sigma = 5$ | Influx of T cells into the GC ($d^{-1}$) | [32] |
| $z = 0.02$ | Average life time of immune complexes on FDCs (d) | |

$B_0$ is the set of centroblasts which have not yet divided. Cells can leave this pool either by dividing ($-\rho B_0$) or by dying ($-\delta_b B_0$) (1.1) where $\rho$ is the division rate and $\delta_b$ is the cell death rate. From experiments it is known that centroblasts divide about 4 times a day and we would therefore need $\rho = 4ln2$ to give growth of the correct size. Kesmir and de Boer however use $\rho = 4$ in their model. Centroblasts divide too quickly as that they would die of age. The main cause of death is lethal mutation in the process of somatic hypermutation. The death rate will therefore be different in the time ranges when somatic hypermutation operates and those when it does not. Shannon and Mehr [51] calculate the proportion of lethal mutations during somatic hypermutation to be 0.28 which ties up with the constant death rate $\delta_b = 0.8$ used in this model. This model therefore neglects the periods of mutation free growth. The dividing centroblasts do not only leave their class $i-1$ but enter the class $i$ which is the class of those cells which have divided $i$ times. Given that they divide in this process we have the influx term, $\rho(1+\alpha_b)B_{i-1}$, into $B_i$ (1.2). $\alpha_b$ models the density dependence of B cell growth and brings in the first non-linearity (1.9). Given that cell division probably also starts as cell density dependent it might have been better to write $2\rho a_B$ which is done in the models presented later. The outflux term is again the same as in the last generation. From the last centroblast generation, centroblasts differentiate into centrocytes upon division and the influx into the centrocytes pool is therefore $d\rho B_n$ (1.3). Cells leave this pool with rate $\mu$ (1.3) and either die or are successful and present antigen for further selection by T cells. The proportion of successful B cells is modelled to be antigen density dependent (1.4). $C_A$ therefore introduces a non-linearity into the equation (1.8). The antigen presenting cells need to interact with T cells

in order to become activated and this activated species $C_T^*$ can either enter the memory cell pool $M$ (1.5) or can recycle and replenish the centroblast pool $B_0$. The probability of recycling is termed $p_r$ and is taken to be $p_r = 0.15$ in order to reproduce the kinetic data. We will later argue that this rate is probably changing with time and in average larger than this chosen value. The ODE for $B_0$ therefore has the influx term $p_r \mu C_T^*$ and for the memory cell dynamics we have the influx of the remaining cells and $(1 - p_r)\mu C_T^*$. The rate $\mu$ was used again since explicit rates for the different centrocyte populations are not known but outflux rates from the centrocyte pool have been determined to be about $2 - 3$ day$^{-1}$. Given that the selection of centrocytes depends on the actual antigen density and the total T cell number, we finally need equations modelling their dynamics. It is assumed that antigen density either decreases by antigen decay with the decay rate $z = 0.02$ day$^{-1}$ or is actively consumed by antigen presenting centrocytes (1.6). This was deduced from the fact that without active antigen consumption antigen stays in the germinal centre for months or years and the half life was therefore assumed to be 50 days. The antigen consumption was modelled to be linearly dependent on the number of antigen presenting cells $C_A$ which depends in a nonlinear manner upon the antigen density (1.8) with $u = 0.15$ being the antigen consumption rate. The T cell pool can be fed by influx $\sigma$ from the outer T cell zone which lies adjacent to the dark zone in the germinal centre or by proliferation which is activated in a density dependent manner by interaction with antigen presenting B cells which gives the term $pa_t C_T^*$. T cells leave the pool by dying with rate $\delta_t = 0.8$.

Table 1.3: Initial values for the GC kinetic model of Kesmir and de Boer [26]

| | |
|---|---|
| $B_0 = 3$ | initial number of centroblasts [32] |
| $B_i = 0$ for $0 < i \leq n$ | centroblast after i divisions |
| C= 0 | centrocytes |
| $C^* = 0$ | centrocytes that are presenting antigen on their surface |
| $C_T^* = 0$ | centrocytes that have been selected by T cells |
| M = 0 | memory cells |
| Ag = 500 | initial number of immune complexes on FDCs |
| T = 0 | T helper cells |

The equations can be solved numerically with a 4th order Runge-Kutta algorithm which was used instead of a Matlab solver in order to have better control by having coded the algorithm explicitly. The initial conditions are given in Table 1.3. The resulting kinetics can be seen in Figure 1.4. Comparison with experimental data in Figure 1.6 shows a very good match especially for the true primary immune response when B cell cell density dependent growth is assumed ($K_b = 10^4$). For cell density independent growth ($K_b = 10^9$) the GC reaction is double the size of the observed ones. The primed primary immune response is modelled by changing the influx of T cells into the GC reaction from $\sigma = 5$ day$^{-1}$ to $\sigma = 50$ day$^{-1}$. This small change leads to an earlier onset of the primed primary response (highest curve in Figure 1.6), which is however not sufficient to capture the experimental data completely. The same is valid for the strength of the response: the model captures qualitatively the higher GC B cell numbers but the numbers are still to small compared to experimental

results. Ignoring recycling (that is, setting $p_r = 0$) leads to the prediction of GC dissolution by day 5 as can be seen in Figure 1.5. This agrees with recent experimental data [10].

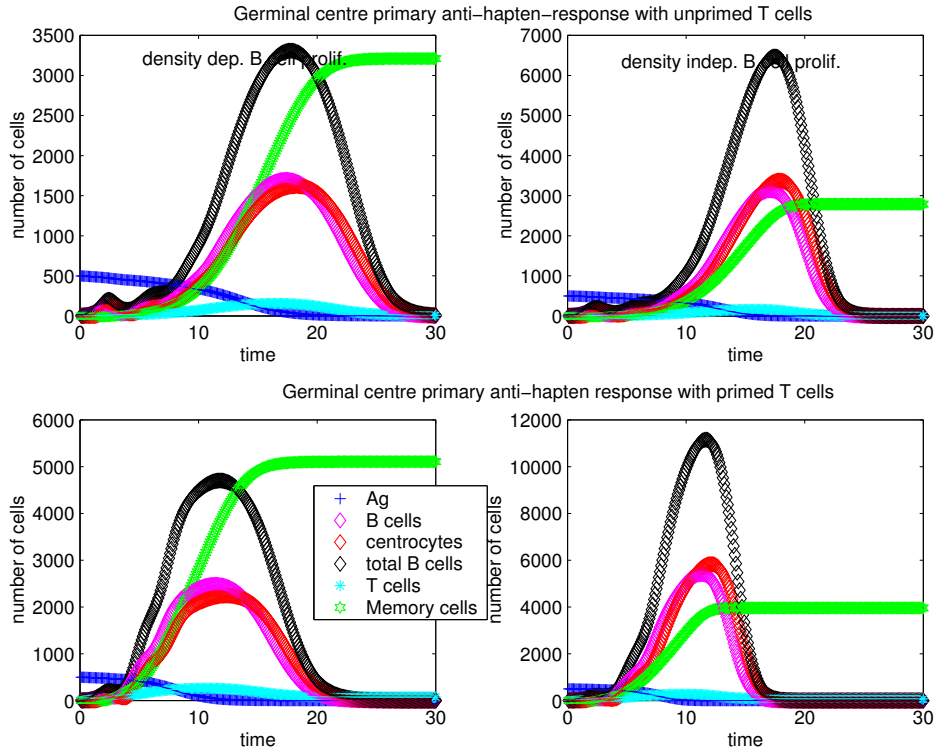



Figure 1.4: Kinetic results of the model of Kesmir and de Boer [26]. (*top*) GC reaction in the true (unprimed) primary immune response. (*bottom*) GC reaction in the primed primary immune response. The GC reaction starts earlier and terminates earlier in the primed case. This is not in agreement with experimental data (see Figure 1.6). Further on, the results for the primed primary immune response show a stronger response than in the unprimed case. This general qualitative behaviour has been captured well by the model while the extend is less than in experimental data (see Figure 1.6). (*LHS*) Germinal centre dynamics with density dependent ($K_b = 10^4$) B cell proliferation.(*RHS*) Germinal centre dynamics with density independent($K_b = 10^9$) B cell proliferation. In case of the true primary immune response, the density dependent model reproduces experimental data concerning the size of the reaction best. The model does however not attempt to explain why the growth of the B cell population should be density dependent with $K_b = 10^4$ being the population size for which the growth rate is half-maximal.

## 1.3 Scope of the Study

The scope of this mathematical study of affinity maturation is to identify the main processes driving affinity maturation. Affinity maturation happens in

special environments, the germinal centres, and this study therefore investigates the germinal centre reaction into which affinity maturation is embedded. The main questions that will be addressed in this study are

- What governs the differentiation of proliferating and mutating B cells (centroblasts) into non-proliferating, non-mutating B cells (centrocytes) which are selected upon the quality of the B cell receptors they express?
- When is the best start of memory cell formation with respect to the efficiency of affinity maturation?
- Which is the best selection policy in order to gain the best affinity maturation of antibodies?
- What is the role of recycling in this process?

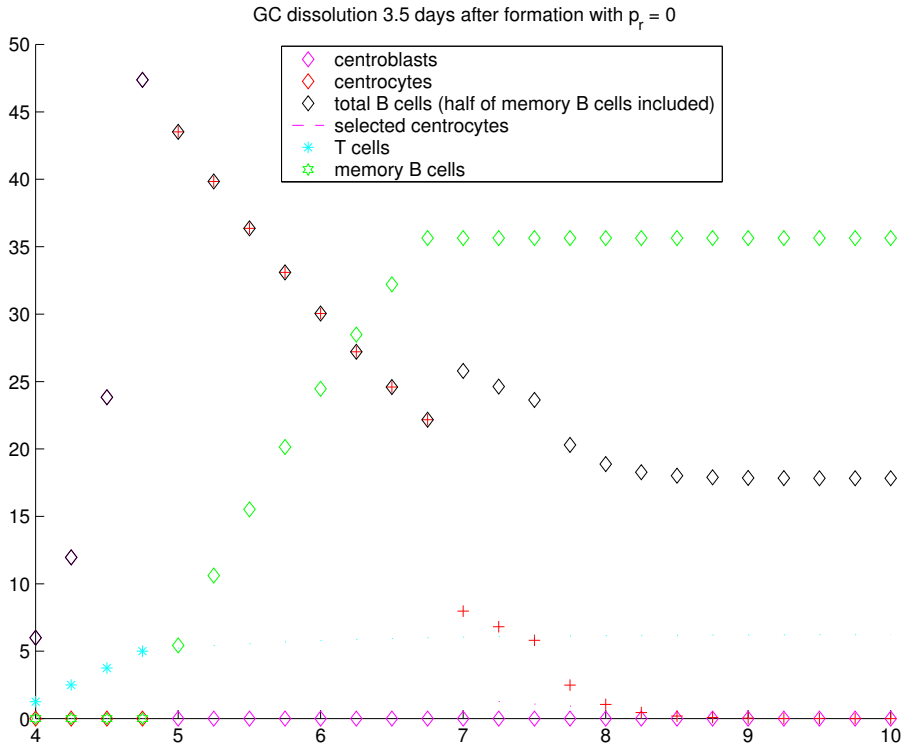



Figure 1.5: GC dissolution by day 5 if centrocytes cannot recycle back to replenish the centroblast pool. The plot shows that the number of centroblasts ($B$) and centrocytes ($C$) goes to zero if centroblasts cannot recycle back while the number of memory cells ($M$) reaches a constant plateau since no selected centrocytes ($C_T^*$) exist which could enter this pool.

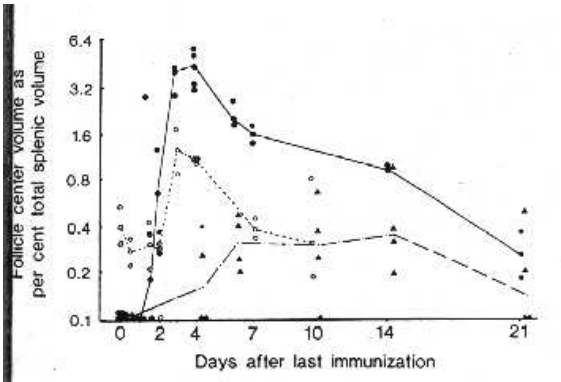



*Figure 4.* The relative size of the follicle center reaction during the fully primary anti-hapten response (triangles), the primary anti-hapten response when T cell help is not limiting (closed circles), and the secondary anti-hapten response (open circles). The immunization groups are described in the legend to Fig. 3 and Sec. 3.1. The size of the follicular reaction is assessed as the percentage of the section which is within follicles and is HIS22$^-$ as specified in Sect. 2.5.1. Each point represents the value for a single rat. Lines are drawn through median values. The time scale represents the time from the last immunization of each rat.

Figure 1.6: GC kinetics measured by Liu et al. (1991) [32]. Note the logarithmic scaling.

# Chapter 2

# Model of Affinity Maturation

## 2.1 Introduction

Modelling affinity maturation is an extension of modelling the GC kinetics and it may therefore seem sensible to build on the model of Kesmir and de Boer which was introduced in Chapter 1. A drawback of this model is that many parameters are unknown and had to be guessed (see Table 1.2) and that the model in itself is already very complex without having added affinity maturation. The non-linearity and the large number of equations prohibit an analytical study which could be expected to provide further insights about the behaviour of the system. The model can however be used to answer three important questions:

1) Is the generation dependency of centroblast to centrocyte differentiation the only sensible assumption or could the regulation of this conversion also be cell density or time dependent?

2) Can antigen density play a decisive role in affinity maturation?

3) Is it more beneficial with respect to affinity maturation to start memory cell formation with the onset of somatic hypermutation or later?

The answer to the first question is clearly that there is no alternative to the generation dependent conversion model. As shown in Appendix B, and briefly reconsidered here, other regulations of the differentiation of centroblasts to centrocytes do not allow one to reproduce all available experimental data. In the case of a cell density or time dependent conversion the equations governing the centroblast ($B$) kinetics in the model of Kesmir an de Boer [26] need to be replaced by

$$\frac{dB}{dt} = p_r C_T^* + (\rho a_b - \delta_b)B - dB \tag{2.1}$$

where $d$ is either cell density or time dependent. As shown explicitly in Appendix B.1 there exists beside the trivial a non-trivial steady state with $C_T^* = 0$ which can be attained if $d$ is constant or cell density dependent as is already obvious from 2.1 and is deduced explicitly in the Appendix. Due to this non-trivial equilibrium point the GC reaction cannot terminate anymore except if

an additional forcing term is introduced as done by Oprea and Perelson [44] which is however difficult to justify biologically.

If we assume time dependency of conversion, conversion needs to start late in order not to obtain a constant non-zero $d$ too early in the response since then a non-trivial equilibrium state could still be attained which prohibits GC termination. Such a late conversion cannot however satisfy the data on early GC termination if recycling is inhibited (see Appendix B.2 for details).

It is therefore necessary to assume a generation dependency of the differentiation of centroblasts into centrocytes.

Concerning question 2 the time dependent and the generation model were investigated whether antigen reduction during the GC reaction could influence selection such that affinity maturation is obtained. This was indeed found (see Appendix B.2 and B.3 and especially figures B.6 and B.9 for details).

With respect to question 3 the model further showed that too early an onset of memory cell formation leads to a lesser extent of affinity maturation (see Appendix B.3). This is probably due to the high proportion of low affinity clones which enter the memory cell pool at the beginning and persist in the memory cell population which prohibits a shift to a high proportion of high affinity clones in case of an early onset of memory cell formation. Further on, the low affinity clones which enter the memory cell pool cannot be further mutated and expanded as centroblasts which is a further disadvantage.

Due to the complexity of the model and the lack of data for important parameters such as the selection proportion $s$, there are no further predictions possible such as restrictions on the possible parameter space for the selection proportion $s$ and the recycling probability $p_r$, which could be gained by a mathematical analysis. Further on, the solution found is highly unstable with respect to parameter variations. Various experiments, however show that nature is robust against such variations [16].

It is therefore necessary to build a new model which can also be studied analytically and which considers a system for which more data are available. Given that non-linear models are in general difficult to be analysed analytically and given that the process can be expected to be highly non-linear the new model is constructed to be semi-linear in the sense that the non-linearity is introduced into the model via parameters. Bounds are obtained for all parameters and in the analysis the parameters are considered constant and the behaviour of the system is deduced for the different ranges of the parameters. With the insights about the behaviour of the system for different sizes of the parameters, the equations governing the parameters can be determined such that biological data can be reproduced. The finally obtained non-linear model can be solved numerically. The second problem concerning the need of a system for which more experimental data are available was solved by modelling the primed primary immune response instead of the true primary immune response which was described above and modelled in Appendix B. In the primed primary immune response an animal is first immunised with a precipitated carrier protein that activates T cells. A month later the animal is again immunised with the carrier protein but this time conjugated to a hapten. A hapten is an agent that is too small to raise an immune response. Conjugated to the carrier

Table 2.1: GC kinetics in the primed primary immune response

| days | Action | References |
|---|---|---|
| 1 | immunisation | |
| first 3 | B blast proliferation with 1 division within 6-7 hours | [32] |
| 3 | first apoptosis (no memory cells yet) | [34] |
| 3 - 4 | differentiation of B blasts into centroblasts, | [32] |
| | onset of somatic hypermutation | |
| | (at 96 hours already two generations of mutations) | [34] |
| 4 | GC formation: centroblast (dark zone) and centrocytes (light zone) | [19], [20], [32] |
| | GC biggest now | |
| 5 | mutated plasma cells can be found (maybe appeared already earlier) | [34] |
| 21 | GC reaction finishes | [19], [20], [32] |

protein it is however recognized by the immune system and raises an immune response. Importantly, the hapten-carrier protein complex can be injected in soluble form. This leads to a faster clearance of the antigen from the body and a sharper response which allows a more accurate description of the process and gives therefore better data. The problem of modelling the true primary immune response already starts with deciding about the onset of the immune response since this is smeared over a time span of several days. The cause for the smeared onset is that the antigen needs to be injected in precipitated form and dissolves only slowly. A draw-back of modelling the primed instead of the true primary immune response is that due to the priming, T cell help is non-limiting and the immune response against the hapten is faster and stronger than in the unprimed case. This is an unfortunate side effect since the mechanisms of the two responses may therefore be different and an understanding of the artificial primed primary immune response does not directly imply an understanding of the true primary immune response. Because of the easier interpretation of the available data for the primed primary immune response it is nevertheless sensible to go ahead with building a mathematical model for this response.

The available kinetic data for the primed primary immune response are summarised in Table 2.1. Further kinetic data available from the literature only concerns small sections of the spleen or the total follicle center volume. The latter is shown as the highest curve in Figure 1.6 and one can see that from day 4 to 7 the follicle center volume halves. It is generally believed that this is due to extensive cell death of cells that were not selected. We will challenge this idea in our model. From day 7 to 14 or 16 the follicle center volume halves again. After day 16 the GC reaction continues to decline. Data on the true primary response [21] suggest that this decrease in cell number may be due to even more stringent selection conditions. For the time after day 21 no data is available but we can assume that the reaction continues to decline in the same way as before. Judging from the GC volume at day 21 about 2000 B cells (10% of the largest population) are still in the germinal center.

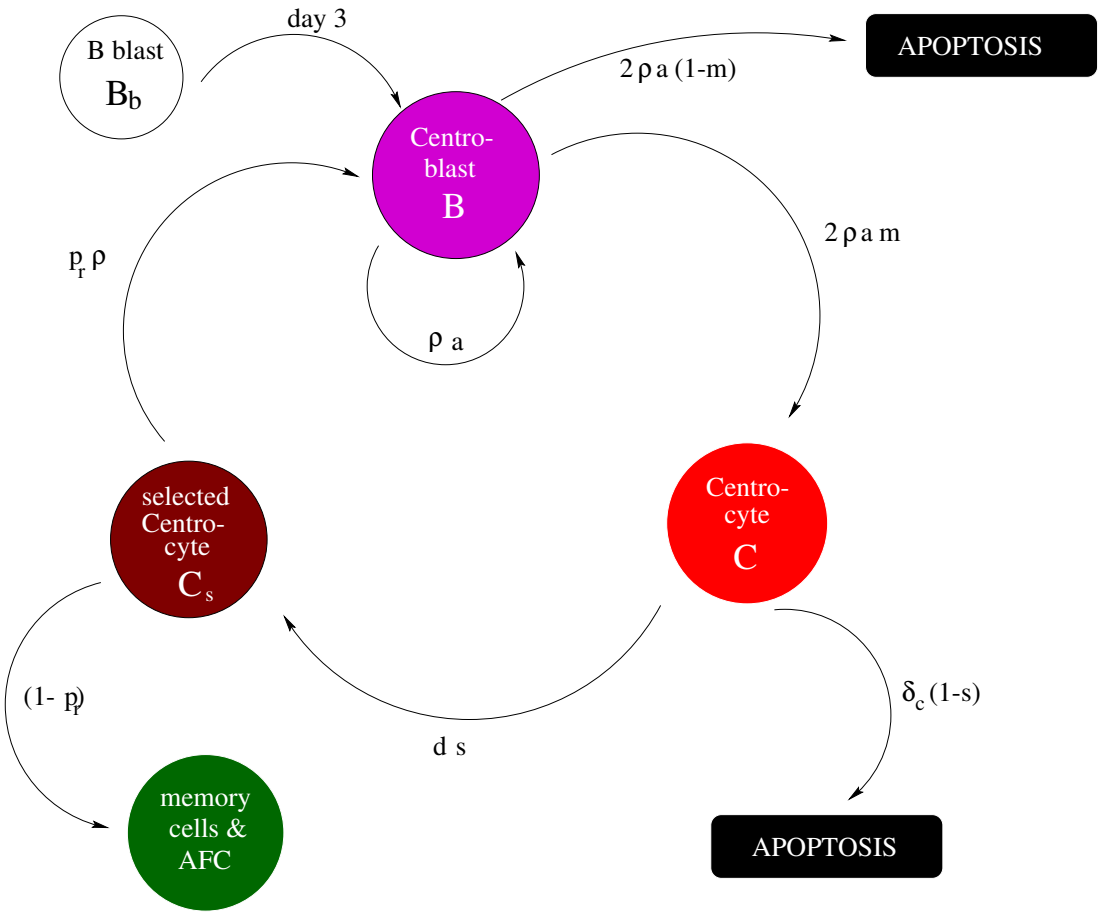



Figure 2.1: Scheme of the model for the primed primary immune response. Abbreviations are explained in Table 2.2.

## 2.2 Model of the Germinal Center Kinetics

Given that the models for the true primary immune response are difficult to analyse properly due to their complexity a very simplistic minimal model is now introduced for the primed primary immune response. In this minimal model the main players of the germinal center reaction are reduced to three, namely centroblasts ($B$), centrocytes ($C$) and selected centrocytes ($C_s$). Additionally, there are memory ($M$), plasma ($PC$) and antibody forming cells ($AFC$) which evolve from selected centrocytes. In the first simple models, we will not distinguish between the three populations. Later on the differentiation between the three population will allow us to use further data in order to evaluate the quality of the model. As can be seen in Figure 2.1 these three populations do not feed back into the general system and we can therefore exclude them mostly from our first analysis and especially from the stability analysis and need only to consider them as outflux terms in the dynamics of selected centrocytes.

During the first three days of the response there is exponential growths

of B blasts which can be modelled by $\frac{dB}{dt} = \rho B$. The division time is 6-7 hours [32] and the proliferation factor is therefore $\rho = 4$ ln2 days$^{-1}$ so that $B(0.25) = 2B(0)$. This ODE can easily be integrated and we obtain $B(t) = B(0)\exp(\rho\Delta t)$. The number of seeding B blasts has been estimated to be five or less [19, 27, 32] and we use $B(0) = 3$. On day 3 therefore 12288 B blasts differentiate into centroblasts which we take as initial condition for the model presented below. Given that B blasts and centroblasts are very similar, they are both labeled $B$ in the equations. With this differentiation the main part of the reaction, which is cyclic, starts. The mathematical formulation of the model is given below. The dynamics incorporated in the model are depicted schematically in Figure 2.1 and the parameters are given in Table 2.2. The unit of time ($t$) is days.

for $t > 3$

$$\frac{dB}{dt} = p_r\rho C_s - \rho B \tag{2.2}$$

$$\frac{dC}{dt} = 2\rho m B - \mu C \qquad \text{with} \quad \mu = ds + \delta_c(1-s) \tag{2.3}$$

$$\frac{dC_s}{dt} = dsC - \rho C_s \tag{2.4}$$

$$\frac{dM}{dt} = (1-p_r)C_s \tag{2.5}$$

Table 2.2: Parameters for the minimal model

| | | |
|---|---|---|
| $B$ | B blasts & centroblasts | |
| $C$ | centrocytes | |
| $C_s$ | centrocytes that have been selected | |
| $p_r \in [0, 1]$ | probability of recycling | |
| $\rho = 4$ ln2 | maximum proliferation rate of centroblast (day$^{-1}$) | [32] |
| $d = 12$ ln2 | Rate of running through the selection process (day$^-1$) | [32] |
| $s =\in [0, 1]$ | selection probability of centrocytes | |
| $m = 0.72$ | probability of non-deleterious mutation | [51] |
| $\delta_c = 1.5$ ln2 | death rate of centrocytes | [36] |

Centroblasts keep on dividing at the same rate $\rho$ as B blasts. The rate of multiplication could be modelled as being cell density dependent as has been done by Kesmir and de Boer [26]. Given that there is however no experimental evidence for such an assumption, this source of nonlinearity will not be included in this simple model. As discussed in the introduction, the conversion of centroblasts into centrocytes needs to be modelled as generation dependent in order to satisfy all available experimental data. As analysis of the model will show, the number of centroblast generations that we require depends critically on the values of the parameters characterising somatic hypermutation. We will here assume the simplest case of generation dependent conversion, namely that after one centroblast cell division and will later show with this assumption we can satisfy the experimental data best. This conversion of centroblasts into centrocytes could either concern only one daughter cell or both of them. In the first case we would however not obtain the observed GC kinetics since the

centroblast pool could only increase but not decrease since no net outflux term would be included and the GC reaction could therefore never terminate. In the model it is therefore assumed that centroblast division directly leads to differentiation of both daughter cells into centrocytes and we therefore have the term $-\rho\, B$ in equation (2.2). Due to somatic hypermutation only the proportion $mB$ survives the cell division and differentiates into centrocytes while the other part of dividing centroblasts $(1-m)B$ is assumed to die at the same rate as the surviving part differentiates. The death rate of centroblasts may well be smaller than the conversion rate. Such a possible difference cannot however be expected to change the modelled kinetics substantially if we assume that centroblasts once committed to apoptosis (programmed cell death) can not take part in the normal cell division process. A smaller death rate would therefore only lead to a slower decay of the total cell number. The surviving centroblast proportion gives rise to the term $2\rho mB$ in equation (2.3). The factor 2 comes in since one centroblast gives raise to two centrocytes and division of centroblasts is assumed to lead directly to differentiation into centrocytes.

Part of the centrocytes ($sC$) becomes selected into the pool $C_s$ at a rate $d$ via interaction with antigen and T cells, whose dynamics are not included in this first simple model. This generates the term $dsC$ in equation (2.4). The other part $((1-s)C)$ undergoes apoptosis with rate $\delta_c$ and the outflux from the centrocyte pool is therefore in total $(ds+\delta_c(1-s))C$, which is given as $\mu C$ in equation 2.3. The selected centrocytes ($C_s$) can then either differentiate into memory ($M$) or plasma cells ($PC$ and $AFC$) with probability $(1-p_r)$ (2.5) or they recycle and replenish the centroblast pool with probability $p_r$. The time needed to recycle is assumed to be, on average, about 6 hours and therefore again $\rho$ is used as a rate constant and we obtain the term $p_r\rho C_s$ in equation 2.2. We further assume that selected centrocytes differentiate at the same rate into memory or plasma cells as they recycle so that the net outflux term out of the pool of selected centrocytes is given by $-\rho C_s$ in equation (2.4). In order to keep the number of plasma and memory cells in a reasonable range we further assume that it takes longer for the centrocytes to develop the memory or plasma cell state than to recycle and chose the rate of becoming a memory or plasma cell to be 1 day$^{-1}$. With this assumption we obtain equation (2.5). Changing this rate would only change the total number of influx cells into the memory and plasma cell pool. The final number of memory B cells was measured to be less than 5 percent of the maximal GC B cell number [55] while the size of the plasma cell pool is unknown and difficult to determine since plasma cells emigrate from germinal centres. A change in the influx rate in this model would therefore need to be compensated by the proportion of cells either becoming memory or plasma cells in order to satisfy the experimental data concerning the size of the memory cell pool.

The non-dimensionalisation of the model is straightforward using

$$t = \tau\tilde{t} \qquad \delta_c = \tau^{-1}\tilde{\delta}_c \qquad d = \tau^{-1}\tilde{d} \qquad \rho = \tau^{-1}\tilde{\rho} \tag{2.6}$$

$$B = Z\tilde{B} \qquad C = Z\tilde{C} \qquad C_s = Z\tilde{C}_s \qquad M = Z\tilde{M} \tag{2.7}$$

where $\tau = 1$ day and we are free to choose $Z$. It is sensible to set $Z$ to be the maximal B cell number so that $B, C, C_s$ and $M$ are all between 0 and 1. Upon dropping the tildes we are left with the same model as above which for that reason will not be repeated again. By comparing the relative sizes of all terms in the above system we see that all must be included. Throughout the rest of this dissertation we will solve the dimensional form of the equations since we wish to compare our results directly with experimental results of other workers [32, 34, 36, 54, 55]. The initial conditions are that all cell populations but the B blasts are zero, while the number of seeding B blasts is 3 [32].

Steady state analysis for the system of equations excluding the equation for M, shows that beside the trivial equilibrium point there exists a second non-trivial one if

$$\mu = \mu_c = 2p_r msd. \tag{2.8}$$

The equilibrium values are:

$$\begin{aligned} B^* &= p_r C_s^* \\ C^* &= \frac{2\rho m}{\mu} B^* \\ C_s^* &= \frac{ds}{\rho} C^* \end{aligned} \tag{2.9}$$

Given that $\mu = ds + \delta_c(1 - s)$ we therefore obtain as a condition for an equilibrium point

$$2p_r mds = ds + \delta_c(1 - s). \tag{2.10}$$

Solving (2.10) for $s$ we obtain for $s$ at the equilibrium point

$$s_c = \frac{\delta_c}{d(2p_r m - 1) + \delta_c}. \tag{2.11}$$

Given that the selection factor $s$ can only take values between 0 and 1 in the model, we obtain as a further condition on the denominator

$$d(2p_r m - 1) + \delta_c \geq \delta_c \tag{2.12}$$

which leaves us with the condition

$$p_r m \geq 0.5 \tag{2.13}$$

in order to attain the equilibrium state within the possible parameter space. Condition (2.13) also ensures that $s_c > 0$ for which we need $p_r m > 0.5 - \frac{\delta_c}{2d} = 0.4375$. Due to somatic hypermutation the survival rate $m$ has been calculated to be about 0.72 [51] or 0.75 [2]. Other sources are more pessimistic and consider $m = 0.5$ [25]. For the latter parameter value of $m$ we would need $p_r = 1$ in order to meet condition (2.13). $p_r$ however cannot attain 1 since then no memory cell formation would be possible (2.5). We therefore have to demand $m > 0.5$ in

order to attain the equilibrium state. For $m \leq 0.5$ we have $\mu > \mu_c$ for all parameters in the parameter space. If we use $m = 0.72$ on the other hand, we only need $p_r \geq 0.69$ in order for our model to be able to attain a non-trivial equilibrium state.

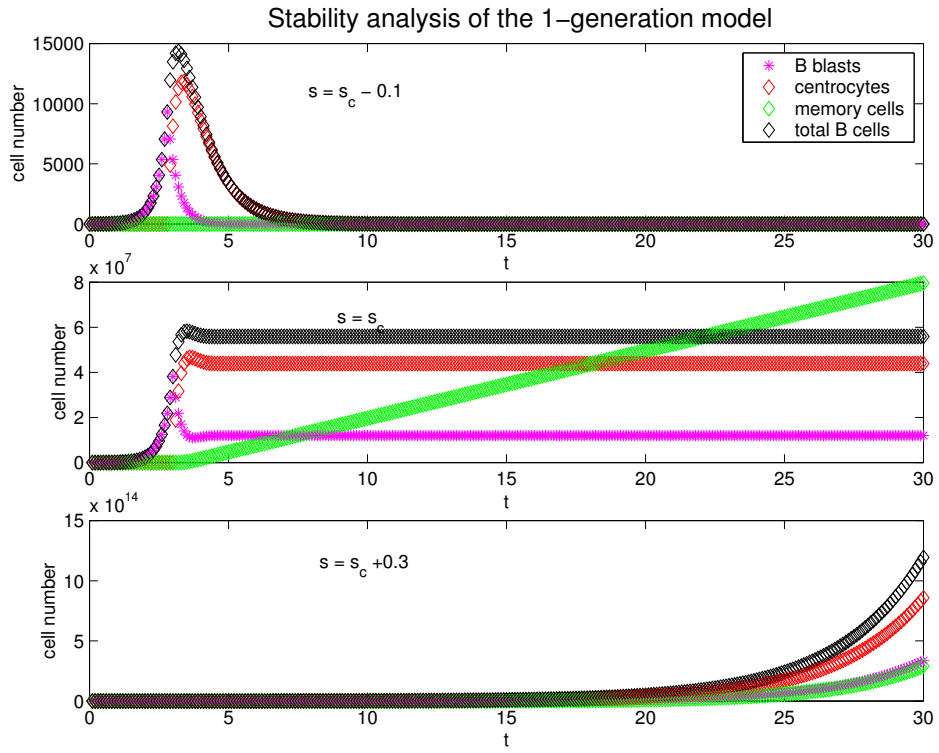



Figure 2.2: GC kinetics of the primed primary immune response in the minimal model where $m = 1$ (no somatic hypermutation included), $p_r = 0.8$ and $s_c = 0.1724$. The three plots show the behaviour for different values of $s$: *top* $s = s_c - 0.1$: solution attains stable equilibrium point 0 for all cell populations; middle $s = s_c$: solution attains non-zero equilibrium point for all cell populations but the memory cells which increase continuously; bottom $s = s_c + 0.3$: the solution explodes for all cell populations

It is now sensible to carry out a stability analysis of the system in order to understand the impact of the last finding. Given that all ODEs are linear we can rewrite the system of equations in matrix form with $\mathbf{v} = [B, C, C_s]'$

$$\dot{\mathbf{v}} = \begin{pmatrix} -\rho & 0 & p_r\rho \\ 2\rho m & -\mu & 0 \\ 0 & ds & -\rho \end{pmatrix} \mathbf{v}$$

and calculate the eigenvalues of the matrix from the characteristic polynomial

$$(\mu + \lambda)(\rho + \lambda)^2 = 2\rho^2 p_r m d s > 0. \tag{2.14}$$

Comparing the factorised form of the general characteristic polynomial of degree 3

$$\lambda^3 - \lambda^2 \sum_i \lambda_i + \lambda \sum_{i<j} \lambda_i \lambda_j - \prod_i \lambda_i = 0 \tag{2.15}$$

where the indices range from 1 to 3 with the characteristic polynomial given in (2.14) we obtain as conditions on $\lambda_i$

$$\begin{aligned} \sum_i \lambda_i &< 0 && (2.16)\\ \sum_{i<j} \lambda_i \lambda_j &> 0 && (2.17)\\ -\prod_i \lambda_i &= \rho^2(\mu - \mu_c) && (2.18) \end{aligned}$$

with $\mu_c = 2p_r mds$ as given in (2.8). For $\mu = \mu_c$ we have $\prod_i \lambda_i = 0$ and therefore w.l.o.g. $\lambda_1 = 0$. From the two other inequalities (2.17, 2.18) follows $\lambda_2\lambda_3 > 0$ and $\lambda_2 + \lambda_3 < 0$ which can only be satisfied by $\lambda_2$, $\lambda_3 < 0$. The steady state is therefore stable and can be non-zero if the starting value (day 3 value) is non-zero since one eigenvalue is zero. This is in agreement with the previous analysis which showed that we have a non-trivial steady state for $\mu = \mu_c$ (2.10). For illustration see the numerical solution in Figure 2.2 middle. For $\mu < \mu_c$ we obtain the conditions $\lambda_1\lambda_2\lambda_3 > 0$ and $\lambda_1+\lambda_2+\lambda_3 < 0$ which can only be satisfied by $\lambda_1 > 0$, $\lambda_2$, $\lambda_3 < 0$. Given that $\lambda_1 > 0$ the critical point is unstable and for $\mu < \mu_c$ the solution therefore explodes as can also be seen in the numerical solution in the bottom plot in Figure 2.2. For $\mu > \mu_c$ we have $\lambda_1\lambda_2\lambda_3 < 0$ and $\lambda_1 + \lambda_2 + \lambda_3 < 0$. This could either be satisfied by $\lambda_1 < 0$, $\lambda_2$, $\lambda_3 > 0$ or by $\lambda_1, \lambda_2, \lambda_3 < 0$. Assuming the first case was correct we would then get $-\lambda_1 > \lambda_2 + \lambda_3 > 0$ and $-\prod_i \lambda_i = \lambda_1(\lambda_2 + \lambda_3) + \lambda_2\lambda_3 < -(\lambda_2 + \lambda_3)^2 + \lambda_2\lambda_3 < 0$ which stands in contradiction to (2.17). We therefore have $\lambda_1, \lambda_2, \lambda_3 < 0$. For $\mu > \mu_c$ - which is always the case in this model if $m \leq 0.5$ - the solution therefore rapidly falls to zero which is the only equilibrium state for $\mu \neq \mu_c$ as can also be seen in the plot in the top of Figure 2.2. This will be exploited in the modelling process for $t > 7$ when the GC reaction slowly declines to zero.

Continuing on the model given by equations (2.2-2.5) we realise that two parameters, the selection probability and the recycling probability, are not known from experiments (see Table 2.2). As deduced above the recycling rate needs to be high in order for our model to work and is taken to be $p_r = 0.8$. This is not a new finding: several groups have argued before that the recycling probability must be high in order to achieve reasonable affinity maturation [38, 44]. The biological justification lies in the fact that clones which do not recycle are lost from the germinal center reaction. Given that improving mutations make up only a very small proportion (less than 10 percent and maybe only 1 per thousand mutations [37]) continual emigration of improved clones would impede a successful affinity maturation. *In vivo* the recycling rate probably varies during the immune response and may critically depend on signals from T cells that

may not only decide whether B cells emigrate as memory or plasma cells but also whether they stay in the germinal center and recycle. We will come back to this idea later but in the first instance only one parameter, the selection rate, is varied in order to keep the analysis simple. The selection factor $s$ is chosen so that the resulting kinetics (see Figure 2.3) reproduce the experimental ones (highest curve in Figure 1.6 where 0.4 splenic volume percent represent about 2000 GC B cellls). We therefore define $s$ by the following function.

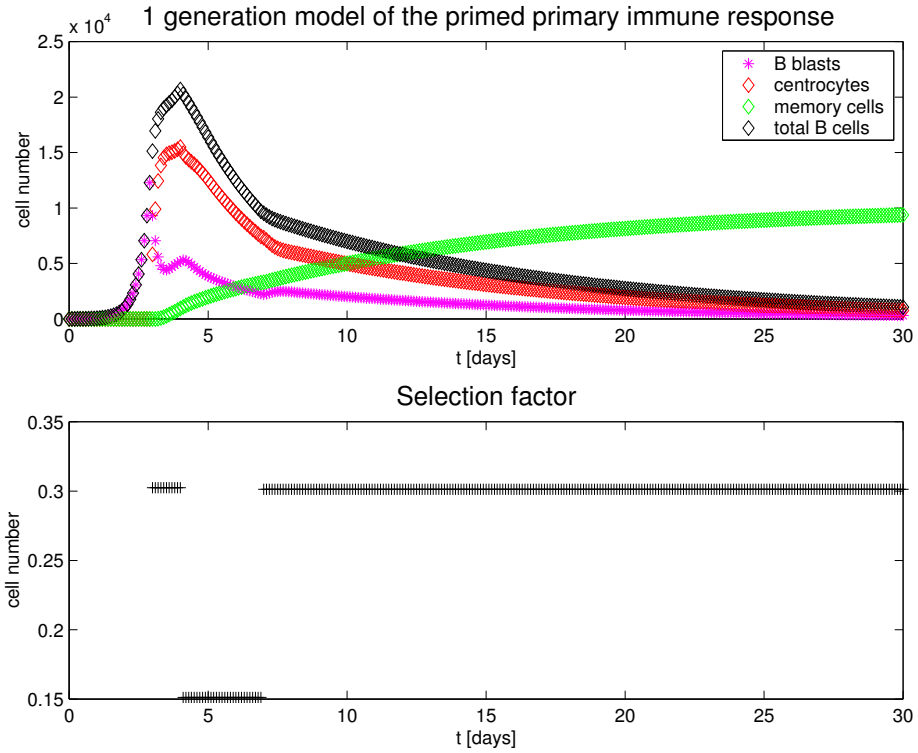



Figure 2.3: *top*: GC kinetics of the primed primary immune response in the minimal model are in good agreement with experimental observations. The total number of B cells attains the maximal value of 20000 at day 4 and declines after that [32]. The number of centrocytes exceeds the number of centroblasts from the time of their formation [36] and memory cell formation starts between day 3 and 4 [34]. *bottom*: The selection factor is varied as given in equations 2.19-2.21 in order to reproduce the GC kinetics.

$$m = 1 \quad \text{and} \quad s = s_c + 0.13 \quad \text{for} \quad 3 < t \leq 4 \tag{2.19}$$

$$m = 0.72 \quad \text{and} \quad s = s_c - 0.3 \quad \text{for} \quad 4 < t < 7 \tag{2.20}$$

$$m = 0.72 \quad \text{and} \quad s = s_c - 0.15 \quad \text{for } t \geq 7 \tag{2.21}$$

The resulting dynamics for $s$ can be seen in Figure 2.3 in the plot at the bottom. While the kinetics shown in the upper plot in Figure 2.3 do not vary much for $3 < t \leq 4$ (2.19) if the selection factor $s$ is varied over the whole

possible range [0, 1], the kinetics become critically dependent on the selection factor for $t > 4$. The first behaviour derives from the fact that differentiation of centroblasts to centrocytes starts at day 3 and selection has therefore a rather limited influence between day 3 and 4. The $s$ values after day 4 follow directly from the analytic stability analysis: between day 4 and 7, $s$ needs to be smaller than $s_c$ in order to capture the rapid shrinking of the cell population. Due to the onset of somatic hypermutation ($m = 0.72$) on day 4, $s_c$ raises from $s_c = 0.17$ to $s_c = 0.45$ which on the other hand relaxes the pressure on $s$ (2.20). After day 7, the cell population shrinks more slowly and $s$ needs to be chosen closer to $s_c$ in order to model this behaviour (2.21). The fact that $s$ is almost constant except for the short time span from day 4 to day 7, which will be shown to be the effect of $p_r$, shows that the selection proportion is independent of any changing external parameters. One could of course argue that even keeping the selection proportion to its initial value implies an increase in selection stringency since due to the affinity increase during the response the selection proportion could be expected to increase. In this case our result would imply that average affinity increase and reduction in antigen density would balance one another. Jacob and coworkers [21] however conclude from their analysis of somatic hypermutation, resulting mutation pattern and affinity increase that either somatic hypermutation terminates by day 16 of the response or the selection stringency strongly increases. The latter is not needed in order to reproduce the GC kinetics in this model and the first has been claimed by several authors before [5]. It is therefore interesting to investigate termination of somatic hypermutation at day 16. As will be shown later, termination of somatic hypermutation at day 16 and introduction of more stringent selection conditions enhances the efficiency of affinity maturation. At this stage it is however already clear from the previous stability analysis that selection stringency needs to be enhanced ($s$ to be reduced) if somatic hypermutation terminates since for increasing hypermutation survival rate $m$ ($m = 0.72$ for $t \leq 16$ and $m = 1$ for $t > 16$), the equilibrium value of $s$, $s_c$, decreases (see (2.11) and Figure 2.2) and in order to prevent the GC reaction from expanding again $s$ has to be chosen smaller than $s_c$. For the selection factor $s$, equation (2.21), which is valid for $t \geq 7$, needs now to be replaced by

$$s = s_c - 0.15 - 0.25\frac{t^n}{t^n + K^n} \qquad \text{with} \qquad K = 16 \qquad n = 20 \qquad (2.22)$$

which introduces the first non-linearity into the system of equations. $K = 16$ was chosen since the selection rate has to fall rapidly around day 16 when somatic hypermutation terminates and because of the needed velocity the Hill curve is chosen very steep with a Hill coefficient of $n = 20$. We do not need to worry about a biological justification for such a high Hill coefficient at this stage since this condition will be replaced in the next step by a more biological assumption and the condition is only meant to investigate the system for a sudden increase in selection stringency upon termination of somatic hypermutation. In nature these two processes may well be coupled such that enhancement of the selection pressure leads to less activation of centrocytes which then leads to a

termination of the mutation program for recycling centrocytes.

The result for this model can be seen in Figure 2.4. The small jump up at day 16 in the total B cell number is due to the fact that the selection factor is still too big in order to prevent expansion of the GC population. Given that the selection factor falls rapidly this has however no large effect.

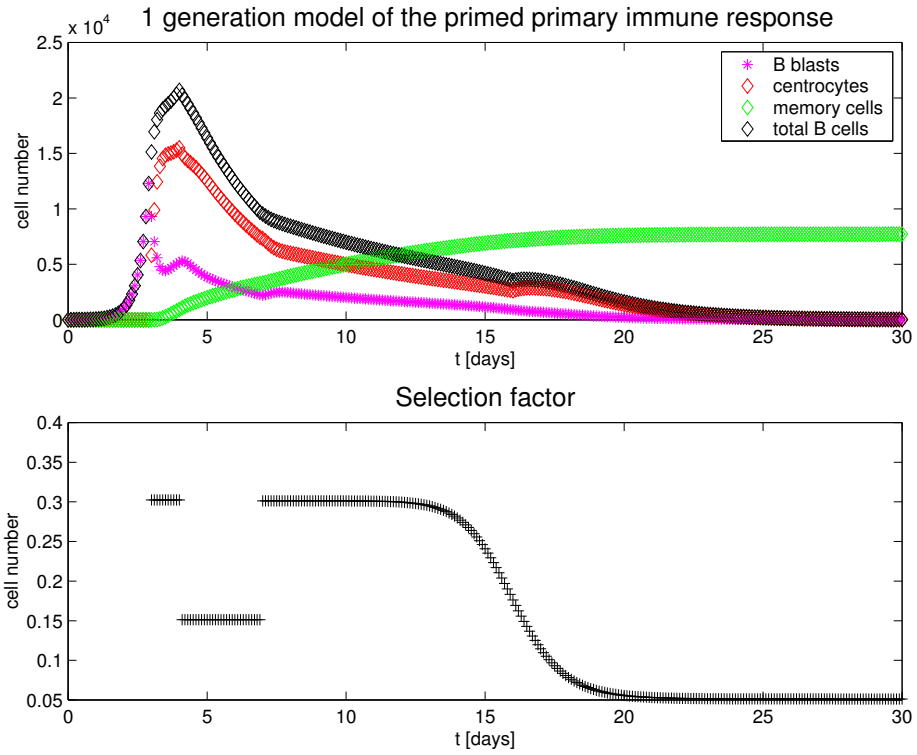



Figure 2.4: *top*: GC kinetics of the primed primary immune response in the minimal model if somatic hypermutation terminates at day 16. The kinetics are similar to those in Figure 2.3 and therefore in good agreement with experimental data. *bottom*: Due to the termination of somatic hypermutation at day 16, the selection factor has to decrease rapidly at day 16 for the GC reaction not to expand again. The selection factor is varied as given in equations 2.19, 2.20, 2.22 in order to reproduce the GC kinetics.

## 2.3 Affinity and Antigen Density Dependence

After having reproduced the GC kinetics with this simple model it is now necessary to find a model for the selection and the recycling rate that allows us to understand the underlying mechanism.

The selection rate has been suggested to be dependent on both B cell receptor (BCR) affinity for the antigen and antigen density in the GC. This may also be the case for the recycling probability since it has been shown that at least the decision about differentiation into memory or plasma cells critically

depends on the expression level of special molecules by T cells [3]. The expression can be triggered via interaction of T cells with B cells which present antigen on their surface [22]. The efficiency of this presentation seems to be dependent on antigen density and BCR affinity [4].

In order to keep the model simple at this stage, the affinities of the B cells are not modelled explicitly but data about the average affinity increase in the GC B cell population is used in order to model the selection factor. It is further assumed that the higher the average affinity of the GC B cell population the higher the consumption of antigen in the selection process.

The increase in the average affinity $\mathcal{A}$ has been measured as the increase in the proportion of high affinity clones in the whole GC B cell population [54]. Figure 1D in [54] shows that this average affinity increases linearly. Jacob and coworkers [21] have previously reported that the mutation frequency grows linearly until day 14 which they suggest to be due to a stepwise incorporation of single point mutations. This linear time dependency of affinity can be modelled by

$$\begin{aligned} \mathcal{A} &= 0.03 && \text{for} \quad t < 4 \\ \mathcal{A} &= 0.09t - 0.33 && \text{for} \quad 4 < t < 7 \\ \mathcal{A} &= 0.3 + 0.025(t-7) && \text{for} \quad 7 \leq t \leq 21 \end{aligned} \tag{2.23}$$

The experimental data is reproduced as dots in the bottom part of Figure 2.10 and Figure 2.11. The line for experimental data in the same plots is the result of equation 2.23. The reason for choosing the curve of the modelled affinity not to exactly follow the experimental data is that the data were obtained for a true primary immune response. We are however interested in a model of the primed primary immune response whose onset is earlier. The experimental data were therefore shifted by 3 days to an earlier start while the end points of the experimental data were kept.

The key hypothesis to be investigated in this dissertation is whether reduction in antigen density can drive affinity maturation. First experiments suggest that selection velocity and success are both dependent on receptor affinity and antigen density. Again we use the simplest model possible and assume that the antigen consumption factor is linearly dependent on the average affinity. This is sensible since the higher the proportion of very good binders the higher the average success of antigen extraction. The antigen consumption factor $u$ is therefore modelled by:

$$u = \xi \frac{\mathcal{A}}{\mathcal{A}_{max}} \qquad \text{with} \quad \mathcal{A}_{max} = 0.65 \qquad \xi = 3 \times 10^{-5} \tag{2.24}$$

The value of $\xi$ was chosen such that consumption of antigen leads to a halving of the initial antigen amount by the time the GC reaction finishes. To obtain this parameter experimentally is difficult and it is only known that the antigen density on follicular dendritic cells (FDCs) varies [34], that antigen can always be detected at the end of the GC reaction and that even after a decrease by 400 times in antigen density, antigen can still be detected [16]. The

consumption factor could therefore be much larger. This would however not change the general results of this model since only the assumption that antigen density reduces at all is critical. If the decrease is larger we only need to adapt other parameters which are dependent on antigen density in order for the model to produce similar results again.

For the total dynamics of the antigen we further assume that natural decay of antigen is more or less irrelevant since this natural decay is much slower than all active processes. The antigen dynamics are therefore only dependent on antigen extraction by centrocytes. It is sensible to assume that we have more extraction the more centrocytes interact with antigen and the more antigen is available since extraction may be facilitated by a higher local antigen density. Assuming further for simplicity a linear influence we are left with $-uC_sAg$ as the term modelling the extraction by selected centrocytes where $Ag$ is the antigen density. Given that centrocytes which do not manage to become selected may extract antigen as well we also need to take this proportion of non-selected centrocytes into account. This cell proportion is taken to be $k(C - C_s)$ and we therefore obtain the second term modelling the antigen dynamics to be $-uk(C - C_s)Ag$ and obtain in total for the antigen dynamics

$$\frac{dAg}{dt} = -(ukC + uC_s(1 - k))Ag \tag{2.25}$$

Since $k$ is again not known from experiments, we assume for simplicity that $k = 0$. This can however easily be changed once experimental data are available. Given however that until now also $u$ and the initial and final antigen density are unknown it is not sensible to explore $k$ at this stage. This model is anyway only meant to investigate as to whether in general antigen consumption can drive affinity maturation by increasing competition between the emerging B cell clones.

A drawback of using experimental data for the affinity increase instead of modelling the affinity maturation process explicitly is that the experimental data of the average affinity also include memory B cells which no longer extract antigen. When using them, we have to assume that memory cells emerge later in the response and do not have a strong influence at the beginning when extraction could influence the kinetics decisively. In a later model we will obtain the average affinity increase directly from the model and can therefore consider only the affinity increase in the centrocyte population.

Now that we have found a relation between the antigen consumption factor $u$ and affinity and have expressed the antigen dynamics in terms of antigen consumption, we can use this newly gained information and express the dynamics of the selection factor $s$ in terms of the antigen density which depends on the average affinity through $u$ (2.24). Selection stringency therefore increases by a decrease of antigen density due to antigen consumption. The antigen density threshold, below which the selection factor decreases according to a Hill function, is chosen such that the selection factor $s$ will be more or less constant until day 16 and decreases then as in the previous model:

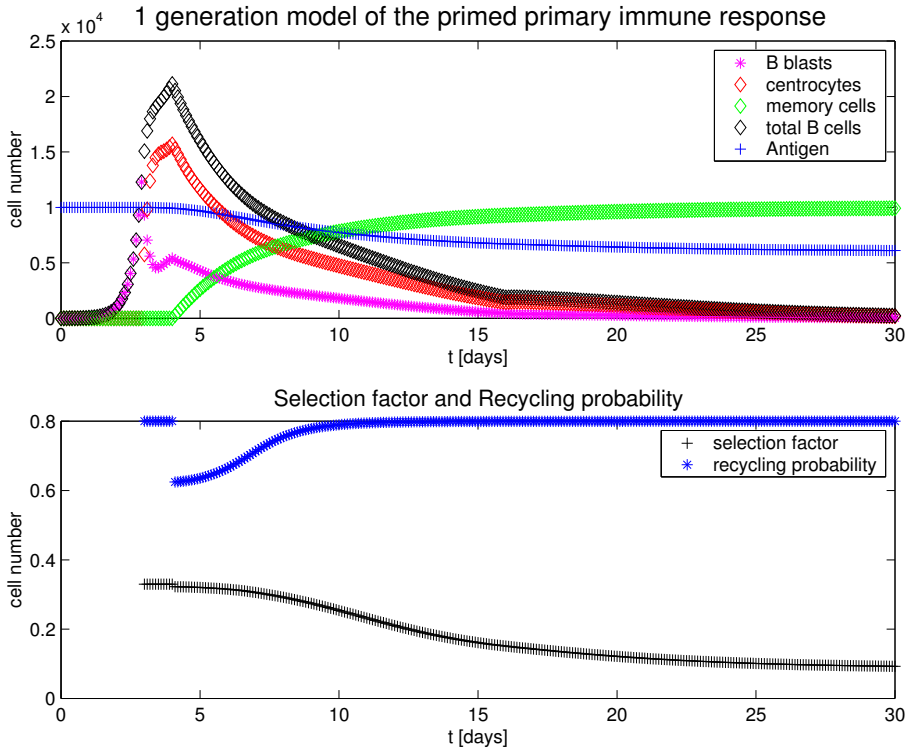



Figure 2.5: *top*: GC kinetics of the primed primary immune response where the selection factor and the recycling probability depend nonlinearly on antigen density and somatic hypermutation terminates on day 16 of the response. The total number of B cells attains the maximal value of about 20000 at day 4 and declines after that [32]. The number of centrocytes exceeds the number of centroblasts from the time of their formation [36] and memory cell formation starts between day 3 and 4 [34]. *Bottom*: The recycling probability drops after the onset of somatic hypermutation at day 4 but recovers quickly. The selection factor falls slowly due to a decrease in antigen availability.

$$s = s_c - h - f\frac{Ag_{min}^n}{Ag_{min}^n + Ag^n} \qquad \text{with} \qquad Ag_{min} = 5000 \qquad n = 10 \qquad (2.26)$$

Given that the selection factor is especially important in the time regime $t > 7$, the value of $s_c$ is calculated with the parameters of this time regime ($p_r = 0.8, m = 0.72$) and we have $s_c = 0.45$. $h$ needs to be introduced since the total B cell number decreases already between day 7 and 16 when antigen consumption is not very important. Therefore the selection factor needs already to be smaller than the equilibrium value of $s$ and in order to reproduce the experimental data it is chosen to be $h = 0.12$. The factor $f$ is needed in order to keep $s$ in the range [0, 1] and we chose $f = 0.3$ in order to reproduce the experimental data.

The Hill coefficient $n$ is a measure of the cooperativity of a process and a

Hill coefficient of 3 is already considered high [58]. The reason that the Hill coefficient had to be chosen that high in this model is that the selection rate needs to fall rapidly and we see from the graph that there is no alternative if we want to satisfy the kinetic data. We have therefore to assume that the fall of the selection factor is almost an on/off response where signalling is changed rapidly when the antigen density and affinity are below a certain threshold. If we understand the rapid decrease in the selection proportion as an effect of a signalling cascade with many amplification steps a high Hill coefficient, which would not be justifiable for single molecule-molecule interactions, can still be realistic.

The antigen density is still high between day 4 and 7, and the selection factor is therefore constant in that time, and the rapid decrease in cell number from day 4 to day 7 cannot be explained by the dynamics of such a selection factor. In reality the selection factor falls probably slightly in that time regime due to emerging clones of lower affinity. This effect is however probably negligible. A fair analysis would require one to analyse the process of affinity maturation by considering more affinity classes so that the extent of low affinity cell formation could be derived from that model. Such a model would also be interesting in other respects as discussed later but is too advanced at this stage since most experimental details are missing in order to build such a model. Neglecting an effect of the selection rate, it is however sensible to assume that the recycling probability decreases strongly soon after the onset of somatic hypermutation and leads to the reduction in the total GC B cell size. Two biological analyses [47, 54] support this assumption and find that early clones of increased affinity seem to preferentially leave the GCs and to differentiate to early plasma cells (AFCs) that produce antibodies as a first defense against the infection. After some time the recycling probability needs to rise again in order to guarantee high efficiency of the germinal center reaction and judging from kinetic data this time point seems to be $t = 7$. The recycling rate is therefore defined by

$$\begin{aligned} p_r &= 0.8 && \text{for} \quad 3 < t < 4 \\ p_r &= 0.6 + 0.2\frac{Ag_{min}^n}{Ag^n + Ag_{min}^n} && \text{for} \quad t \geq 4 \end{aligned} \tag{2.27}$$

with $Ag_{min} = 9000$, $n = 20$. The critical antigen density $Ag_{min}$ had to be chosen higher than for the selection rate since this switch happens earlier than that in the selection rate. The Hill coefficient $n$ had to be chosen even higher so that we more or less model an on/off response. This model gives an idea of the sort of compromise the system has to make between the two opposing interests of an early availability of reasonably good antibodies as a first line of defense against the infection and the final high output of high affinity antibodies. The resulting kinetics, which can be seen in Figure 2.5, are very similar to those in Figure 2.3, and compare therefore similarly well with the experimental results.

## 2.4 Modelling Affinity Maturation

We are finally left to deduce the affinity increase with model parameters. Given that in the experimental work which we referred to so far, only low, middle and high affinity clones are distinguished [54], it is sensible at this stage only to consider two species, namely high and low affinity clones. We keep track of the cell numbers of the low as well of the high affinity population by using vectors of size two where the first argument refers to the number of cells with low affinity of the given cell species and the second argument to the number of cells with high affinity. The two components are referred to by subscripts. Mutation is modelled by applying a mutation matrix $\mathbf{M}$ and $m$ is therefore replaced by $m\mathbf{M}$ in equation (2.3). Given that we assume somatic hypermutation only to take place between day 3.5 [34] and day 16 [5, 21], we have for $t \in [3.5, 16]$ $m = 0.72$ and $\mathbf{M}$ as given in equation (2.75). For all other times we have $m = 1$ and $\mathbf{M}$ being the unit matrix. The constants differ for high and low affinity clones and are therefore written as pairs of numbers where the first argument refers to the number of cells with low affinity of the given cell species and the second argument to the number of cells with high affinity. In explicit form the system which we are going to solve looks as follows

for $t \leq 3$

$$\frac{dB}{dt} = \rho B \tag{2.28}$$

for $t > 3$

$$\begin{aligned}
\frac{dB_1}{dt} &= p_r \rho C_{s1} - \rho B_1 && (2.29)\\
\frac{dB_2}{dt} &= p_r \rho C_{s2} - \rho B_2 && (2.30)\\
\frac{dC_1}{dt} &= 2\rho m(\mathbf{M}_{11} B_1 + \mathbf{M}_{12} B_2) - \mu_1 C_1 && (2.31)\\
\frac{dC_2}{dt} &= 2\rho m(\mathbf{M}_{21} B_1 + \mathbf{M}_{22} B_2) - \mu_2 C_2 && (2.32)\\
\frac{dC_{s1}}{dt} &= d s_1 C_1 - \rho C_{s1} && (2.33)\\
\frac{dC_{s2}}{dt} &= d s_2 C_2 - \rho C_{s2} && (2.34)\\
\frac{dM_1}{dt} &= (1 - p_{r1}) C_{s1} && (2.35)\\
\frac{dM_2}{dt} &= (1 - p_{r2}) C_{s2} && (2.36)
\end{aligned}$$

with $\mu_i = d s_i + \delta_c(1 - s_i)$.

The biological relevance of the different entries of $\mathbf{M}$ is as follows:

$\mathbf{M}_{11}$ - Proportion of low affinity cells that remain low affinity

$\mathbf{M}_{12}$ - Proportion of high affinity cells that become low affinity

$\mathbf{M}_{21}$ - Proportion of low affinity cells that become high affinity

$\mathbf{M}_{22}$ - Proportion of high affinity cells that remain high affinity

Given that the total number of cells does not change, the proportions need to sum to 1, so $\mathbf{M}_{11} + \mathbf{M}_{21} = 1$ and $\mathbf{M}_{12} + \mathbf{M}_{22} = 1$.

### 2.4.1 Analytical Analysis of the Model

The non-dimensionalisation can be carried out as given by equations (2.6) and given that the non-dimensionalised equations do not differ from the dimensional ones except for the tildes we drop the tildes and the new equations are therefore not given again. The non-dimensional form shows that all terms are of similar size and need to be incorporated in the model. As before, we solve the dimensional model in order to be able to directly compare our results with experimental data.

It is now sensible to determine the equilibrium points together with the subset of the parameter space for which they exist. Beside the trivial equilibrium point there also exists a non-trivial equilibrium point for $B, C, C_s$ given by

$$B_1^* = p_{r1} C_{s1}^* \qquad B_2^* = p_{r2} C_{s2}^* \tag{2.37}$$

$$C_1^* = \frac{2\rho m}{\mu_1}(\mathbf{M}_{11} B_1^* + \mathbf{M}_{12} B_2^*) \qquad C_2^* = \frac{2\rho m}{\mu_2}(\mathbf{M}_{21} B_1^* + \mathbf{M}_{22} B_2^*) \tag{2.38}$$

$$C_{s1}^* = \frac{d s_1}{\rho} C_1^* \qquad C_{s2}^* = \frac{d s_2}{\rho} C_2^* \tag{2.39}$$

if

$$\mathbf{M}_{12}\mathbf{M}_{21} = \left(\frac{1}{K_1} - \mathbf{M}_{11}\right)\left(\frac{1}{K_2} - \mathbf{M}_{22}\right) \tag{2.40}$$

where

$$K_1 = 2md\frac{p_{r1} s_1}{\mu_1} \qquad K_2 = 2md\frac{p_{r2} s_2}{\mu_2}. \tag{2.41}$$

The range of $K_1$ and $K_2$ is given by $K_1, K_2 \in [0, 2m]$ and we see that the upper limit depends on $m$ but cannot be larger than 2. As calculated by others [51], about 26 percent of mutations lead to an affinity change and improving and worsening mutations therefore have to add up to this proportion which gives the condition $\mathbf{M}_{12} + \mathbf{M}_{21} = 2 \times 0.26 = 0.52$. The factor 2 comes in since the sum over all entries of $\mathbf{M}$ is 2. After substitution into 2.40 and solving of 2.40 for $\mathbf{M}_{11}$ we further obtain

$$\mathbf{M}_{11} = \frac{12K_1K_2 + 25 - 37K_2}{25(K_1 - K_2)} \tag{2.42}$$

In general $\mathbf{M}_{11}$ can only take values out of [0, 1] and since at least 74 percent of the mutations do not lead to an affinity change $\mathbf{M}_{11} \in [0.74\,, 1]$. From all data available from the literature the parameter space for $\mathbf{M}_{11}$ is probably even more restricted with $\mathbf{M}_{11} > 0.9$. Figure 2.6 shows the plots of four solutions of (2.42) for different values of $\mathbf{M}_{11}$ in the $K_1 - K_2$-space. We see from there

that the shape of the resulting curves completely differs for $\mathbf{M}_{11} = 0$ and $(\mathbf{M}_{11} = 0.74, \mathbf{M}_{11} = 0.99$. We can further rearrange (2.42) and obtain

$$K_2 = 25\frac{K_1\mathbf{M}_{11} - 1}{-37 + 12K_1 + 25\mathbf{M}_1 1}. \tag{2.43}$$

From (2.43) we see that that for $\mathbf{M}_{11} = 1$ we have $K_2 = \frac{25}{12}$ for all $K_1$ which gives the third possible shape - a horizontal line. Given that this $K_2$ does not lie in the range of $K_2$, we can already conclude that for $\mathbf{M}_{11} = 1$, no non-trivial steady state can be attained.

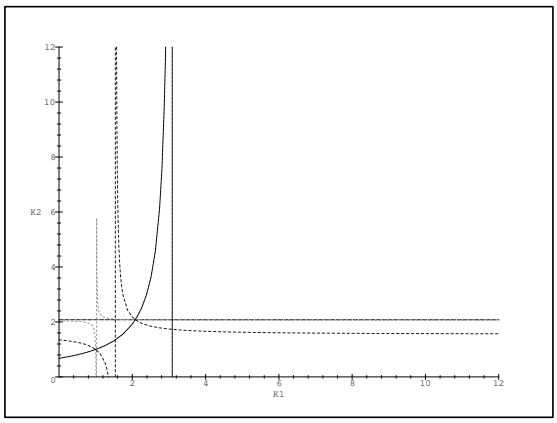



Figure 2.6: Parameter space for which the system 2.29-2.34 attains a non-trivial equilibrium state. The horizontal line is obtained for $\mathbf{M}_{11} = 1$. The curve with the asymptote furthest right is obtained for $\mathbf{M}_{11} = 0$, the curve with the pole in the middle was obtained for $\mathbf{M}_{11} = 0.74$ and the curve with the pole the furthest left was obtained for $\mathbf{M}_{11} = 0.99$.

From Figure 2.6 we can deduce the region in $K_1 - K_2$ space for which the system can attain a non-trivial equilibrium state in dependence of the range of $\mathbf{M}_{11}$. If we allow $0 < \mathbf{M}_{11} < 1$ we see that the parameter space is limited by the three curves given by $\mathbf{M}_{11} = 1$, $\mathbf{M}_{11} = 0.\bar{9}$ and $\mathbf{M}_{11} = 0$. If we further restrict the range of $\mathbf{M}_{11}$ to $l < \mathbf{M}_{11} < 1$ the curve for $\mathbf{M}_{11} = l$ is the third limiting curve instead of that for $\mathbf{M}_{11} = 0$ and we see that the larger $l$ the smaller the region for which a non-trivial equilibrium state can be attained. If we assume that $\mathbf{M}_{11}$ is of the order 0.95 then the system is robust against small changes in $\mathbf{M}_{11}$ since the region where the non-trivial equilibrium point can be attained is changed only slightly. We further see that at least one $K_i$ needs to be small in order to attain a non-trivial equilibrium state. $K_i$ can be made small by either choosing a small selection rate $s_i$ or a small recycling rate $p_{ri}$.

It would now be interesting to know about the stability of the equilibrium points in the different regions. The characteristic polynomial is given by

$$\lambda^6 + a_5\lambda^5 + a_4\lambda^4 + a_3\lambda^3 + a_2\lambda^2 + a_1\lambda + a_0 = 0 \tag{2.44}$$

where

$$
\begin{aligned}
a_5 &= \mu_2 + \mu_1 + 4\rho \qquad (2.45)\\
a_4 &= 4\rho(\mu_1 + \mu_2) + \mu_1\mu_2 + 6\rho^2 \\
a_3 &= 4\rho^3 - 1.48\rho^2 K_2\mu_2 + 6\rho^2(\mu_1 + \mu_2) + 4\rho\mu_1\mu_2 + \rho^2\mathbf{M}_{11}(K_2\mu_2 - K_1\mu_1) \\
a_2 &= \rho^4 + \rho^3(4(\mu_1 + \mu_2) + 2(\mathbf{M}_{11}(K_2\mu_2 - K_1\mu_1) - 1.48K_2\mu_2)) \\
&+ \rho^2(\mu_1\mu_2(6 - 1.48K_2 + \mathbf{M}_{11}(K_2 - K_1)) \\
a_1 &= \rho^4(\mu_1(1 - \mathbf{M}_{11}K_1) + \mu_2(1 + \mathbf{M}_{11}K_2 - 1.48K_2)) \\
&+ \rho^3\mu_2\mu_1(4 - 2.96K_2 + 2\mathbf{M}_{11}(K_2 - K_1)) \\
a_0 &= \rho^4\mu_1\mu_2(1 - K_1\mathbf{M}_{11} - 1.48K_2 + 0.48K_1K_2 + K_2\mathbf{M}_{11})
\end{aligned}
$$

Given that all parameters are greater than or equal to zero, we have for all possible parameters $a_4, a_5 \geq 0$. Furthermore given that $K_1, K_2 \in [0,\, 2m]$ we also have $a_2, a_3 > 0$ while $a_0, a_1$ can take either sign. The characteristic polynomial can be factorised in terms of the eigenvalues with the general formula being

$$(\lambda - \lambda_1)(\lambda - \lambda_2)(\lambda - \lambda_3)(\lambda - \lambda_4)(\lambda - \lambda_5)(\lambda - \lambda_6) = 0. \qquad (2.46)$$

Comparing this general formula with 2.44 and 2.45 we obtain

$$
\begin{aligned}
a_0 &= \lambda_1\lambda_2\lambda_3\lambda_4\lambda_5\lambda_6 && (2.47)\\
a_1 &= -\sum_{i<j<k<l<m} \lambda_i\lambda_j\lambda_k\lambda_l\lambda_m && (2.48)\\
a_2 &= \sum_{i<j<k<l} \lambda_i\lambda_j\lambda_k\lambda_l && (2.49)\\
a_3 &= -\sum_{i<j<k} \lambda_i\lambda_j\lambda_k && (2.50)\\
a_4 &= \sum_{i<j} \lambda_i\lambda_j > 0 && (2.51)\\
a_5 &= -\sum_{i} \lambda_i > 0 && (2.52)
\end{aligned}
$$

where the indices range from 1 to 6.

Let us start with considering the case $a_0 = 0$ which requires $\mathbf{M}_{11}$ to take the value given by equation (2.42) and we have already determined the possible parameter space for $a_0 = 0$ which is shown on the LHS of Figure 2.7 and 2.8. $\lambda_1 = 0$ is one possible eigenvalue and the system can attain a non-zero equilibrium as discussed above which is unstable for most possible parameters as we will derive now. Let us first consider the case when $a_1 < 0$. If $a_0 = 0$ w.l.o.g $\lambda_1 = 0$ and therefore $a_1 = -\lambda_2\lambda_3\lambda_4\lambda_5\lambda_6$. We see that $a_1 < 0$ is only possible if at least one eigenvalue is larger than zero. The eigenstate is therefore unstable and the region in the parameter space to which this applies can be seen in Figure 2.7 and 2.8 for two different ranges of $\mathbf{M}_{11}$.

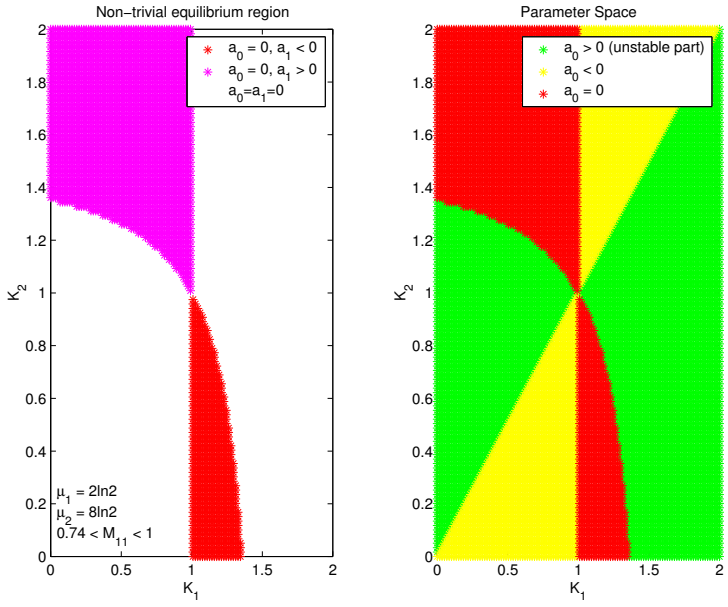



Figure 2.7: (*LHS*) The parameter space for which the system 2.29-2.34 attains a non-trivial equilibrium state is shown in colour ($0.74 < \mathbf{M}_{11} < 1$). (*RHS*) The regions in the parameter space for which the steady state is unstable is shown in color. For this choice of $s_1, s_2$ ($\mu_1 = 2\ln 2, \mu_2 = 8\ln 2$) no region can be found where the steady state is stable.

In the next case $a_1 > 0$ we require at least w.l.o.g $\lambda_2 < 0$. We need again to distinguish two cases. For $a_2 \leq 0$ - which can however not be attained in our model - we have as a condition on $\lambda_2$

$$\lambda_2 \geq -\frac{\lambda_3\lambda_4\lambda_5\lambda_6}{\sum_{i<j<k}(\lambda_i\lambda_j\lambda_k)} \tag{2.53}$$

where the indices range from 3 to 6. This condition leads to a contradiction if we assume eigenvalues for all $\lambda_i < 0$ and thus we require at least one eigenvalue to be greater zero and therefore the eigenstate is unstable. For $a_2 > 0$ the condition on $\lambda_2$ can be satisfied also if we assume all $\lambda_i < 0$. We must therefore check $a_3$. If $a_3 \leq 0$ - what is again not possible to be attained in this parameter space - we have $\sum_{i,j,k=1}^{6} \lambda_i\lambda_j\lambda_k > 0$ which can only be satisfied if at least one eigenvalues is larger than zero. If $a_3 > 0$ we have $a_1, a_2, a_3, a_4, a_5 > 0$ and this gives us the conditions $\lambda_2 < 0$ (2.48), $\lambda_2 < -(\lambda_3 + \lambda_4 + \lambda_5 + \lambda_6)$ (2.52) and $\sum_{i<j} \lambda_i\lambda_j > 0$ (2.51). Substituting the inequality for $\lambda_2$ into the last inequality we obtain $(\sum_i \lambda_i)^2 < \sum_{i<j<k} \lambda_i\lambda_j\lambda_k$ where the indices range from 3 to 6. We see that this inequality cannot be satisfied if all $\lambda_i$ are of the same sign and therefore not all eigenvalues can be negative and this eigenstate is also unstable.

We finally need to investigate the case $a_0 = 0, a_1 = 0$. We now have w.l.o.g. $\lambda_1 = 0 = \lambda_2$ and therefore $a_2 = \lambda_3\lambda_4\lambda_5\lambda_6$. If $a_2 < 0$ we need again at least one $\lambda_i$ to be larger than zero and this eigenstate is therefore unstable. For $a_2 = 0$, we have w.l.o.g. $\lambda_3 = 0$ and therefore $a_3 = -\lambda_4\lambda_5\lambda_6$. If $a_3 < 0$ we

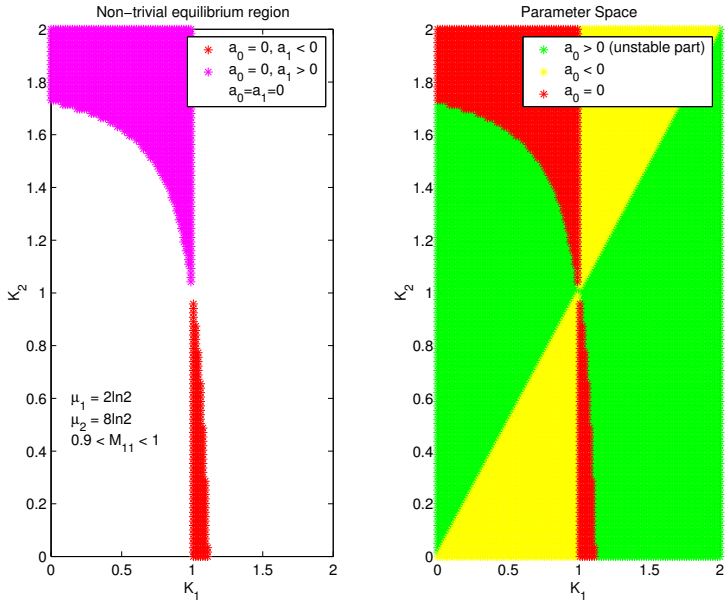



Figure 2.8: (*LHS*) The parameter space for which the system 2.29-2.34 attains a non-trivial equilibrium state is shown in colour ($0.9 < \mathbf{M}_{11} < 1$). (*RHS*) The regions in the parameter space for which the steady state is unstable is shown in color. For this choice of $s_1, s_2$ ($\mu_1 = 2\ln 2, \mu_2 = 8\ln 2$) no region can be found where the steady state is stable.

need again at least one eigenvalue to be larger than zero and the eigenstate is unstable. For $a_3 = 0$ we have w.l.o.g $\lambda_4 = 0$ and given that $a_4 = \lambda_5\lambda_6 > 0$ and $a_5 = \lambda_5 + \lambda_6 < 0$ all eigenvalues are less or equal zero and we have therefore found a stable, non-trivial equilibrium state. If $a_3 > 0$ we either have $\lambda_4 < 0$ and $\lambda_5, \lambda_6 > 0$ (case 1) or $\lambda_4, \lambda_5, \lambda_6 < 0$ (case 2). If we assume case 1, we have $a_4 = \lambda_4(\lambda_5 + \lambda_6) + \lambda_5\lambda_6 > 0$ which implies $\lambda_5\lambda_6 > -\lambda_4(\lambda_5 + \lambda_6)$. From $a_5 = \lambda_4 + \lambda_5 + \lambda_6 < 0$ we further have $-\lambda_4 > \lambda_5 + \lambda_6$ which gives together the condition $\lambda_5\lambda_6 > (\lambda_5 + \lambda_6)^2$ which gives a contradiction. We therefore have case 2 and all eigenvalues are less or equal zero. Non-trivial equilibrium states are therefore stably attained if $a_0 = a_1 = a_2 = 0$ and $a_3 \geq 0$. We however know that within the possible parameter space $a_2 > 0$, a case which we still need to consider. We still have $\lambda_1 = \lambda_2 = 0$ and in order to satisfy $a_4, a_5 > 0$ we also need $\lambda_3, \lambda_4 < 0$ and $\lambda_5, \lambda_6$ to be of one sign. Let us first assume that the latter eigenvalues are both positive. From $a_4 > 0$ we further have

$$\lambda_3(\lambda_4 + \lambda_5 + \lambda_6) + \lambda_4(\lambda_5 + \lambda_6) + \lambda_5\lambda_6 > 0. \tag{2.54}$$

From $a_5 > 0$ we however have $\lambda_3 < -(\lambda_4 + \lambda_5 + \lambda_6)$ which replaced in (2.54) gives a contradiction if $\lambda_5, \lambda_6 > 0$ since for $\lambda_5, \lambda_6 > 0$ we have $(\lambda_4 + \lambda_5 + \lambda_6)^2 > \lambda_4(\lambda_5 + \lambda_6) + \lambda_5\lambda_6$. If $\lambda_5, \lambda_6 < 0$ we can satisfy all conditions and we therefore have found a stable non-trivial steady state where all eigenvalues are equal to or less than zero. It is attained if $K_1, K_2$ satisfy the following condition

$$K_1^2 - \frac{K_2(37\rho(\mu_1-\mu_2)+12K_2\mu_2(2\mu_1+\rho))+25\mu_2(\rho+2\mu_1)}{12\mu_1K_2(\rho+2\mu_2)}K_1 - \frac{25}{12} = 0 \tag{2.55}$$

which is only satisfied for very few parameter choices, especially if $K_1 = K_2$ and $\mu_1 = \mu_2$ which implies $p_{r1} = p_{r2}$.

We are left to investigate the trivial equilibrium point and we will start to investigate the system for the case $a_0 < 0$. Given that $a_0 = \prod_{i=1}^{6}\lambda_i$, $a_0 < 0$ cannot be satisfied if for all eigenvalues $\lambda_i \leq 0$ and this steady state is therefore also unstable. The parameter space affected can be seen on the RHS of Figure 2.7 and 2.8.

For $a_0 > 0$ always an even number of eigenvalues needs to be negative and we see that $\lambda_i < 0$ for all $i$ is again impossible if $a_1 \leq 0$. For $a_1 > 0$ w.l.o.g. $\lambda_1, \lambda_2 < 0$ and we again need to distinguish two cases. For $a_2 \leq 0$ - a case which is again not contained in the possible parameter space - the same argument as before (2.53) applies and the eigenvalues cannot all be negative since we have the condition

$$0 > \lambda_1 + \lambda_2 > -\frac{(\lambda_1\lambda_2+\lambda_5\lambda_6)(\lambda_3\lambda_4)}{\sum_{i<j<k}\lambda_i\lambda_j\lambda_k} \tag{2.56}$$

where the indices range from 3 to 6 and this gives a contradiction if we assume all eigenvalues to be negative. For $a_1, a_2 > 0$ we need to investigate $a_3$ and find as before that for $a_3 \leq 0$ it is impossible for all eigenvalues to be smaller or equal zero. For $a_0, a_1, a_2, a_3, a_4, a_5 > 0$ we require $\lambda_1, \lambda_2 < 0$ (2.47, 2.48) and could have all $\lambda_i$ negative. In order to have $a_0 > 0$ we need

$$K_2 > 25\frac{K_1\mathbf{M}_{11}-1}{-37+12K_1+25\mathbf{M}_{11}} \quad \text{if} \quad K_1 > \frac{1.48-\mathbf{M}_{11}}{0.48} \tag{2.57}$$

$$K_2 < 25\frac{K_1\mathbf{M}_{11}-1}{-37+12K_1+25\mathbf{M}_{11}} \quad \text{if} \quad K_1 < \frac{1.48-\mathbf{M}_{11}}{0.48} \tag{2.58}$$

There can only exist a $K_2$ satisfying (2.58) if $K_1 < \frac{1}{\mathbf{M}_{11}}$. The $K_1, K_2$ satisfying (2.57) are not contained in the possible range of $K_1, K_2$. $a_0 > 0$ can therefore only be attained for small $K_1, K_2$. In order to have $a_1 > 0$ $K_1$ and $K_2$ need to satisfy the following inequalities

$$K_2 < \frac{\rho^4\left(\frac{\mu_1}{\mu_2}(1-\mathbf{M}_{11}K_1)+1\right)-\rho^3\mu_1(4-2\mathbf{M}_{11}K_1)}{\rho^4(\mathbf{M}_{11}-1.48)+\rho^3\mu_1(2\mathbf{M}_{11}-2.96)} \tag{2.59}$$

$$K_1 < \frac{4-\rho(\frac{1}{\mu_2}+\frac{1}{\mu_1})}{\mathbf{M}_{11}(2-\frac{\rho}{\mu_2})} \tag{2.60}$$

We see that the existence of a possibly stable trivial equilibrium point strongly depends on the parameters $s, p_r$ chosen. To prove that this eigenstate is indeed stable would be tedious and is omitted. The numerical solution given later will show that there exist a parameter space for which the solution

tends to zero. In line with the analysis above this parameter space is however very small and the choice of $s, p_r$ is very much restricted such that $K_1, K_2$ are indeed small. This will help us to draw conclusions about the parameter space used by nature.

We have further shown that the wider the range of $\mathbf{M}$ the larger the possible range for $K_1$, $K_2$, for which a non-trivial equilibrium point can be attained. In nature the proportion of beneficial mutations will vary since the process is random and we probably have $\mathbf{M}_{11} \in [0.9, 1)$. The model shows that the germinal center reaction is robust against such fluctuations since the band of non-trivial equilibrium points created by such fluctuations in the $K_1 - K_2$-space is thin and the behaviour of the system can be expected not to vary much upon such fluctuations.

Given that the main question of this dissertation concerns the process of affinity maturation it is now of interest to determine the restrictions on the parameters such that we indeed obtain affinity maturation.

We can analyse the efficiency of affinity maturation best by defining

$$\dot{T}_1 = \dot{B}_1 + \dot{C}_1 + \dot{C_{s1}} + \dot{M}_1 \tag{2.61}$$
$$\dot{T}_2 = \dot{B}_2 + \dot{C}_2 + \dot{C_{s2}} + \dot{M}_2. \tag{2.62}$$

so that $T_1$ represents the rate of increase of low affinity cells and $T_2$ represents the increase of high affinity cells. We therefore have a net affinity increase if $\dot{T}_1 < \dot{T}_2$. This inequality is satisfied if

$$C_{s1} < C_{s2}\frac{1-p_{r2}}{1-p_{r1}} \tag{2.63}$$
$$C_1 > C_2\frac{1-s_2}{1-s_1} \tag{2.64}$$
$$\frac{B_1}{B_2} < \frac{-1+2m(\mathbf{M}_{22}-\mathbf{M}_{12})}{-1+2m(\mathbf{M}_{11}-\mathbf{M}_{21})} = \frac{-1+2m(2.48-2\mathbf{M}_{11})}{-1+2m(2\mathbf{M}_{11}-1)} \tag{2.65}$$

From inequality (2.63) we see that affinity maturation is favored if high affinity clones recycle with less probability than low affinity clones ($p_{r2} < p_{r1}$). We will come back to this idea soon when we analyse the mutation matrix in more detail. Inequality (2.64) gives the intuitively understandable insight that it is most beneficial for affinity maturation if low affinity clones get less selected than high affinity clones ($s_1 < s_2$).

Given that the LHS of inequality (2.65) cannot become smaller than 0, we need $\mathbf{M}_{11} < 0.89$ in order to be able to obtain an affinity increase. The RHS goes to zero when $\mathbf{M}_{11}$ approaches its upper limit. The limit given above will be larger in total since the three terms have been analysed independently so far. Bringing them together should allow to use slightly larger values for $\mathbf{M}_{11}$. It is however unclear if this then allows affinity maturation to happen for realistic values of $\mathbf{M}_{11}$ ($\mathbf{M}_{11} > 0.95$) and it is therefore worth investigating whether the

introduction of more centroblast generations helps to widen the possible range of $\mathbf{M}_{11}$.

Before following this idea it is however worth to investigate the effect of a termination of somatic hypermutation on affinity maturation. In case of a termination of somatic hypermutation $\mathbf{M}$ becomes the unit matrix and in (2.65) we have $\frac{B_1}{B_2} < 1$ . This condition can be easily satisfied by introducing more stringent selection conditions which reduce the number of $B_1$ cells. The $B_2$ cells get further multiplied and they soon dominate the germinal center reaction. From this it is obvious that it is beneficial to terminate somatic hypermutation before the germinal center reaction finishes in order to be able to further expand the high affinity clones without the hazard to lose them because of worsening mutations. Equally obviously somatic hypermutation must not terminate before high affinity clones have evolved. Given that high affinity clones have about 8 mutations and assuming that one way through the cycle takes about a day we need about 8 days of somatic hypermutation. Given that not every mutation is beneficial the 12 days allowed for somatic hypermutation to take place seem to be reasonable.

**Extension to several centroblast generations**

The general model considering $n$ divisions before conversion is given by

for $t \leq 3$

$$\frac{dB}{dt} = \rho B \tag{2.66}$$

for $t > 3$

$$\begin{aligned}
\frac{dB^0}{dt} &= p_r \rho C_s - \rho B^0 && (2.67)\\
\frac{dB^j}{dt} &= 2\eta\rho B^{j-1} - \rho B^j \qquad \text{for j = 1, ..., n} && (2.68)\\
\frac{dC}{dt} &= 2\rho m \mathbf{M} B^n - \mu C \qquad \text{with} \quad \mu = ds + \delta_c(1-s) && (2.69)\\
\frac{dC_s}{dt} &= dsC - \rho C_s && (2.70)\\
\frac{dM}{dt} &= (1-p_r)C_s && (2.71)
\end{aligned}$$

where the upper B indices indicate the centroblast generation since we reserve the lower B indices as the vector indices distinguishing low and high affinity cell populations. In this model, we have assumed that somatic hypermutation always acts on the last generation while $\eta$ can either take the value $m$ (somatic hypermutation takes place) or 1 (no somatic hypermutation). We will further assume that somatic hypermutation starts on day 3.5 [34] and stops on day 16 [5, 21]. For $t \in [3.5, 16]$ we therefore have $m = 0.72$ and $\mathbf{M}$ as given in (2.75) while for all other times $m = 1$ and $\mathbf{M}$ being the unit matrix.

Comparison of (2.66-2.70) with the one generation model (2.28-2.36) shows that we need to modify equation (2.65) to

$$\frac{\sum_i B_1^i}{\sum_j B_2^j} < \frac{-1 + 2m(\mathbf{M}_{22} - \mathbf{M}_{12})}{-1 + 2m(\mathbf{M}_{11} - \mathbf{M}_{21})} = \frac{-1 + 2m(2.48 - 2\mathbf{M}_{11})}{-1 + 2m(2\mathbf{M}_{11} - 1)} \tag{2.72}$$

for $i, j = 1, .., n$. The effect of several centroblast generations is that the LHS of 2.72 goes to zero if the matrix leads to a net shift of cells from low affinity (bin 1) to high affinity (bin 2). We will investigate in the following under which condition the matrix acts this way. If the LHS can be made very small, we can use much higher values for $\mathbf{M}_{11}$ since, as stated before, for $\mathbf{M}_{11}$ tending against its upper limit the RHS of (2.72) falls to zero. This would then allow the system to achieve affinity maturation with a small proportion of beneficial mutations.

Obviously, there is a net shift of the mutation matrix $\mathbf{M}$ to high affinity if the population of low affinity centroblasts is larger than the population of high affinity centroblasts by more than $\frac{\mathbf{M}_{12}}{\mathbf{M}_{21}}$. Introduction of several centroblast generations leads to a multiple application of the matrix $\mathbf{M}$ on the centroblast vector. This however does not change the condition given above as can easy be seen from the explicit calculation of $\mathbf{M}^2$:

$$\mathbf{M}^2 = \begin{pmatrix} \mathbf{M}_{11}^2 + \mathbf{M}_{12}\mathbf{M}_{21} & \mathbf{M}_{12}(\mathbf{M}_{11} + \mathbf{M}_{22}) \\ \mathbf{M}_{21}(\mathbf{M}_{11} + \mathbf{M}_{22}) & \mathbf{M}_{22}^2 + \mathbf{M}_{12}\mathbf{M}_{21} \end{pmatrix}$$

From this we see that the ratio between worsening and improving mutations $\frac{\mathbf{M}_{12}}{\mathbf{M}_{21}}$ is constant if the matrix is multiplied by itself. This implies that if the population of low affinity clones is larger than the population of high affinity clones by more than $\frac{\mathbf{M}_{12}}{\mathbf{M}_{21}}$, then we have a net increase in the high affinity population upon application of this matrix. If the proportion of high affinity clones is however higher, then this matrix reduces this proportion. In the limit we can therefore only attain this ratio by consecutive application of this matrix. This is illustrated in Figure 2.9, and we further see that the increase in the proportion of high affinity clones per application of the mutation matrix is highest when the proportion of high affinity clones is smallest and if $n$, the number of times the mutation matrix has already been applied, is small.

**Conclusion from the above analysis** Nature would work the most efficient if somatic hypermutation worked on a small number of centroblast generations ($n < 10$) and if the initial and recycling centroblast population had a very small proportion of high affinity clones. This has indeed been shown for the initial centroblast population which was found to consist of 3 percent high affinity clones [54]. In order to keep the proportion of high affinity centroblasts low, the recycling probability for high affinity centroblasts needs to be much smaller than for low affinity clones, which we already deduced from inequality (2.63). This is a new insight about the importance of this parameter for affinity maturation and raises the question of how high affinity clones could be generated from low affinity clones if clones of improved affinity hardly recycle and high affinity clones cannot be generated from low affinity clones in one round. This conceptual problem however only arises because of the simplicity of our model

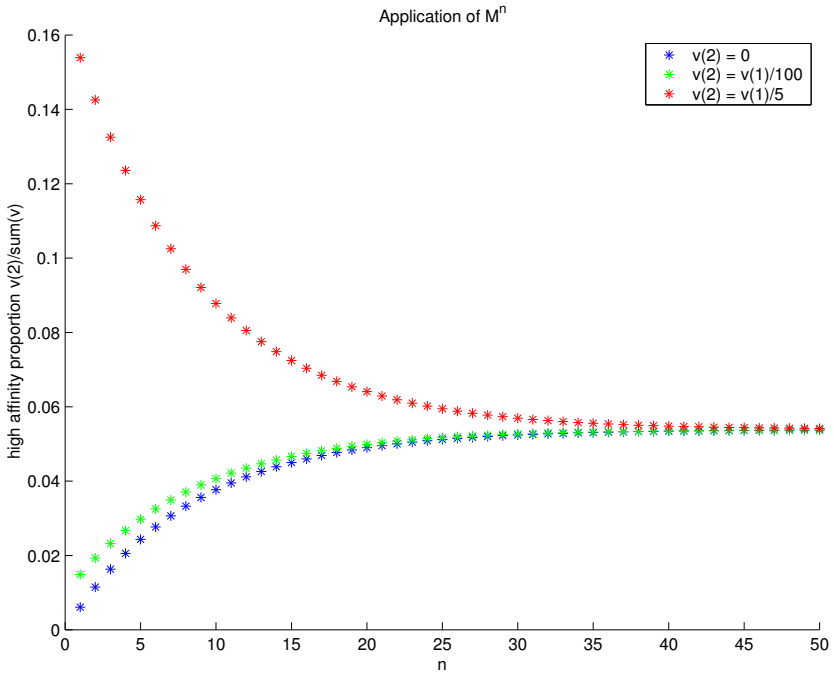



Figure 2.9: Consecutive application of the mutation matrix **M**: The proportion of high affinity cells $\frac{v(2)}{\sum_i v(i)}$ is plotted against the number of times $n$ the mutation matrix **M** was applied. Dependent on the initial proportion of high affinity cells v(2) given in the legend in the inset, the shift per application of the mutation matrix is of different size.

which only considers two different affinities so that a shift from low to high affinity *is* possible in this model. At this stage it is therefore beneficial to consider an advanced model with ten bins. The number 10 is sensible since experimentalists find that high affinity B cells differ in their antibody coding genes by about 8 mutations from germline genes. Assuming that every one of these mutations changes the affinity of the antibody it is sensible to use 8 bins for improved affinity, one for the starting affinity and one for reduced/no affinity. While cells below the starting bin undergo apoptosis when trying to interact with antigen, cells much above the starting bin are selected into the plasma cell pool or into the memory cell pool. The cells in the bins in between mostly recycle, some of them may also enter the memory pool. The threshold above which cells definitely leave the GC as memory or plasma cells can be assumed to increase during the germinal center reaction. This is in agreement with the analysis of the two bin model: once most of the population has gone say from bin 2 to bin 3, bin 3 acts as the low affinity bin in our model and is assigned the recycling probability for low affinity cells instead of that of high affinity cells. Therefore the recycling probability changes with time for the different bins and finally even clones of relatively high affinity recycle and are expanded. In this model, high affinity clones preferentially leave the GC reaction at the

beginning. This is also intuitively understandable since at the beginning a high affinity clone, which was generated by chance, would be lost with high probability once it goes through mutation again since most of the mutations worsen the antibody. Additionally, the body needs early high affinity clones in order to hold the invader in check. Early immigration is therefore beneficial for the efficiency of affinity maturation and for the early immune response. Once however many clones have reached the next affinity bin and mutation acts on a wide platform, mutations are beneficial since they will not lead to a complete elimination of the already gained beneficial mutations but there is a good chance that affinity is even enhanced. The loss of early high affinity clones has been described earlier [47] and it was suggested that this is due to a stochasticity in selection. It has been remarked [33] that many biological reactions which are suggested to be based on stochasticity are simply not yet understood and in this case here this model suggests that the loss of early high affinity clones is based on a deterministic process which selects high affinity clones to preferentially leave the GC reaction at the beginning. The activation to leave the GC reaction is probably dependent on both receptor-antigen affinity and antigen density. Given that the antigen density decreases due to antigen consumption by centrocytes, the recycling rate increases during the GC reaction which allows also the expansion of higher affinity clones.

In total we conclude that understanding the mechanism of recycling may be key to understand affinity maturation. It is sensible to assume that recycling regulates affinity maturation since selection should only have a protective function against the emergence of self-reactive clones. It is not sensible to eliminate even weak binders which can be used as plasma cells as a first defense against the invader. From this model, the regulation of which clones stay in the germinal center reaction and which enter the plasma cell pool or the memory cell pool respectively is the important step which drives affinity maturation. Furthermore the model strongly supports the concept of an early termination of somatic hypermutation at about day 16 since without such a termination affinity maturation would be less efficient and a need for more stringent selection conditions could not easily be reasoned. Termination of somatic hypermutation allows the expansion of the high affinity B cell population without the hazard of worsening mutations.

**Reconsidering the hypermutation survival rate in the several generation model:** We found previously that we cannot reproduce the GC kinetics of the primed primary immune response (Figure 1.6) if $m \leq 0.5$ which leads to $\mu < \mu_c$ which in turn leads to an early termination of the GC reaction. Several experiments suggest that centroblast may run through at least two cell divisions before differentiation into centrocytes [31, 32, 34]. It is therefore interesting to investigate the impact of several centroblast generations on the parameter restrictions mentioned above. If we again calculate $s_c$, we obtain as condition on $p_r$ in analogy to (2.13)

$$m\eta^{n-1} \geq \frac{1}{2^n p_r}. \tag{2.73}$$

Dependent on how many $\eta$s actually take the value $m$ and how many generations we consider we can now tolerate very low values for $m$. As an example, if $n = 10$ as considered in the model of Kesmir and de Boer [26] and $\eta = 1$ for all generations than we can satisfy (2.73) for $p_r$ close to 1 already for $m \geq 10^{-3}$. We can rewrite (2.73) and obtain

$$p_r \geq \frac{1}{2^n m \eta^{n-1}}. \tag{2.74}$$

From (2.74) we see that the more generations we consider the smaller the value of $p_r$ that satiesfies the equilibrium condition as long as the denominator in (2.74) is less than 1. This is intuitively understandable since the more expansion in the centroblast population the less need for recycling. This may explain why Kesmir and de Boer only need $p_r = 0.15$ in their model [26] while other groups demanded high values of $p_r$ in the range $p_r \geq 0.7$ in order for affinity maturation to work [38, 44] since Kesmir and de Boer do not include any direct diminishing effects of mutation on the proliferation rate ($m = 1$ in their model) but only a general death rate for centroblasts and are considering 10 generations of centroblasts.

### 2.4.2 Numerical Simulation of the Model

It is finally interesting to explicitly solve the 1 generation model (equations (2.28-2.36)) and the two generation model (equations (2.66 - 2.71) with $j = 2$) and to compare the results with the analytic predictions and the experimental data.

The new object in the equations compared to the models before is the mutation matrix $\mathbf{M}$ for which we need to find the biological correct entries. The selection rate $s$ and the recycling probability $p_r$ will then be chosen as derived by the analytical analysis such that the kinetic data are reproduced.

In order to find the correct entries for $\mathbf{M}$ we use calculations by others [51] that estimate 53 percent of all mutations to be silent and 28 percent to be lethal. Therefore from the surviving 72 percent, 74 percent have not changed affinity while 26 percent have. We cannot expect that more than 10 percent of all mutations which change the affinity (or about 2 percent of all mutations) are beneficial. Manser even assumes that only 0.1 percent of all mutations are beneficial [37] which however may be quite pessimistic. Assuming that 10 percent of all changing mutations are beneficial we obtain as mutation matrix

$$\mathbf{M} = \begin{pmatrix} 0.948 & 0.468 \\ 0.052 & 0.532 \end{pmatrix} \tag{2.75}$$

which is derived as follows. If 10 percent of all changing mutations were beneficial, 2.6 percent of all low affinity clones would be promoted to high affinity in every round of mutation. We therefore have $\mathbf{M}_{21} = 0.1 \times 0.26 \times 2 = 0.052$ where the factor 2 comes in since the sum over all entries of $\mathbf{M}$ is 2. The remaining part of the low affinity clones remains of low affinity and we therefore find $\mathbf{M}_{11} = 1 - 0.052 = 0.948$. Given that we assume that 26% of all mutations change the affinity, $(26 - 2.6)\% = 23.4\%$ must reduce the affinity so

that $\mathbf{M}_{12} = 0.234 * 2 \times 2 = 0.468$. The remaining high affinity clones remain of high affinity and we find for the last matrix entry $\mathbf{M}_{22} = 1 - 0.468 = 0.532$.

Given that the division rate is $4\,day^{-1}$ and we apply the mutation matrix continuously in every time step, we need to take $M$ to the $\frac{4day-1}{\frac{1}{dt}} = 0.4$ with $dt = 0.1$ being our numerical finite time difference. Our final $\mathbf{M}$ is therefore given by:

$$\mathbf{M} = \begin{pmatrix} 0.9746 & 0.229 \\ 0.0254 & 0.771 \end{pmatrix}$$

These mutations are now changing the proportion between high and low affinity clones which is calculated from

$$\mathcal{A} = \frac{B_2 + C_2 + C_{s2} + M_2}{\sum_i (B_i + C_i + C_{si} + M_i)}. \tag{2.76}$$

It is no longer sensible to consider an affinity dependence of the consumption factor after the results in the previous models. Additionally, the main affinity increase happens in the memory cell population and there is no experimental data available showing that high affinity B cells extract more antigen than low affinity ones. We therefore choose $u = 2.5 \times 10^{-5}$. The antigen dynamics are still modelled as given in equation (2.25).

Given that the above analysis claims that several centroblast generations would be beneficial for affinity maturation it is interesting to study a one and a two generation model. Both exploit results from the previous analysis for the choice of the selection factor $s$ and the recycling probability $p_r$. In order to gain maximal affinity increase we need to choose $s_1$ small while $s_2$ has to be large. The recycling probability, on the other hand needs to be chosen high for low affinity clones ($p_{r1}$) and low for high affinity clones ($p_{r2}$). With time also the recycling probability for high affinity clones has to increase reflecting the stronger competition for activating signals because of reduction of available antigen. In a multi bin model the threshold bin for which the recycling probability is high would rise. We therefore have

$$\mathbf{s} = \begin{pmatrix} f\frac{Ag^n}{Ag^n_{min_s}+Ag^n} \\ \frac{Ag^n}{Ag^n_{min_s}+Ag^n} \end{pmatrix} \qquad n = 15 \tag{2.77}$$

$$\mathbf{p_r} = \begin{pmatrix} 0.95 \\ 0.05 + 0.7\frac{Ag^n_{min_p}}{Ag^n_{min_p}+Ag^n} \end{pmatrix} \qquad n = 15 \qquad Ag_{minp} = 7500$$

with $f = 0.17, Ag_{min_s} = 4500$ in the 1 generation model and $f = 0.14, Ag_{min_s} = 6000$ in the 2 generation model.

The centrocytes which do not recycle can either differentiate into memory or plasma cells. Early plasma cells, the antibody forming cells ($AFC$), are of extreme high affinity and their formation stops between day 10 and day 14 [54]. Memory cell ($M$) formation starts between day 4 and day 5 [34] and plasma cell formation continues after $AFC$ formation into the plasma cell ($PC$) pool. It is

important to distinguish between these cell populations since memory cells stay at the edge of the germinal centre and were counted when the affinity increase was measured by experimentalists. Plasma cells however leave the germinal centre and do not count anymore. AFCs have been measured explicitly in the experiments and it may help in the analysis to have a further value to compare with data. We therefore have as additional equations at the end of every time step:

for $t < 5$

$$AFC(t+dt) = AFC(t) + (1-p_r)C_s dt; \tag{2.78}$$

for $5 \leq t < 12$

$$\begin{aligned} AFC(t+dt) &= AFC(t) + f_1(1-p_r)C_s dt & (2.79)\\ M(t+dt) &= M(t) + f_2(1-p_r)C_s dt; & (2.80) \end{aligned}$$

for $t \geq 12$

$$\begin{aligned} PC(t+dt) &= PC(t) + f_1(1-p_r)C_s dt & (2.81)\\ M(t+dt) &= M(t) + f_2(1-p_r)C_s dt. & (2.82) \end{aligned}$$

The parameters $f_1$, $f_2$ were chosen as $f_1 = 0.6$, $f_2 = 0.4$ in order to satisfy the experimental result that the memory cell population is smaller than 5 percent of the maximal GC B cell number which is about $2 \times 10^4$. If we choose the rate at which selected centrocytes differentiate into memory or plasma cells to deviate from the value which has been assumed so far (1 day$^{-1}$)[1], we would need to adapt $f_1$, $f_2$ accordingly. Given that the total number of plasma cells (PCs) has no influence on the key results of this model such a change cannot be expected to have a large impact on the model.

We have now determined equations for $s(Ag), p_r(Ag)$ and obtained the mutation matrix. Solving equations (2.28)-(2.36) for the 1 generation model and (2.66) - (2.71) with $j = 2$ for the 2 generation model while using equations (2.78-2.4.2) for AFC, plasma cell and memory cell dynamics, 2.25 for the antigen dynamics and the newly determined equations for the parameters $s(Ag), p_r(Ag)$ yields for the 1 generation model Figure 2.10 and for the 2 generation model Figure 2.11. The upper plot shows in both figures the germinal centre kinetics which behave mostly as described before. One should however note that for the 2 generation model the centrocyte population is of about the same size as the centroblast population for most of the germinal centre reaction. This is not in good concert with experimental data [36]. Comparing the plots of affinity maturation (bottom plots) shows that as expected from our analysis the affinity increase is larger in the 2 generation model. The total difference is however so small that taken together with the deviations in the GC kinetics for the 2 generation model it seems that the 1 generation model describes affinity maturation best. In favor for both models is the proportion of high affinity AFCs at day 14. Although nothing was specifically undertaken to influence this number, the proportion given in the literature (56 percent) [54] is reproduced well by both models (53 percent). The 1 generation model reproduces

[1]The rate is first needed in (2.5) and discussed in that context.

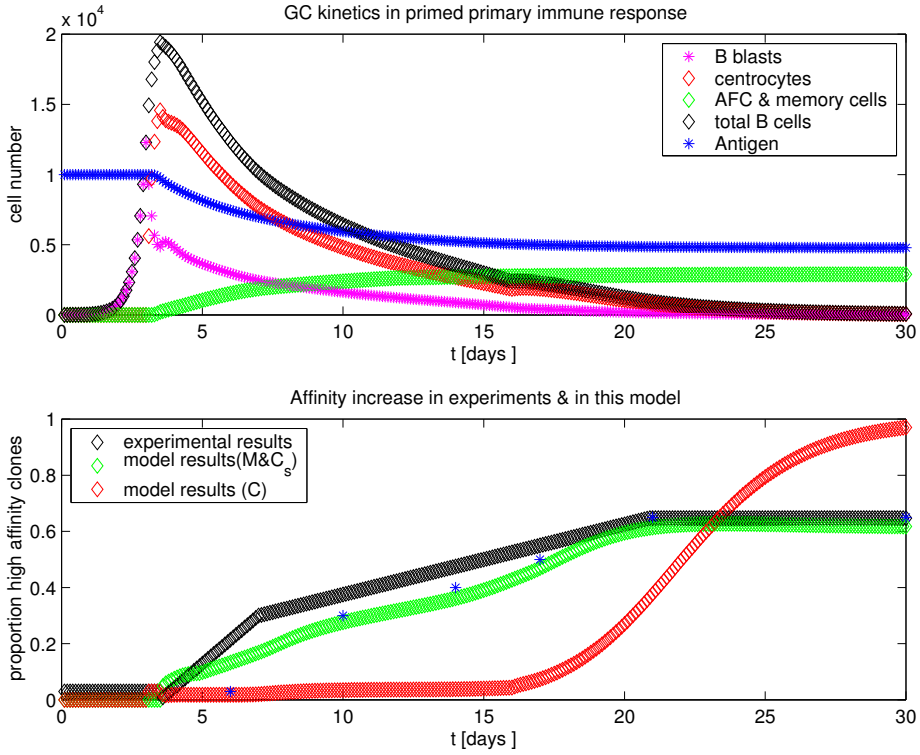



Figure 2.10: (*top*) GC kinetics of the primed primary immune response in the 1 generation model where selection ($s$) and recycling ($p_r$) is dependent on antigen density and somatic hypermutation terminates at day 16. The dynamics of all cell populations behave as described before. (*bottom*) Affinity maturation: the model results are close to the experimental ones (dots and marked line). Until day 16 the affinity increase is largely due to an affinity increase in the memory population. After the termination of somatic hypermutation on day 16 the average affinity increases again substantially due to an affinity increase in the centrocyte population.

therefore all data which are available from the literature and allows us to make predictions about the recycling and selection rate. The last step to take is the building of a multi bin model. Given that however neither entries for the much more complex mutation matrix nor values for the different entries of $s$ or $p_r$ are known, it is sensible to wait for more experimental data before undertaking a detailed modelling approach.

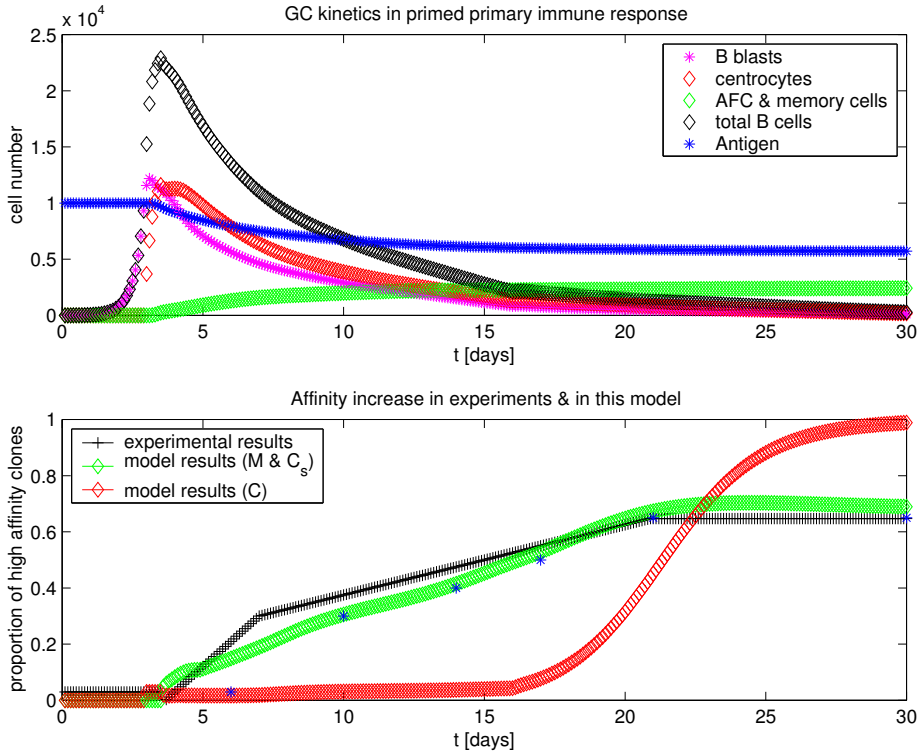



Figure 2.11: (*top*) GC kinetics of the primed primary immune response in the 2 generation model where selection ($s$) and recycling ($p_r$) is dependent on antigen density and somatic hypermutation terminates at day 16. The dynamics of all cell populations behave as described before. (*bottom*) Affinity maturation: the model results are close to the experimental ones (dots and marked line). Until day 16 the affinity increase is largely due to an affinity increase in the memory population. After the termination of somatic hypermutation on day 16 the average affinity increases again substantially due to an affinity increase in the centrocyte population.

# Chapter 3

# Conclusion

## 3.1 Summary of Results and Discussion

The key results of this analysis of affinity maturation concern predictions about the selection rate $s$ and the recycling probability $p_r$. It was further shown that a termination of somatic hypermutation at about day 16 is beneficial for affinity maturation. Finally the analysis suggests that a one generation model fits the available experimental data best.

The mathematical analysis shows that both the selection rate $s$ and the recycling probability $p_r$ need to be dynamic with respect to time. The latter is a new proposal and follows from analysis of the efficiency of affinity maturation. Affinity maturation is most efficient if mutation is acting on a population with only a small proportion of high affinity clones. This is due to the deleterious nature of most changing mutations. Nature works therefore the most efficient if clones with a high affinity compared to the current average affinity emigrate from the GC reaction and either enter the memory or plasma cell pool. With time the average affinity increases and fewer clones have a much higher relative affinity and so the recycling probability for clones of higher affinity increases which allows also expansion of high affinity clones. The early emigration of high affinity clones has been described previously [47, 54] but was understood to be due to a stochasticity in the selection and was viewed as a failure of the system. The model presented in this dissertation suggests that the early emigration is a deterministic process and is beneficial for affinity maturation and for the defense of the organism against the invader since the early emigrants produce antibodies which support the organism's first defense. This finding is also in good agreement with another experimental result where a transgene which coded for a high affinity antibody was inserted into the genome of an animal [62]. The animal nevertheless produced a similar memory cell repertoire as the control animals without the transgene. This is in favor for the deterministic early emigration of high affinity clones which therefore do not dominate the response and in the later response animals without the transgene have obtained antibodies of comparable affinity by mutation while the antibody encoded by the transgene can accumulate worsening mutations. The model also explains the results of Hannum and coworkers [16] which find that the germinal centre

reaction is more or less normal even if the animals cannot deposit antigen on FDCs due to the lack of soluble antibodies. Their data shows that the GC cell numbers are even higher than in the control animals while the activation of centrocytes is less. Due to less activation presumably more cells recycle and the GC reaction is therefore stable. The activation may be less since antigen cannot be displayed professionally on FDCs but needs to be recognised in other - maybe even in soluble - form which elicits less response [4].

The selection factor needs to be chosen in the opposite way to the recycling rate and is high for high affinity clones and low for low affinity clones. This is also intuitively understandable. With time the competition for antigen becomes harder since due to extraction of antigen by centrocytes the antigen density decreases. Therefore the selection proportion of low and high affinity clones decreases with time.

Less activation due to less antigen availability may then finally switch off somatic hypermutation which needs to happen together with an increase in selection stringency as this model shows. This correlation may be due to a connection between activating signals during centrocyte selection and signals for continuation of somatic hypermutation after centrocytes have recycled. The analysis of this model further shows that termination of somatic hypermutation before the end of the germinal center reaction is beneficial for affinity maturation since it allows the expansion of high affinity clones without the hazard of losing the clone due to worsening mutations.

Finally the kinetics for models with one or more centroblast generations show that it is only for the one generation model that centrocytes outnumber centroblasts for the main part of the response as has been described by experimentalists [36]. We can conclude from this that the differentiation of centroblasts into centrocytes happens after one generations. This result takes away the burden of arguing how centroblasts may sense through how many generations they may have gone already.

## 3.2 Further Work

Given that the model presented in this dissertation answers all the questions that we started with and reproduces all experimental data available it only remains to be challenged experimentally. It would be useful if data was available concerning the dependency of B cell activation and selection on antigen density and affinity. Furthermore it would be interesting to know what impact antigen density and affinity have on the decision whether a selected centrocyte differentiates into a memory or plasma cell or recycles back and replenishes the centroblast pool. In order to extend the model to a multi affinity bin model we would need data for all rates and for the entries in the mutation matrix. The latter especially will be very difficult to measure. Finally it would be interesting if the question concerning the regulation of the differentiation of centroblasts into centrocytes could be resolved experimentally.

Even without further data it would be interesting to extend the model to understand what regulates differentiation of selected centrocytes into memory

or plasma cells or makes them recycle. T cells can be expected to play a major role in this process and would need to be included in such a model. Given the success of the approach taken so far, it seems sensible to build on this model and to add assumptions again by following the semi-linear way as presented in this dissertation. Combination of the two models should allow a more or less complete picture of the germinal centre reaction.

A completely different modelling approach would be the use of a cellular automaton model. The advantage of such a simulation technique is the inclusion of details about the spatial organisation of the germinal centres which was neglected in the continuous model presented in this dissertation and which would be difficult to be analysed in a continuous PDE model. In order to build such a cellular automaton model, it would however be necessary to have data about the migration time of different cell types in the germinal centre and these data are currently not available [34].

# Part II: Simulation of Biological Membranes

# Chapter 4

# Introduction to Biological Membranes

In the previous chapters we derived a model for affinity maturation in the immune system with which we can make predictions about which processes may drive affinity maturation. We saw that antigen extraction and the resulting decrease in antigen density may be crucial in driving affinity maturation. We will now consider mechanistic details of the cell-cell interaction process which finally leads to antigen extraction.

Selection is based on how well centrocytes interact with antigen located in the light zone of the germinal centre [35]. We will follow the current view that the antigen with which centrocytes are interacting is presented on the surface of follicular dendritic cells (FDCs) [35]. In a model system it was recently found that interaction of B cells with membrane tethered antigen leads to the formation of organised structures in the contact zone [4]: While antigen, the antigen receptor and molecules which are activating B cells concentrate in the contact zone, inhibitory molecules are expelled. Beside proteins also lipids (see figure 4.1 for an example) and the cytoskeleton undergo a re-organisation: The glycolipid sphingomyelin GM1, which can be detected by Cholera Toxin subunit B (CTB), concentrates in the contact zone as do components of the cytoskeleton, such as actin. Similar structures have also been observed between T cells and antigen presenting cells (APCs) [28, 39, 40, 41, 57]. The current view is that this dynamic rearrangement of proteins into organised supramolecular activation clusters is driven primarily by active cytoskeletal processes [11, 64].

A recent mathematical study [46] however shows that the essential characteristics of synaptic patterns observed in living cells can result from spontaneous self-assembly processes. Active cellular interventions are superimposed on these self-organising tendencies and may also serve to regulate spontaneous processes. For most parameters the mathematical study uses values determined in experiments. Parameters characterising the membrane constitution of the synapse forming cells are however unknown and values from other experimental systems were used. Given that the study nevertheless reproduces the data on synapse formation, membrane structure seems not to be important for spontaneous self-assembly processes which lead to synapse formation. Membrane structure may

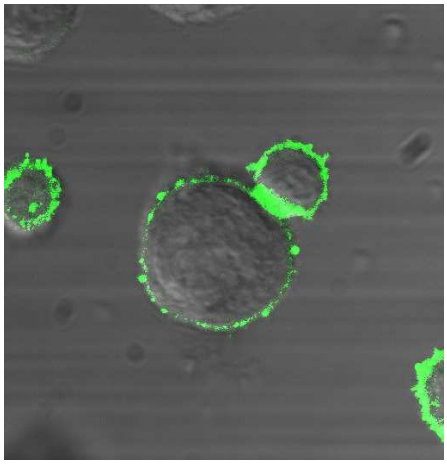


Figure 4.1: B cell (small) interacting with a cell that is displaying antigen: GM1 is concentrated in the contact zone as revealed by CTB-staining

however regulate synapse formation via its influence on active cellular actions carried out by the cytoskeleton. The lipids which are found to concentrate in the contact zone belong to the class of raft lipids and raft lipids have been discussed to have various effects on the cytoskeleton and on intracellular signalling. Further on lipid domain formation may also support extraction and subsequent endocytosis of antigen as theoretical analysis of vesicle budding [29] suggests. Intramembrane domains have an edge energy proportional to the length of the boundary of this domain with its environment. In order to minimise this edge energy, the domain has a tendency to attain a circular shape and the edge energy can be further minimised if the domain forms a bud. Because of this edge energy, the domain must bud as soon as its linear size exceeds a certain critical size even if it has no spontaneous curvature. The raft domains may however have spontaneous curvature since one of its main constituent, the sphingolipids, reside only in the outer leaflet [58] which induces an asymmetric membrane composition (e.g. the two leaflets of the membrane differ in their composition) and this has been shown to lead to a spontaneous curvature [29]. That lipid structure can aid endocytosis is also supported by experiments [9] which show that membrane domains consisting of raft lipids and a GPI-protein form invaginations of $72-250$ nm in size. These invaginations were found to be involved in the internalisation process of the GPI-protein. A phase separation between raft lipids in the contact zone and other lipids may therefore also support extraction and internalisation of antigens out of the opposing membrane which requires budding of a membrane vesicle into the cell [1].

Understanding how membrane structure may facilitate internalisation may also help to explain how endocytosis has evolved in nature since it may have been "easier" to improve a process that happens by the intrinsic properties of cell components than to invent the endocytosis machinery from scratch. Membrane composition in "modern" cells will however probably not solely drive internalisation (endocytosis) of the receptors but it may decisively support the en-

docytotic process which is otherwise driven by proteins such as the clathrin mediated pathway. In this context it is worth mentioning that clathrin molecules and components of the cytoskeleton were also found to concentrate in the contact zone. Additionally, src kinases, that have been reported to reside in rafts, are able to induce clathrin self-assembly which finally leads to internalisation [63]. In line with that, destroying rafts by cholesterol depletion inhibits clathrin mediated endocytosis [49, 59].

We conclude that it is of interest to investigate which processes lead to such a phase separation of lipids in the membrane upon cell-cell interaction. Before continuing with a model of lipid phase separation, some background about general membrane architecture will be given in the next section.

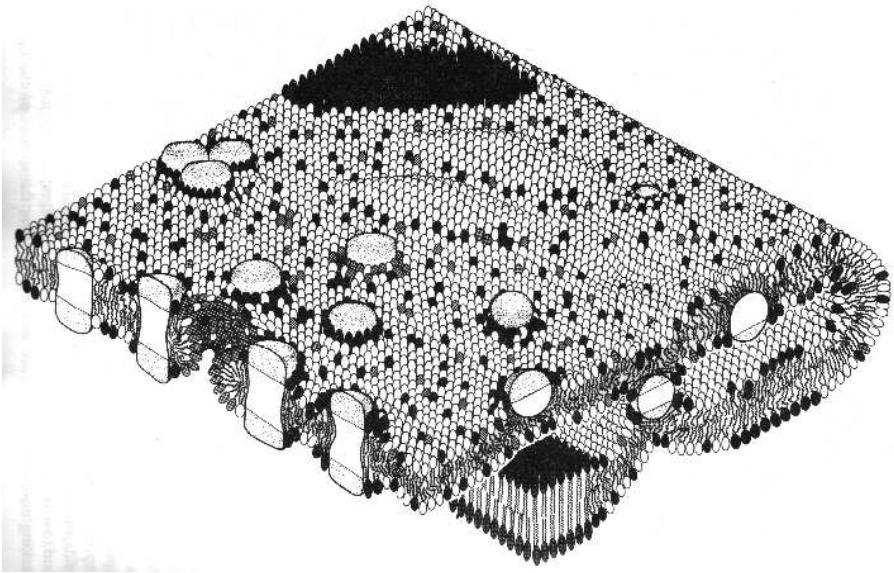


Figure 4.2: Schematic figure of a biological membrane taken from [18]. The lipid contents of different membranes varies from as little as 25% up to 80% by weight. At highly curved regions the outer convex face contains mainly cone-shaped lipids while the inner concave face has more wedge-shaped lipids. Note how stressed regions may adopt a locally non-bilayer structure.

## 4.1 Membrane architecture

Membranes are built up out of two layers of lipids and of proteins that are solved in the lipid bilayer. Every lipid has a hydrophobic tail (fatty acid chain) and a hydrophilic head. The hydrophobic tails of the two bilayers point towards one another, while the hydrophilic heads interact with the aqueous environment. Transmembrane proteins have a hydrophobic part which spans the bilayer ($\pm 20$ amino acids) and hydrophilic parts that interact with the aqueous environment [1]. Although membranes are impermeable to many compounds and start to rupture as soon as their area is changed by about 1% [29], they are still fluid.

The diffusion coefficient of lipids in a variety of membranes is about $1\mu m^2 s^{-1}$. Thus, a phospholipid molecule diffuses an average distance of $2\mu m$ in 1 s. This means that a lipid molecule can travel from one end of a bacterium (single cell organism) to the other in a second. Proteins are in general much slower than lipids [58].

In the current model of membrane structure lipids mainly play the role of a solvent for membrane proteins that have functions in transport, signalling and stabilisation. It is however striking that more than 100 different lipids have been characterized and lipid species are distributed asymmetrically over the exoplasmic and cytoplasmic leaflets of the membrane [1]. This asymmetry is retained since lipids are restricted to lateral movement and flip only rarely between the two layers due to energetic constraints [58]. More recently it has been proposed that membranes also show a lateral organisation of lipids in small microdomains termed rafts and that this membrane structure has functional relevance [53]. This is however still controversial since these microdomains are too small and unstable - if they exist at all - to be easily measurable [12, 24, 61].

Rafts are believed to be mainly constituted from two sorts of lipids: sphingolipids and cholesterol. Sphingolipids have long hydrophobic tails, bulky hydrophilic heads and are only found in the exoplasmic leaflet while cholesterol is a rather small lipid that is found in both leaflets. These two lipids together form thicker membranes than other lipids [48]. It has been suggested that this increased membrane thickness leads to preferential association of these microdomains with transmembrane proteins with a long hydrophobic transmembrane domain or with proteins with glycosyl phosphatidyl inositol (GPI) or acyl anchor, that are only inserted into the membranes without spanning them. Membrane proteins with short transmembrane regions are on the other hand believed to be excluded since their residence in these membrane microdomains would be energetically costly due to the interaction of polar protein parts with hydrophobic lipid parts. The same argument (but the other way round) applies to proteins with long transmembrane regions that try to interact with thinner parts of the membrane and thus the association of membrane proteins with different lipid domains is suggested to be selective [42, 60].

## 4.2 Model of Lipid Distribution on Membranes

Given that we are interested in spontaneous processes we neglect all active cellular actions such as mediated by the cytoskeleton in the model of the phase separation between raft lipids and other lipids. The driving forces for the domain formation of raft lipids in the contact zone are assumed to be an attractive potential for raft lipids in the contact zone and lipid-lipid interactions. The attractive potential is due to the favorable interaction of a certain group of proteins (src kinases, GPI proteins), which become engaged in the contact zone, with this lipid [4, 53]. The gain in energy by interaction between lipids of one sort can be justified by the geometry of lipids as has been discussed above: It is unfavorable for a long raft lipid to interact with a small non-raft lipid.

### 4.2.1 Analytic solution for spherical cells

The problem can be analysed analytically [30] if we neglect lipid-lipid interactions and further simplify the model by assuming the other cell to be a wall decorated with adhesive stickers (adhesion molecules) to which the remaining cell binds. These stickers represent both the proteins which are engaged in the contact zone and the adhering raft lipids. In order to keep the geometry simple the cell is further assumed to be of spherical shape. In the strong adhesion regime the cell therefore forms a spherical cap upon interaction with the wall, and this strong adhesion regime applies if

$$|W| \gg 2\frac{\pi\kappa}{A_{Me}} \tag{4.1}$$

where W is the adhesion energy per area in the contact zone, $\kappa$ is the bending rigidity of the lipid bilayer (of the order $10^{-19}J$) and $A_{Me}$ is the total membrane area . This yields the condition that the adhesion energy per $\mu m$ must be larger then a few $kT$ (thermal energy unit) in order to work in the strong adhesion regime. This is easily achieved since each attractive molecular interaction is expected to contribute a binding energy of a least $kT$ and every sticker is only of the size of a few Å($10^{-10}m$).

The size of the contact zone is balanced by two forces. While the attractive force enlarges the contact zone to its maximum another force opposes against the shape change introduced by the enlargement of the contact zone. The shape change can only lead to a change in volume since we require area conservation for biological reasons. In biological membranes, the total number of lipids is more or less fixed and membranes are inelastic with respect to stretching from which area conservation directly follows. In order to describe the opposing force by a physical equation we assume that a change in volume changes the osmotic pressure balance across the membrane. This assumption implies that channels in the cell membrane cannot rapidly balance the osmotic pressure change due to the volume change. This assumption probably does not reflect biological reality where cells do not need to preserve a spherical shape and can therefore attain the cell shape which maximises the contact area but leads to only small deviations in area and volume. Furthermore, in real cells the cytoskeleton has a large impact on cell shape transformations. Given that we are however interested in spontaneous processes, we neglect influences of the cytoskeleton throughout this study and use this simple model.

Therefore, assuming that the opposing force is due to osmotic stress and that the osmotic pressure difference is balanced by the lateral membrane tension $\Sigma$ we obtain

$$\Sigma = \frac{T\frac{\mathcal{N}_{in}}{V} - \rho_{ex}}{2M} \tag{4.2}$$

where $M$ is the mean curvature of the membrane, $\mathcal{N}_{in}$ is the total number of osmotic relevant particles inside the cell, $V$ is the cell volume and $\rho_{ex}$ is the concentration of osmotic relevant particles outside the cell.

Combining 4.2 with the Young-Dupree equation for the effective contact angle $\theta$

$$|W| = \Sigma(1 + \cos\theta), \tag{4.3}$$

with equations expressing the geometric quantities such as the contact area, the radius, the effective contact angle ad the vesicle volume in terms of the cell radius $R_{Me}$ of the unbound sphere and in terms of the dimensionless cell height $h \equiv \frac{H}{2R_{Me}}$ where $H$ is the dimensional height of the cell, yields the implicit equation

$$\left(\alpha \frac{h}{1-h^2} + \beta\right) h(3-h^2) = 2. \tag{4.4}$$

The two dimensionless parameters $\alpha$ and $\beta$ are given by

$$\alpha \equiv \frac{8\pi}{3} \frac{|W| R_{Me}^2}{T\mathcal{N}_{in}} \qquad \beta \equiv \frac{4\pi}{3} \frac{\rho_{ex} R_{Me}^3}{\mathcal{N}_{in}}. \tag{4.5}$$

In order to calculate $|W|$ dependent on $h$ we consider a gas of adhesion molecules in the membrane. The binding energy of one adhesion molecule with the wall surface is denoted by $|U|$, the lateral sticker size by $a$. We can calculate $|W|$ analytically by using a grand canonical description in which one couples the cell membrane to a reservoir of adhesion molecules with the fugacity

$$\zeta \equiv \exp\left(\frac{\mu}{kT}\right) \tag{4.6}$$

where $\mu$ is the chemical potential of the adhesion molecules.

The grand canonical partition function is then given by

$$\mathcal{Z} = \left(1 + \zeta \exp\left(\frac{|U|}{T}\right)\right)^{\Omega_b} (1+\zeta)^{\Omega_{ub}} \tag{4.7}$$

with $\Omega_b$ and $\Omega_{ub}$ the number of bound and unbound membrane segments respectively.

From this one can determine the adhesion energy per area $|W|$ to be

$$|W| = \frac{|U|}{a^2} \frac{f_\zeta \exp\left(\frac{|U|}{T}\right)}{1 + f_\zeta \exp\left(\frac{|U|}{T}\right)} \tag{4.8}$$

where the function $f_\zeta$ is given by

$$f_\zeta = 0.5(\gamma + \sqrt{\gamma^2 + \delta}) \tag{4.9}$$

which depends on the parameters

$$\gamma = \frac{n}{1-n} - \exp\left(-\frac{|U|}{T}\right) - 0.5(1-h^2)\frac{1 - \exp\left(-\frac{|U|}{T}\right)}{1-n} \tag{4.10}$$

$$\delta = 4\exp\left(-\frac{|U|}{T}\right)\frac{n}{1-n} \tag{4.11}$$

Equation 4.4 finally depends on the following four dimensionless parameters

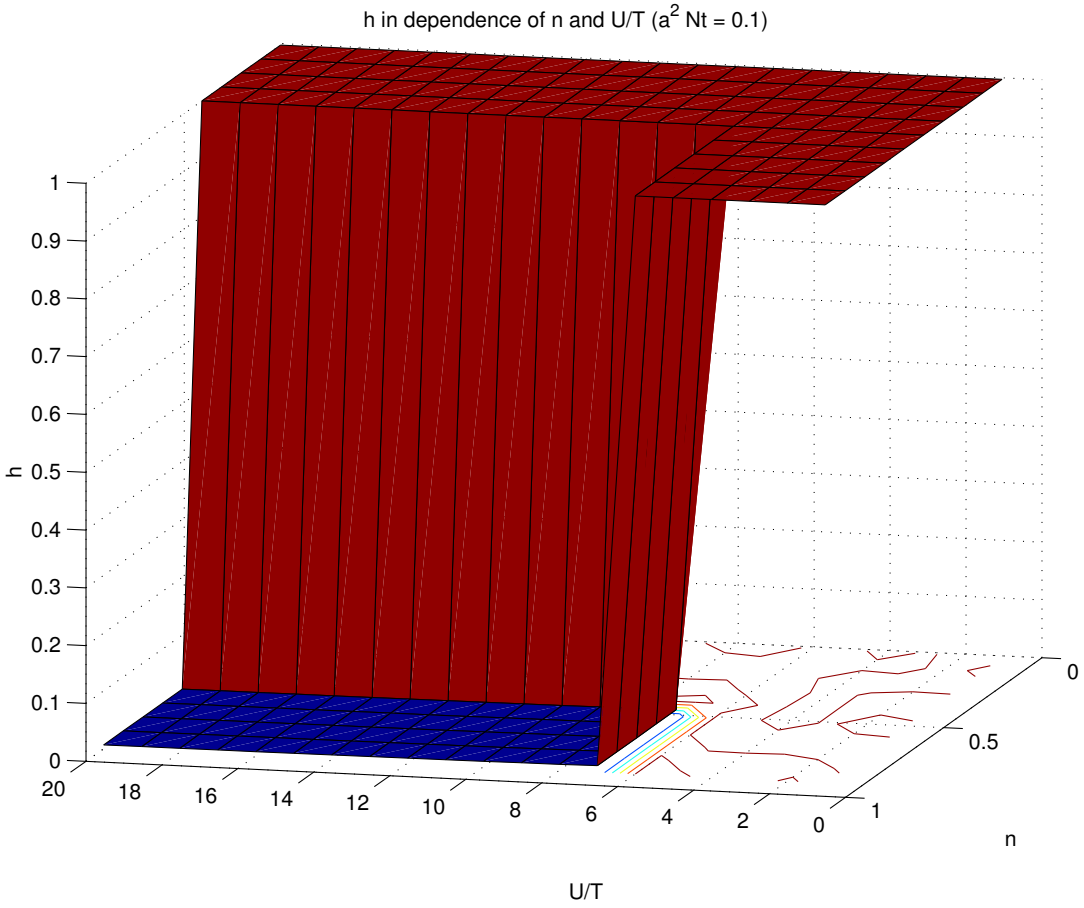



Figure 4.3: The solution of equation 4.4 for h in the range $n \in [0, 1]$ and $\frac{|U|}{T} \in [0, 20]$ with $a^2 N_t = 0.1$.

- the relative adhesion strength

$$\frac{|U|}{T} \frac{R_{Me}^2}{a^2} \frac{1}{\mathcal{N}_{in}} \tag{4.12}$$

- the particle number fraction

$$\frac{\rho_{ex} R_{Me}^3}{\mathcal{N}_{in}} \tag{4.13}$$

- the adhesion molecule density $n$
- the adhesion molecule binding 'strength' $\exp\left(\frac{|U|}{T}\right)$.

In a cell the sticker density $n$ and the binding energy $\frac{U}{T}$ can vary while $a^2 \mathcal{N}_{in}$ can be assumed to be more or less fixed. For simplicity, we further set the bulk concentration of osmotic relevant particles $\rho_{ex}$ to zero and are left with two free parameters, $n$ and $\frac{U}{T}$. It is now sensible to explore (4.4) by investigating its behaviour when either $n$ or $\frac{U}{T}$ go to zero or $n$ goes to 1 or $\frac{U}{T}$ to infinity. If

$U \to 0$ we see that $|W| \to 0$ and therefore $\alpha \to 0$ and (4.4) can only be satisfied if $h \to 1$. If $\frac{U}{T} \to \infty$ we find $\alpha \to \infty$ and need therefore $h \to 0$ in order to satisfy (4.4). The sticker density $n$ does not change this overall behaviour dependent on $\frac{U}{T}$ but influences the behaviour in the way that large sticker densities work in favor of a small cell height $h$. The same is also found in the numerical analysis of (4.4) as can be seen in Figure 4.3[1]. The plot shows that the cell takes a flattened shape for large adhesion binding strength ($\frac{|U|}{T} \gg 1$) and low adhesion molecule density ($n \to 0$). This is also intuitively understandable since the higher the adhesion strength the higher the tendency to enlarge the contact zone (reduce h) and the lower the sticker density the smaller the possible contact zone ($h \to 1$). For the numerical solution $a^2\mathcal{N} = 0.1$ is chosen for computational reasons although this value is too large for biological systems. For biological lipids we have $a \leq 10^{-9}$m and $a^2\mathcal{N}_{in} = 0.1$ therefore requires $N_t = 10^{17}$ molecules. Given that the initial volume is about $V = 113\mu m^3$ the internal cell concentration would be about $c = 2 \times 10^{30} M$ while normal cells are about 1 molar. It is however only interesting to see the general behaviour of the solution and for smaller values of $a^2\mathcal{N}_{in}$ the total values handled by the computer become too large. Computational problems with too large numbers also forces us to explore the equations for $\frac{|U|}{T} \leq 20$.

## 4.3 Scope of the study

Experiments with B cells shown the accumulation of a special sort of lipids in the contact zone where the B cell interacts with a second cell. It is unknown which processes drive such a re-organisation of the membrane structure and it is therefore of interest to analyse the impact of protein-lipid and lipid-lipid interactions on lipid domain formation.

In this dissertation a simplistic model of membrane lipid dynamics is investigated by the use of Monte Carlo methods. The lipid-protein interactions are only studied indirectly by assuming that proteins which attract this special lipid species are all engaged in the contact zone. This can then be modelled by applying an affinity field in the contact zone which attracts only the lipid sort found to accumulate but not the other lipids.

The size of the emerging lipid domains is analysed with respect to temperature and strength of lipid-lipid and lipid-protein interactions by determination of the correlation function.

[1]The Matlab program code is given in the Appendix D.1.

# Chapter 5

# Methods

## 5.1 General Setup

The impact of cell-cell interaction on the lipid dynamics, is investigated by the use of a Monte Carlo method [43]. In order to keep track of the cell surface lipids, the various lipids are divided up into two classes: lipid class $A$ contains all lipids that are attracted into the contact zone between the two cells (approximately $10-15\%$ of all lipids) and its members are assigned the numerical value $\lambda = +1$, while lipid class $I$ contains all those lipids that are indifferent towards this attraction and the members of this lipid class are assigned the numerical value $\lambda = -1$.

Two different cell shapes are investigated in this dissertation: in a first model cells are taken to be of torus shape (cylinder with periodic boundary conditions) while in the second model the more realistic shape of a sphere is considered. From the analytical analysis in Chapter 4.2.1 we know that it is sensible to consider a strong adhesion regime in the contact zone between the two cells and due to this strong adhesion the contact zone is flat while the remaining cell body forms a spherical cap if cells are taken to be of spherical shape (see Figure 5.1 for illustration).

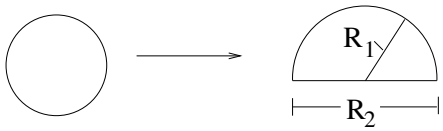



Figure 5.1: The cell becomes flattened upon interaction with a second cell. The second cell is omitted and replaced by application of an affinity field in the "contact zone".

We can then further simplify the model by considering only one cell. The interactions with the second cell can be replaced by the application of an affinity field in the former contact zone which attracts lipid $A$ and to which lipid $I$ is indifferent (see Figure 5.2 for illustration).

The equilibrium shape of the cell emerges from the balance between two forces. One force acts to maximise the contact zone where the affinity field

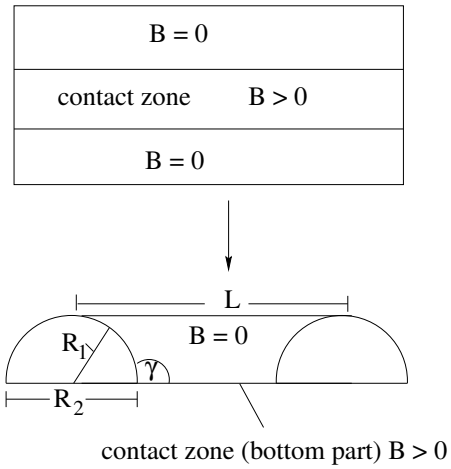



Figure 5.2: Replacement of the second cell by application of an affinity field on the flattened part of the cell. Here cells have been taken to be of cylinder shape.

$B$ is applied while the other force opposes this action by minimising volume reductions which are a consequence of the enlargement of the contact zone as discussed previously.

## 5.2 Monte Carlo Method

In the Monte Carlo simulation shape changes and lipid movements take place with a probability $P$ depending on the change of the inner energy $H$ introduced into the system through this action. In the Monte Carlo method used here, this probability $P$ is given by

$$P(\mu \to \nu) = \begin{cases} e^{-\beta \Delta H} & \text{if } \Delta H > 0 \\ 1 & \text{otherwise} \end{cases} \tag{5.1}$$

where $\Delta H$ is the energy difference between the two states $\mu$ and $\nu$, and $\beta = \frac{1}{kT}$ is the temperature factor.

The inner energy $H$ of the system depends on local interactions between neighbouring lipids, on the affinity field in the contact zone, and on the actual volume of the cell. The energy functional H is therefore given by

$$H = -J \sum_{<ij>} \lambda_i \lambda_j - \sum_i B_i(\lambda_i + 1) - \frac{\mathcal{N}_{in}}{\beta} \ln \frac{V_{new}}{V} \tag{5.2}$$

where J is a positive constant which is modelling the interaction energy between nearest-neighbour lipids $< ij >$, and B is the external "affinity" field. $B_i$ is therefore zero outside the contact zone and $> 0$ inside the contact zone. The last term in (5.2) is derived by integrating $dH = -pdV$ which models the energy change due to mechanical work. The osmotic pressure $p$ is given by $p = \frac{\mathcal{N}_{in}}{\beta V}$ where $\mathcal{N}_{in}$ is the number of osmotic relevant particles inside the cell and V is the cell volume.

As can be seen from the first term in (5.2) a neighbourhood of similar lipids leads to a negative contribution to the inner energy while a mixture of lipids from different classes leads to positive contribution. The biological justification for modelling the accumulation of lipids of the same sort as energetically favorable while evaluating interactions between lipids of different classes as energetically costly lies in the chemical properties of these lipids. Lipids of the two classes have for instance different lengths so that interaction of lipids from different classes leads to a microscopy ruffled membrane where full separation of the hydrophilic heads from the hydrophobic tails is impeded as outlined in the introduction. Hydrophobic and hydrophilic compounds however repel one another and bringing them close together is therefore energetic costly.

The second term in equation (5.2) is chosen such that only lipids of group $A$ ($\lambda_i = 1$) feel an attractive force in the contact zone, while lipids from group $I$ are indifferent.

The third term in equation (5.2) models the inner energy increase due to a volume reduction as discussed before. The enlargement of the contact zone which goes hand in hand with a volume reduction may nevertheless make such a step energetic favorable.

## 5.3 The Algorithm

The simulation was programmed in the language C and the simulation was run on a computer with a 466 MHz Celeron processor and MMX CPU. The algorithms differ for the case when cells either take a cylinder or a spherical shape and will be presented separately.

### 5.3.1 Algorithm for Simulation of Cylinder Cells

The main parts of the program, which is organised into four parts, will be described in the following. $10^9$ simulation steps took about 1 hour on the computer equipped as described above.

**Algorithm**

1) Initiation

2) Time loop: for $(t = 0; t <$ final time; $t++)\{$

   i) Lipid diffusion (Kawasaki algorithm)

   ii) Calculation of diffusion distance

   iii) Shape change (once a sweep)$\}$

**Initiation** In the initiation module lipids get distributed randomly over the lattice and the initial internal energy is calculated. It is important to arrange the lists of lipids on the lattice carefully at this stage in order to avoid unnessary waste of computing time on searches of entries later on. This is especially important for the efficient calculation of diffusion.

**Spin exchange** In the Kawasaki algorithm one lipid and a neighboring lipid (local interactions) are picked randomly in every step of the simulation as is illustrated in Figure 5.3. Next neighbours can be located north, south, east and west of the original lipid. These two lipids can exchange their position with a probability according to (5.1). From (5.2) it is obvious that it is not sensible to carry out any further calculations if both lipids belong to the same lipid class and have therefore the same numerical value $\lambda$ since $\Delta H = 0$ for this swap and the exchange probability is therefore $P = 1$. If the spins are different, the energy difference due to the swap needs to be calculated. In order to spare computational time this calculation does not consider all interaction energies but only those that have changed. The change of energy due to new interactions can be calculated from

$$\Delta H = 2J \left( \lambda_i^\mu \sum_{k \neq j,\ \text{n.n. to i}} \lambda_k^\mu + \lambda_j^\mu \sum_{n \neq i,\ \text{n.n. to j}} \lambda_n^\mu \right) \tag{5.3}$$

where $\lambda_i$ and $\lambda_j$ are the two swapping lipids and the lipids under the sum are the next neighbour lipids. In case of Figure 5.3, the lipids under the sum for the first term would be lipid 1,2 and 3 and for the second term lipid 4,5 and 6.

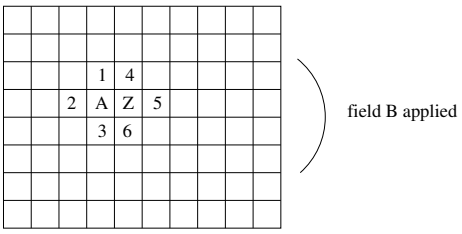



Figure 5.3: Sketch illustrating the calculation of inner energy: In order to calculate the inner energy for lipid $A$ we need to consider its interaction with 1,2,3 and $Z$ and the attraction of the field $B$ on $A$.

The change of energy due to lipid $A$ moving into or out of the affinity field is calculated from

$$\Delta H = B_i(\lambda_i - \lambda_j) + B_j(\lambda_j - \lambda_i) \tag{5.4}$$

with $B_i$ being the field where $\lambda_i$ moved to and from where $\lambda_j$ moved away from. The other way round applies to $B_j$.

If the energy difference is negative the spins are always swapped ($P = 1$) while a swapping happens with less probability as given in (5.1) if the energy difference is positive.

**Diffusion** Diffusion is calculated by determining at every time step the average of the distance of all lipids from their starting point. The diffusion in x and y direction is considered separately. At this stage it is very important to organise the lists to minimise computation time in updating them. This is

achieved by having three different lists: one with the actual lipid distribution on the lattice, one that stores how far a lipid has moved on the lattice and one that correlates the lipids on the lattice with the correct lipids in the list of diffusion since the places in the latter are fixed while the places on the lattice are dynamically changing.

**Shape change** Once a sweep the cell is allowed to change its contact angle $\gamma$ (see Figure 5.4 for illustration). Due to the conservation of area, once the contact angle is chosen the cell form is completely determined and we can calculate radius and volume of the cell from $\gamma$ and the known surface area. The surface area of the cell can be determined most easily by considering the shape of the unbound cell which will have perfect cylindrical form. The conserved area is therefore $A = 2\pi rl$ with $r$ being the initial cell radius (about $3\mu m$ for B cells) and $l$ the length of the cylinder.

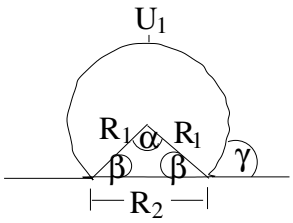



Figure 5.4: Notation for the calculation of the geometric properties of the deformed cylinder

Upon change of $\gamma$, the radius of the remaining part of the cylinder and the length of the flat part can be calculated by exploiting the conservation of the length of the circumference of the deformed circle (the length of the cylinder is also fixed). Using the notation in Figure 5.4 we obtain for the total circumference

$$U_T = U_1 + R_2 = 2\pi r \tag{5.5}$$

For the circle part of the circumference we find

$$U_1 = 2\pi R_1 \left(1 - \frac{\alpha}{2\pi}\right) \tag{5.6}$$

$R_2$ can be calculated by exploiting the fact that the triangle is isosceles.

$$\begin{aligned} \cos(\beta) &= \frac{R_2}{2R_1} \Leftrightarrow R_2 = 2R_1 \cos(\beta) \\ \beta &= \left|\frac{\pi - \alpha}{2}\right| \\ \gamma &= \frac{\alpha}{2} \end{aligned} \tag{5.7}$$

Combining (5.5)-(5.7) and putting the initial radius of the cell to $r = 3\hat{R}$ with $\hat{R} = 1\mu$m we end up with the following formula for the dimensionless parameters $R_1$ and $R_2$:

$$\frac{R_1}{\hat{R}} = \frac{3\pi}{\pi(1-\frac{\gamma}{\pi}) + \cos|\frac{\pi}{2} - \gamma|} \tag{5.8}$$

$$\frac{R_2}{\hat{R}} = 2\,R_1\,\cos|\frac{\pi}{2} - \gamma|. \tag{5.9}$$

In order to determine the number of rows corresponding to the contact zone where the affinity field is applied, the share of membrane in the contact zone on the total membrane is calculated from $\frac{R2}{U_T}$. It is convenient to change the size of the affinity field always in steps of two rows symmetrical around the middle of the mesh. Given that the share of the contact zone on the total membrane is normally some rational and not an even number the largest even number $E$ that is smaller than the calculated rational is taken as number of rows belonging to the contact zone where the affinity field is applied. The remainder is not neglected but incorporated in the simulations by applying a weaker affinity field to the two rows adjacent to the affinity field. This weaker field is chosen proportional to this remainder and we therefore have

$$B_i = \mathcal{A} \quad \text{for} \quad i \in \left[\frac{L-E}{2}, \frac{L+E}{2}\right] \tag{5.10}$$

$$B_i = \frac{L\frac{R2}{U_T} - E}{2}\mathcal{A} \quad \text{for} \quad i = \frac{L-E}{2} - 1 \wedge i = \frac{L+E}{2} + 1 \tag{5.11}$$

$$B_i = 0 \quad \text{for} \quad i \in \left[1, \frac{L-E}{2} - 2\right] \cap \left[\frac{L+E}{2} + 2, L\right] \tag{5.12}$$

with $L$ being the lattice size which was chosen $L = 100$ if not indicated otherwise and $\mathcal{A}$ being a real, positive number modelling the binding energy. The new volume can be calculated from

$$V = 2\pi R_1 \left(1 - \frac{\alpha}{2\pi}\right) L = \frac{6\pi^2\,(1-\frac{\gamma}{\pi})\,L}{\pi(1-\frac{\gamma}{\pi}) + \cos|\frac{\pi}{2} - \gamma|} \tag{5.13}$$

and we obtain for the relative volume change:

$$\frac{V}{V_0} = \frac{2\pi R_1\,(1-\frac{\alpha}{2\pi})\,L}{2\pi r L} = \frac{(1-\frac{\gamma}{\pi})}{(1-\frac{\gamma}{\pi}) + \frac{1}{\pi}\cos|\frac{\pi}{2} - \gamma|} \tag{5.14}$$

The new volume and the change in B both lead to a change in $H$ (5.2) and the energy difference to the last configuration $\Delta H$ determines the probability $P$ for the acceptance of the move.

### 5.3.2 Algorithm for Simulation of Spherical Cells

The algorithm for spherical cells is organised into three parts, which will be described in the following. $4 \times 10^7$ simulation steps took 1 hour on the computer about which details were given above.

**Algorithm**

1) Initiation

2) Time loop: for $(t = 0; t <$ final time; $t++)\{$

   i) Shape change (once a sweep)

   ii) Lipid diffusion$\}$

**Initiation** A given number of lipid $A$ molecules (in general between 14000 and 15000) is distributed randomly on the sphere surface. Given that we consider a continuous surface instead of a lattice we do not have to model every lipid explicitly but can only consider lipid $A$ molecules and can assume that the lipid $I$ molecules fill the gaps the lipid $A$ molecules leave on the surface. This approach allows to model larger systems than otherwise possible.

**Shape change** Once per sweep the shape of the cell can change by the choice of a new contact angle between cell body and contact zone. This new contact angle $\gamma$ is chosen to vary only slightly from the previous contact angle $g$ and is determined by $\gamma = g + \varrho$ where $\varrho$ is chosen randomly with $\varrho \in [-\frac{\pi}{20}, \frac{\pi}{20}]$. As in the cylinder case all further parameters of the cell can be calculated once the contact angle is chosen since we require the cell surface area to be conserved. We therefore have

$$R_{new} = \frac{3\pi}{\pi - \gamma + \cos|\frac{\pi}{2} - \gamma|} \tag{5.15}$$

$$R_{con} = R_{new} \times \cos|\frac{\pi}{2} - \gamma| \tag{5.16}$$

$$h_{new} = R_{new}(1 + \cos(\gamma)) \tag{5.17}$$

$$V_{new} = \frac{\pi}{3} h_{new}^2 (3R_{new} - h_{new}) \tag{5.18}$$

where $R_{new}$ is the radius of the new configuration, $R_{con}$ is the new radius of the contact zone, $h_{new}$ is the new height of the cell and $V_{new}$ is the new volume. The center of the sphere is always the zero point. By using equation (5.2) we can calculate the change in the inner energy $\Delta H$ introduced into the system through the shape change. Equation (5.1) then gives the probability for the move.

If the shape change is accepted the sphere needs to be replotted which implies that the lipids need to be mapped to new positions. The first step in this process is the determination of which spins are mapped onto the spherical part and which spins are mapped into the contact zone. Due to the differences if the contact angle $\gamma$ either increases or decreases it is sensible to consider the two cases separately.

**$\gamma$ increases** If the contact angle $\gamma$ increases the contact zone becomes enlarged. Given that we neither mean to stretch the membrane nor wish to change neighbor interactions more than necessary it is sensible to map the lipids above

a critical z-coordinate $z_c$ onto the new spherical cap and the lipids below the critical z-coordinate $z_c$ into the edge parts of the contact zone. Lipids which already reside in the contact zone stay at their position and fill the center part of the contact zone. Only the z-coordinate of the position vector of these lipids will change since the center of the sphere is always the zero point and for increasing $\gamma$ the z-coordinate of the contact zone therefore also increases. The critical z-coordinate $z_c$ is chosen such that the surface area of the old cap above this is equivalent to the new surface area cap. The surface area of a spherical cap is given by $A = 2\pi rh$ where h is the cell height of the spherical cap and we therefore obtain for the critical cell hight $h_c$ and the critical z-coordinate $z_c$

$$h_c = \frac{R_{new}h_{new}}{R_{old}} \tag{5.19}$$

$$z_c = R_{old} - h_c = R_{old} - \frac{R_{new}h_{new}}{R_{old}} \tag{5.20}$$

Every lipid which stays on the spherical part is turned such that its angle with the z-axis changes by

$$\psi = \theta_o - \theta_n. \tag{5.21}$$

The old angle of the lipid with the z-axis $\theta_o$ can easily be determined since the position of the lipid is known in cartesian coordinates and we therefore have $\theta_o = \arccos\frac{z}{R_{old}}$ where $z$ is the z-coordinate of the lipid. The new angle with the z-axis $\theta_n$ can be determined from

$$\theta_n = \theta_o \frac{\vartheta_{max_n}}{\vartheta_{max_o}} \tag{5.22}$$

where $\vartheta_{max_o} = \arccos\frac{h_c}{R_{old}}$ is the angle a position vector with z-coordinate $z_c$ would have with the z-axis and $\vartheta_{max_n} = \pi - \gamma$ is the maximal $\theta$ on the new sphere. The turn by $\psi$ around the z-axis is accomplished by

$$\vec{s}_n = \frac{R_{new}}{R_{old}} \left(\cos(\psi)\vec{s}_o + sin(\psi)\vec{v}\right) \tag{5.23}$$

where $\vec{s}_n$ is the new position vector of the lipid while $\vec{s}_o$ is the old position vector of the lipid. $\vec{v}$ is the vector which is orthogonal to the axis of the turn $\vec{u}$ given by

$$\vec{u} = \begin{pmatrix} \hat{y} \\ -\hat{x} \\ 0 \end{pmatrix} \tag{5.24}$$

where $\hat{x} = \frac{x}{\sqrt{(x^2+y^2)}}$, $\hat{y} = \frac{y}{\sqrt{(x^2+y^2)}}$ and the original position vector $\vec{s}_o$. We therefore have

$$\vec{v} = \vec{u} \times \vec{s}_o. \tag{5.25}$$

The lipids which have a z-coordinate less than $z_c$ but do not already reside in the contact zone need to be mapped there by

$$x_n = \left(R_{con_o} + \frac{(R_{con} - R_{con_o})(z + h_{old} - R_{old}}{z_c + h_{old} - R_{old}}\right) \frac{x}{\sqrt{x^2 + y^2}} \quad (5.26)$$

$$y_n = \left(R_{con_o} + \frac{(R_{con} - R_{con_o})(z + h_{old} - R_{old})}{z_c + h_{old} - R_{old}}\right) \frac{y}{\sqrt{x^2 + y^2}} \quad (5.27)$$

$$z_n = R_{new} - h_{new}. \quad (5.28)$$

where $R_{con_o}$ is the contact radius of the sphere before the shape change. For all lipids already residing in the contact zone we have

$$x_n = x \quad (5.29)$$

$$y_n = y \quad (5.30)$$

$$z_n = R_{new} - h_{new}. \quad (5.31)$$

**$\gamma$ decreases** If the contact angle $\gamma$ decreases the contact zone shrinks and we need to consider three different cases. Those lipids which are in the central part of the contact zone stay in the contact zone while those lipids which are situated at the edge are mapped onto the spherical part. The lipids on the spherical part stay on the spherical part but need to be mapped to new locations since the shapes of the old and the new cap differ. The latter is accomplished by using (5.21) and (5.23) again with $\theta_o = \arccos \frac{z}{R_{old}}$ where z is the z-coordinate of the lipid. $\theta_n$ is now given by

$$\theta_n = \theta_o \frac{\vartheta_{max_n}}{\vartheta_{max_o}} \quad (5.32)$$

where

$$\vartheta_{max_n} = \arccos\left(\frac{R_{new} - h_{old}\frac{R_{old}}{R_{new}}}{R_{new}}\right) \quad (5.33)$$

and $\vartheta_{max_o} = \pi - \gamma$ as before.

The lipids which reside on the original sphere in the contact zone but whose distance to the center $d$ is larger than the radius of the new contact zone $R_{con}$ need to be mapped onto the spherical part of the new sphere. This is accomplished by using (5.21) and (5.23) again with

$$\theta_n = \pi - \gamma - \frac{(\pi - \gamma - \vartheta_{max_o})(d - R_{con})}{R_{con_o} - R_{con}} \quad (5.34)$$

and $\theta_o = \arccos\left(\frac{z}{|\vec{s}_o|}\right)$.

The lipids which stay in the contact zone only change the z-coordinate to $z = R_{new} - h_{new}$.

**Lipid Diffusion** In every step a lipid is chosen randomly and is allowed to move at maximum the distance $\delta = \frac{3\pi}{20}$. The move can only be accepted if the lipid stays in a minimal distance $d_{min}$ to all other lipids. The acceptance probability is otherwise given by (5.1).

If the spin which is chosen to be moved happens to be located on the spherical part then it is turned around a randomly chosen axis $\vec{u}$ (of length $R_{old}$) by a randomly chosen angle $\psi \in [0, \frac{\delta}{R_{old}}]$. For this move again equations 5.21) and (5.23) can be used. If the lipid moves beyond the edge of the spherical cap it needs to be projected on the contact zone by

$$x_n = \sigma \frac{x_o}{L_{xy}} \tag{5.35}$$

$$y_n = \sigma \frac{y_o}{L_{xy}} \tag{5.36}$$

$$z_n = R_{new} - h_{new}. \tag{5.37}$$

where $\sigma = R_{con_o} - d$ and $L_{xy} = \sqrt{x^2 + y^2}$. $d$ is the arclength beyond the spherical cap and can be calculated from

$$d = R_{old}(\psi - \arccos \chi) \tag{5.38}$$

$$\chi = \frac{z(R_{old} - h_{old})}{z^2 + u^2} + \sqrt{\Upsilon} \tag{5.39}$$

$$\Upsilon = \frac{u^2 - (h_{old} - R_{old})^2}{z^2 + u^2} + \left( \frac{z(h_{old} - R_{old})}{u^2 + z^2} \right)^2 \tag{5.40}$$

If the contact zone is so small that lipids can even cross the contact zone when moving from one spherical part to the other, then this needs also be considered, but the method of mapping has already been described above.

If the chosen spin is located in the contact zone the lipid can only move in two dimensions and the movement of the lipid is modelled by adding a displacement vector $\vec{v}_d = \frac{3\pi}{20}\vec{u}$ where $\vec{u}$ is a unit vector in any random direction with the z-component being zero. The new coordinates of the lipid are then given by $\vec{s}_n = \vec{s}_o + \vec{v}_d$. If the lipid happens to move the distance $D$ beyond the limit of the contact zone it is mapped onto the spherical part by setting

$$\psi = \frac{D}{R_{old}} \tag{5.41}$$

and using (5.23, 5.24, 5.25).

# Chapter 6

# Results of the Membrane Simulation

## 6.1 Results for cells of cylinder shape

The cylinder cell simulation is first tested by monitoring the diffusion of the lipids on the cell surface. Subsequently the behaviour of lipids in the contact zone, especially with respect to domain formation, is investigated.

### 6.1.1 Diffusion of lipids in the membrane

The Kawasaki algorithm, which was used in the simulation, allows to model the diffusion of lipids in the membrane. As discussed before [17] we expect for weak interactions between lipids

$$s^2 = 2D_T t \tag{6.1}$$

where $s$ is the distance travelled from the starting position, $D_T$ is the diffusion coefficient and $t$ the time passed. This linear relation between $s^2$ and $t$ is indeed observed for $J = 0.05$ as can be seen in Figure 6.1. Due to the applied field in x-direction, lipid A (spin 1 in Figure 6.1) moves slower in that direction, while the movement in y-direction is free. The other lipids feel the field less and are only inhibited in their diffusion in x-direction if an exchange with lipid $A$ is impossible due to the applied field. The difference between the diffusion velocity in x- and y-direction is therefore much smaller than in case of lipid $A$.

#### Concentration of lipid A in the contact zone

In the simulation an external field $B$ attracts lipid $A$ but is indifferent towards the other lipid class. Simulation for different proportions of lipid $A$ on the total lipid amount, shows that the higher the share of lipid $A$, the faster the contact zone is completely filled with lipid $A$ (see Figure 6.2). In equilibrium the contact zone is therefore always completely filled with lipid $A$ (see Figure 6.3) if not strong interactions between the lipids ($J$ large) lead to trapping of lipid $A$ in small patches elsewhere on the cylinder. Then the minimal energy configuration cannot attained.

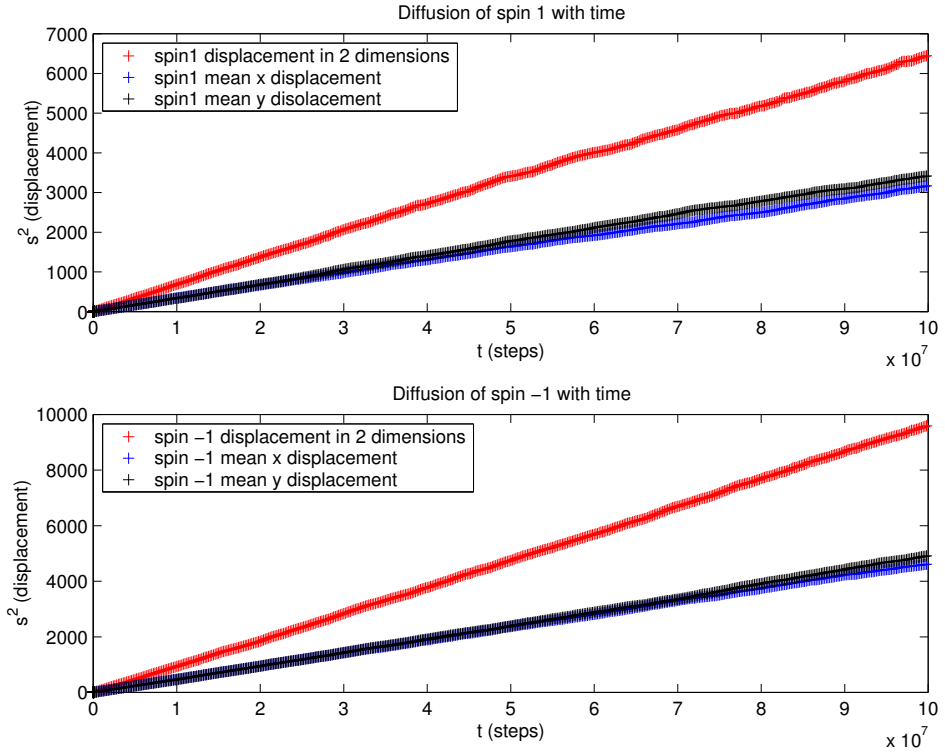



Figure 6.1: Diffusion of lipids on the cylinder cell surface. (*top*) Lipid $A$: Due to the applied field, lipid $A$ diffuses more slowly in x-direction than in y-direction. (*bottom*) Lipid I: For lipid $I$ diffusion is almost the same in both directions. Lipid $I$ is only effected by the field when it is blocked by interaction with lipid $A$ which senses the field.

### 6.1.2 Equilibrium cell shape

If we leave the contact angle free to change the equilibrium shape is balanced between the tendency to enlarge the contact zone to its maximum due the attractive potential $B$ and an opposing force due to the volume reduction which raises the osmotic pressure. From the analytic analysis given above we know how the height of the sperical cells depends on the sticker density $n$ and on the applied field $U$ if lipids cannot interact. We can reproduce the result by setting $J = 0$ in our simulation (see Figure 6.4). Given that mathematical analysis cannot be used to derive any results if lipids can interact, it is especially interesting to study that case numerically. For small interaction potential ($J = 0.05$) or high temperatures ($T = 50$) we reproduce the analytic results (see Figure 6.4 and 6.5). For large interaction potentials ($J \gg 0$) at low temperatures the lipids form patches on the cell surface and are trapped in this configuration. The minimal energy configuration cannot therefore be attained within reasonable time and the cylinder does not flatten as quickly as is the case when the temperature is high or the interaction potential J small (data not shown).

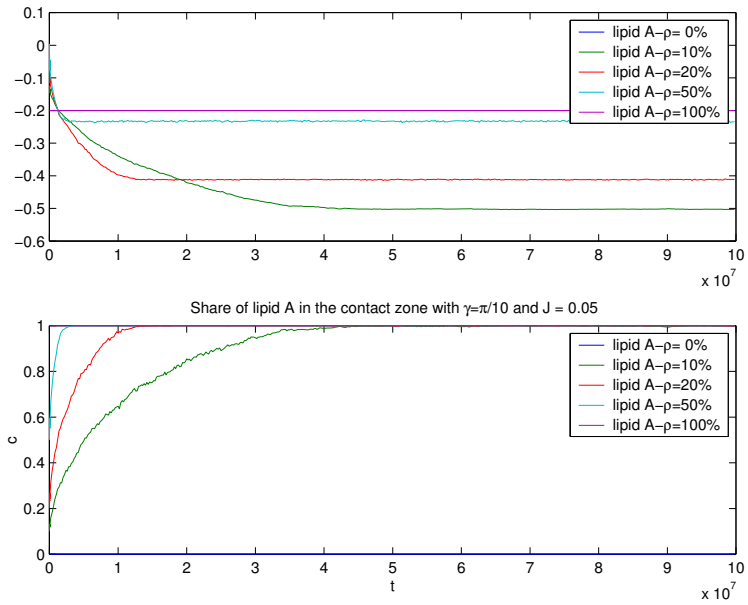



Figure 6.2: (*top*)Inner energy and (*bottom*) concentration of lipid A in the contact zone for various shares of A on the total lipid amount

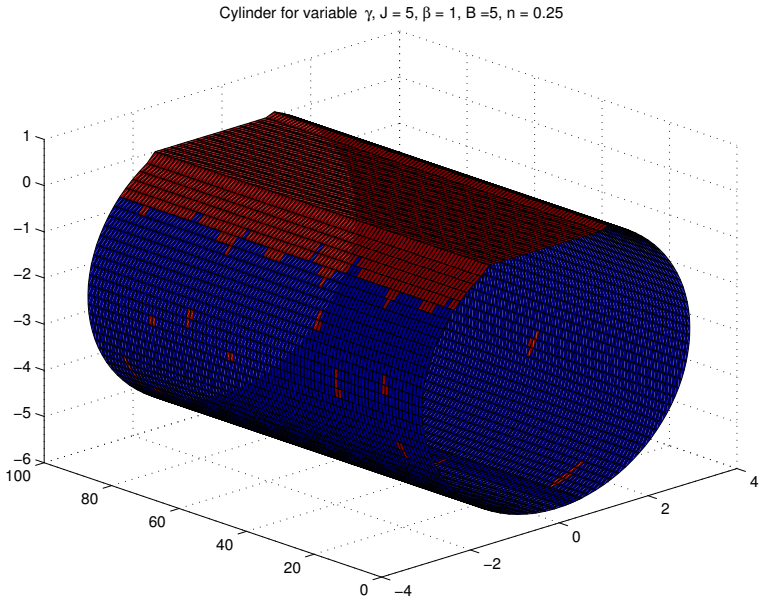



Figure 6.3: Distribution of lipids in equilibrium when the contact angle $\gamma$ is left to vary and the lipid density is $n = 0.25$. Those lipids A (red) which do not find space in the contact zone accumulate at the border.

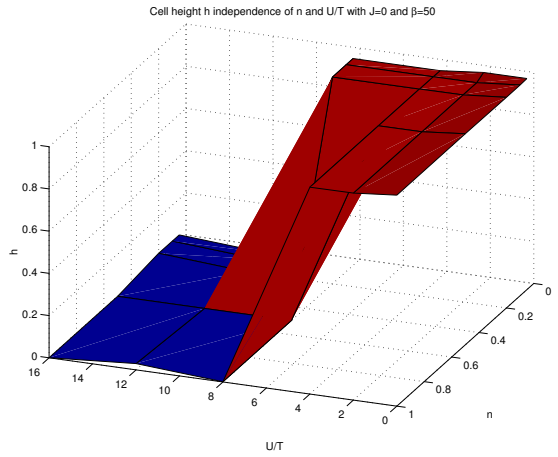



Figure 6.4: Cell height in dependence of sticker density $n$ and binding energy $\frac{U}{T}$ with no interactions between lipids ($J = 0$) and $T = 50$

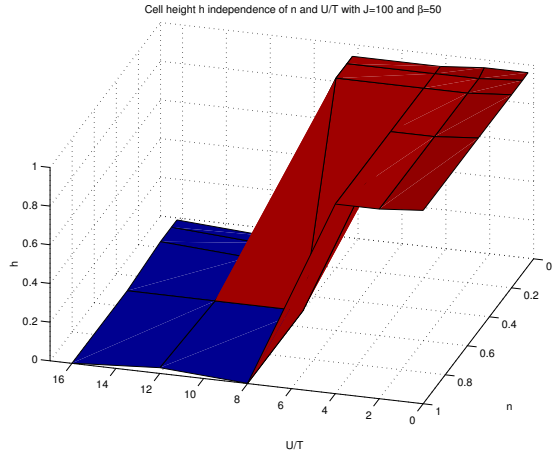



Figure 6.5: Cell height in dependence of sticker density $n$ and binding energy $\frac{U}{T}$ with interactions between lipids ($J = 100$) and $T = 50$

### 6.1.3 Domain Formation and Phase Transition

**Temperature dependent Domain Formation** Dependent on the temperature and on the applied field the two lipid sorts can be expected to organise in domains. This can be investigated by determination of the correlation function which is defined as [6]

$$\begin{aligned} G(r) &= \sum_{|r_i - r_j| = r} (< \lambda_i - < \lambda_i >>< \lambda_j - < \lambda_j >>) \\ &= \sum_{|r_i - r_j| = r} (< \lambda_i \lambda_j > - < \lambda_i >< \lambda_j >) \end{aligned}$$

and can therefore be determined from experimental data by

$$G(r) = \frac{1}{N_r} \sum_{|r_i - r_j| = r} \left( \lambda_i \lambda_j - \frac{1}{N^2} (\sum_k \lambda_k)^2 \right). \tag{6.2}$$

where $|r_i - r_j|$ denotes the distance between the two lipids $\lambda_i$, $\lambda_j$, $N_r$ the number of lipids in distance $r$, and $N$ the total number of lipids. If two lipids in distance $r$ belong to the same lipid class we therefore have a positive contribution to $G(r)$ while for two lipids in distance $r$ from different lipid classes we have a negative contribution to $G(r)$. From this we see that the decrease of $G(r)$ with distance $r$ tells us something about the size of lipid clusters. A measure of the size of such domains is the correlation length $\zeta$ which is in two dimension related to $G(r)$ as given below

$$G(r) = C K_0 \left( \frac{r}{\zeta} \right) \tag{6.3}$$

where $C$ is a constant, $K_0$ a modified Bessel function and $\zeta$ the correlation length [6]. As is clear from (6.3) the correlation falls off exponentially with distance $r$. At separations of more than a few times $\zeta$ the fluctuations in the order parameter are essentially uncorrelated. At the critical point the correlation length is only limited by the physical size of the system and the fluctuations are no longer microscopic. The correlation length can only be obtained from the measured correlation function by fitting the modified Bessel function $K_0$ to the correlation function. Given that we have two free parameters, this step is work intensive and as we are only interested in estimating the point of phase transition the exponential shape of the correlation function was exploited and an exponential function is fitted to the correlation function where we assume $G(r) \sim \exp(-\frac{r}{\xi})$. In order to estimate how well the parameter $\xi$ obtained from the exponential fit correlates with the correlation length $\zeta$ obtained from fitting a Bessel function, the modified Bessel function $K_0$ is plotted with the $\zeta = \xi$. As Figure 6.6 shows the correlation length $\zeta$ must be much larger than $\xi$ in order to fit the correlation functions obtained in experiments.

We however also see that for both the Bessel functions and the exponential functions $\zeta$ and $\xi$ respectively become smaller the steaper the correlation function is. We can therefore expect $\xi$ obtained from the exponential fit to at

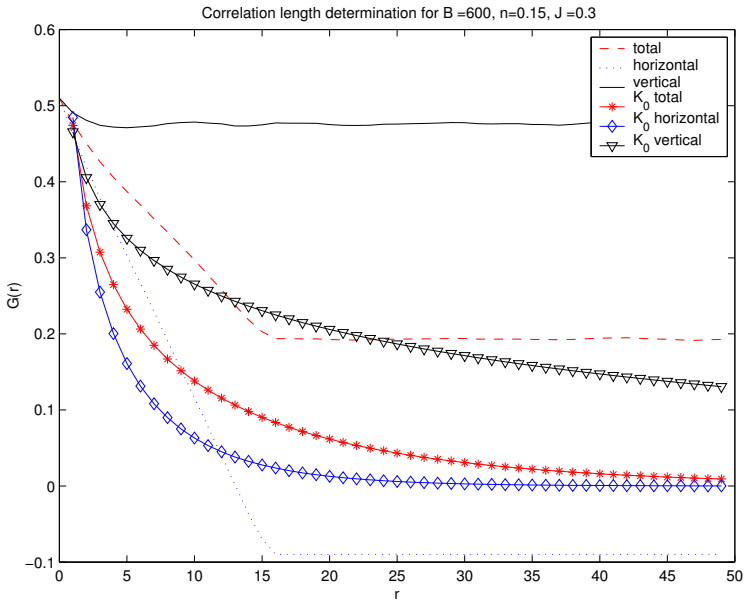



Figure 6.6: The correlation function for the cylinder cells fitted with a modified Bessel function.

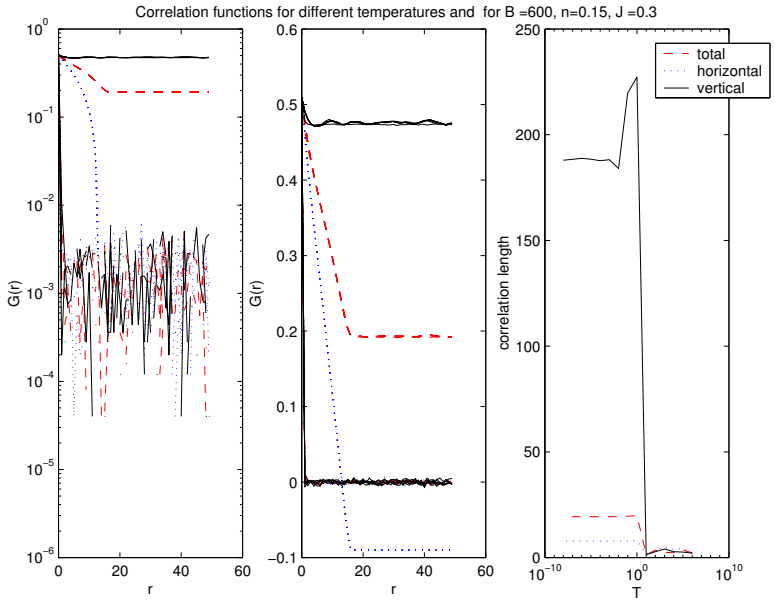



Figure 6.7: The correlation function for the cylinder cells for $J \neq 0$. (*left*) The correlation function on a logarithmic scale for different temperatures measured in vertical or horizontal or both directions. (*middle*) The correlation function on a linear scale for different temperatures measured in vertical or horizontal or both directions. (*right*) A parameter determined out of the correlation function given in the two panels on the left and indicating a phase transition at $T = 1$.

least indicate approximately the point of phase transition since a large change in the correlation function will also have an impact on the parameter $\xi$ obtained from the exponential fit. The result is shown in Figure 6.7 and we see that the parameter $\xi$ indicates a phase transition at $\beta = 1$. The impact of the lipid-lipid interactions on the phase transition was investigated by repeating the same measurement for $J = 0$ and Figure 6.8 shows that the lipid-lipid interaction does not change the equilibrium domain size and the critical point for phase transition.

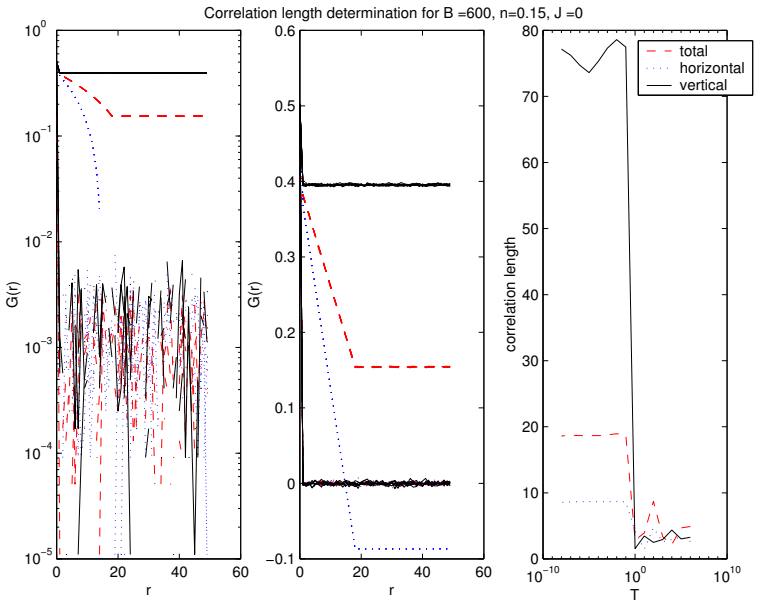



Figure 6.8: The correlation function for the cylinder cells for $J = 0$. (*left*) The correlation function on a logarithmic scale for different temperatures measured in vertical or horizontal or both directions. (*middle*) The correlation function on a linear scale for different temperatures measured in vertical or horizontal or both directions. (*right*) A parameter determined out of the correlation function given in the two panels on the left and indicating a phase transition at $T = 1$.

**Affinity Field induced Domain Formation** The affinity field attracts lipids of one sort into a special domain the contact zone. We can therefore expect that an increase in the field strength will lead to an increase in the size of the domains. In case of the cylinder cell it will also introduce an anisotropie into the correlation function since in vertical direction the domains are only limited by the size of the system upon formation of the contact zone while in horizontal direction the size of the domains is much smaller. Figure 6.9 indeed shows that the anisotropie becomes stronger the higher the applied field $B$ and this is also intuitively understandable.

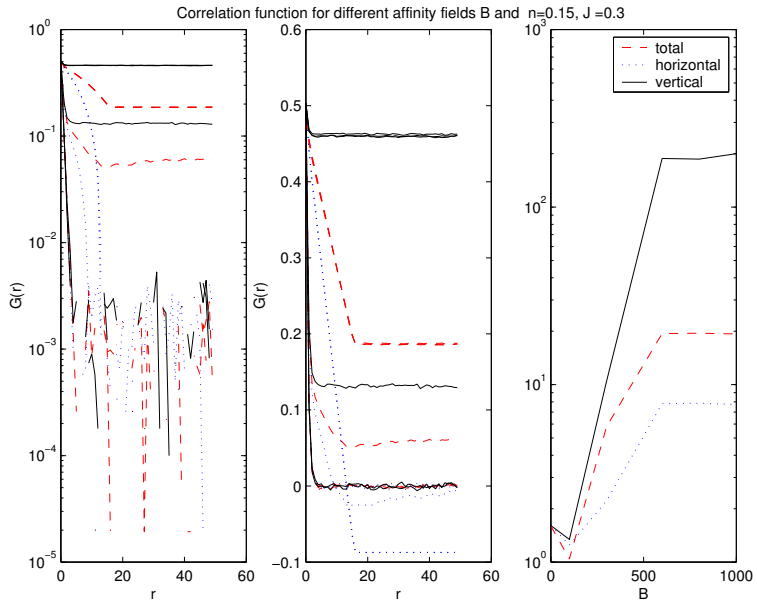



Figure 6.9: The correlation function for the cylinder cells for different affinity fields $B$. (*left*) The correlation function on a logarithmic scale for different affinity fields $B$ measured in vertical or horizontal or both directions. (*middle*) The correlation function on a linear scale for affinity fields $B$ measured in vertical or horizontal or both directions. (*right*) A parameter determined out of the correlation function given in the two panels on the left and showing an anisotropie in the correlation function for increasing affinity field $B$.

## 6.2 Results for Cells of Sperical Shape

Figure 6.10 shows the initial distribution of lipids on the sphere. As expected, the affinity field $B$ which is acting on the contact zone attracts lipids $A$ and leads to their accumulation in the contact zone (Figure 6.12 top panel and Figure 6.11). The equilibrium shape depends on the applied field $B$ and the concentration of osmotic relevant particles $\mathcal{N}_{in}$ inside the cell. Given that it takes more than $10^9$ time steps in order to attain the equilibrium for $T = 0.01$ (see Figure 6.12 top panel) and $4 \times 10^7$ simulation steps take about 1 hour, the study of the equilibrium behaviour for various sticker densities $n$, affinity fields $B$ and temperatures $T$ has to be postponed to later research. From the data obtained so far we can however expect similar data as for the cylinder simulations.

Furthermore it will be interesting to study the domain formation in some more detail. As we do not use any grid, and spins are free to locate anywhere on the sphere we can expect hexagonal array formation of lipid $A$ in the contact zone once the contact zone is completely filled since upon hexagonal array formation the lipids have the densest packing allowing a maximal number of lipids to be attracted by the affinity field. Such hexagonal packing has also been observed in other studies of lipid dynamics [50].

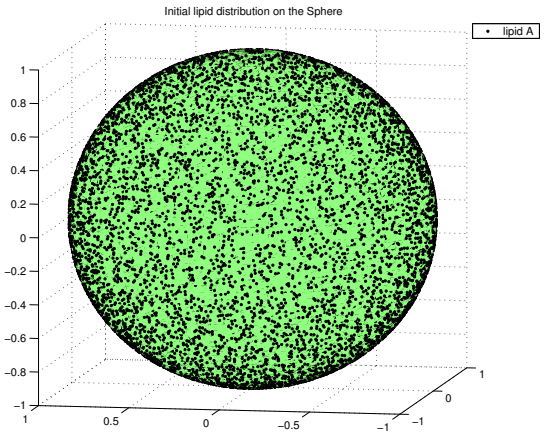



Figure 6.10: Initial lipid distribution on spherical cells

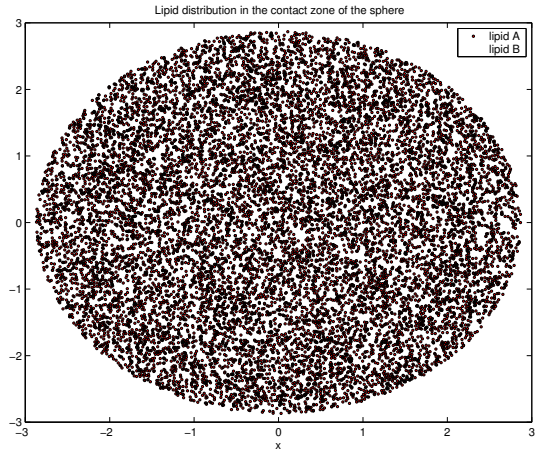



Figure 6.11: Contact zone of spherical cell. Lipid $A$ accumulates in the contact zone.

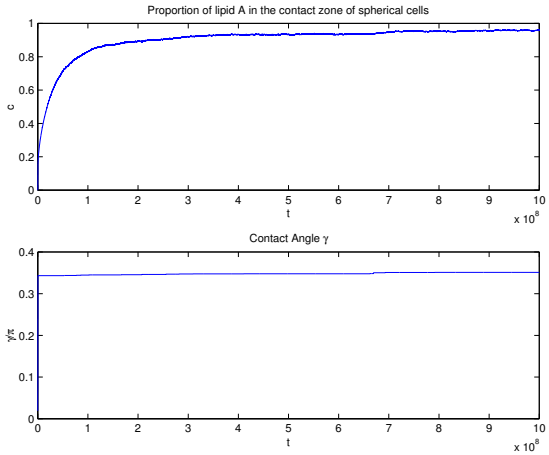



Figure 6.12: (*top*) Proportion of lipid $A$ in the contact zone. (*bottom*) Contact angle $\frac{\gamma}{\pi}$

# Chapter 7

# Conclusion from the Membrane Studies

## 7.1 Summary of Results and Discussion

The analysis of the lipid behaviour on the cell surface upon cell-cell interaction shows that the driving force for lipid domain formation in the contact zone are lipid-protein interactions which are modelled as affinity field applied in that region. Interactions between lipids seem not to be important for this phenomenon to occur and may even prohibit a formation of this equilibrium conformation due to trapping of lipids in patches elsewhere on the cell surface. The size of the contact zone strongly depends on the sticker density, the height of the applied field and the force opposing volume reduction as was also deduced analytically [30]. Domain formation depends on the height of the applied field and the strength of lipid interaction as analysed by the use of correlation functions.

First results from the simulations of spherical cells show that the general behaviour is similar to that of cylinder cells. It will however be interesting to study the lipid domain structure in the contact zone of spherical cells in some greater detail since in this simulation no grid is used and lipids are free to arrange in the formation which is energetic most favorable. This formation is expected to be hexagonal.

## 7.2 Further Work

As discussed above, the simulation of spherical cells needs to be further analysed with respect to lipid arrangement in the contact zone. Further on, the model described in this dissertation represents the most simple possible for the processes wished to be investigated. It would however be interesting not only to consider attracted and indifferent lipids but to distinguish between protein stickers and these lipids and to add repeller proteins. In such a simulation, the protein stickers would be attracted to the contact zone and lipid A would be attracted to these stickers while repelled by repeller proteins. One can then investigate three different szenarios:

1) The repellers are also attracted to the contact zone which should lead to domain formation inside the contact zone.

2) Repelleres and stickers have different attraction potential to the contact zone which should lead to the exclusion of the one which feels less attraction.

3) Stickers and repellers have different length such that one sort of them can interact with the other cell while being only at the edge of the contact zone. We would expect to see ring formation in this case.

In order to further understand antigen extraction it would also be interesting to investigate how these domains may support a budding of the membrane. This is especially interesting if the mixture of stickers and repellers leads to the formation of several smaller domains.

Finally it would be interesting to model two interacting cells explicitly. We are then free to change the sticker density independently on both cells which may yield interesting equilibrium conformations.

# Bibliography


[1] B. Alberts, D. Bray, J. Lewis, M. Raff, K. Roberts, and J.D. Watson, *Molecular biology of the cell*, Garland Publisher, 1989.

[2] D. Allen, A. Cumano, R. Dildrop, C. Kocks, K. Rajewsky, N. Rajewsky, J. Roes, F. Sablitzky, and M. Siekevitz, *Timing, genetic requirements and functional consequences of somatic hypermutation during b cell development*, Immunol. Rev. **96** (1987), 5–22.

[3] C. Arpin, J. Dechanet, C. Van Kooten, P. Merville, G. Grouard, F. Briere, J. Banchereau, and Y.J. Liu, *Generation of memory B cells and plasma cells in vitro*, Science **268** (1995), 720–722.

[4] F.D. Batista, D. Iber, and M.S. Neuberger, *B cells aquire antigen from target cells after synapse formation*, Nature **411** (2001), 489–494.

[5] C. Berek and C. Milstein, *The dynamic nature of the antibody repertoire*, Immunological Reviews **105** (1988), 5–26.

[6] J. Binney, *The theory of critical phenomena : an introduction to the renormalization group*, Oxford University Press, 1992.

[7] E.A. Clark and J.A. Ledbetter, Nature **367** (1994), 425–428.

[8] J.J. Cohen, R.C. Duke, V.A. Fadok, and K.S. Sellins, *Apoptosis and programmed cell death in immunity*, Annu. Rev. Immunol. **10** (1992), 267ff.

[9] E.M. Danielsen and B. van Deurs, J. Cell Biology **131** (1995), 939–950.

[10] C. García de Vinuesa, M.C. Cook, J. Ball, M. Drew, Y. Sunners, M. Cascalho, M. Wabl, G.G.B. Klaus, and I.C.M. MacLennan, *Germinal centers without t cells*, J. Exp. Med. **191** (2000), 485–493.

[11] M.L. Dustin and J.A. Cooper, *The immunological synapse and the actin cytoskeleton: molecular hardware for t cell signaling*, Nat. Immunol. **1** (2000), 23–29.

[12] T. Friedrichson and T.V. Kurzchalia, *Microdomains of GPI-anchored proteins in living cells revealed by crosslinking*, Nature **394** (1998), 802–805.

[13] C.C.G. Goodnow, *Chance encounters and organized rendezvous*, Immunological Reviews **156** (1997), 5–10.

[14] D. Gray, Immunology **65** (1988), 73–79.

[15] S. Han, B. Zheng, J. DalPorto, and G. Kelsoe, J. Exp. Med. **182** (1995), 1635–1644.

[16] L.G. Hannum, A.M. Haberman, S.M. Anderson, and M.J: Shlomchik, *Germinal center initiation, variable gene region hypermutation, and mutant B cell selection without detectable immune complexes on follicular dendritic cells*, J. Exp. Med. **192** (2000), 931–942.

[17] D. Iber, *Membrane structure and function*, Special Topic in Numerical Methods in Medicine (2001).

[18] J. Israelachvili, *Intermolecular and surface forces*, Academic Press, 1992.

[19] J. Jacob, R. Kassir, and G. Kelsoe, *In situ studies of the primary immune response to (4-hydroxy-3-nitrophenyl)acetyl. I. the architecture and dynamics of responding cell populations*, J. Exp. Med. **173** (1991), 1165–1175.

[20] J. Jacob and G. Kelsoe, *In situ studies of the primary immune response to (4-hydroxy-3-nitrophenyl)acetyl. II. a common clonal origin for periarteriolar lymphoid sheath-associated foci and germinal centers*, J. Exp. Med. **176** (1992), 679–687.

[21] J. Jacob, J. Przylepa, C. Miller, and G. Kelsoe, *In situ studies of the primary immune response to (4-hydroxy-3-nitrophenyl)acetyl. III. the kinetics of V region mutation and selection in germinal center B cells*, J. Exp. Med. **178** (1993), 1293–1307.

[22] C.A. Janeway and P. Travers, *Immunology. the immune system in health and disease*, Garland Publisher, 1997.

[23] G. Kelsoe, *The germinal center: a crucible for lymphocyte selection*, Semin. Immunol. **8** (1996), 179ff.

[24] A.K. Kenworthy, N. Petranova, and M. Edidin, *High-resolution FRET microscopy of cholera toxin B-subunit and GPI-anchored proteins in cell plasma membranes*, Molecular Biology of the Cell **11** (2000), 1645–1655.

[25] T.B. Kepler and A.S. Perelson, *Somatic hypermutation in B cells: an optimal control treatment*, J. Theor. Biol. **164** (1993), 37–64.

[26] C. Kesmir and R.J. de Boer, *A mathematical model on germinal center kinetics and termination*, Journal of Immunology **163** (1999), 2463–2469.

[27] F.G.M. Kroese, A.S. Wubena, H.G. Seijen, and P. Nieuwenhuis, Eur. J. Immunol. **17** (1987), 1069–1072.

[28] O. Leupin, R. Zaru, T. Laroche, S. Muller, and S. Valitutti, *Exclusion of CD45 from the T-cell receptor signaling area in antigen-stimulated T lymphocytes*, Curr Biol. **9** (2000), 277–280.

[29] R. Lipowsky, *Vesicles and biomembranes*, Encyclopedia of Applied Physics **23** (1998), 199–222.

[30] R Lipowsky, personal communication (2001).

[31] Y.-J. Liu, C. Barthelemy, and O. de Bouteiller, *The differences in survival and phenotype between centroblasts and centrocytes*, InVivo Immunology (1994), 213–218.

[32] Y.L. Liu, J. Zhang, E.Y.T. Chan, and I.C.M. MacLennan, *Sites of specific B cell activation in primary and secondary responses to T-cell-dependent and T-cell-independent antigens*, Eur J Immunol **21** (1991), 2951–2962.

[33] M. Mackey, Leverhulme Trust Lecture Series in Mathematical Biology (2001).

[34] I.C.M. MacLennan, personal communication (2001).

[35] I.C.M. MacLennan, C. Garciá de Vinuesa, and M. Casamayor-Palleja, Phil Trans R Soc Lond B **355** (2000), 345–350.

[36] I.C.M. MacLennan, Y.L. Liu, S. Oldfield, J. Zhang, and P.J.L. Lane, Curr Top Microbiol Immunol **159** (1990), 37–64.

[37] T. Manser, *The efficiency of antibody affinity maturation: can the rate of B-cell division be limiting?*, Immunology Today **11** (1990), 305–308.

[38] M. Meyer-Hermann, A. Deutsch, and M. Or-Guil, *Recycling probability and dynamical properties of germinal center reactions*, J Theor Biol **210** (2001), 265–285.

[39] C.R. Monks, B.A. Freiberg, H. Kupfer, N. Sciaky, and A. Kupfer, *Three-dimensional segregation of supramolecular activation clusters in T cells*, Nature **395** (1998), 82–86.

[40] CR Monks, H. Kupfer, I. Tamir, A. Barlow, and A. Kupfer, *Selective modulation of protein kinase c-theta during t-cell activation*, Nature **385** (1997), 83–86.

[41] S. Muller, S. Demotz, C. Bulliard, and S. Valitutti, *Kinetics and extent of protein tyrosine kinase activation in individual T cells upon antigenic stimulation*, Immunology **97** (1999), 287–293.

[42] S. Munro, *Localization of proteins to the golgi apparatus*, Trends Cell Biol **8** (1998), no. 1, 11–15.

[43] M.E.J. Newman and G.T. Barkema, *Monte carlo methods in statistical physics*, Oxford University Press, 1999.

[44] M. Oprea and A.S. Perelson, *Somatic mutation leads to efficient affinity maturation when centrocytes recycle back to centroblasts*, Journal of Immunology **158** (1997), 5155–5162.

[45] J.M. Dal Porto, A.M. Haberman, M.J. Shlomchik, and G. Kelsoe, *Antigen drives very low affinity B cells to become plasmacytes and enter germinal centers*, J.Immunol. **161** (1998), 5373–5381.

[46] S.Y. Qi, J.T. Groves, and A.K. Chakraborty, *Synaptic pattern formation during cellular recognition*, PNAS **98** (2001), 6548–6553.

[47] M.D. Radmacher, G. Kelsoe, and T.B. Kepler, *Predicted and inferred waiting times for key mutants in the germinal centre reaction: Evidence for stochasticity in selection*, Immunology and Cell Biology **76** (1998), 373–381.

[48] J. Ren, S. Lew, Z. Wang, and E. London, *Transmembrane orientation of hydrophobic $\alpha$-helices is regulated both by the relationship of helix length to bilayer thinkness and by the cholesterol concentration*, Biochemistry **36** (1997), 10213–10220.

[49] S.K. Rodal, G. Skretting, Q. Garred, F. Vilhardt, B.van Deurs, and K. Sandvig, Mol Biol Cell **10** (1999), 961–974.

[50] M.C. Sabra, J.C.M. Uitdehaag, and A. Watts, *General model for lipid-mediated two-dimensional array formation of membrane proteins: application to bacteriorhodopsin*, Biophysical Journal **75** (1998), 1180–1188.

[51] M. Shannon and R. Mehr, *Reconciling repertoire shift with affinity maturation: The role of deleterious mutations*, Journal of Immunology **162** (1999), 3950–3956.

[52] K.M. Shokat and C.C.G. Goodnow, Nature **375** (1995), 334–338.

[53] K. Simons and E. Ikonen, *Functional rafts in cell membranes*, Nature **387** (1997), no. 5, 569–572.

[54] K.G.C. Smith, A. Light, G.J.V. Nossal, and D.M. Tarlinton, *The extent of affintiy maturation differs between the memory and antibody-forming cell compartments in the primary immune response*, EMBO **16** (1997), 2996–3006.

[55] K.G.C. Smith, U. Weiss, K. Rajewski, G.J.V. Nossal, and D.M. Tarlinton, *Bcl-2 increases memory b cell recruitment but does not perturb selection in the germinal centers*, Immunity **1** (1994), 803–813.

[56] M.E. Smith and W.L. Ford, Immunology **49** (1983), 83–94.

[57] A.I. Sperling, J.R. Sedy, N. Manjunath, A. Kupfer, B. Ardman, and J.K. Burkhardt, *TCR signaling induces selective exclusion of CD43 from the t cell-antigen-presenting cell contact site*, J Immunol. **161** (1998), 6459–6462.

[58] L. Stryer, *Biochemistry*, W.H. Freeman and Company, 1995.

[59] A. Subtil, I. Gauderov, K. Kobylarz, M.A. Lampson, J.H. Keen, and T.E. McGraw, Proc Natl Acad Sci **96** (1999), 6775–6780.

[60] M.L. Thomas, Current Opinion in Immunology **11** (1999), 270–276.

[61] R. Varma and S. Mayor, *GPI-anchored proteins are organized in submicron domains at the cell surface*, Nature **394** (1998), 798–801.

[62] K.A. Vora and T. Manser, *Altering the antibody repertoire via transgene homologous recombination: evidence for global and clone-autonomous regulation of antigen-driven B cell differentiation*, J Exp Med **181** (1995), 271–281.

[63] A. Wilde, E.C. Beattie, L. Lem, D.A. Riethof, S.-H. Liu, W.C. Mobley, P. Soriano, and F.M. Brodsky, Cell **96** (1999), 677–687.

[64] C. Wulfing and M.M. Davis, *A receptor/cytoskeletal movement triggered by costimulation during t cell activation*, Science **282** (1998), 2266–2269.

# Appendix A

# Glossary

The definitions in this Glossary follow those given in [22].

The **adaptive** immune response is the response of antigen-specific lymphocytes to antigen, including the development of immunological memory. Adaptive immune responses are generated by clonal selection of lymphocytes. Adaptive immune responses are distinct from innate and non-adaptive phases of immunity, which are not mediated by clonal selection of antigen-specific lymphocytes. Adaptive immune responses are also known as **acquired immune responses**.

**Affinity** is the strength of binding of one molecule to another at a single site, such as the binding of a monovalent Fab fragment of antibody to a monovalent antigen.

**Affinity maturation** refers to the increase in affinity of the antibodies produced during the course of a humoral immune response. It is particularly prominent in secondary and subsequent immunizations.

An **antibody** is a protein which binds specifically to a particular substance - the antigen. Each antibody molecule has a unique structure, that enables it to bind specifically to its corresponding antigen, but all antibodies have the same overall structure and are known collectively as immunoglobulins. Antibodies are produced by plasma cells in response to infection or immunization, and bind to and neutralize pathogens or prepare them for uptake and destruction by phygocytes.

An **antigen** ($Ag$) is any molecule that can bind specifically to an antibody.

T and B lymphocytes collectively bear on their surface highly diverse **antigen receptors** capable of recognizing a wide diversity of antigens. Each individual lymphocyte bears receptors of a single antigen specificity.

**Antigen presentation** describes the display of antigen as peptide fragments bound to MHC molecules on the surface of a cell; all T cells recognize antigen

only when it is presented in this way.

**Antigen presenting cells** are highly specialized cells that can process antigens and display peptide fragments on the cell surface together with molecules required for lymphocyte activation. The main antigen-presenting cells for T cells are dendritic cells, macrophages, and B cells, whereas the main antigen-presenting cells for B cells are follicular dendritic cells.

**Apoptosis**, or programmed cell death, is a form of cell death in which the cell activates an internal death program.

A **B cell** or **B lymphocyte**, is one of the two major types of lymphocyte. The antigen receptor on B lymphocytes, sometimes called the B-cell receptor, is a cell-surface immunoglobulin. On activation by antigen, B cells differentiate into cells producing antibody molecules of the same antigen-specificity as this receptor.

**Centroblasts** ($B$) are large, rapidly dividing cells found in germinal centres, and are the cells in which somatic hypermutation is believed to occur. Antibody-secreting and memory B cells derive from these cells.

**Centrocytes** ($C$) are the small, non-proliferating B cells in germinal centres that derive from centroblasts. They may mature into antibody-secreting plasma cells or memory B cells, or may undergo apoptosis, depending on their receptor's interaction with antigen.

**Effector cells** are lymphocytes that can mediate the removal of pathogens from the body without the need for further differentiation , as distinct from naive lymphocytes, which must proliferate and differentiate before they can mediate effector functions, and memory cells, which must differentiate and often proliferate before they become effector cells.

The **follicular dendritic cells** (FDC) of lymphoid follicles are cells of uncertain origin with long branching processes that make intimate contact with many different B cells. They have Fc receptors that are not internalized by receptor-mediated endocytosis and thus hold antigen:antibody complexes on the surface for long periods. These cells are crucial in selecting antigen-binding B cells during antibody responses.

**Germinal centres** (GC) in secondary lymphoid tissues are sites of intense B-cell proliferation, selection, maturation, and death during antibody responses. Germinal centres form around follicular dendritic cell networks when activated B cells migrate into lymphoid follicles.

**Haptens** are molecules which can bind antibody but cannot by themselves elicit an immune response. Haptens must be chemically linked to protein carriers to elicit antibody and T-cell responses.

The **immune response** is the response made by the host to defend itself against a pathogen.

A **plasmablast** is a B cell in a lymph node that already shows some features of a plasma cell.

**Plasma cells** ($PC$) are terminally differentiated B lymphocytes and are the main antibody-secreting cells of the body. They are found in the medulla of the lymph nodes, in splenic red pulp, and in bone marrow.

During T-dependent antibody responses, a **primary focus** (plural, **primary foci**) of B-cell activation forms in the vicinity of the margin between T and B cell areas of lymphoid tissue. Here, the T and B cells interact and B cells can directly into antibody-forming cells or migrate to lymphoid follicles for further proliferation and differentiation.

Lymphoid tissues contain lymphoid follicles made up of follicular dendritic cells and B lymphocytes. The **primary follicles** contain resting B lymphocytes and are the site at which germinal centres form when they are entered by activated B cells, forming secondary follicles.
The **primary immune response** is the adaptive immune response to an initial exposure to antigen. **Primary immunization**, also known as priming, generates both the primary immune response and immunological memory.

A cell is said to be **selected** by antigen when its receptors bind that antigen. If the cell starts to proliferate as a result, this is called clonal selection, and the cell founds a clone; if the cell is killed as a result of binding antigen, this is called negative selection or clonal deletion.

**T cells**, or **T lymphocytes**, are a subset of lymphocytes defined by their development in the thymus and by heterodimeric receptors associated with the proteins of the CD3 complex.

# Appendix B

# Extension of 1.2 to Affinity Maturation

The process of affinity maturation and the germinal center (GC) kinetics are mutually dependent since mutation and the selection rate determine the death rate while proliferation and recycling allow expansion of high affinity clones which supports affinity maturation. A model of the GC kinetics which reproduces the measured kinetics reasonably well is therefore needed first. In the framework of these GC kinetics the selection mechanism can then be embedded and investigated. The model of Kesmir and de Boer [26], which has been discussed in detail in Chapter 1, is the only model proposed so far that reproduces the various measured germinal center kinetics reasonably well whilst staying close to biological reality. It is therefore sensible to build a first model of affinity maturation based on this model. Before actually further complicating the model by embedding affinity maturation, it is however interesting to first investigate two variants of the model with regard to the centroblast dynamics since in the model of Kesmir and de Boer [26] these dynamics are governed by a large set of ODEs (4-10) and it would already be a large simplification to replace these equations (1.1-1.2) by one equation. Additionally due to the fact that it is yet unknown which signal leads to the differentiation of centroblasts into centrocytes, it is also of interest to further investigate this step with respect to possible other mechanisms that may regulate conversion. In the model of Kesmir and de Boer [26] the differentiation of centroblasts into centrocytes is modelled to be generation dependent and the different generations until conversion are modelled explicitly generating 4 to 10 odes. Generally speaking, one could imagine three different mechanisms for the regulation of centroblast to centrocyte differentiation: the differentiation rate could either be cell density dependent, time dependent, or again generation dependent, with the number of generations before conversion being at best 1 or at least not more than 3.

As we will see in section B.1 making the conversion rate cell density dependent leads to two more equilibrium points beside the trivial one. One is for negative cell numbers and can therefore be neglected. The third one however is quickly attained and the GC reaction is trapped and cannot terminate anymore. Perelson and coworkers [44] solved this problem by forcing an outflux

of all GC cells at the time when the GC reaction should terminate. There is however no biological justification for such a forcing condition.

The second mechanism of a time dependent conversion factor (section B.2) does not introduce any new stable states and the GC kinetics can be well reproduced. Given that the model is much easier to handle than that of Kesmir and de Boer a first crude model of affinity maturation will be presented based on this kinetic model. This model will give us an idea of important interactions and required constraints. The time dependent conversion mechanism cannot however account for the rapid loss of germinal centers if recycling of centrocytes into the centroblast pool is impossible.

The time dependent model cannot therefore be correct and we will need to go back to a generation dependent model which is presented in section B.3. Modelling the selection process explicitly allows to reproduce the experimental data of the true primary immune response even better than by the model of Kesmir and de Boer [26]. We further find that memory cell formation needs to start well after the onset of somatic hypermutation in order to reproduce the experimental data on affinity maturation [54]. The model is however very complex which prohibits an analytical analysis and too many parameters are still unknown which also limits the numerical analysis. Due to the lack of analytical insights it is not possible to find a large parameter space in which the solution is stable which is discouraging since nature can be expected to be robust against small parameter variations. All these problems are solved in a further model presented in Chapter 2 where the primed primary immune response is considered, for which more data is available from the literature.

## B.1 Density Dependent Centroblast-Centrocyte Conversion

It is well known that cells can sense the cell density in the population and adapt for instance their growth rate accordingly [1]. Centroblasts might therefore differentiate to centrocytes dependent on cell density. In order to investigate this possibility the model of Kesmir and de Boer [26] was used except for the equation governing the centroblast kinetics (1.1-1.2) which were changed to one equation, namely

$$\frac{dB}{dt} = p_r C_T^* + (\rho a_b - \delta_b)B - dB \tag{B.1}$$

with

$$d = D\rho_c \qquad \rho_c = B(t) + C(t) \qquad D = 10^{-3} \quad \text{day}^{-1}. \tag{B.2}$$

where $d$ represents the cell density dependent conversion factor which can be further split into a constant term $D$ and the cell density dependent term $\rho_c$. Only centrocytes and centroblasts were included into the conversion factor since they make up the largest cell proportion in the GC beside memory cells which are located at the edge of the GC and are assumed not to have an influence on cell density in the GC. The premultiplier of $D = 10^{-3}$ day$^{-1}$ is necessary

since d has been determined to be of order $1\,day^{-1}$ and the total centroblast and centrocyte population is of order 1000 [32].

Analysis of the system of equations[1] yields the 2 following non-trivial stable states

$$A_0 = 0 \qquad C_{A0} = 0 \qquad C_0^* = 0 \qquad C_{T0}^* = 0 \tag{B.3}$$

$$B_0 = -\frac{k_1}{2k_2} \pm \frac{1}{2}\sqrt{\frac{k_1^2}{k_2^2} - 4\frac{k_3}{k_2}} \qquad C_0 = \frac{D\rho B_0^2}{\mu - D\rho B_0} \qquad T_0 = \frac{\sigma}{\delta_T} \tag{B.4}$$

$$k_1 = K_b(\rho + Dk_4) + \delta_b(k_4 - K_b) \qquad k_2 = \delta_b + Dk_4 \tag{B.5}$$

$$k_3 = K_b k_4(\rho - \delta_b) \qquad k_4 = \frac{\mu}{D\rho} \tag{B.6}$$

Using the values of the constants specified in Table 1.2 except for using $\rho = 4ln2$ instead of $\rho = 4$, which was wrong in the model of Kesmir and de Boer, and choosing $K_b = 10^3$ we obtain as steady state values

$$B_0 = 536 \qquad C_0 = 526 \qquad T_0 = 62.5. \tag{B.7}$$

The graphical output for $K_b = 10^3$ can be seen in Figure B.1. As we see the non-trivial equilibrium point is quickly attained and the germinal centre reaction cannot terminate. Given that in equilibrium $C_T^* = 0$, it is obvious from (B.1) that the non-trivial equilibrium point is also attained when $d = const$ and $d < (\rho - \delta_b)$. We will discuss the implications of this problem later but will first finish the analysis of this model.

It is worth noting that the steady state formula for B drastically simplifies in the case $K_b \gg B$ as is the case for $K_b = 10^9$. We then obtain

$$B_0 = \frac{\mu(\rho - \delta_b)}{d(\mu + \rho(\rho - \delta_b))} \tag{B.8}$$

.

After having determined equilibrium values for the variables we can now finally use them to set up a model in dimensionless form. It is sensible to nondimensionalise as follows

$$B = B_0\tilde{B} \tag{B.9}$$

$$C = B_0\tilde{C} \qquad C^* = B_0\tilde{C^*} \qquad C_A = B_0\tilde{C_A} \tag{B.10}$$

$$C_T^* = T_0\tilde{C_T^*} \qquad M = (1 - p_r)T_0\tilde{M} \qquad T = T_0\tilde{T} \tag{B.11}$$

$$A = A_k\tilde{A} \qquad \text{with} \qquad A_k = \frac{uB_0}{z} \tag{B.12}$$

$$d = B_0\tilde{d} \tag{B.13}$$

$$a_b = \frac{\tilde{K_b}}{\tilde{K_b} + \tilde{B}} \qquad \text{with} \qquad K_b = B_0\tilde{K_b} \tag{B.14}$$

$$a_T = \frac{\tilde{K_T}}{\tilde{K_T} + \tilde{T}} \qquad \text{with} \qquad K_T = T_0\tilde{K_T} \tag{B.15}$$

[1]Explicit calculations are given in Appendix F.1.1.

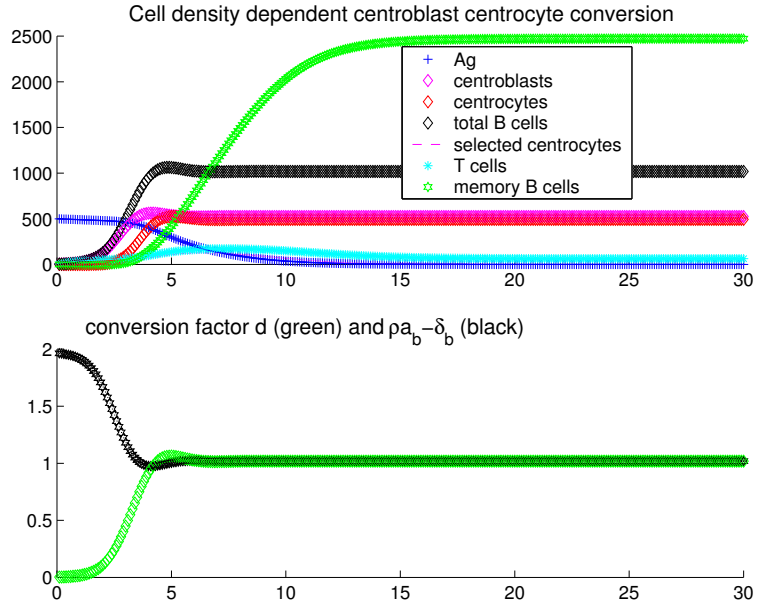



Figure B.1: (*top*) Germinal centre dynamics with density dependent centroblast-centrocyte conversion for $K_b = 10^3$. (*bottom*) The non-trivial equilibrium point is attained once $\rho a_b - \delta_b = d$ since $C^*_{T0} = 0$. It is obvious that the same happens if $d$ is constant and $d \leq \rho - \delta_b$ since $a_b \in [0, 1]$.

$$t = \tau\tilde{t} \qquad \text{with} \qquad \tau = 1 \quad \text{day} \tag{B.16}$$

The constants are either dimensionless or have dimension $t^{-1}$. We can therefore nondimensionalise them with $\tau$, and $\tau$ cancels out of all ODEs. The dimensionless model is given below where the tildes have been omitted for for notational simplicity:

$$\frac{dB}{dt} = p_r \frac{T_0}{B_0} C^*_T + (\rho a_b - \delta_b - dB_0)\, B \tag{B.17}$$

$$\frac{dC}{dt} = d\rho B_0 B - \mu C \tag{B.18}$$

$$\frac{dC^*}{dt} = \mu(C_A - C^*) \tag{B.19}$$

$$\frac{dM}{dt} = \mu\, C^*_T \tag{B.20}$$

$$\frac{dA}{dt} = z(A - C_A) \tag{B.21}$$

$$\frac{dT}{dt} = \delta_T(1 - T) + \rho a_T C^*_T \tag{B.22}$$

$$\tag{B.23}$$

$$C_A = \frac{CA}{s_A + A} \qquad \text{with} \qquad s_A = \frac{s_A}{A_k} \tag{B.24}$$

$$C_T = \frac{C^* T}{s_T + C^*} \qquad \text{with} \qquad s_T = k_4 s_T \tag{B.25}$$

By comparing the relative sizes of all terms in the above system we see that all must be included. Throughout the rest of this dissertation we will solve the dimensional form of the given model since we wish to compare the results directly with experimental results.

We are left with the problem of GC termination. Perelson and coworkers faced the same problem with a slightly different model that also relied on cell density dependent centroblast centrocyte differentiation and they solved the problem by introducing a sudden emigration of GC cells at the time when biologists measured the dissolution of germinal centres [44]. This is however a very artificial approach that cannot explain anything about the underlying mechanism. Moreover, their kinetics do not capture the measured kinetics as shows by comparison of their results in Figure B.2 with experimental data in Figure 1.6.

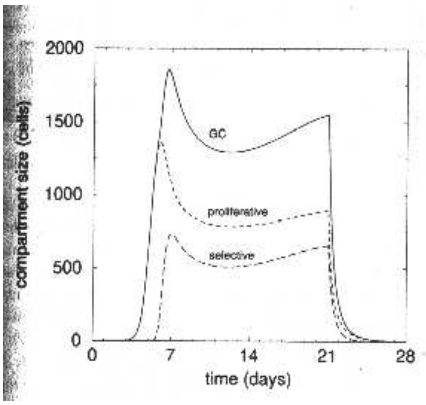



Figure B.2: /small GC kinetics modelled with density dependent conversion by Oprea and Perelson (1997)[44]

Due to the nontrivial stable state, a cell density dependent conversion factor therefore seems unreasonable to describe the GC kinetics. Also biological data may oppose this mechanism: it is known that GCs can host various numbers of cells during different type of responses [32] and this makes a limitation in space very unlikely.

## B.2 Time Dependent Centroblast-Centrocyte Conversion

As shown in the last section, a non-trivial stable state, which impedes GC termination, is always reached if the conversion rate is chosen constant or dependent on cell numbers. A much more promising approach is to assume time dependence of centroblast to centrocyte conversion. A biological interpretation of this would be that with constitution of a germinal centre a compound is produced that needs to reach some critical concentration within the germinal centre in order to induce centroblast differentiation.

Table B.1: GC kinetics of the true primary immune response

| day | Action | References |
|---|---|---|
| 1 | immunisation | |
| 1-4 | antigen gets delivered to the secondary lymphoid organs, | |
| | B cell interact with antigen and T cells (T cell help limiting) | |
| 4 | 3-5 B blasts are seeding the follicles and are starting to proliferate | [32] |
| 7/8 | GC formation: centroblast (dark zone) and centrocytes (light zone) | [19], [20], [32] |
| | onset of somatic hypermutation | [21] |
| 12-14 | GC reaction peaks | [19], [20], [32] |
| | centrocytes outnumber centroblasts | [36] |
| 16-21 | GC reaction declines | [19], [20], [32] |
| 21 | GC reaction finishes | [19], [20], [32] |

### B.2.1 Kinetics of GC reaction

As in the density dependent conversion model we keep all equations from Kesmir's and de Boer's model [26] but those that describe the centroblasts dynamics. The centroblasts dynamic is then described by

$$\frac{dB}{dt} = p_r C_T^* + (\rho a_b - \delta_b)B - d(t)B \tag{B.26}$$

We have now a time-dependent conversion factor $d(t)$ which is chosen to be

$$d(t) = 2.5 * \frac{t^n}{t_c^n + t^n} \tag{B.27}$$

From experiments we know that the true primary immune response is maximal at about day 14 and falls rapidly after this time [32](reproduced as lowest curve in Figure 1.6). In order to obtain an expansion of the B cell population at the beginning we need a net increase of centroblasts - the only population in the GC which can multiply - which is only possible if $\rho a_b - \delta_b > d$. After day 14 the reaction has to decline and given that a measure on centroblasts multiplication only slowly affects the GC kinetics we set $\rho a_b - \delta_b < d$ from day 10 on. Given that $a_b$ is large for small cell numbers and vice versa the term on the LHS increases again once the cell numbers decrease due to $\rho a_b - \delta_b < d$ as can also be seen in the bottom plot of Figure B.3. The conversion factor therefore needs to grow faster than $a_b$ and we therefore need to model it by a steep Hill function ($n = 8$) centered around $t = t_c = 15$.

Due to the experimental restrictions discussed in Chapter 2, in the true primary immune response the onset of the immune reaction is not very well defined and lies somewhere between day 1 and day 5 and we chose day 3 as a starting point. When comparing the experimental and model results one needs to take this into account. All in all, comparison of Figure 1.6 with the numerical solution[2] of the time dependent model in Figure B.3 shows a reasonable match that should be sufficient to build a first model of affinity maturation on these kinetics. The advantage of the model is its relative simplicity although the nonlinear terms still prohibit an mathematical analysis of the affinity maturation process modelled below. The main drawback of this model is however

[2]see Appendix F.2 for an explicit program

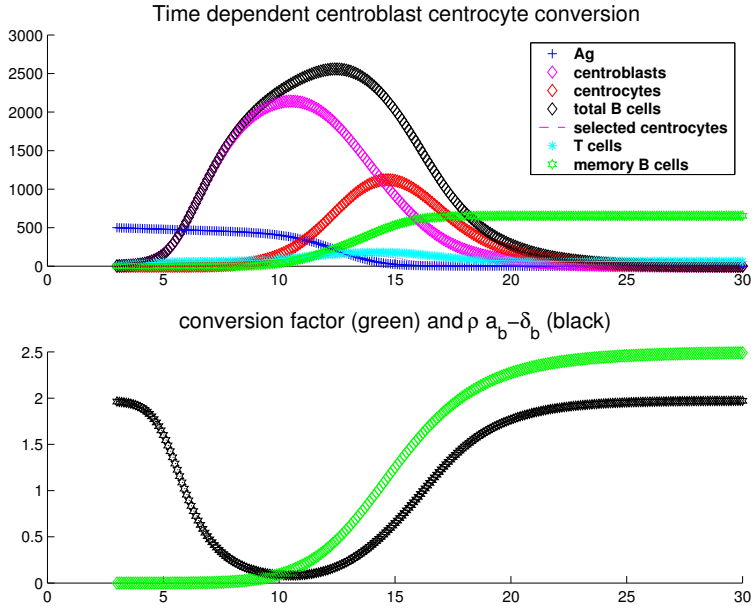



Figure B.3: (*top*) Germinal centre dynamics with time dependent centroblast-centrocyte conversion. (*bottom*) The two curves $\rho a_b - \delta_b$ and $d$ are plotted. If we neglect the recycling term, we have $\frac{dB}{dt} > 0$ for $\rho a_b - \delta_b > d$ and vice versa.

that the centrocyte population is emerging late which is not in good agreement with experimental data. We will fix this problem in the next model but the analysis of affinity maturation with this model will give us some basic ideas about possible mechanisms for affinity maturation.

### B.2.2 Affinity maturation

There are two unsolved problems concerning affinity maturation. One is the question of how mutations are introduced into the genes coding for antibodies - and only into these and not elsewhere in the body where they might cause cancer. Connected with the question on the mechanism are questions concerning rate and timing of the process. This has been studied in some model systems but it is unclear how representative these systems are for general immune responses. In the models of affinity maturation in this dissertation representative data will be used, otherwise the process of somatic hypermutation will be treated as a black box - which it still is.

The second unsolved problem concerns the selection process. When the body becomes infected, most B cells do not bind this antigen at all and the few which can recognise it only bind with very low affinity ($K = 5 \times 10^4 - 1.3 \times 10^6 M^{-1}$ [45] - in the models it will be assumed that the starting affinity is $K = 10^3 M^{-1}$). These weakly binding cells need to go through several rounds of expansion, mutation and selection for their antibodies to become improved. These rounds are only sensible if the affinity threshold of selection rises with time. As first experiments suggest, this time dynamic threshold may be realised

in terms of a dependence of the success of selection not only on receptor affinity but also on antigen density in the germinal centres. The antigen density decreases during the germinal center reaction since centrocytes extract antigen during the selection process [4].

In order to investigate whether an antigen density dependent threshold can drive affinity maturation in general, an oversimplistic model is considered first which uses the set of odes for the time dependent model described above and a simple model of the mutation process.

The first complication of the simple time dependent model lies in the fact that the B cells gain a new property, namely affinity. Given that the affinity of a B cell receptor towards its antigen can lie between $0\,M^{-1}$ and $10^{10}\,M^{-1}$ and affinities change by a factor of at most 10 per mutation (with few exceptions) a logarithmic scale was used for the affinities which runs from 0 to 10. The accuracy at which affinity can be determined is limited and it is therefore sensible not to treat affinity as a continuous variable but to group cells of similar affinity in one affinity bin. Due to the limitations in experimental accuracy it is not sensible to consider more than 100 such affinity bins. This number of bins will allow us later to compare the modelling results with experimental ones once they have been measured. The model that will be presented in the following is adapted to the 100 bin model and does not work if we reduce the number of affinity bins substantially. This is due to the fact that we need our affinity threshold to raise in small steps. If we have less bins, then cells of a larger range of affinities get killed once the threshold value reaches the next affinity bin and this number is then too high for the reaction to continue. This is a realistic result since in nature the affinity threshold can also be expected to rise continuously and not to jump which would kill cells of a larger range of affinities at once.

Mathematically we have therefore introduced a vector of size 100 that stores the cell numbers in the different affinity bins. The dynamics of cells in every bin are governed by their own system of odes and the number of odes rises in total from 6 to 402. Cells can change bins only by mutation. Mathematically this is achieved by applying a mutation matrix $\mathbf{M}$ at the end of every time step for $t > 7$ such that

$$B = \mathbf{M}B \tag{B.28}$$

**Modelling mutation** During somatic hypermutation on average one mutation is introduced per cell genome per generation [5, 37]. We will now use the oversimplistic assumption that mutations lead to a Gaussian distribution of the resulting new antibody affinities around the initial affinity and we therefore have the mutation matrix $\mathbf{M}$ given by

$$\mathbf{M}_{ij} = \frac{\exp\left(-\frac{(i-j)^2}{100}\right)}{\sum_{j=1}^{100}\exp\left(-\frac{(i-j)^2}{100}\right)} \qquad i,j = 1,..,100 \tag{B.29}$$

The denominator in (B.29) is needed in order for the column sum to be equal to 1 so that neither cells are lost nor amplified due to this matrix. Death

and cell division are still modelled by explicit rates in the ODEs. The Gaussian distribution is not in agreement with experimental data and another model will be proposed later that uses more realistic assumptions. The current assumption leads however to a very simple mutation matrix which redistributes the cells in the different bins according to the given probabilities. The middle row of this mutation matrix is shown in Figure B.4. In nature, mutation is a statistical, random process. Although the cell numbers are not large enough to justify the use of average values they are used nontheless for the sake of simplicity. A statistical analysis may be worth attempting at a later stage.

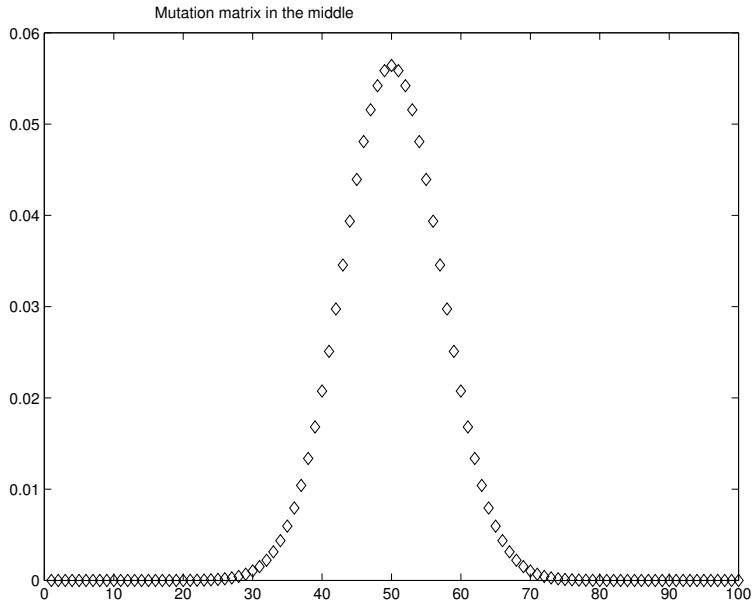



Figure B.4: Distribution of values in a row in the mutation matrix

**Modelling selection** At the end of every time step cells are killed if their affinity is too low. Given that we sorted cells into affinity bins, cells out of the affinity bins below a threshold bin are killed. The threshold bin ($T_B$) is dependent on antigen density as follows

$$T_B = 2\theta \frac{s_b^5}{s_b^5 + Ag^5}. \tag{B.30}$$

The dependency between the threshold bin and antigen density is modelled as a Hill function which implies that as long $Ag \gg s_b$ the threshold is close to zero and almost all clones survive and are expanded. However, once the antigen falls to $s_b = 100$ the threshold increases. $s_b$ is chosen this small in order to give the system time to produce mutants with an affinity sufficiently high to cope with the selection rules. When the antigen density approaches zero the threshold further raises to its maximum which is $T_{Bmax} = 66$. The reason for choosing $\theta$ to be 33 is that the starting affinity in the model is set to be 30 and an affinity change by a factor 10 per mutation is viewed as very good. Given

that we leave time for several divisions and mutations before differentiation into centrocytes and selection, a high proportion of cells can be expected to reach the threshold before the start of selection. If $\theta$ is chosen to be 39 or higher, affinity maturation does not take place and the GC dissolves by day 10.

As can be seen below, without the antigen dependent threshold, the GC reaction terminates by day 10 and affinity maturation towards high affinity clones is not achieved (Figure B.5). The antigen density dependent model (Figure B.6) however gives the anticipated result[3].

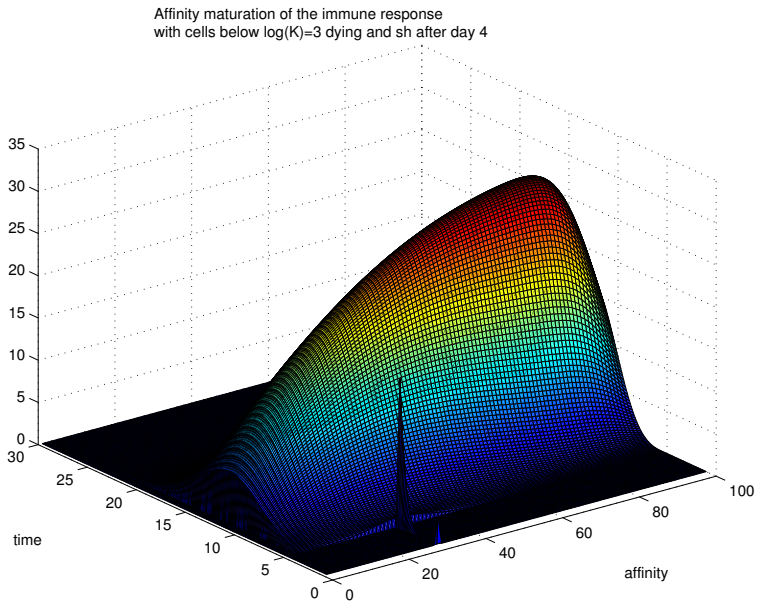



Figure B.5: Affinity development of centrocytes without density dependent selection. The starting condition can be seen as a peak at day 3 and affinity bin 30. From there the reaction evolves but the shift to high affinity is small as can be seen from the small cell numbers (z-axis).

Taken together this model shows that antigen density can drive affinity maturation. The model needs however to be more realistic in order to further help understanding affinity maturation. There are three main points that need to be changed to achieve this. First of all, the time dependent model predicts differentiation of centroblasts into centrocytes which occurs too late. This has several effects. First of all the centrocyte population remains smaller than the centroblast population for almost all the time which is not in agreement with observations of MacLennan and coworkers [36]. Then recycling of centrocytes back into the centroblast pool is not needed in this model to maintain the GC reaction. This is due to the late onset of conversion since until the onset of conversion all cells - regardless of their affinity - are protected from negative selection and survive. The mutation matrix has therefore enough time to shift a high number of cells to high affinity until selection starts properly and it is

[3]The program code to the numerical solutions is given in the Appendix F.2.2.

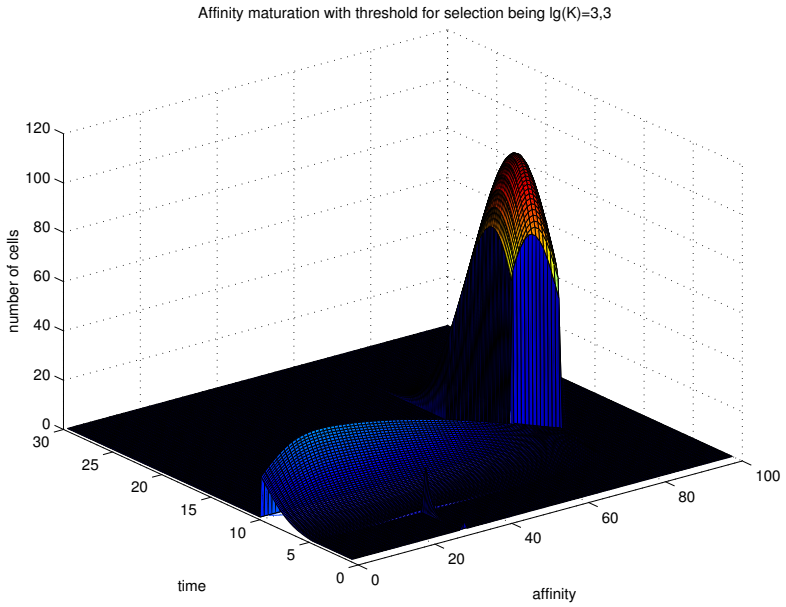



Figure B.6: Affinity development of centrocytes with density dependent selection, $\theta = 33$. At day 10 there is shift of low affinity clones to high affinity.

therefore not required that the best binder recycles and gets amplified in order to maintain the reaction. Additionally, at the time of conversion, the GCs are already meant to reduce in size so that no recycling is needed at all. Beside several convincing mathematical analyses [38, 44], it has also recently been shown experimentally that abolishment of recycling of centrocytes back into the centroblast pool leads to the dissolution of GCs within 3.5 days after their formation [10]. A third point to be improved is the mutation matrix: mutations do not induce a Gaussian distribution around the initial affinity but a discrete shift to few defined affinities. Furthermore, the antigen density does not go to zero during a germinal center reaction. All these points will be considered in the next model.

## B.3 Generation dependent Centroblast-Centrocyte Conversion

### B.3.1 Model

GC formation has been described to take place at day four of the true primary immune response [21] and this generation dependent model therefore starts at day four without considering any mutations since somatic hypermutation does not start before day seven [21]. Furthermore centroblasts are assumed to initially multiply for one day until they all differentiate to centrocytes on day 5. This assumption is necessary in order to reach the cell numbers reported in the literature. As already discussed, *in vivo* the onset of proliferation is smeared over the time span of day 0 to 4. Since no explicit data is available on the

probability of the start of proliferation at each possible time point, it is sensible to use the simplest model which we do here. For the affinity maturation model only the cell numbers at day seven are relevant. The reason for not starting the model at day seven with the right cell numbers is that the proportion of cells in the different populations (centroblast, centrocyte, selected centrocytes) have not been determined experimentally and need to be taken from the model. At day seven somatic hypermutation and negative selection of centrocytes which were previously excluded are then introduced.

We therefore have the following sets of odes:

For day 4 to 5:

$$\frac{dB}{dt} = \rho a_b B \tag{B.31}$$

$$\frac{dT}{dt} = \sigma \tag{B.32}$$

where the GC T cell population is assumed to initially only grow due to influx ($\sigma = 5$) from the outer T cell zone where T cells interact with T cells and are activated to proliferate and enter the GC kinetics (B.32). As discussed before, at day 5 all centrocytes differentiate to centrocytes: $C = B$ and $B = 0$. Given that in this model, centroblasts have differentiated completely into centrocytes by day 5, we are left with the following set of odes for the time period day 5 to day 30:

$$\frac{dC}{dt} = -\kappa C_A H_T \tag{B.33}$$

$$\frac{dC_T^*}{dt} = \kappa C_A H_T \tag{B.34}$$

$$\frac{dAg}{dt} = -zAg - 2quC_A \tag{B.35}$$

$$\frac{dT}{dt} = \sigma + (pa_T H_C - \delta_T)T \tag{B.36}$$

$$C_A = \frac{CAg}{Ag + s_a} \qquad H_T = \frac{T}{T + K_t} \qquad K_t = \frac{C}{20} \qquad H_C = \frac{C_T^*}{C_T^* + s_T} \tag{B.37}$$

Centrocytes ($C$) are selected into the pool of selected centrocytes ($C_T^*$) in non-linear dependence upon antigen ($C_A$) and T cell availability ($H_T$) as has already been discussed in the context of the model of Kesmir and de Boer in Chapter 1.2. We therefore have $\kappa C_A H_T$ as outflux from the $C$ pool and as influx into the $C_T^*$ pool. $\kappa$ is deduced later on page 109. The saturation constant for B cells binding to FDCs is chosen to be $s_a = 10^9$ and the saturation constant for T cell centrocyte interaction is chosen to be $s_t = 50$.

Equation (B.35) models the Ag dynamics. The initial Ag amount is taken to be $10^7$ Ag molecules per FDC. Assuming that there exist 100 FDCs per GC we therefore start with $10^9$ Ag molecules. Antigen can be reduced due to natural decay with decay rate $z$ or by extraction during the selection of Centrocytes with consumption rate $u$. The threshold below which no further antigen

extraction is possible is assumed to be $10^3$ antigen molecules per FDC, so $10^5$ molecules per GC. The consumption of antigen per centrocyte $u$ is assumed to be $10^5$ molecules since below this amount of antigen availability no successful extraction and presentation is possible. $q$ works as a Heaviside function in equation (B.35) which prohibits antigen extraction at all if the amount needed to be extracted due to this equation exceeds the amount of antigen available but as the resulting solutions show (Figure B.9 and B.11 middle panel) the antigen amount does not fall to a critical number so that this function is not really needed in the model. The factor 2 comes in since the saturation constant for B cells binding to FDCs is chosen equal to the initial number of antigen molecules so that the starting value for $C_A$ is $0.5C$ which is fixed by introducing the factor 2.

We still need to model the fate of the selected centrocytes ($C_T^*$) and their dynamics are modelled by discrete equations in order to have a better control over the model which will prove useful when introducing mutation and selection since then we will be faced by many experimentally undetermined parameters that need to be guessed sensibly in order for the model to work. The discrete conditions imposed at the end of every time step ($dt = 0.1$) are given by

$$\begin{aligned} B(t) &= B(t-dt) + p_r C_T^*, && \text{(B.38)} \\ M(t) &= M(t-dt) + (1-p_r) C_T^*, && \text{(B.39)} \\ C(t) &= C(t) + B(t-2.5), && \text{(B.40)} \\ B(t-2.5) &= 0, && \text{(B.41)} \\ C(t-0.25) &= 0.\times C(t-0.25) && \text{(B.42)} \end{aligned}$$

The selected centrocytes $C_T^*$ can either recycle into the centroblast pool $B$ with probability $p_r$ (B.38) or differentiate into memory cells $M$ with probability $1-p_r$ (B.39). The value chosen for the parameter $p_r$ is discussed on page 110. In case of the memory cells the equation used here is simply the integrated form of the ODE already given in the model of Kesmir and de Boer (1.5) with the only difference that the rate of formation is chosen to be 1 instead of $\rho$. Integration of the ODE is simple since the ODE describing the memory cell kinetics is independent of the memory cell number itself. Out of the centroblast pool cells differentiate after 10 generations (2.5 days) into centrocytes (B.40-B.41). 10 generations is about the same number that is favorably used in the model of Kesmir and de Boer. This is not surprising since both models are very similar. The time delay of 10 days is incorporated into the model by setting up ten more ODEs which represent the different generations a centroblast goes through as in the model of Kesmir and de Boer. In the numerical solution recycling centroblasts are stored in different matrix columns according to the time at which they recycle. The different columns of the matrix can be regarded as normal $B$ vectors on which the normal continuous ODE for centroblast expansion (B.31) is imposed. The transfer from the centrocyte state into the centroblast one and back are not modelled by rates but are assumed to be complete (discrete) transfers as we have already assumed for the differentiation of centroblasts into centrocytes at day 5. Centrocytes that are not selected die after one day and

after about 6 hours half of the population is dead [31] (B.42).

The first check of the kinetic model is whether inhibiting recycling leads to germinal center dissolution until day 5 as has been measured experimentally [10]. Figure B.7 shows that this is indeed the fact.

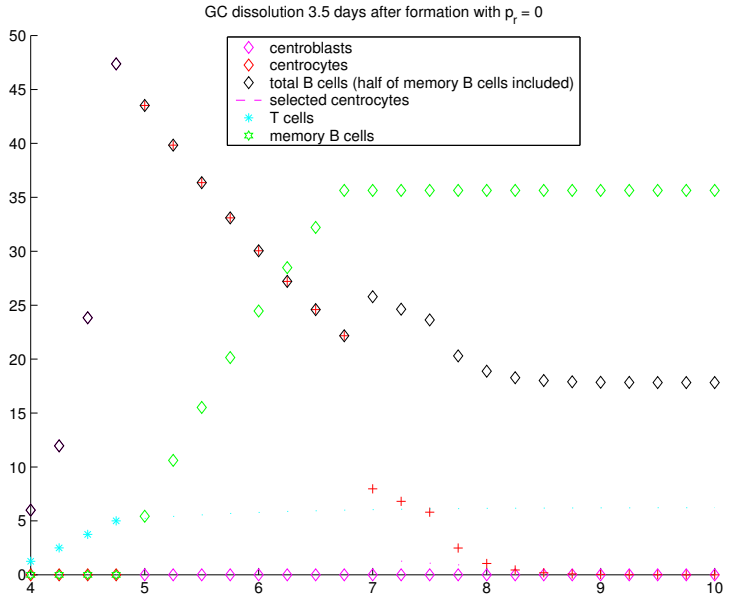



Figure B.7: Germinal centers dissolve within 3.5 days if recycling is inhibited ($p_r = 0$) which can be seen from the fact that the centroblast and centrocyte populations go to zero. The memory cells are only located at the edge of the germinal centre and their presence does not inhibit the involution of GC centres due to missing cells.

At day seven somatic hypermutation finally starts. The model needs to be supplemented by a module that takes care of the affinity changes introduced by mutations and one module responsible for selection. Mutations are introduced by multiplying the centroblast matrix $B$ once per generation with a mutation matrix $\mathbf{M}$ such that

$$B = \mathbf{M}B. \tag{B.43}$$

The mutation matrix redistributes the cells in new rows (affinity bins) of the centroblast matrix as has been described previously although this time a more realistic mutation matrix is introduced. After differentiation, centrocytes are then selected upon affinity and antigen density. The antigen density reduces during the GC reaction with a natural decay $z$ and by extraction of antigen with rate $u$ while the average affinity increases due to selection and multiplication of selected clones. Given that the affinity threshold for selection is modelled dependent upon antigen density it rises with time.

Table B.2: Symbols used in the mutation matrix with discrete affinty shifts

| | |
|---|---|
| $v_1$ | m*0.0171 |
| a | 0.72 - $\sum_{i=2}^{100} \mathbf{M}_{ij}$ |
| b | $v_1$ |
| c | $\frac{v_1}{3}$ |
| d | 0.57 |
| d1 | d+0.15-$v_1$ |
| e | $\frac{v_1}{2}$ |
| f | 1.5 |
| g | $v_1$ |
| h | $\frac{v_1}{f}$ |
| i | row index |
| j | column index |
| m | 1.5 |

**Mutations** On average one mutation is introduced per cell genome per cell cycle. As calculated from available experimental data [51], more than half of the mutations will not change the affinity of the receptor, about 28% are deleterious leading to the death of the cell and the rest change the affinity in a way that the cell remains viable. This proportion (15% in the model) causes the cell to change the affinity bin in the model. Most of these mutations will reduce the affinity of the receptor and only a few are beneficial. The following sparse mutation matrix is therefore introduced from which - for space reasons - only rows and columns 1,30,40,50,60,65,80,90,100 are printed - the remaining elements are all zero except for elements 1 to 29 in row 30 which are of value $b$. The numerical values of the variables are given in Table B.2.

$$\begin{pmatrix} 1 \\ 30 \\ 40 \\ 50 \\ 60 \\ 65 \\ 80 \\ 90 \\ 100 \end{pmatrix} = \begin{pmatrix} d1 & \dots & a & \dots & a & \dots & a & \dots & a & \dots & a & \dots & a & \dots & a & \dots & a \\ b & b & d & \dots & c & \dots & c & \dots & c & \dots & 0 & \dots & 0 & \dots & 0 & \dots & 0 \\ 0 & \dots & c & \dots & d & \dots & e & \dots & e & \dots & 0 & \dots & 0 & \dots & 0 & \dots & 0 \\ 0 & \dots & c & \dots & e & \dots & d & \dots & 0 & \dots & g & \dots & 0 & \dots & 0 & \dots & 0 \\ 0 & \dots & c & \dots & e & \dots & 0 & \dots & d & \dots & 0 & \dots & 0 & \dots & g & \dots & 0 \\ 0 & \dots & 0 & \dots & 0 & \dots & g & \dots & 0 & \dots & d & \dots & g & \dots & 0 & \dots & 0 \\ 0 & \dots & 0 & \dots & 0 & \dots & 0 & \dots & 0 & \dots & g & \dots & d & \dots & 0 & \dots & h \\ 0 & \dots & 0 & \dots & 0 & \dots & 0 & \dots & g & \dots & 0 & \dots & 0 & \dots & d & \dots & h \\ 0 & \dots & 0 & \dots & 0 & \dots & 0 & \dots & 0 & \dots & 0 & \dots & h & \dots & h & \dots & d \end{pmatrix}$$

On the diagonal we have the value $d = 0.57$ which represents the proportion of silent mutations which do not change the affinity of the clones. (1,1) is an exception and we have $d1 = d + 0.15 - m * 1.171$ since the clones of the lowest affinity cannot further lose affinity and the proportion staying in (1,1) is therefore higher. For the other entries in the first row we have

$$\mathbf{M}_{1j} = 0.72 - \sum_{i=2}^{100} \mathbf{M}_{ij} \qquad j = 2, .., 100. \tag{B.44}$$

Cells in affinity bins below the starting affinity (i = 30) are assumed only to be able to lose their affinity completely and enter into the first row or to mutate to the starting affinity (bin 30). We therefore have

$$\mathbf{M}_{30j} = v_1 = 0.0171m \qquad j = 1, .., 29. \tag{B.45}$$

The remaining off-diagonal entries which are all symmetric model the affinity jumps introduced by mutation. These jumps are happening on a random basis and if we average over a large number of mutations against different antigens almost every jump - which is smaller than 30 - will have occurred. For one special antigen however similar affinity jumps happen in different animals independently. We can therefore assume a set of fixed favored jumps and neglect other possibilities without loss of generality. The entries for the jumps are in general symmetric since mutations are assumed to be reversible in every step by back mutation. Exceptions are those mutations that destroy the antibody completely. These off-diagonal entries are coded by the letters $c$ to $h$ whose values are given in Table B.2.

**Selection** Selection is dependent on both affinity and antigen density and the threshold is therefore a curve in the affinity-antigen density space. Experiments are currently running to determine this threshold curve, but these data are not yet available. This of course limits our study since without these experimental data too many parameters are unknown. The scope of this model can therefore only be investigated in general to determine whether such an antigen density dependent selection mechanism is also possible with the more realistic assumptions made so far.

Following the advice of experimentalists, a threshold curve $f(x)$ with

$$f(x) = \frac{12.5}{x-4} \qquad\qquad f^{-1}(x) = \frac{12.5}{x} + 4 \tag{B.46}$$

was chosen arbitrarily. The plot of $f(x)$ can be seen in Figure B.8. The higher the affinity of the BCRs on a centrocyte and the more antigen available the higher the proportion of selected centrocytes. To include this assumption in the model the distance of every parameter pair from the threshold curve needs to be determined at every time step. In order to spare computational time the distance was determined in the 1-norm for every affinity-antigen pair above the threshold curve by

$$\lambda(\beta) = 0.5 \left( \left| \log_{10} Ag - f^{-1}\left(\frac{\beta}{10}\right) \right| + \left| \frac{\beta}{10} - f(\log_{10} Ag) \right| \right) \tag{B.47}$$

with $\beta$ denoting the affinity bin. First experiments suggest that not only does the selection proportion increases with increasing $\lambda$ but also the rate of conversion on the path $C \to CTA \to B$. We could incorporate this detail by differential delay equations whose delays depend on $\lambda$. We however use a simpler approach and assume that faster conversion means faster return into the centroblast pool where the cells are expanded. We can therefore introduce

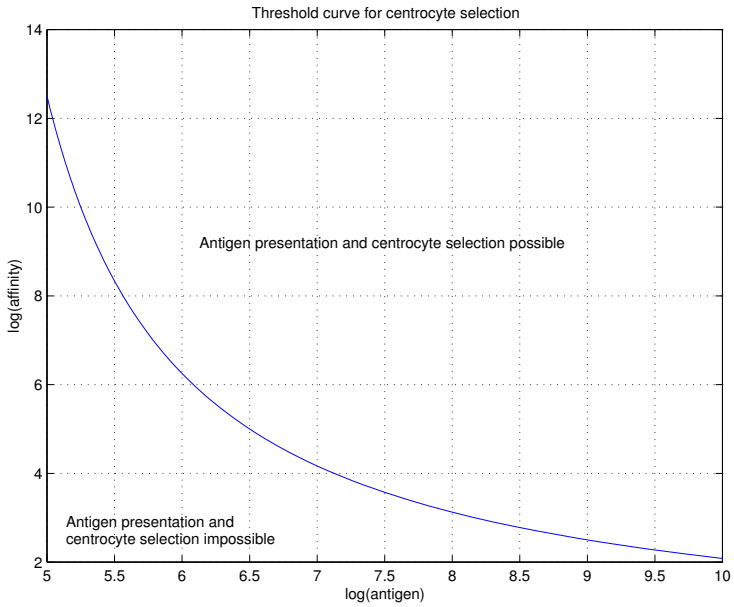



Figure B.8: Threshold curve $f(x)$ (B.46) for antigen density and affinity dependent centrocyte selection used in the model: for parameter pairs under the curve selection is difficult, above the curve selection improves with distance from the curve.

a constant $\kappa$ in (B.33),(B.34) which also leads to an increase in cell numbers dependent on $\lambda$.

$$\kappa(\beta) = \frac{8}{7}\lambda(\beta) + \frac{8}{7} \quad \text{if} \quad \lambda(\beta) \leq 1.2 \tag{B.48}$$

$$\kappa(\beta) = g\lambda(\beta) \quad \text{if} \quad \lambda(\beta) > 1.2 \tag{B.49}$$

with $g \in [2, 3]$.

$\kappa$ can take values between 0 and 30 but most of the time remains smaller than 10 and $\kappa = 0$ implies no selection. The value of $g$ influences the kinetics of the GC. For $g = 2$ there is slower affinity maturation and the GC reaction is largest at day 12 while for $g = 3$, the affinity maturation is faster and the maximum of the GC reaction is attained at day 16. This is directly understandable since the higher $g$ the more high affinity clones get expanded.

**AFC formation** We have now determined all parameters needed to solve the model (equations (B.33-B.37). Before actually turning to the numerical solution we still need to add one further equation concerning the AFC formation. By day 14 centrocytes with affinity higher than $10^{8.5}$ are selected into the AFC pool and we therefore have for $7 \leq t < 14$:

$$AFC(t) = AFC(t - dt) + \sum_{i>85} C^*_{Ti} \tag{B.50}$$

where the index $i$ refers to the $i$th entry of the vector $C^*_{Ti}$. AFCs directly leave the GCs and are therefore lost for the GC reaction.

**Recycling and Memory cell formation** In agreement with previous work of Perelson and coworkers [44] the probability of recycling of the centrocyte back into the centroblast pool was chosen to be 100% until the start of memory cell formation and 70% afterwards. The remaining 30% go into the memory pool. The starting point of memory cell formation in the true primary immune response is believed to lie around day 10. It was interesting to test what impact an onset of memory cell formation at day 7 or day 10 would have on the kinetics. Interestingly the kinetics are very different and one would hope that comparison with the experimental data would lead to a conclusion on this point. Unfortunately this is only limited the case since the most important data point at day 10 is not well measured in the experiment [32]. All data points are the mean of the values obtained from four different rats. One rat however gives a very odd result on day 10 (GC reaction finished). If one excludes the rat from the calculation one obtains Figure B.13 which is similar to the kinetics from Figure B.9 where the memory compartment is not formed before day 10. Inclusion of the rat gives the kinetics of Figure B.11 where the memory compartment is formed with the onset of somatic hypermutation. In order to compare the size of the GC reaction one needs to convert the spleen volumes given in Figure B.13 and B.14 into cell numbers. The total spleen has in average about $5 \times 10^5$ cells. 0.4% splenic volume would therefore be about 2000 B cells.

### B.3.2 Results

The model shows the impact of a late versus an early start of memory cell formation on the GC kinetics and on affinity maturation. Despite these clear differences in the model results which respect to GC kinetics it is difficult to derive any conclusions from the kinetic data of Liu and coworkers in Figure 1.6 [32]. Comparison with further data available from the literature however strongly supports the assumption that memory cell formation starts at day 10. The curve for the total GC B cell number from the day 10 model (top panel in Figure B.9) has almost the same height and shape as the one directly obtained from experiments if the critical rat (termination of GC reaction by day 10) is excluded (Figure B.14). Additionally the average affinity increase (bottom panel in Figure B.9) also reproduces well the data found in the literature [54]. This is in contrast to the model where memory cell formation starts at day 7. The curve for the total cell numbers (top plot in Figure B.11) has a similar shape as the one obtained from experiments (Figure B.13). The height is however different and the total cell numbers obtained from the model are much to high. Affinity maturation is less efficient than in the day 10 model (bottom plot in Figure B.11) and does not agree with the experimental results. The smaller extent of affinity maturation in the day 7 model is also evident by comparing Figure B.10 (day 10 model) and Figure B.12 (day 7 model). Both Figures show the number of B cells per affinity bin over time and the shift to higher affinities is much larger in the day 10 model than in the day 7 model.

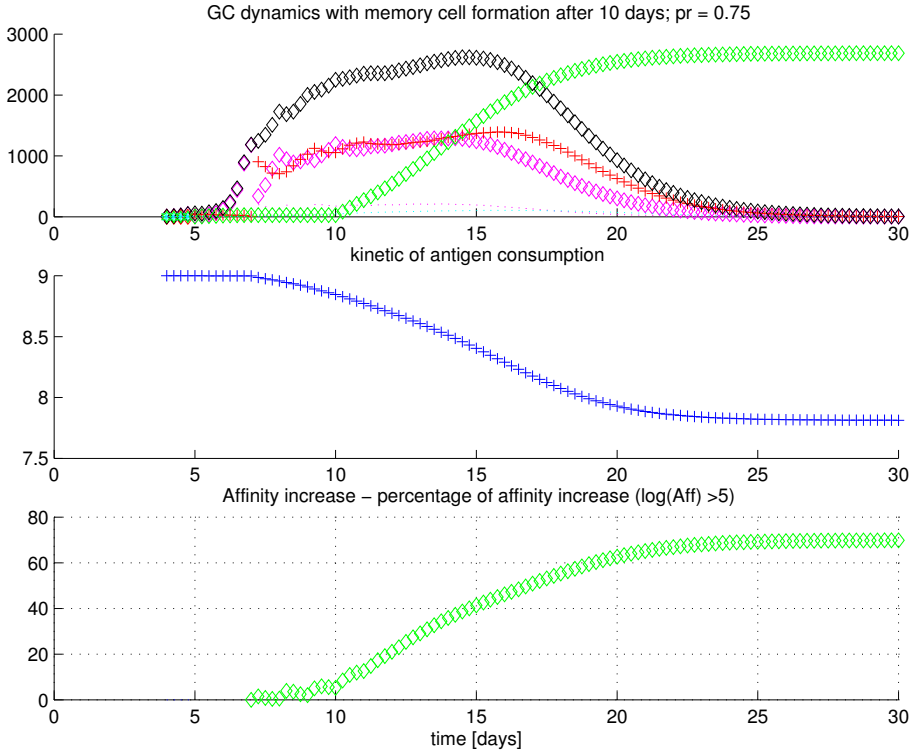



Figure B.9: GC kinetics with discrete mutation matrix, onset of somatic hypermutation at day 3 after GC formation, memory compartment formation after day 10 and antigen density dependent selection ($\kappa = 3 \quad \lambda$). (*top*) GC kinetics: the color code is used as in the figures before. The curve for the total cell numbers has exactly the same height and shape as the one obtained from experiments (Figure B.13). Memory cell formation starts at day 10. The size of centrocyte and centroblast pools are about the same size which is a result of considering several centroblast generations but is not in good agreement with experimental data [36]. (*middle*) Plot of the antigen dynamics. (*bottom*) Affinity increase over time. The result is in good agreement with experimental data [54].

Problems with both models are that the size of the centrocyte and the centroblast pool are of about the same size which is not in good agreement with experimental data [36] and that the model is not robust against parameter variations. The first problem is a result of considering several centroblast generations since this enlarges the centroblast pool. The second problem also cannot easily be fixed in this model since the complexity of the model prohibits an analytic stability analysis which might yield a sufficiently wide parameter range for which the model is stable or at least further insights into why the model cannot be stable. Both problems are fixed in the main model of the primed primary immune response presented in Chapter 2.

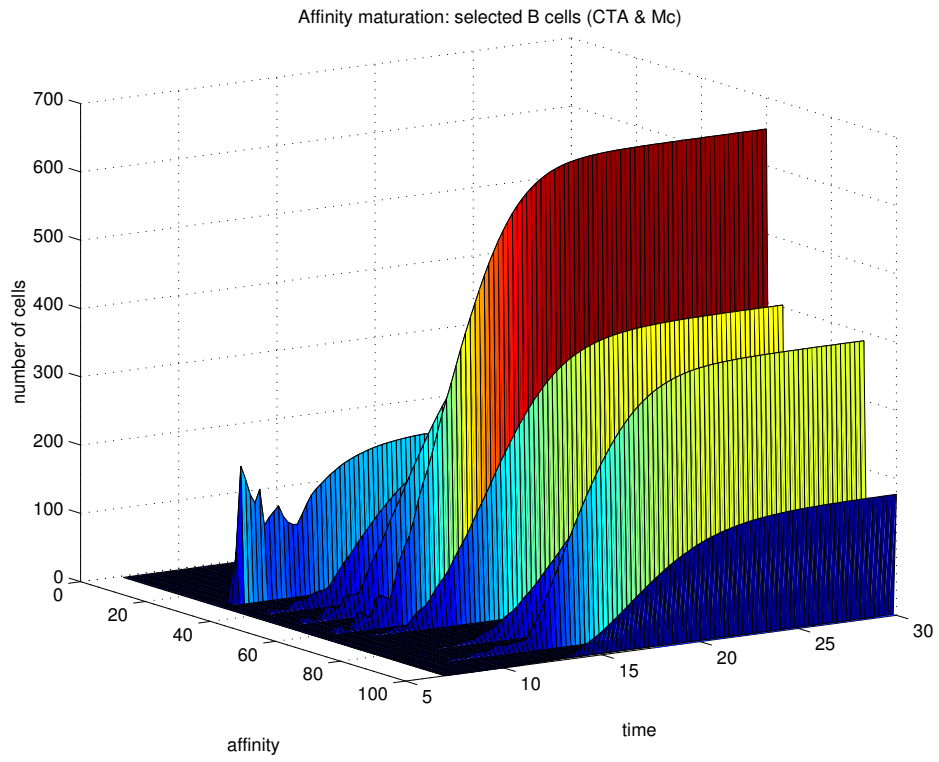



Figure B.10: Affinity maturation with discrete mutation matrix, onset of somatic hypermutation at day 3 after GC formation and antigen density dependent selection. The starting affinity bin is 30. About day 10 there is a first shift to higher affinities (bin 40-60). By day 15 clones are further shifted to higher affinity and reach the highest affinity (bin 100).

## B.4 Conclusion

From modelling the differentiation rate from centroblasts to centrocytes either cell density, time or generation dependent we have shown that the latter approach best reproduces available data. The generation dependent model presented in the last section includes an hypothesis on the affinity maturation process and reproduces the kinetics of the GC reaction in the true primary immune response [32] and data concerning affinity maturation well [54]. We can therefore conclude that a with time decreasing antigen density can indeed drive affinity maturation in the way observed in the germinal centre reaction. The fact that the final memory B cell pool consists out of 65 percent high affinity clones could be reproduced by assuming a continuous influx of selected centrocytes into the memory pool instead of assuming a further selection step before entry of selected centrocytes into the memory pool.

The results of the model further suggest that it is beneficial for the efficiency of affinity maturation if memory cell formation starts some time after the onset of somatic hypermutation. That memory cell formation indeed starts later than somatic hypermutation has already been shown for the primed primary

immune response [34] but is still unclear in the case of the true primary immune response.

Unfortunately, many parameters needed in this model are still unknown and assumptions had to be made concerning the parameter space. Given that some parameters such as the important threshold function $f(x)$ was chosen somewhat arbitrarily, no conclusions about uniqueness can be made. The model only presents one possible solution and cannot exclude others. Furthermore, the model is very unstable against parameter changes. This is however not acceptable since biological processes are in general very robust against changes of parameters over quite a large range. A stability analysis which might yield some information about stable regions is not straightforward because of the complexity of the model.

Pursuing this modelling approach has however given some insights that prove helpful when constructing a simpler model. First of all it seems sensible to restrict the analysis to three cell species: centroblasts, centrocytes and selected centrocytes while the effects of T cells and antigen can be modelled by time dependent parameters in the first instance. A further insight comes from modelling memory cell formation: here we used different times for the onset of memory cell formation and the proportion of recycling centrocytes varied therefore with time. This is an idea which is worth to be followed up in a simpler model which is presented in Chapter 2.

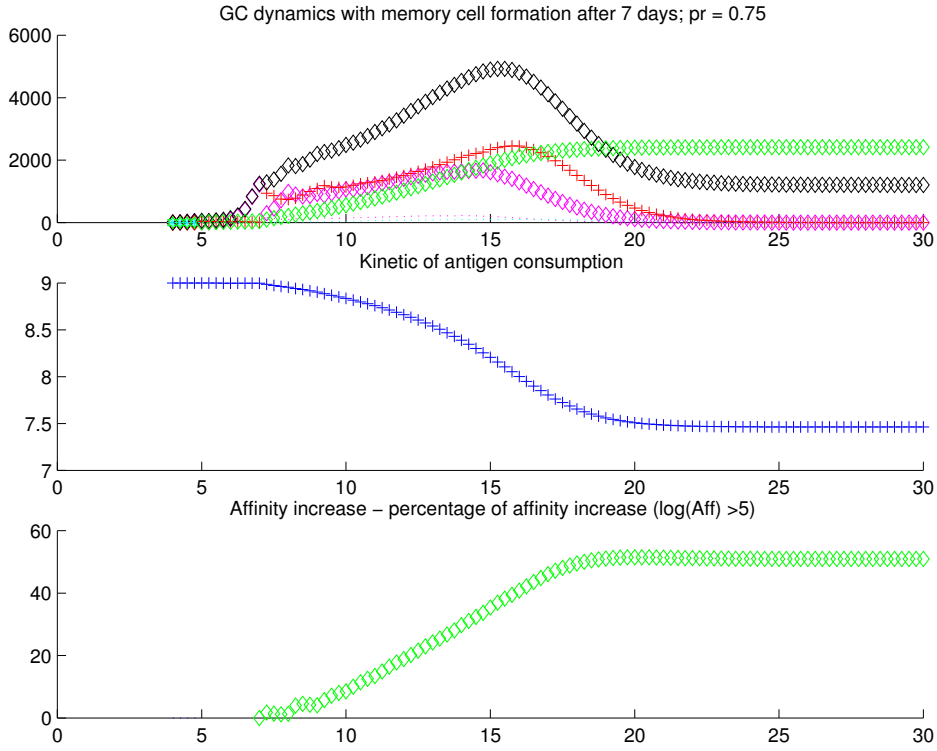



Figure B.11: GC kinetics with discrete mutation matrix, onset of somatic hypermutation at day 3 after GC formation (day 7), memory compartment formation from day 7 on and antigen density dependent selection ($\kappa = 2 \quad \lambda$). (*top*) GC kinetics: the color code is used as in the figures before. The curve for the total cell numbers has a similar shape as the one obtained from experiments (Figure B.13). The height is however different and the total cell numbers obtained from the model are much too high. Memory cell formation starts at day 7. The size of the centrocyte and centroblast pool is of about the same size which is a result of considering several centroblast generations but is not in good agreement with experimental data [36]. (*middle*) Plot of the antigen dynamics. (*bottom*) Affinity increase over time. The result is in less good agreement with experimental data [54] than the result obtained if memory cell formation is assumed to start at day 10.

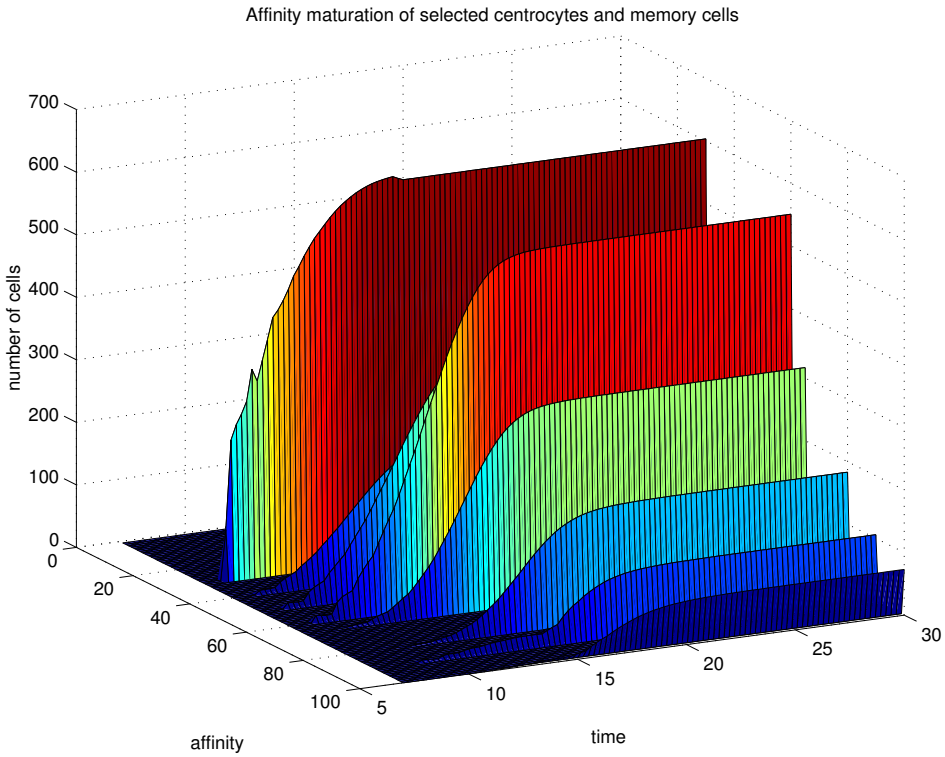



Figure B.12: Affinity maturation with discrete mutation matrix, onset of somatic hypermutation at day 3 after GC formation and antigen density dependent selection. The starting affinity bin is 30. About day 10 there is a first shift to higher affinities (bin 40-60). By day 15 clones are further shifted to higher affinity and reach the highest affinity (bin 100). The total shift to higher affinities is less than in the model where memory cell formation starts at day 10.

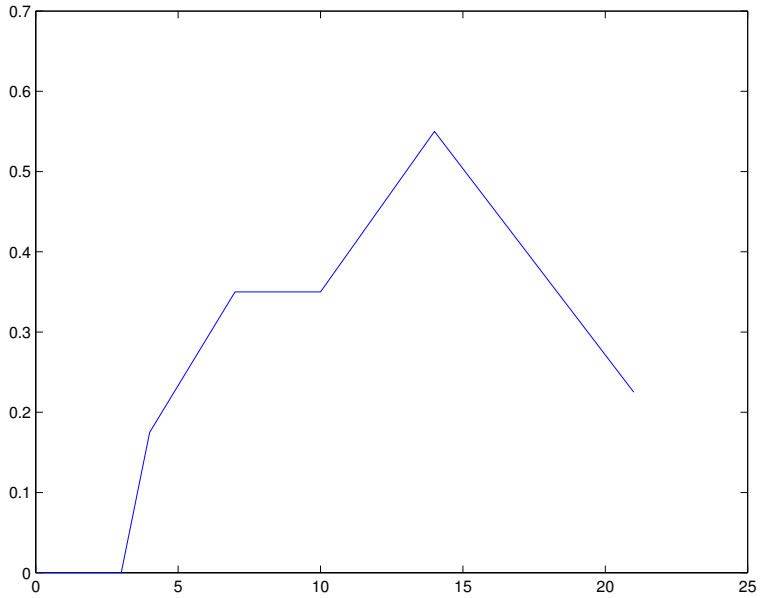



Figure B.13: GC kinetics as measured by Liu et al. [32] with all rats included

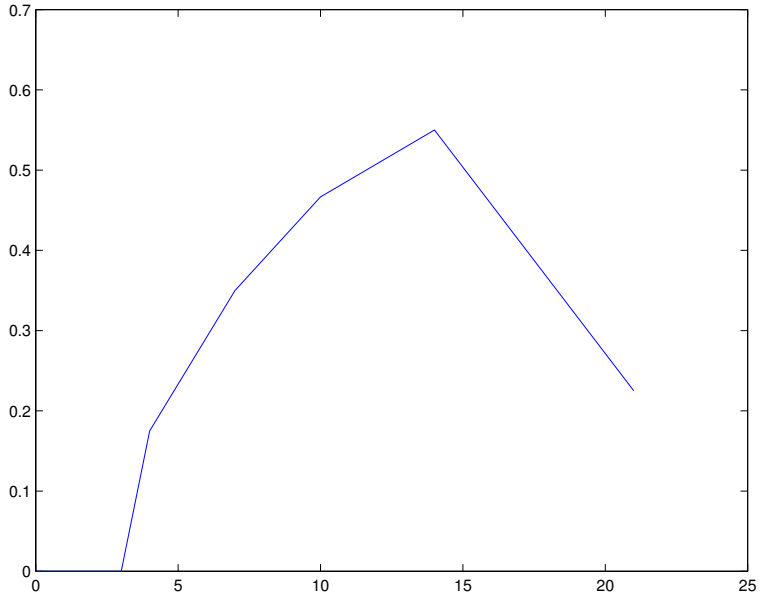



Figure B.14: GC kinetics as measured by Liu et al. [32] with 1 rat at day 10 excluded

# Appendix C

# Program Codes for Chapter 2

## C.1 Program to the Numerical Solutions of the Model in 2.2

The plot showing for the stability analysis was obtained by using the program

```
% model for affinity maturation in primed response


% parameters
dt = 0.1;

Bb  = 3; % number of seeding B blasts
C = 0; % number of centrocytes
Cs = 0; % number of selected centrocytes
C1 = 0;
Ag = 0; % number of antigen complexes
M = 0; % number of memory cells

ln2 = log(2)/log(exp(1));
rho = 4*ln2; % maximum proliferation rate of centroblast (day^-1)
d = 12 * ln2; % time to run through selection process
s = 0.5;  % selection probability
Kt = 18; % Hill coefficient for s
dc = 1.5*ln2;  % death rate for non-selected centrocytes
pr = 0.8; % probability of recycling
m=1;
sc = dc/(d*(2*pr*m-1)+dc);
l = 7;


figure

% Runge-Kutta method
```

```
for t=0:dt:2.8
   bb1 = rho*Bb;
   bb2 = rho*(Bb+bb1*dt/2);
bb3 = rho*(Bb+bb2*dt/2);
   bb4 = rho*(Bb+bb3*dt);

   Bb = Bb+dt*(bb1+2*bb2+2*bb3+bb4)/6;
   T = Bb;
   CT =0;

subplot(3,1,1)
plot(t,B,'m--^', t, CT, ':r', t, M, '-g', t, T, 'k--d');
legend('B blasts', 'centrocytes', 'memory cells', 'total B cells');
hold on,
pause(0);
end

B = Bb;

for t=2.8+dt:dt:4
   m = 1;  % no somatic hypermutation
   %s = 0.5 * Kt^l/((t-3)^l+Kt^l);
   s = sc-0.1;
   s = 0;
 mu = d*s+dc*(1-s);

   k1 = rho*(pr*Cs-B);
   ck1 = 2*rho*m*B - mu*C;
   cak1 = d*s*C-rho*Cs;
   c1 = rho*(pr*Cs-C1);

   k2 =  rho*(pr*Cs-(B+k1*dt/2));
ck2=  2*rho*m*B - mu*(C+ck1*dt/2);
cak2 = d*s*C-rho*(Cs+cak1*dt/2);
c2 = rho*(pr*Cs-C1+c1*dt/2);

   k3 =  rho*(pr*Cs-(B+k2*dt/2));
ck3=  2*rho*m*B - mu*(C+ck2*dt/2);
cak3 = d*s*C-rho*(Cs+cak2*dt/2);
   c3 = rho*(pr*Cs-C1+c2*dt/2);

   k4 =  rho*(pr*Cs-(B+k3*dt));
ck4=  2*rho*m*B - mu*(C+ck3*dt);
cak4 = d*s*C-rho*(Cs+cak3*dt);
   c4 = rho*(pr*Cs-C1+c3*dt);

M = M + (1-pr)*Cs*dt;
```

```
B = B+dt*(k1+2*k2+2*k3+k4)/6;
C = C+dt*(ck1+2*ck2+2*ck3+ck4)/6; % dynamics of centrocytes
Cs= Cs + dt*(cak1+2*cak2+2*cak3+cak4)/6; % dynamics of Ag-Centrocytes

T = B+C+Cs;
CT = C+Cs;

% plotting
subplot(3,1,1)
plot(t,B,'--m', t, CT, ':r', t, M, '-g', t, T, '--kd');
legend('B blasts', 'centrocytes', 'memory cells', 'total B cells');
hold on,
pause(0);
end

for t=4+dt:dt:30
   %m = 0.72;  % non-deleterious mutation rate
   m = 1;
   s = sc-0.1;
   s = 0;
  mu = d*s+dc*(1-s);


   k1 = rho*(pr*Cs-B);
   ck1 = 2*rho*m*B - mu*C;
   cak1 = d*s*C-rho*Cs;

   k2 =  rho*(pr*Cs-(B+k1*dt/2));
ck2=  2*rho*m*B - mu*(C+ck1*dt/2);
cak2 = d*s*C-rho*(Cs+cak1*dt/2);

   k3 =  rho*(pr*Cs-(B+k2*dt/2));
ck3=  2*rho*m*B - mu*(C+ck2*dt/2);
cak3 = d*s*C-rho*(Cs+cak2*dt/2);

   k4 =  rho*(pr*Cs-(B+k3*dt));
ck4=  2*rho*m*B - mu*(C+ck3*dt);
cak4 = d*s*C-rho*(Cs+cak3*dt);


M = M + (1-pr)*Cs*dt;
B = B+dt*(k1+2*k2+2*k3+k4)/6;
C = C+dt*(ck1+2*ck2+2*ck3+ck4)/6; % dynamics of centrocytes
Cs= Cs + dt*(cak1+2*cak2+2*cak3+cak4)/6; % dynamics of Ag-Centrocytes


T = B+C+Cs;
```

```
CT = C+Cs;

% plotting
subplot(3,1,1)
plot(t,B,'--m', t, CT, ':r', t, M, '-g', t, T, '--kd');
legend('B blasts', 'centrocytes', 'memory cells', 'total B cells');
hold on,
pause(0);
end



% Runge-Kutta method
for t=dt:dt:3
   bb1 = rho*Bb;
   bb2 = rho*(Bb+bb1*dt/2);
bb3 = rho*(Bb+bb2*dt/2);
   bb4 = rho*(Bb+bb3*dt);

   Bb = Bb+dt*(bb1+2*bb2+2*bb3+bb4)/6;
   T = Bb;
   CT =0;

   subplot(3,1,2)
   plot(t,Bb,'m*', t, CT, 'rd', t, M, 'gd', t, T, 'kd');
   hold on


end

B = Bb;

for t=3+dt:dt:4
   m = 1;  % no somatic hypermutation
   %s = 0.5 * Kt^l/((t-3)^l+Kt^l);
   s = sc;
   mu = d*s+dc*(1-s);


   k1 = rho*(pr*Cs-B);
   ck1 = 2*rho*m*B - mu*C;
   cak1 = d*s*C-rho*Cs;
   c1 = rho*(pr*Cs-C1);

   k2 =  rho*(pr*Cs-(B+k1*dt/2));
ck2=  2*rho*m*B - mu*(C+ck1*dt/2);
cak2 = d*s*C-rho*(Cs+cak1*dt/2);
```

```
c2 = rho*(pr*Cs-C1+c1*dt/2);

   k3 =  rho*(pr*Cs-(B+k2*dt/2));
ck3=  2*rho*m*B - mu*(C+ck2*dt/2);
cak3 = d*s*C-rho*(Cs+cak2*dt/2);
   c3 = rho*(pr*Cs-C1+c2*dt/2);

   k4 =  rho*(pr*Cs-(B+k3*dt));
ck4=  2*rho*m*B - mu*(C+ck3*dt);
cak4 = d*s*C-rho*(Cs+cak3*dt);
   c4 = rho*(pr*Cs-C1+c3*dt);

M = M + (1-pr)*Cs*dt;
B = B+dt*(k1+2*k2+2*k3+k4)/6;
C = C+dt*(ck1+2*ck2+2*ck3+ck4)/6; % dynamics of centrocytes
Cs= Cs + dt*(cak1+2*cak2+2*cak3+cak4)/6; % dynamics of Ag-Centrocytes

T = B+C+Cs;
CT = C+Cs;

% plotting
subplot(3,1,2)
plot(t,B,'m*', t, CT, 'rd', t, M, 'gd', t, T, 'kd');
legend('B blasts', 'centrocytes', 'memory cells', 'total B cells');
hold on,
pause(0);

end

for t=4+dt:dt:30
   %m = 0.72;  % non-deleterious mutation rate
   m = 1;
   s = sc;
mu = d*s+dc*(1-s);

   k1 = rho*(pr*Cs-B);
   ck1 = 2*rho*m*B - mu*C;
   cak1 = d*s*C-rho*Cs;
   c1 = rho*(pr*Cs-C1);

   k2 =  rho*(pr*Cs-(B+k1*dt/2));
ck2=  2*rho*m*B - mu*(C+ck1*dt/2);
cak2 = d*s*C-rho*(Cs+cak1*dt/2);
c2 = rho*(pr*Cs-C1+c1*dt/2);

   k3 =  rho*(pr*Cs-(B+k2*dt/2));
ck3=  2*rho*m*B - mu*(C+ck2*dt/2);
```

```
cak3 = d*s*C-rho*(Cs+cak2*dt/2);
   c3 = rho*(pr*Cs-C1+c2*dt/2);

   k4 =  rho*(pr*Cs-(B+k3*dt));
ck4=  2*rho*m*B - mu*(C+ck3*dt);
cak4 = d*s*C-rho*(Cs+cak3*dt);
   c4 = rho*(pr*Cs-C1+c3*dt);

   M = M + (1-pr)*Cs*dt;
B = B+dt*(k1+2*k2+2*k3+k4)/6;
C = C+dt*(ck1+2*ck2+2*ck3+ck4)/6; % dynamics of centrocytes
Cs= Cs + dt*(cak1+2*cak2+2*cak3+cak4)/6; % dynamics of Ag-Centrocytes

C1 =pr*Cs;

T = B+C+Cs;
CT = C+Cs;

% plotting
subplot(3,1,2)
plot(t,B,'--m', t, CT, ':r', t, M, '-g', t, T, '--kd');
legend('B blasts', 'centrocytes', 'memory cells', 'total B cells');
hold on,
pause(0);
end



% Runge-Kutta method
for t=dt:dt:3
   bb1 = rho*Bb;
   bb2 = rho*(Bb+bb1*dt/2);
bb3 = rho*(Bb+bb2*dt/2);
   bb4 = rho*(Bb+bb3*dt);

   Bb = Bb+dt*(bb1+2*bb2+2*bb3+bb4)/6;
   T = Bb;
   CT =0;

   subplot(3,1,3)
   plot(t,Bb,'m*', t, CT, 'rd', t, M, 'gd', t, T, 'kd');
   hold on


end

B = Bb;
```

```
for t=3+dt:dt:4
   m = 1;  % no somatic hypermutation
   %s = 0.5 * Kt^l/((t-3)^l+Kt^l);
   s = sc+0.3;
 mu = d*s+dc*(1-s);


   k1 = rho*(pr*Cs-B);
   ck1 = 2*rho*m*B - mu*C;
   cak1 = d*s*C-rho*Cs;
   c1 = rho*(pr*Cs-C1);

   k2 =  rho*(pr*Cs-(B+k1*dt/2));
ck2=  2*rho*m*B - mu*(C+ck1*dt/2);
cak2 = d*s*C-rho*(Cs+cak1*dt/2);
c2 = rho*(pr*Cs-C1+c1*dt/2);

   k3 =  rho*(pr*Cs-(B+k2*dt/2));
ck3=  2*rho*m*B - mu*(C+ck2*dt/2);
cak3 = d*s*C-rho*(Cs+cak2*dt/2);
   c3 = rho*(pr*Cs-C1+c2*dt/2);

   k4 =  rho*(pr*Cs-(B+k3*dt));
ck4=  2*rho*m*B - mu*(C+ck3*dt);
cak4 = d*s*C-rho*(Cs+cak3*dt);
   c4 = rho*(pr*Cs-C1+c3*dt);

M = M + (1-pr)*Cs*dt;
B = B+dt*(k1+2*k2+2*k3+k4)/6;
C = C+dt*(ck1+2*ck2+2*ck3+ck4)/6; % dynamics of centrocytes
Cs= Cs + dt*(cak1+2*cak2+2*cak3+cak4)/6; % dynamics of Ag-Centrocytes

T = B+C+Cs;
CT = C+Cs;

% plotting
subplot(3,1,3)
plot(t,B,'m*', t, CT, 'rd', t, M, 'gd', t, T, 'kd');
legend('B blasts', 'centrocytes', 'memory cells', 'total B cells');
hold on,
pause(0);

end

for t=4+dt:dt:30
   %m = 0.72;  % non-deleterious mutation rate
```

```
   m = 1;
   s = sc + 0.3;
mu = d*s+dc*(1-s);


   k1 = rho*(pr*Cs-B);
   ck1 = 2*rho*m*B - mu*C;
   cak1 = d*s*C-rho*Cs;
   c1 = rho*(pr*Cs-C1);

   k2 =  rho*(pr*Cs-(B+k1*dt/2));
ck2=  2*rho*m*B - mu*(C+ck1*dt/2);
cak2 = d*s*C-rho*(Cs+cak1*dt/2);
c2 = rho*(pr*Cs-C1+c1*dt/2);

   k3 =  rho*(pr*Cs-(B+k2*dt/2));
ck3=  2*rho*m*B - mu*(C+ck2*dt/2);
cak3 = d*s*C-rho*(Cs+cak2*dt/2);
   c3 = rho*(pr*Cs-C1+c2*dt/2);

   k4 =  rho*(pr*Cs-(B+k3*dt));
ck4=  2*rho*m*B - mu*(C+ck3*dt);
cak4 = d*s*C-rho*(Cs+cak3*dt);
   c4 = rho*(pr*Cs-C1+c3*dt);

M = M + (1-pr)*Cs*dt;
B = B+dt*(k1+2*k2+2*k3+k4)/6;
C = C+dt*(ck1+2*ck2+2*ck3+ck4)/6; % dynamics of centrocytes
Cs= Cs + dt*(cak1+2*cak2+2*cak3+cak4)/6; % dynamics of Ag-Centrocytes

C1 =pr*Cs;

T = B+C+Cs;
CT = C+Cs;

% plotting
subplot(3,1,3)
plot(t,B,'--m', t, CT, ':r', t, M, '-g', t, T, '--kd');
legend('B blasts', 'centrocytes', 'memory cells', 'total B cells');
hold on,
pause(0);
end
```

The program code for the simple model where the selection factor is constant except for the time regime $4 < t < 7$ is not given explicitly.

The program code for the simple model when somatic hypermutation terminates at day 16 and the selection stringency needs therefore to be increased

is given below

## C.2 Program to the Numerical Solutions of the Model in 2.4

The sign of $a_0$ and $a_1$ in the range of $K_1, K_2$ was determined by using the following Matlab code

```
% algorithm in order to determine the sign of a_0 and a_1 ...
% for the range of K1(i) and K2(j)%


r = 4*log(2);
rho = r;
m = 0.72;
d = 12*log(2);
mu1 = 2*log(2);
mu2 = 8*log(2);
M11 = 0.95;

K1 = linspace(0,2,120);
K2 = linspace(0,2,120);

ck = 0;
k = 0;
dk = 0;
dk1 = 0;
dk2 = 0;
dk3 = 0;
dk4 = 0;
for i=1:120
   for j = 1:120
      Z(i,j) =  0.04*(12.*K1(i)*K2(j)+25.-37.*K2(j))/(K1(i)-1.*K2(j));


         pol1 = (1/12*(37*rho*mu1*K1(i)*K2(j)+24*mu1*mu2*K2(j)^2*K1(i)-...
               50*mu1*mu2*K2(j)+12*rho*K2(j)^2*mu2*K1(i)-37*rho*K2(j)*mu2*K1(i)...
               +25*rho*mu2*K1(i)+50*mu1*mu2*K1(i)-25*rho*mu1*K2(j))/mu1/K2(j)/(rho+2*m

         pol2 = -1/12*(25*rho^2*K2(j)-24*rho*K2(j)^2*mu2*K1(i)-25*rho^2*K1(i)+...
               50*rho*K2(j)*mu2+100*rho*mu1*K2(j)+125*mu1*mu2*K2(j)+74*rho*K2(j)*mu2*K
               -100*rho*mu2*K1(i)-125*mu1*mu2*K1(i)-12*mu1*mu2*K2(j)^2*K1(i)-...
               74*rho*mu1*K1(i)*K2(j)-50*rho*mu1*K1(i))/mu1/K2(j)/(mu2+2*rho);

            pol3 = -.4000000000e-1*rho*(-100.*rho^2*K2(j)+100.*rho^2*K1(i)-150.*rho*mu
               +125.*rho*mu1*K1(i)-100.*mu1*mu2*K2(j)+100.*mu1*mu2*K1(i)-125.*rho*mu2*
```

```
                150.*rho*mu2*K1(i)-37.*rho*mu2*K2(j)*K1(i)+12.*rho*mu2*K2(j)^2*K1(i)+
                37.*rho*mu1*K1(i)*K2(j)-12.*rho*mu1*K1(i)^2*K2(j))/(K2(j)-1.*K1(i));



            pol1a = 25.*(-1.*rho*mu2-1.*rho*mu1+rho*M11*K1(i)*mu1-4.*mu1*mu2+...
               2.*M11*K1(i)*mu1*mu2)/mu2/(-74.*mu1+25.*rho*M11-37.*rho+50.*M11*mu1);
            pol2a = -25.*(4.*rho*mu1+6.*mu1*mu2-1.*M11*K1(i)*mu1*mu2+...
               4.*rho*mu2-2.*rho*M11*K1(i)*mu1+rho^2)/mu2/(-37.*mu1+50.*rho*M11+...
               25.*M11*mu1-74.*rho);
            pola3 = -25.*(4.*rho^2+6.*rho*mu1+4.*mu1*mu2+6.*rho*mu2-...
               1.*rho*M11*K1(i)*mu1)/rho/mu2/(-37.+25.*M11);

if (Z(i,j) <= 0.74) % M11 > RHS , a0 > 0
   if (K2(j) <= pol1a) % a1 <= 0 eigenvalue > 0
      dk = dk +1;
      d1(dk,1) = i;
      d1(dk,2) = j;
      d1(dk,3) = 1;
   else
      if (K2(j) <= pol2a) % a2 <= 0 eigenvalue > 0
         dk = dk +1;
      d1(dk,1) = i;
      d1(dk,2) = j;
      d1(dk,3) = 1;
      else
         if (K2(j) <= pola3) % a3 < 0 eigenvalue > 0
            dk = dk +1;
      d1(dk,1) = i;
      d1(dk,2) = j;
      d1(dk,3) = 1;
         else
            if (K2(j) > pola3) % a3 > 0 eigenvalue ?
            dk4 = dk4 +1;
       d4(dk4,1) = i;
       d4(dk4,2) = j;
            d4(dk4,3) = 1;
            end
         end
      end
   end
end

      if (Z(i,j) >= 1) % M11 < RHS , a0 < 0; eigenvalue > 0
         ck = ck+1;
         c(ck,1) = i;
         c(ck,2) = j;
```

```
         c(ck,3) = 4;
      end


if (Z(i,j) < 1 & Z(i,j) > 0.74)
    k = k+1;
         b(k,1) = i;
         b(k,2) = j;
         m11 = Z(i,j);

         if (K1(i)^2 < pol1)
            b(k,3) = -1; % a0 = 0; a1 < 0
         end

         if (K1(i)^2 ==  pol1 & K1(i)^2 == pol2 & pol3 >= 0)
            b(k,3) = 5; % a0 = 0; a1 = a2= 0, a3 >= 0
         else
            if (K1(i)^2 ==  pol1 & K1(i)^2 == pol2 & pol3 < 0)
               b(k,3) = 6; %a0 = 0; a1 = a2= 0, a3 < 0
            end
         end

         if (K1(i)^2 > pol1)
            if (K1(i)^2 > pol2)
                 b(k,3) = 1; % a0 = 0; a1 > 0, a2 > 0
              else
                 if (K1(i)^2 < pol2)
                    b(k,3) = 2; % a0 = 0; a1 > 0, a2 < 0
                 end
            end
         end

      end
   end
end



figure


b0 = find(b(:,3) < 0);
b1 = find(b(:,3) > 0 & b(:,3) <5 );
b3 = find(b(:,3) >=5);
```

```
subplot(1,2,1)
plot(K1(b(b0,1)),K2(b(b0,2)),'r*',K1(b(b1,1)),K2(b(b1,2)),'m*',...
   K1(b(b3,1)),K2(b(b3,2)),'b*'),
legend('a_0 = 0, a_1 < 0', 'a_0 = 0, a_1 > 0', 'a_0=a_1=0')
title('Non-trivial equilibrium region')
text(10,2,'\mu_1 = 5 ln(2) \mu_2 = 10 ln(2) 0.9 < M_{11} < 1')
xlabel('K1'),
ylabel('K2')

subplot(1,2,2)
plot(K1(d1(:,1)),K2(d1(:,2)),'g*',K1(c(:,1)),K2(c(:,2)),'y*', ...
   K1(b(:,1)),K2(b(:,2)),'r*')
title('Parameter Space')
legend('a_0 > 0 (unstable part)', 'a_0 < 0', 'a_0 = 0')
xlabel('K1'),
ylabel('K2')

hold on
```

For the 1-generation model, solutions were obtained via the following program

```
% model for affinity maturation in primed response

% model uses only kinetic data and obtains affinity increase from model %
% this affinity increaes feeds back into the model for antigen extraction%
% and the selection factor is finally dependent on antigen density

% resulting kineitcs optimal %




% parameters
dt = 0.1;

Bb  = 3; % number of seeding B blasts
C = 0; % number of centrocytes
Cs = 0; % number of selected centrocytes
Ag = 10000; % number of antigen complexes
M = 0; % number of memory cells
PC = 0;
AFC = 0;
Aff = 3;
```

```
affg = 0;
affgmax = 0.7;

ln2 = log(2);
rho = 4*ln2; % maximum proliferation rate of centroblast (day^-1)
d = 10 * ln2; % time to run through selection process
mu = 4*ln2;
s = 0.5;  % selection probability
Kt = 18; % Hill coefficient for s
dc = 1.5*ln2;  % death rate for non-selected centrocytes
pr = 0.8; % probability of recycling
u = 0.000025; % percent of antigen complex extracted by centrocyte
k = 0;  % percent of non-selected centrocytes extracting antigen
l = 7;
a = 1;


figure

% Runge-Kutta method
for t=dt:dt:3
   bb1 = rho*Bb;
   bb2 = rho*(Bb+bb1*dt/2);
bb3 = rho*(Bb+bb2*dt/2);
   bb4 = rho*(Bb+bb3*dt);

   Bb = Bb+dt*(bb1+2*bb2+2*bb3+bb4)/6;
   T = Bb;
   CT =0;

     affg = 0;
   affgc = 0;

   subplot(2,1,1),
   plot(t,Bb,'m*', t, CT, 'rd', t, M, 'gd', t, T, 'kd', t, Ag, 'b*'),
   legend('B blasts', 'centrocytes', 'AFC & memory cells', 'total B cells', ...
   'Antigen'),
   hold on


   subplot(2,1,2),
plot(t, Aff/100, 'kd', t,affg,'gd', t, affgc, 'rd'),
hold on


end
```

```
B = Bb;
Affmax = 65;
l2 = 15;


for t=3+dt:dt:3.5
   m = 1;  % no somatic hypermutation

   affgc = 0.03;
   s = 0.5;
   mu = d*s+(1-s)*dc;

   k1 = rho*(pr.*Cs-B);
   ck1 = 2*rho*m*B - mu.*C;
   cak1 = d*s.*C-rho*Cs;
   c1 = -(u*k*sum(C)+u*sum(Cs)*(1-k))*Ag;

   k2 =  rho*(pr.*Cs-(B+k1*dt/2));
ck2=  2*rho*m*B - mu.*(C+ck1*dt/2);
cak2 = d*s.*C-rho*(Cs+cak1*dt/2);
   c2 = -(u*k*sum(C)+u*sum(Cs)*(1-k))*(Ag+c1*dt/2);

   k3 =  rho*(pr.*Cs-(B+k2*dt/2));
ck3=  2*rho*m*B - mu.*(C+ck2*dt/2);
cak3 = d*s.*C-rho*(Cs+cak2*dt/2);
   c3 = -(u*k*sum(C)+u*sum(Cs)*(1-k))*(Ag+c2*dt/2);

   k4 =  rho*(pr.*Cs-(B+k3*dt));
ck4=  2*rho*m*B - mu.*(C+ck3*dt);
cak4 = d*s.*C-rho*(Cs+cak3*dt);
   c4 = -(u*k*sum(C)+u*sum(Cs)*(1-k))*(Ag+c3*dt);

AFC = AFC + (1-pr).*Cs*dt;
B = B+dt*(k1+2*k2+2*k3+k4)/6;
C = C+dt*(ck1+2*ck2+2*ck3+ck4)/6; % dynamics of centrocytes
Cs= Cs + dt*(cak1+2*cak2+2*cak3+cak4)/6; % dynamics of Ag-Centrocytes
Ag = Ag + dt*(c1+2*c2+2*c3+c4)/6;

T = B+C+Cs;
CT = C+Cs;

% plotting
pause(0);
subplot(2,1,1),
plot(t,B,'m*', t, CT, 'rd', t, M+AFC, 'gd', t, T, 'kd', t, Ag, 'b*'),
title('GC kinetics in primed primary immune response'),
hold on,
```

```
subplot(2,1,2),
plot(t, Aff/100, 'kd',t,affg,'gd', t, affgc, 'rd'),
hold on

end

B = [0.97*B,0.03*B]'; % 3% are high affinity clones
C = [0.97*C,0.03*C]';
Cs = [0.97*Cs,0.03*Cs]';
M = [0.97*M,0.03*M]';
PC  = [0.97*PC,0.03*PC]';
AFC = [0.97*AFC,0.03*AFC]';

%MM = [0.96, 0.07; 0.04, 0.93]; % 1/3 beneficial mutation
%MM = [0.94, 0.06; 0.06, 0.94];  % 1/2 beneficial mutation
%MM = [0.986, 0.246; 0.014, 0.754]; % Manser I mutation matrix (0.1% beneficial)
%MM = [0.986, 0.123; 0.014, 0.877]; % Manser II mutation matrix (0.1% beneficial)
MM = [0.9746, 0.229; 0.0254, 0.7710]; % 10% beneficial mutation of 26 % change
% 1% of total beneficial
%MM = [0.9152, 0.1696; 0.0848, 0.8304]; % 1/3 beneficial mutation of 26 % change
%MM = [0.9364, 0.0636; 0.1908, 0.8092]; % 1/4 beneficial mutation of 26 % change



%MM = [0.97, 0.07; 0.03, 0.93]; % 1/3 beneficial mutation


affgmax = 0.7;
Ag18 = 7000;
Ag1 = 8000;
Ag2 = 5500;
Ag3 = 5000;

n = 50;
n1 = 50;

for t=3.5+dt:dt:30
   s =[0.17*Ag^n1/(Ag3^n1+Ag^n1),1*Ag^n1/(Ag3^n1+Ag^n1)]';
   pr = [0.95, (0.05 +0.7*(1-Ag^n/(Ag18^n+Ag^n)))]';

   if t <= 16
      m = 0.72; % non-deleterious mutation rate
   else
      m = 1;
end
```

```
   if t < 7
      Aff = 29.97/3.5*t-29.94;
   end

  if t >= 7
     if t <= 21
        Aff = 30+2.5*(t-7);
     end
  end

  affgc = C(2)/sum(C);
  mu = d*s+(1-s)*dc;


   k1 = rho*(pr.*Cs-B);
   ck1 = 2*rho*m*B - mu.*C;
   cak1 = d*s.*C-rho*Cs;
   c1 = -(u*k*sum(C)+u*sum(Cs)*(1-k))*Ag;

   k2 =  rho*(pr.*Cs-(B+k1*dt/2));
ck2=  2*rho*m*B - mu.*(C+ck1*dt/2);
cak2 = d*s.*C-rho*(Cs+cak1*dt/2);
   c2 = -(u*k*sum(C)+u*sum(Cs)*(1-k))*(Ag+c1*dt/2);

   k3 =  rho*(pr.*Cs-(B+k2*dt/2));
ck3=  2*rho*m*B - mu.*(C+ck2*dt/2);
cak3 = d*s.*C-rho*(Cs+cak2*dt/2);
   c3 = -(u*k*sum(C)+u*sum(Cs)*(1-k))*(Ag+c2*dt/2);

   k4 =  rho*(pr.*Cs-(B+k3*dt));
ck4=  2*rho*m*B - mu.*(C+ck3*dt);
cak4 = d*s.*C-rho*(Cs+cak3*dt);
   c4 = -(u*k*sum(C)+u*sum(Cs)*(1-k))*(Ag+c3*dt);



if t >=5
   if t < 12
      AFC = AFC + 0.6*(ones(2,1)-pr).*Cs*dt;
      M = M + 0.4*(ones(2,1)-pr).*Cs*dt;
   else
      PC = PC + 0.6*(ones(2,1)-pr).*Cs*dt;
      M = M + 0.4*(ones(2,1)-pr).*Cs*dt;
   end
else
   AFC = AFC + (ones(2,1)-pr).*Cs*dt;
end
```

```
B = B+dt*(k1+2*k2+2*k3+k4)/6;
C = C+dt*(ck1+2*ck2+2*ck3+ck4)/6; % dynamics of centrocytes
Cs= Cs + dt*(cak1+2*cak2+2*cak3+cak4)/6; % dynamics of Ag-Centrocytes
Ag = Ag + dt*(c1+2*c2+2*c3+c4)/6;

if t <=16
B = MM*B;
end

T = sum(B)+sum(C)+sum(Cs);
CT = sum(C)+sum(Cs);
BT = sum(B);

affg = (Cs(2)+M(2))/(sum(Cs)+sum(M));
affgc = C(2)/sum(C);

% plotting
pause(0),
subplot(2,1,1),
plot(t,BT,'m*', t, CT, 'rd', t, sum(M)+sum(AFC), 'gd', t, T, 'kd', t, Ag, 'b*'),
title('GC kinetics in primed primary immune response'),
hold on


subplot(2,1,2),
plot(t, Aff/100, 'kd', t,affg,'gd', t, affgc, 'rd'),
legend('experimental results','model results(M&C_s)','model results (C)',2),
title('Affinity increase in experiments & in this model'),
hold on

if t == 10
   AFC10 = AFC
end

if t == 14
   AFC14 = AFC
end
end


Av = [6, 3; 10, 30; 14, 40; 17, 50; 21, 65; 30, 65];
subplot(2,1,2),
hold on,
plot(Av(:,1), Av(:,2)/100, 'b*'),
```

For the 2-generation model, solutions were obtained via the following program

```
% model for affinity maturation in primed response

% model uses only kinetic data and obtains affinity increase from model %
% this affinity increaes feeds back into the model for antigen extraction%
% and the selection factor is finally dependent on antigen density

% resulting kineitcs optimal %




% parameters
dt = 0.1;

Bb  = 3; % number of seeding B blasts
B1 = 0;
C = 0; % number of centrocytes
Cs = 0; % number of selected centrocytes
Ag = 10000; % number of antigen complexes
M = 0; % number of memory cells
PC = 0;
AFC = 0;
Aff = 3;
affg = 0;
affgmax = 0.7;

ln2 = log(2);
rho = 4*ln2; % maximum proliferation rate of centroblast (day^-1)
d = 10 * ln2; % time to run through selection process
mu = 4*ln2;
s = 0.5;  % selection probability
Kt = 18; % Hill coefficient for s
dc = 1.5*ln2;  % death rate for non-selected centrocytes
pr = 0.8; % probability of recycling
u = 0.000025; % percent of antigen complex extracted by centrocyte
k = 0;  % percent of non-selected centrocytes extracting antigen
l = 7;
a = 1;


figure

% Runge-Kutta method
```

```
for t=dt:dt:2.9
   bb1 = rho*Bb;
   bb2 = rho*(Bb+bb1*dt/2);
bb3 = rho*(Bb+bb2*dt/2);
   bb4 = rho*(Bb+bb3*dt);

   Bb = Bb+dt*(bb1+2*bb2+2*bb3+bb4)/6;
   T = Bb;
   CT =0;

     affg = 0;
   affgc = 0;

   subplot(2,1,1),
   plot(t,Bb,'m*', t, CT, 'rd', t, M, 'gd', t, T, 'kd', t, Ag, 'b*'),
   legend('B blasts', 'centrocytes', 'AFC & memory cells', 'total B cells', ...
   'Antigen'),
   hold on


   subplot(2,1,2),
plot(t, Aff/100, 'k+-', t,affg,'gd-', t, affgc, 'rd-'),
hold on


end

B = Bb;
Affmax = 65;
l2 = 15;


for t=3:dt:3.5
   m = 1;  % no somatic hypermutation

   affgc = 0.03;
   s = 0.5;
   mu = d*s+(1-s)*dc;

   k1 = rho*(pr.*Cs-B);
   bk1 = 2*rho*m*B - rho.*B1;
   ck1 = 2*rho*m*B1 - mu.*C;
   cak1 = d*s.*C-rho*Cs;
   c1 = -(u*k*sum(C)+u*sum(Cs)*(1-k))*Ag;

   k2 =  rho*(pr.*Cs-(B+k1*dt/2));
   bk2=  2*rho*m*B - rho.*(B1+bk1*dt/2);
```

```
ck2=  2*rho*m*B - mu.*(C+ck1*dt/2);
cak2 = d*s.*C-rho*(Cs+cak1*dt/2);
   c2 = -(u*k*sum(C)+u*sum(Cs)*(1-k))*(Ag+c1*dt/2);

   k3 =  rho*(pr.*Cs-(B+k2*dt/2));
   bk3=  2*rho*m*B - rho.*(B1+bk2*dt/2);
ck3=  2*rho*m*B - mu.*(C+ck2*dt/2);
cak3 = d*s.*C-rho*(Cs+cak2*dt/2);
   c3 = -(u*k*sum(C)+u*sum(Cs)*(1-k))*(Ag+c2*dt/2);

   k4 =  rho*(pr.*Cs-(B+k3*dt));
   bk4=  2*rho*m*B - rho.*(B1+bk3*dt);
ck4=  2*rho*m*B - mu.*(C+ck3*dt);
cak4 = d*s.*C-rho*(Cs+cak3*dt);
   c4 = -(u*k*sum(C)+u*sum(Cs)*(1-k))*(Ag+c3*dt);

AFC = AFC + (1-pr).*Cs*dt;
B = B+dt*(k1+2*k2+2*k3+k4)/6;
B1 = B1 +dt*(bk1+2*bk2+2*bk3+bk4)/6;
C = C+dt*(ck1+2*ck2+2*ck3+ck4)/6; % dynamics of centrocytes
Cs= Cs + dt*(cak1+2*cak2+2*cak3+cak4)/6; % dynamics of Ag-Centrocytes
Ag = Ag + dt*(c1+2*c2+2*c3+c4)/6;

T = B+B1+C+Cs;
CT = C+Cs;

% plotting
pause(0);
subplot(2,1,1),
plot(t,B+B1,'m*', t, CT, 'rd', t, M+AFC, 'gd', t, T, 'kd', t, Ag, 'b*'),
title('GC kinetics in primed primary immune response'),
hold on,

subplot(2,1,2),
plot(t, Aff/100, 'k+-', t,affg,'gd-', t, affgc, 'rd-'),
hold on

end

B = [0.97*B,0.03*B]'; % 3% are high affinity clones
B1 = [0.97*B1, 0.03*B1]';
C = [0.97*C,0.03*C]';
Cs = [0.97*Cs,0.03*Cs]';
M = [0.97*M,0.03*M]';
PC  = [0.97*PC,0.03*PC]';
AFC = [0.97*AFC,0.03*AFC]';
```

```
%MM = [0.96, 0.07; 0.04, 0.93]; % 1/3 beneficial mutation
%MM = [0.94, 0.06; 0.06, 0.94];  % 1/2 beneficial mutation
%MM = [0.986, 0.246; 0.014, 0.754]; % Manser I mutation matrix (1% beneficial)
%MM = [0.986, 0.123; 0.014, 0.877]; % Manser II mutation matrix (1% beneficial)

%MM = [0.97, 0.07; 0.03, 0.93]; % 1/3 beneficial mutation
MM = [0.9746, 0.229; 0.0254, 0.7710]; % 10% beneficial mutation of 26 % change
% 1% of total beneficial


affgmax = 0.7;
Ag18 = 7500;
Ag1 = 8000;
Ag2 = 5500;
Ag3 = 6000;

n = 50;
n1 = 50;

for t=3.5+dt:dt:30
   s =[0.14*Ag^n1/(Ag3^n1+Ag^n1),1*Ag^n1/(Ag3^n1+Ag^n1)]'; %  s(2) needs to be smaller

   if t <= 16
      m = 0.72; % non-deleterious mutation proportion
else
      m = 1;
end

   if t < 7
      Aff = 9*t-33;
   end

  if t >= 7
     if t <= 21
        Aff = 30+2.5*(t-7);
     end
  end

  affgc = C(2)/sum(C);
   mu = d*s+(1-s)*dc;

  pr = [(0.95+0*(1-Ag^n/(Ag18^n+Ag^n))), (0.05 +0.7*(1-Ag^n/(Ag18^n+Ag^n)))]';
  %if t<7
  %   if t>4
 %      pr = [0.95,0.05]';
   %    s = [0.13,1]';
   %  end
```

```
   %end

     k1 = rho*(pr.*Cs-B);
   bk1 = 2*rho*m*B - rho.*B1;
   ck1 = 2*rho*m*B1 - mu.*C;
   cak1 = d*s.*C-rho*Cs;
   c1 = -(u*k*sum(C)+u*sum(Cs)*(1-k))*Ag;

   k2 =  rho*(pr.*Cs-(B+k1*dt/2));
   bk2=  2*rho*m*B - rho.*(B1+bk1*dt/2);
ck2=  2*rho*m*B - mu.*(C+ck1*dt/2);
cak2 = d*s.*C-rho*(Cs+cak1*dt/2);
   c2 = -(u*k*sum(C)+u*sum(Cs)*(1-k))*(Ag+c1*dt/2);

   k3 =  rho*(pr.*Cs-(B+k2*dt/2));
   bk3=  2*rho*m*B - rho.*(B1+bk2*dt/2);
ck3=  2*rho*m*B - mu.*(C+ck2*dt/2);
cak3 = d*s.*C-rho*(Cs+cak2*dt/2);
   c3 = -(u*k*sum(C)+u*sum(Cs)*(1-k))*(Ag+c2*dt/2);

   k4 =  rho*(pr.*Cs-(B+k3*dt));
   bk4=  2*rho*m*B - rho.*(B1+bk3*dt);
ck4=  2*rho*m*B - mu.*(C+ck3*dt);
cak4 = d*s.*C-rho*(Cs+cak3*dt);
   c4 = -(u*k*sum(C)+u*sum(Cs)*(1-k))*(Ag+c3*dt);



if t >=5
   if t < 12
      AFC = AFC + 0.6*(ones(2,1)-pr).*Cs*dt;
      M = M + 0.4*(ones(2,1)-pr).*Cs*dt;
   else
      PC = PC + 0.6*(ones(2,1)-pr).*Cs*dt;
      M = M + 0.4*(ones(2,1)-pr).*Cs*dt;
   end
else
   AFC = AFC + (ones(2,1)-pr).*Cs*dt;
end

B = B+dt*(k1+2*k2+2*k3+k4)/6;
B1 = B1+dt*(bk1+2*bk2+2*bk3+bk4)/6;
C = C+dt*(ck1+2*ck2+2*ck3+ck4)/6; % dynamics of centrocytes
Cs= Cs + dt*(cak1+2*cak2+2*cak3+cak4)/6; % dynamics of Ag-Centrocytes
Ag = Ag + dt*(c1+2*c2+2*c3+c4)/6;

if t <=16
```

```
   B = MM*B;
   B1 = MM*B1;
end

T = sum(B)+sum(C)+sum(Cs)+sum(B1);
CT = sum(C)+sum(Cs);
BT = sum(B)+sum(B1);

affg = (Cs(2)+M(2))/(sum(Cs)+sum(M));
affgc = C(2)/sum(C);

% plotting
pause(0),
subplot(2,1,1),
plot(t,BT,'m*', t, CT, 'rd', t, sum(M)+sum(AFC), 'gd', t, T, 'kd', t, Ag, 'b*'),
title('GC kinetics in primed primary immune response'),
hold on


subplot(2,1,2),
plot(t, Aff/100, '--k+', t,affg,'--gd', t, affgc, '--rd'),
legend('experimental results','model results (M & C_s)', 'model results (C)',2),
title('Affinity increase in experiments & in this model'),
hold on

if t == 10
   AFC10 = AFC
end

if t == 14
   AFC14 = AFC
end
end


Av = [6, 3; 10, 30; 14, 40; 17, 50; 21, 65; 30, 65];
subplot(2,1,2),
hold on,
plot(Av(:,1), Av(:,2)/100, 'b*'),
```

# Appendix D

# Numerical Solution used in Chapter 4

## D.1 Numerical solution of equation 4.4

The analytic solution for the geometry of spherical cells binding to a surface decorated with adhesion molecules was visualised using the following Matlab programs

```
% Determine h in Lipowsky's equation
format long;

%UT = 1;
R = 3;
rho = 0;
Nin = 10^(10);

k3 = 10^-1;

i = 0;
for n = 0.05:0.1:0.95
   for k0 = 0:1:20
   i = i+1;
k1 = k0*R^2/k3;
k2 = rho*R^3/Nin;

   if n > 0.5
      if k0 < 7
         [a,fz] = fzero('f', 0.8,[],k0,k1,k2,n);
      else
         [a,fz] = fzero('f', 0.01,[],k0,k1,k2,n);
      end
   else
      if n < 0.1
         [a,fz] = fzero('f', 0.7,[],k0,k1,k2,n);
```

```
      else
       if k0 < 10
          [a,fz] = fzero('f', 0.8,[],k0,k1,k2,n);
      else
            [a,fz] = fzero('f', 0.4,[],k0,k1,k2,n);
         end
      end
   end

L(i,1)=n;
L(i,2)=k0;
L(i,3)=a;
L(i,4)=fz;

end
end
%c=find(L(:,3)<0);
%L(c,3)=0;

%d=find(L(:,3)>1);
%L(c,3) = 1;

% plotting
for(i=1:10)
   z(i,:)=L((21*(i-1)+1):(21*i),3)';
end



n = linspace(0.01,0.91,10);
k0 = linspace(0,20,21);

figure
surfc(k0,n,z);
xlabel('U/T');
ylabel('n');
zlabel('h');
title('h in dependence of n and U/T');
axis([0 20 0 1 0 1]);
```

The function f is given in another M-file

```
function k = f(x,k0,k1,k2,n)

g = n/(1-n)-exp(-k0)-0.5*(1-x^2)*(1-exp(-k0))/(1-n);
d = 4*exp(-k0)*n/(1-n);
```

```
fs = 0.5*(g+sqrt(g^2+d));

u = 8*pi/3*k1*fs*exp(k0)/(1+fs*exp(k0));
v = 4*pi/3*k2;

k = (u*x/(1-x^2)+v)*x*(3-x^2)-2;
```

# Appendix E

# Program Codes for Simulations presented in Chapter 6

## E.1 Programs for the Simulation of Cylinder Cells

### E.1.1 C Program for the Simulation of Cylinder Cells

Simulation in which the contact angle can change in every sweep

### E.1.2 Matlab Programs for Visualisation of the Results

The relevant Matlab programs for visualisation of the results are given below:

In order to plot the time dependency of the inner energy and the concentration of lipid A in the contact zone the program ctvol.m was used given below

```
%%%%%%%% Results of C simulation %%%%%%%%%%
clear

load kUa4gVs1.dat

load kGgV.dat

Ns0 = kGgV(:,4);
b  = kGgV(1,3);
L = 100;
F = b/L;
F2 = L*b;
N = L*L;
al = N;

M0 = kUa4gVs1;

subplot(2,1,1)
```

```
plot(M0(:,1), M0(:,3));
legend('B=2');
title('Inner Energy decrease for cylinder variable {\gamma} and J = 0.05')
xlabel('t');
ylabel('U');

%subplot(2,1,2)
%plot(M0(:,1), M0(:,3),M1(:,1), M1(:,3),M2(:,1), M2(:,3), M3(:,1), M3(:,3), M4(:,1),
%xlabel('t');
%ylabel('U');


%subplot(2,1,1)
%plot(M0(:,1), M0(:,2)/(F*Ns0(1)),M1(:,1), M1(:,2)/(F*Ns0(2)),M2(:,1), M2(:,2)/(F*Ns
%legend('aff=0','aff=10','aff=100','aff=1000','aff=10000','aff=100000');
%title('Concentration of lipid A in the contact zone for {\gamma}={\pi}/4 and J = 0
%xlabel('t');
%ylabel('c');

subplot(2,1,2)
plot(M0(:,1), M0(:,2)/F2);
legend('B=2');
title('Share of lipid A in the contact zone with variable {\gamma} and J = 0.05')
xlabel('t');
ylabel('c');
```

in order to visulise the final cylinder the program cylplotv.m was used

```
clear

load kGgV.dat
load spinsV.dat

%parameter

L = kGgV(1,2);
b = kGgV(1,3);
g =kGgV(1,6);

R1 = 3*pi/(pi-g+cos(abs(pi/2-g)))
h = R1*cos(g);


% coordinates
y = linspace(1,L,L);
z = zeros(L,L);
```

```
phi = -pi/2;
for i=1:(L-b)/2+2
phi = phi+(pi/2-g-(-pi/2))/((L-b)/2+1);
   x(i) = R1*cos(phi);
   z(:,i)=-h + R1*sin(phi);
end

for i = (L-b)/2+3:L/2+b/2+3
phi=phi+2*g/b;
   x(i) = R1*cos(phi);
   z(:,i)=0;
end

for i=L/2+b/2+4:L
phi = phi+ (pi/2-g-(-pi/2))/((L-b)/2-4);
   x(i) = R1*cos(phi);
   z(:,i)=-h + R1*sin(phi);
end

cc = length(spinsV);
% plotting
c = spinsV(cc-99:cc,:)';

surf(x,y,z,c)
title('Contact zone for {\gamma}={\pi}')
get(1);
set(1,'colormap',vga);
```

and in order to determine diffusion the program diffn.m was used

```
clear

%load C:\\Cprogrammes\diff.dat

load diffsV.dat
diff = diffsV;
subplot(2,1,1)
plot(diff(:,1), (diff(:,2)), 'r+',diff(:,1), (diff(:,4)), 'b+',diff(:,1), (diff(:,6)),
%axis([0 10^5 0 15]);
title('Diffusion of spin 1 with time')
   legend('spin1 displacement in 2 dimensions', 'spin1 mean x displacement', 'spin1 me
   xlabel('t (steps)')
ylabel('{s^2} (displacement)')

subplot(2,1,2)
plot(diff(:,1), (diff(:,3)), 'r+',diff(:,1), (diff(:,5)), 'b+', diff(:,1), (diff(:,7))
%axis([0 10^5 0 15]);
```

```
title('Diffusion of spin -1 with time')
legend('spin -1 displacement in 2 dimensions','spin -1 mean x displacement', 'spin -
   xlabel('t (steps)')
ylabel('{s^2} (displacement)')
```

.

Simulation in which the contact angle is kept fixed and the time course for different lipid A proportions were analysed by the following Matlab programs.

cspinden.m plots U(t) and the increase of lipid A in the contact zone with time

```
%%%%%%%%% Results of C simulation %%%%%%%%%%%%
clear

load kUa4ghs0.dat
load kUa4ghs1.dat
load kUa4ghs2.dat
load kUa4ghs5.dat
load kUa4ghsh.dat

load kGgh.dat



Ns0 = kGgh(:,4);
b  = kGgh(1,3);
L = 100;
F = b/L;
F2 = L*b;
N = L*L;
al = N;

M0 = kUa4ghs0;
M1 = kUa4ghs1;
M2 = kUa4ghs2;
M3 = kUa4ghs5;
M4 = kUa4ghsh;


subplot(2,1,1)
plot(M0(:,1), M0(:,3),M1(:,1), M1(:,3),M2(:,1), M2(:,3), M3(:,1), M3(:,3), M4(:,1),
legend('lipid A-{\rho}= 0%','lipid A-{\rho}=10%','lipid A-{\rho}=20%','lipid A-{\rho
title('Inner Energy decrease for cylinder with {\gamma}={\pi}/10 and J = 0.05')
xlabel('t');
ylabel('U');
```

```
subplot(2,1,2)
plot(M0(:,1), M0(:,2)/F2, M1(:,1), M1(:,2)/F2, M2(:,1), M2(:,2)/F2, M3(:,1), M3(:,2)/F
legend('lipid A-{\rho}= 0%','lipid A-{\rho}=10%','lipid A-{\rho}=20%','lipid A-{\rho}=
title('Share of lipid A in the contact zone with {\gamma}={\pi}/10 and J = 0.05')
xlabel('t');
ylabel('c');
```

cylplots.m plots the relevant cylinder geometry

```
% Matlab code to plot cylinder from data produces with
% kftotspin2.cpp

clear

load kGgh.dat
load spins1.dat % choose data file which you want to look at
% angle for all the same

spinsh = spins1; % set parameter right
%parameter

L = kGgh(1,2);
b = kGgh(1,3);
g = kGgh(1,6);

R1 = 3*pi/(pi-g+cos(abs(pi/2-g)))
h = R1*cos(g);


% coordinates
y = linspace(1,L,L);
z = zeros(L,L);

phi = -pi/2;
for i=1:(L-b)/2+2
phi = phi+(pi/2-g-(-pi/2))/((L-b)/2+1);
   x(i) = R1*cos(phi);
   z(:,i)=-h + R1*sin(phi);
end

for i = (L-b)/2+3:L/2+b/2+3
phi=phi+2*g/b;
   x(i) = R1*cos(phi);
   z(:,i)=0;
end

for i=L/2+b/2+4:L
```

```
phi = phi+ (pi/2-g-(-pi/2))/((L-b)/2-4);
   x(i) = R1*cos(phi);
   z(:,i)=-h + R1*sin(phi);
end


% plotting
c = spinsh(901:1000,:)';

surf(x,y,z,c)
title('Contact zone for {\gamma}={\pi}')
get(1);
set(1,'colormap',vga);
```

## E.2 C Program for the Simulations of Spherical Cells

The sphere was simulated by the code given below. The Matlab programs used for plotting the results are omitted for space limitations.

```
 /* BEST PROGRAM so far for nonlocalised lipids on cell surface

angle are changed dynamically and neighbors are interacting*/



 /* saving and loading of old data works */


/* beta   = inverse temperature
 * theta  = angle between r and z-axis (0,0,1)
 * phi   = angle between r and x-axis (1,0,0)
 * L      = constant edge length of lattice
 * nv[]   = vector of neighbour coordinates*/


#include <math.h>
#include <stdio.h>
#include <stdlib.h>
#include <time.h>
#include "ran3.cpp"

#define proplipidA 0.15
#define Lipidtotal 20000
#define N Lipidtotal
#define tf 50000*Lipidtotal /* number of time steps */
#define J 0.5
#define B 5
```

```
#define beta 100
#define Nt 1000
#define R 3

#define boxmax 50
#define phiboxmax 50
#define indtheta 50
#define indphi 50
#define Rconmax 1.41421356237310*R
#define abstmin 0.025  /* urspruenglich 0.05*/
#define abstlim 0.05
#define abstmin2 0.000625 /* 0.025 urspruenglich wenn abstmin = 0.05*/
#define abstlim2 0.0025


/* for aequidistant spins (dist = 0.1/R) would need Thresacc = 0.99944560623298 */
/* for non-overlapping lpids need Thresacc = 0.99999998611111 */

#define Thresacc 0.99999998611111 /*0.99999444444959*/
#define Thresneigh 0.99935026039497 /*0.99875026039497*/
#define pi 3.1415926535
#define PI3_20 0.47123889803847 /* 3*pi/20 */
#define PI3 9.42477796076938 /* 3*pi */


int Lspin[Lipidtotal][5];
int Lz[102][5000];
int LW[6000][1000];
int Lipidtotal1;
int Ns0,Ns1;
int zbox,zboxmax,thetaboxMax;
int i,j,k;
int t,td; /* time variable */
int spinnumber; /* number of chosen spin */
int sig;
int l5,l,spinlim;
int Ns2=0;
int counternew;


double Rold=R,hold=2*R,Rconold=0,g=0; /* variables that need to be saved for next run
double H,DH,dH;
double vect[3];
double thetaMax;
double cosw,sinw;
double gammaw;
double winkelold,winkelnew,winkeldiff;
```

```
double Lxy;
double V,Vf;
double R2 = 9;
double Rhelp;
double Rcon=0;
double Rnew = R;
double hnew=2*R;
double spv[Lipidtotal][6];
double spvR[3];
double spvnew[3];
double vp[3],helpv[3],helpv2[3];
double r2,L;
double dist,dist1,d,d2; /* distance parameters */
double wp,wp1;



long* dummy;



FILE *fp; /* File pointer */
/*FILE *fpen2; */ /* File pointer */
FILE *fpc;
FILE *fpg;
/*FILE *fpw;*/

int Ns1det(void);

int phiboxdet(double phiw1, double thetaw1);
int thetadet(double theta1);
int phidet(double phiw2);
double phiwdet(double vector9[]);
double thetawdet(double vector10[]);

double scalarproduct(double u[],double v[]);
double scalprodxy(double u[],double v[]);

void fileread();
void saveini();
void saveend();
void starts();
void distancedet(double vect[], int m);
void distance(double vector11[], int l);
void change(double Rold4, double hold4);
void drehung(int spinindex, double winkeldiff);
void initiation(); /* sets up the grid */
```

```
void move(double Rold3, double hold3);
void newbox(int spinnumber7,double Rold7,double hold7,double Rconold7);
void phiboxchange(int spinnumber8, double Rconold8);
void topch();
void geomch(double Rnew, double hnew, double Rold2, double Rconold2);



/* functions in order to determine neighbor interactions*/
double interboxes(double vector1[], int spinnumber1, double Rcon1);
double sphereroutine(double vector2[], int spinnumber2);
double circleroutine(double vector3[], int spinnumber3, double Rcon3);
double borderroutine(double vector4[],int spinnumber4,int phiboxb);
double schleifephi(double vector5[],int spinnumber5,int indexs1, int indexs2);
double neighbor(int spin, double vector6[], int spinnumber6);

void main()
{
/* fpen2 = fopen("Hverg.dat", "a");
fpw = fopen("winkel.dat", "w"); */

/* Seed the random-number generator with current time so that
    * the numbers will be different every time we run.
    */
/*srand( (unsigned)time( NULL ) );*/

dummy = new long; *dummy=-254128; ran3(dummy);
*dummy = 1;

/* initiliaze either from new or take previous values
as starting values*/

int beta_n=0;
/*clear();*/

if (beta_n >0){
fileread();
H = 0;}
else{
starts();
saveini();
thetaMax = pi-g;
thetaboxMax = thetadet(thetaMax);
}


for (t=0; t<tf; t++){
```

```
move(Rold, hold);


if (spv[spinnumber][5] > (Rold +0.1)){
printf("zu gross %f\t %f\t %f\t %f\n", spv[spinnumber][5], gammaw, g, Rold);
break;
}

if (spv[spinnumber][5]  < Rold-hold-0.1){
printf("zu klein %d\t %d\t %f\t %f\t %f\t %f\n", t, spinnumber, spv[spinnumber][5],
break;
}

double Le = sqrt(spv[spinnumber][3]*spv[spinnumber][3]+spv[spinnumber][4]*spv[spinnu
if (spv[spinnumber][5]  == Rold-hold && Le > Rconold){
printf("contact %d\t %d\t %f\t %f\n", t, spinnumber, Le, Rconold);
break;
}

if ((t % N)== 0){
printf("time %d\n", t);
topch();

int Ns1number = Ns1det();
fpg = fopen("gammaw.dat", "a");
fprintf(fpg, "%d\t %f\t %f\n", t, g, gammaw);
fclose(fpg);

fpc = fopen("conc.dat", "a");
fprintf(fpc, "%d\t %d\t %f\t %d\n", t, Ns1, H, Ns1number);
fclose(fpc);
}

} /* end time loop*/


/* fclose(fpen2);
fclose(fpw);*/
saveend();
} /* end main loop */



double scalarproduct(double u[],double v[])
{
double p;
p = u[0]*v[0]+u[1]*v[1]+u[2]*v[2];
```

```
return p;
}

double scalprodxy(double u[],double v[])
{
double p;
p = u[0]*v[0]+u[1]*v[1];
return p;
}



void saveini()
{
fp = fopen("sphereini.dat", "w");
for (i=0; i<Lipidtotal1; i++){
fprintf(fp, "%f\t %f\t %f\n", spv[i][3], spv[i][4], spv[i][5]);}
fclose(fp);

fp = fopen("spinini.dat", "w");
for (i=0; i<Lipidtotal1; i++){
fprintf(fp, "%d\n", Lspin[i][0]);}
fclose(fp);

}

void saveend()
{
fp = fopen("sphereend.dat", "w");
for (i=0; i<Lipidtotal1; i++){
fprintf(fp, "%lf\t %lf\t %lf\t %lf\t %lf\t %.7lf\n", spv[i][0], spv[i][1], spv[i][2],s
fclose(fp);

fp = fopen("spinend.dat", "w");
for (i=0; i<Lipidtotal1; i++){
fprintf(fp, "%d\t %d\t %d\n", Lspin[i][0], Lspin[i][1],Lspin[i][2]);}
fclose(fp);


fp = fopen("Lz0.dat", "w");
for (i = 0; i <102; i++){
fprintf(fp,"%d\n", Lz[i][0]);}
fclose(fp);

fp = fopen("LW0.dat", "w");
for (i = 0; i <6000; i++){
fprintf(fp,"%d\n", LW[i][0]);}
```

```
fclose(fp);


fp = fopen("Lz.dat", "w");
for (i = 0; i <102; i++){
for (j = 0; j <Lz[i][0]+1; j++){
fprintf(fp,"%d\t", Lz[i][j]);
/*printf("%d\n", Lz[i][j]);*/}
fprintf(fp,"\n");}
fclose(fp);

fp = fopen("LW.dat", "w");
for (i = 0; i <6000; i++){
for (j = 0; j <LW[i][0]+1; j++){
fprintf(fp,"%d\t", LW[i][j]);
}
fprintf(fp,"\n");}
fclose(fp);


fp = fopen("data.dat", "w");
fprintf(fp, "%f\t %f\t %f\t %f\t %f\t %d\t %d\t %f\t %f\t %d\t %d\n", V, g, Rold, Rc
fclose(fp);




}


void fileread()
{

int Lz0[102][1], LW0[6000][1];

fp = fopen("data.dat", "r");
fscanf(fp,"%lf %lf %lf %lf %lf %d %d %lf %lf %d %d", &V, &g, &Rold, &Rconold, &hold,
fclose(fp);

fp = fopen("sphereend.dat", "r");
for (i = 0; i <Lipidtotal1; i++){
for (j = 0; j <6; j++){
fscanf(fp,"%lf", &spv[i][j]);
}}
fclose(fp);
```

```
fp = fopen("spinend.dat", "r");
for (i = 0; i <Lipidtotal1; i++){
for (j = 0; j <3; j++){
fscanf(fp,"%d", &Lspin[i][j]);
}}
fclose(fp);

fp = fopen("Lz0.dat", "r");
for (i = 0; i <102; i++){
fscanf(fp,"%d", &Lz0[i][0]);}
fclose(fp);

fp = fopen("LW0.dat", "r");
for (i = 0; i <6000; i++){
fscanf(fp,"%d", &LW0[i][0]);}
fclose(fp);

fp = fopen("Lz.dat", "r");
for (i = 0; i <102; i++){
for (j = 0; j <Lz0[i][0]+1; j++){
fscanf(fp,"%d", &Lz[i][j]);}
}
fclose(fp);


fp = fopen("LW.dat", "r");
for (i = 0; i <6000; i++){
for (j = 0; j <LW0[i][0]+1; j++){
fscanf(fp,"%d", &LW[i][j]);
}
}
fclose(fp);


}




/* Inititation */

void starts()
{
/* parameter in loops*/
int nrs;
int l5;
```

```
int m;
int signal;
for (i=0; i<102; i++){
Lz[i][0] = 0;}

double k5;
double p1,t1;
double sinp,sint,cosp,cost;
double x,y,z;
double a1[3];


double Rstart = 3.;
double hstart = 6.;
double hight = -3.;
double Height = boxmax/hstart;
Rconold = 0;
V = 4*pi*Rstart*Rstart*Rstart/3;
g = 0;
Ns1 = 0;
Ns0 = 0; /* initial number of lipids A */



/* Initial spin distribution on sphere surface with r = 3
 * Determine angle coordinates randomly and test distance
 * if too close (d<0.01) reject,
 * take as next neighbor if distance d < 0.15 (<10 neighbors)*/


i = 0;

l5 = 0;
while (l5 < indtheta){
k5 = (2*l5+1)*pi/(2*indtheta);
nrs = (int) (R2*sin(k5))+(int) (2*ran3(dummy));

if (l5 == indtheta -2){
spinlim = i;}

for (j = 0; j<indphi; j++){
LW[l5*indphi+j][0] = nrs;
m = 1;

while (m < nrs+1){
signal = 0;
```

```
if ((i % 1000) == 0) {
printf("%d\n", i);}

while (signal == 0){
sig = 1;

/* coordinate choice */
p1 = j*2*pi/indphi + 2*pi*ran3(dummy)/indphi; /*phi*/
t1 = k5 - pi/(2*indtheta) + pi*ran3(dummy)/indtheta; /*theta*/
t1 = fmod(t1,pi);
cost = cos(t1);
sint = sqrt(1-cost*cost);
cosp = cos(p1);
sinp = sqrt(1-cosp*cosp);
if (p1 > pi){
sinp = -sinp;}

x = R*sint*cosp;
y = R*sint*sinp;
z = R*cost;

spv[i][0] = x;
spv[i][1] = y;
spv[i][2] = z;
spv[i][3] = x;
spv[i][4] = y;
spv[i][5] = z;



/* calculate distance to previous spins */
a1[0] = spv[i][3];
a1[1] = spv[i][4];
a1[2] = spv[i][5];

distancedet(a1,m);
signal = sig;
} /* end while (signal == 0) loop */



/* make list with spinnumbers in dependence of angle box*/
LW[l5*indphi+j][m] = i;
Lspin[i][3] = l5*indphi+j;
Lspin[i][4] = m;
```

```
/* putting Spin into z-Box */
zbox = (int) ((spv[i][5]-hight)*Height);
Lz[zbox][0] += 1;
Lz[zbox][Lz[zbox][0]]=i;

/* coordinates in spin list */
Lspin[i][1] = zbox;
Lspin[i][2] = Lz[zbox][0];

/* initial spin configuration with 10 % spin = 1*/
r2 = ran3(dummy);

if (r2 < proplipidA){
Lspin[i][0] = 1;
Ns0 +=1;}
else{
Lspin[i][0] = 1;}
i++;
m++;

} /* end while (m<nrs) loop*/

} /* end for (j<58) loop */
l5++;
} /* end while (k5 < pi) loop */

Lipidtotal1 = i;
printf("%d\t %d\n", Ns0, Lipidtotal1);

} /* end starts loop*/



void distancedet(double vect[], int m)
{
int par1,par2;
if (l5 < 1) {
for (l = 0; l < i; l++){
distance(vect, l);}
}

else {
if (l5 > (indtheta-2)){
for (l = spinlim; l < i; l++){
distance(vect, l);}
}
else {
```

```
par1 = l5*indphi+j;
par2 = (l5-1)*indphi+j;
for (k = 1; k < m; k++){
l = LW[par1][k];
distance(vect, l);}
for (k = 1; k < LW[par1-1][0]+1; k++){
l = LW[par1-1][k];
distance(vect, l);}
for (k = 1; k < LW[par2][0]+1; k++){
l = LW[par2][k];
distance(vect, l);}
for (k = 1; k < LW[par2+1][0]+1; k++){
l = LW[par2+1][k];
distance(vect, l);}
for (k = 1; k < LW[par2-1][0]+1; k++){
l = LW[par2-1][k];
distance(vect, l);}
}
}
}


void distance(double vector11[], int l)
{
double a3[3];
a3[0] = vector11[0] - spv[l][3];
a3[1] = vector11[1] - spv[l][4];
a3[2] = vector11[2] - spv[l][5];

wp = scalarproduct(a3,a3);
/* printf("wp %f\t, %f\n", wp, abstmin2);*/

if (wp < abstmin2){
sig=0;}
/*if (wp > Thresacc) {
sig = 0;}*/
}




void move(double Rold3, double hold3)
{
double disp[2];
double scal,theta,costh;
double thetamax = pi/50;
double dthe;
```

```
double height = Rold3-hold3;
double sv[3]; /* keeps initial values of spv[spinnumber][]*/
sv[0] = spv[spinnumber][3];
sv[1] = spv[spinnumber][4];
sv[2] = spv[spinnumber][5];


/* 1) choose one spin
 * 2) turn around perpendicular axis
 * 3) aquire new co-ordinates */

/* 1) choose a spin randomly */
spinnumber = (int) (Lipidtotal1 * ran3(dummy));
if (spinnumber == Lipidtotal1){ /* otherwise overflow */
spinnumber = Lipidtotal1-1;}



if (spv[spinnumber][5] > (height)){
/* 2) turn around perpendicular axis */
/* generate a vector vp on a random basis that is perpendicular to the cosen spin ve
wp = 2;

while (wp > 1) {
vect[0] = 2*ran3(dummy)-1;
vect[1] = 2*ran3(dummy)-1;
vect[2] = 2*ran3(dummy)-1;

wp = scalarproduct(vect,vect);
}

dist1 = sqrt(wp);


helpv[0] = vect[0]/dist1;
helpv[1] = vect[1]/dist1;
helpv[2] = vect[2]/dist1;

spvR[0] = spv[spinnumber][3]/Rold3;
spvR[1] = spv[spinnumber][4]/Rold3;
spvR[2] = spv[spinnumber][5]/Rold3;



costh = spvR[0]*helpv[0]+spvR[1]*helpv[1]+spvR[2]*helpv[2];
```

```
helpv2[0] = costh*spvR[0];
helpv2[1] = costh*spvR[1];
helpv2[2] = costh*spvR[2];

/* perpendicular vector */
vp[0] = helpv2[0] - helpv[0];
vp[1] = helpv2[1] - helpv[1];
vp[2] = helpv2[2] - helpv[2];

wp1 = scalarproduct(vp, vp);
dist = sqrt(wp1);



vp[0] = Rold3*vp[0]/dist;
vp[1] = Rold3*vp[1]/dist;
vp[2] = Rold3*vp[2]/dist;



/* turning */
theta = thetamax*ran3(dummy);

double sint = sin(theta);
double cost = cos(theta);

spvnew[0] = cost*spv[spinnumber][3]+sint*vp[0];
spvnew[1] = cost*spv[spinnumber][4]+sint*vp[1];
spvnew[2] = cost*spv[spinnumber][5]+sint*vp[2];


if (spvnew[2] < height){
/*determination of arc length beyond plate */
double arg = (vp[2]*vp[2]-height*height)/(vp[2]*vp[2]+spv[spinnumber][5]*spv[spinnumbe
if (arg < 0 && arg > -0.0001) {
arg = 0;}

costh = height*spv[spinnumber][5]/(vp[2]*vp[2]+spv[spinnumber][5]*spv[spinnumber][5])+

if (costh > 1 && costh < 1.01){
costh = 1;}
double dth = acos(costh);

d = Rold3*(theta-dth);
/* Take out full turns around cell */
d = fmod(d,(2*Rconold+(1-g/pi)*Rold3));
```

```
/*printf("%f\t %f\t %f\t %f\t %f\n", theta, dth, arg ,d, spv[spinnumber][5]-height);
if (d<0) {
printf("d \n");
d= 0;}

arg = spvnew[0]*spvnew[0]+spvnew[1]*spvnew[1];
L = sqrt(arg);


if ((Rconold-d) >= (-Rconold)) {
scal = (Rconold-d)/L;


/*projection on circle */
spvnew[2] = height;
spvnew[0] = scal*spvnew[0];
spvnew[1] = scal*spvnew[1];
}
else {
/* Turn back onto sphere */
dthe = (d-2*Rconold)/Rold3;

cosw = cos(dthe);
sinw = sin(dthe);


/* projection of spvnew to the edge of the circle in opposite direction*/

spvR[0] = -Rconold*spvnew[0]/L;
spvR[1] = -Rconold*spvnew[1]/L;
spvR[2] = height;


Lxy = sqrt(spvR[0]*spvR[0]+spvR[1]*spvR[1]);

/* perpendicular vector to spvR and u)*/
vp[0] = -spvR[0]*spvR[2]/Lxy;
vp[1] = -spvR[1]*spvR[2]/Lxy;
vp[2] = (spvR[0]*spvR[0]+spvR[1]*spvR[1])/Lxy;

L = sqrt(scalarproduct(vp,vp));

vp[0] = vp[0]/L;
vp[1] = vp[1]/L;
vp[2] = vp[2]/L;

L = sqrt(scalarproduct(spvR,spvR));
```

```
spvR[0] = spvR[0]/L;
spvR[1] = spvR[1]/L;
spvR[2] = spvR[2]/L;

/* TURN */

spvnew[0] = cosw*spvR[0]+sinw*vp[0];
spvnew[1] = cosw*spvR[1]+sinw*vp[1];
spvnew[2] = cosw*spvR[2]+sinw*vp[2];

L = sqrt(scalarproduct(spvnew,spvnew));

spvnew[0] = Rold3*spvnew[0]/L;
spvnew[1] = Rold3*spvnew[1]/L;
spvnew[2] = Rold3*spvnew[2]/L;

}

}
double arg = spvnew[0]*spvnew[0]+spvnew[1]*spvnew[1];
L = sqrt(arg);

if (L > Rconold && spvnew[2] < height) {
printf("FATALFATAL  %f\t %f\t %f\n", d, scal, Rconold);}

if (L > Rconold && spvnew[2] == height) {
printf("FATALcontact  %f\t %f\t %f\n", d, scal, Rconold);}

if ( spvnew[2] < height) {
printf("FATALhoehe  %f\t %f\t %f\n", d, Rold3, Rconold);}

}

if (spv[spinnumber][5] == (height)){
wp = 2;

while (wp > 1) {
disp[0] = 2*ran3(dummy)-1;
disp[1] = 2*ran3(dummy)-1;

wp = disp[0]*disp[0]+disp[1]*disp[1];
}


disp[0] = PI3_20*disp[0];
disp[1] = PI3_20*disp[1];
```

```
spvnew[0] = spv[spinnumber][3]+disp[0];
spvnew[1] = spv[spinnumber][4]+disp[1];
spvnew[2] = height;


Lxy = sqrt(spvnew[0]*spvnew[0]+spvnew[1]*spvnew[1]);


if ( Lxy > Rconold){
dthe = (Lxy-Rconold)/Rold3;

cosw = cos(dthe);
sinw = sin(dthe);


/* projection of spvnew to the edge of the circle */

spvR[0] = Rconold*spvnew[0]/Lxy;
spvR[1] = Rconold*spvnew[1]/Lxy;
spvR[2] = height;


Lxy = sqrt(spvR[0]*spvR[0]+spvR[1]*spvR[1]);

/* perpendicular vector to spvR and u)*/
vp[0] = -spvR[0]*spvR[2]/Lxy;
vp[1] = -spvR[1]*spvR[2]/Lxy;
vp[2] = (spvR[0]*spvR[0]+spvR[1]*spvR[1])/Lxy;

L = sqrt(scalarproduct(vp,vp));

vp[0] = vp[0]/L;
vp[1] = vp[1]/L;
vp[2] = vp[2]/L;

L = sqrt(scalarproduct(spvR,spvR));

spvR[0] = spvR[0]/L;
spvR[1] = spvR[1]/L;
spvR[2] = spvR[2]/L;

/* TURN */

spvnew[0] = cosw*spvR[0]+sinw*vp[0];
spvnew[1] = cosw*spvR[1]+sinw*vp[1];
spvnew[2] = cosw*spvR[2]+sinw*vp[2];
```

```
L = sqrt(scalarproduct(spvnew,spvnew));

spvnew[0] = Rold3*spvnew[0]/L;
spvnew[1] = Rold3*spvnew[1]/L;
spvnew[2] = Rold3*spvnew[2]/L;

}

}

double dHi;
double dHi1=interboxes(spvnew, spinnumber,Rconold);
double dHi2=interboxes(sv,spinnumber,Rconold);

if (dHi2 > 50000){
dHi = 0;}
else{
dHi = dHi1-dHi2;}


/* Energy calculation for move */
/* Lipid B always moves */


if (Lspin[spinnumber][0] == -1){
dH = dHi;}

if (Lspin[spinnumber][0] == 1){
if ((spvnew[2] == height) && (spv[spinnumber][5] == height)){
dH = dHi;}

if ((spvnew[2] > height) && (spv[spinnumber][5] > height)){
dH = dHi;}

if ((spvnew[2] == height) && (spv[spinnumber][5] > height)){
dH = -B+dHi;}

if ((spvnew[2] > height) && (spv[spinnumber][5] == height)){
dH = B+dHi;}
}


if (dH <= 0){

if (Lspin[spinnumber][0] == 1){
if ((spvnew[2] == height) && (spv[spinnumber][5] > (height))){
```

```
Ns1 += 1;}

if ((spvnew[2] > height) && (spv[spinnumber][5] <= (height))){
Ns1 -= 1;}
}

change(Rold3,hold3);



L = sqrt(spv[spinnumber][3]*spv[spinnumber][3]+spv[spinnumber][4]*spv[spinnumber][4]
if (L>Rconold && spv[spinnumber][5] == (Rold3-hold3)){
printf("Rconproblem");
spv[spinnumber][3] = Rconold* spv[spinnumber][3]/L;
spv[spinnumber][4] = Rconold*spv[spinnumber][4]/L;
}

H += dH;
}


if (dH > 0){
r2 = ran3(dummy);

if (r2 <exp(-beta*dH)) {

/*printf("energy %f\t %d\t %f\n", dHi, Lspin[spinnumber][0], dH);*/
if (Lspin[spinnumber][0] == 1){
if ((spvnew[2] == height) && (spv[spinnumber][5] > height)){
Ns1 += 1;}

if ((spvnew[2] > height) && (spv[spinnumber][5] == height)){
Ns1 -= 1;}

}

change(Rold3,hold3);

H += dH;
}
}

/* if (t % N == 0){
fprintf(fpen2, "%d\t %f\t %f\t %f\t %f\n", t, dHi, dH, DH, H);}
printf("%d\t %f\t %f\t %f\t %f\n", t, dHi, dH, DH, H);*/
} /* end move() */
```

```
void change(double Rold4, double hold4)
{
spv[spinnumber][3] = spvnew[0];
spv[spinnumber][4] = spvnew[1];
spv[spinnumber][5] = spvnew[2];

newbox(spinnumber, Rold4, hold4, Rconold);
}



void newbox(int spinnumber7, double Rold7, double hold7, double Rconold7)
{
/* local variables */
float zbox1;
double Lb;
double Height = Rold7-hold7;


/* determine new z box */
if (spv[spinnumber7][5] > Height){
zbox1 = (float)((spv[spinnumber7][5]-Height)*boxmax);
zbox = (int)(zbox1/hold7);
}
else {
L = sqrt(spv[spinnumber7][3]*spv[spinnumber7][3]+spv[spinnumber7][4]*spv[spinnumber7][
Lb = L/Rconold7;
zbox = boxmax+1 + (int)(Lb*boxmax);
}


if (zbox != Lspin[spinnumber7][1]){
/* 1) throw out the spin out of the zbox it has been in */

int pos1 = Lspin[spinnumber7][1];
int pos2 = Lspin[spinnumber7][2];
int pos3 = Lz[pos1][0];
int pos4 = Lz[pos1][pos3];
int pos5 = Lz[pos1][0];

Lz[pos1][pos2]=pos4;
Lspin[pos4][1] = pos1;
Lspin[pos4][2] = pos2;
Lz[pos1][0] = pos5-1;
```

```
/* 2) put into new box */
Lz[zbox][0] += 1;
Lz[zbox][Lz[zbox][0]]=spinnumber7;
Lspin[spinnumber7][1] = zbox;
Lspin[spinnumber7][2] = Lz[zbox][0];
}



phiboxchange(spinnumber7, Rconold7);

}


void phiboxchange(int spinnumber8, double Rconold8)
{
int phiBOX;
double phiw;

/* Determine new phibox*/
double spvV[3];
spvV[0] = spv[spinnumber8][3];
spvV[1] = spv[spinnumber8][4];
spvV[2] = spv[spinnumber8][5];

phiw = phiwdet(spvV);

if (spv[spinnumber8][5] > (Rconold8-hold)){
double theta5 = thetawdet(spvV);
phiBOX = phiboxdet(phiw,theta5);
}

else {
double Le = sqrt(scalprodxy(spvV,spvV));
int Rbox = 51+(int) (((Rconold8-Le)/(Rconmax)) *boxmax);
int phibox1 = phidet(phiw);

phiBOX = Rbox*indphi+phibox1;
}

int box = Lspin[spinnumber8][3];
int pos = Lspin[spinnumber8][4];
int endpos = LW[box][0];

if (phiBOX != box){
/* throw out of old phi-box */
LW[box][pos]=LW[box][endpos];
```

```
Lspin[LW[box][endpos]][3] = box;
Lspin[LW[box][endpos]][4] = pos;
LW[box][0] -= 1;

/* put into new phibox*/
LW[phiBOX][0] += 1;
LW[phiBOX][LW[phiBOX][0]] = spinnumber8;
Lspin[spinnumber8][3] = phiBOX;
Lspin[spinnumber8][4] = LW[phiBOX][0];
}

}

double phiwdet(double vector9[])
{
double phiw1;
/*printf("%f\t %f\t %f\n", vect[1], vect[0], vect[1]/vect[0]);*/
if (vector9[0] == 0 && vector9[1] == 0){
phiw1 = 0;}
else {
phiw1 = atan2(vector9[1],vector9[0]);}
if (phiw1 < 0){
phiw1 = 2*pi+phiw1;}

return phiw1;
}



double thetawdet(double vector10[])
{
Lxy = sqrt(scalprodxy(vector10,vector10));
double theta1 = atan(Lxy/vector10[2]);
if (theta1 < 0) {
theta1 = pi+theta1;}

return theta1;
}



int phidet(double phiw2)
{
int j = (int) (phiw2*indphi/(2*pi));
return j;
}
```

```
int thetadet(double theta1)
{
int hzahl = (int) (theta1*indtheta/pi);
if (hzahl == indtheta){
hzahl -= 1;}
return hzahl;
}

int phiboxdet(double phiw1, double theta1)
{
int PHIBOX;
/* put into new phibox */
int l4 = thetadet(theta1);
j = phidet(phiw1);
PHIBOX =  l4*indphi + j ;

return PHIBOX;
}

double interboxes(double vector1[], int spinnumber1, double Rcon1)
{
double dHI1;

if (vector1[2] == (Rold-hold)){ /* on circle */
dHI1 = circleroutine(vector1,spinnumber1,Rcon1);
}
else {
dHI1 = sphereroutine(vector1,spinnumber1);
}

return dHI1;

}

double sphereroutine(double vector2[], int spinnumber2)
{
double dHI2 =0;
int phiboxs;

double phi2 = phiwdet(vector2);
phiboxs = phidet(phi2);

double theta2 = thetawdet(vector2);
int thetabox = thetadet(theta2);


if (thetabox > 2){
```

```
if (thetabox < (thetaboxMax -2)){
for (j = (thetabox-1); j <= (thetabox+1); j++){
if (fabs(dHI2) > 50000){
break;}
for (i = (phiboxs-1); i <= (phiboxs+1); i++){
if (fabs(dHI2) > 50000){
break;}
dHI2 += schleifephi(vector2,spinnumber2,i,j);
}
}
}
else{
dHI2 += borderroutine(vector2,spinnumber2,phiboxs);

}
}
else{
for (j = 0; j <= (thetabox+1); j++){
if (fabs(dHI2) > 50000){
break;}
for (i = 0; i <= phiboxmax; i++){
if (fabs(dHI2) > 50000){
break;}
dHI2 += schleifephi(vector2,spinnumber2,i,j);

}
}
}

return dHI2;

}



double circleroutine(double vector3[], int spinnumber3,double Rcon3)
{
double dHI3=0;
double Le = scalprodxy(vector3,vector3);

int Rbox = 51+(int) (((Rcon3-Le)/(Rconmax)) *boxmax);
double phi1 = phiwdet(vector3);
int phiboxc = phidet(phi1);

if (Rbox > 53){ /* spin not at circle border*/
if (Le > (2*Rcon3/(Rconmax))){ /* spin not in center*/
for(j = (Rbox-1); j <= (Rbox+1); j++){
```

```
if (fabs(dHI3) > 50000){
break;}
for (i=(phiboxc-1); i <=(phiboxc+1); i++){
if (fabs(dHI3) > 50000){
break;}
dHI3 += schleifephi(vector3,spinnumber3,i,j);

}
}
}
else{
if (Rbox <= 100){
for(j = (Rbox-1); j <= (Rbox+1); j++){
if (fabs(dHI3) > 50000){
break;}
for (i=0; i < phiboxmax; i++){
if (fabs(dHI3) > 50000){
break;}
dHI3 += schleifephi(vector3,spinnumber3,i,j);

}
}
}
else{
for(j = (Rbox-1); j <= Rbox; j++){
if (fabs(dHI3) > 50000){
break;}
for (i=0; i < phiboxmax; i++){
dHI3 += schleifephi(vector3,spinnumber3,i,j);

}
}
}

}
}
else{
dHI3 += borderroutine(vector3,spinnumber3,phiboxc);
}

return dHI3;

}


double borderroutine(double vector4[],int spinnumber4,int phiboxb)
{
```

```
double dHI4 = 0;
int index1, index2;

for (index1=(phiboxb-1); index1 <=(phiboxb+1); index1++){
if (fabs(dHI4) > 50000){
break;}
for(index2 = 51; index2 <= 53; index2++){
dHI4 += schleifephi(vector4,spinnumber4,index1,index2);
}
for (index2 = (thetaboxMax-2); index2 <= thetaboxMax; index2++){
dHI4 += schleifephi(vector4,spinnumber4,index1,index2);
}
}
return dHI4;
}




double schleifephi(double vector5[],int spinnumber5,int indexs1, int indexs2)
{
int ks1;
double dHI5=0;
int par = indexs2 *indphi+indexs1;
for (ks1=1; (ks1 <= LW[par][0]) && (fabs(dHI5) < 50000); ks1++ ){
int spinneigh = LW[par][k];
dHI5 += neighbor(spinneigh,vector5,spinnumber5);
}

return dHI5;
}






double neighbor(int spin, double vector6[], int spinnumber6)
{
double dist2, dHI6=0;
double vector7[3];

/* difference vector */
vector7[0] = spv[spin][3]-vector6[0];
vector7[1] = spv[spin][4]-vector6[1];
vector7[2] = spv[spin][5]-vector6[2];
```

```
dist2 =  scalarproduct(vector7,vector7);

if (dist2 < abstmin2){
dHI6 = 1000000;}
else if (dist2 < abstlim2) {
dHI6 = -J*(Lspin[spinnumber6][0]*Lspin[spin][0]);}

return dHI6;
}



void topch()
{
/* 1) choose a new contact angle */
r2 = pi*ran3(dummy)/10-pi/20;
gammaw = g+r2;

if (gammaw < 0) {
gammaw = -gammaw;}

gammaw = fmod(gammaw, pi);


/* 2) calculate energy change upon topology change
calculate size of contact zone
calculate attractive potential
calculate volume constraint

size of contact zone */
if (gammaw > pi/2) {
Rnew = PI3/(pi-gammaw+cos(-(pi/2-gammaw)));
Rcon = Rnew * cos(-(pi/2-gammaw));}
else {
Rnew = PI3/(pi-gammaw+cos(pi/2-gammaw));
Rcon = Rnew * cos(pi/2-gammaw);}

hnew = Rnew*(1+cos(gammaw));
Vf = pi*hnew*hnew*(3*Rnew-hnew)/3;


/* Distinguish case
1) g > gammaw
2) g < gammaw*/


/* determine rows that belong to sphere cap */
```

```
/* Height on previous spherical object that will belong to new spherical part*/
double hsphere = Rnew*hnew/Rold;

/* CASE gammaw > g */
/* determine energy change due to attractive potential*/

int SUM = 0;
if (gammaw > g){
zboxmax = (int) (((hold-hsphere)/hold)*boxmax);

for (j=0; j<zboxmax; j++){
for (k = 1; k <= Lz[j][0]; k++){
SUM -= (Lspin[Lz[j][k]][0]+1);}
}
for (k = 1; k <= Lz[zboxmax][0]; k++){
if ((spv[Lz[zboxmax][k]][5] < (Rold-hsphere)) && (spv[Lz[zboxmax][k]][5] > (Rold-hold)
SUM -= (Lspin[Lz[zboxmax][k]][0]+1);}
}
}


if (gammaw < g){
zboxmax = boxmax+1 + (int) ((Rcon/Rconold)*boxmax);


for (j=zboxmax+1; j<2*boxmax +1; j++){
for (k = 1; k < Lz[j][0]+1; k++){
SUM += Lspin[Lz[j][k]][0]+1;}
}

for (k = 1; k < Lz[zboxmax][0]+1; k++){
L = sqrt(spv[Lz[zboxmax][k]][3]*spv[Lz[zboxmax][k]][3]+spv[Lz[zboxmax][k]][4]*spv[Lz[z
if (L > Rcon){
SUM += Lspin[Lz[zboxmax][k]][0]+1;}

}

}

int DH2;
DH2 = B * SUM;

/* volume constraint */
double DH1 = -Nt*N*log(Vf/V)/beta;
DH = (float) DH1 + (float) DH2;

/*printf("energy %d\t %d\t %f\t %f\t %f\t %f\t %f\n", SUM, DH2, DH, DH1, (Vf/V), Vf, V
```

```
if (DH <= 0){
H += DH;
geomch(Rnew, hnew,Rold, Rconold);
V = Vf;
g = gammaw;
thetaMax = pi-g;
thetaboxMax = thetadet(thetaMax);
Rold=Rnew;
Rconold = Rcon;
hold = hnew;

Ns1 -= (int) ((float) SUM/2.);

}

if (DH > 0) {
r2 = ran3(dummy);

if (r2 < exp(-beta*DH)){
H += DH;
geomch(Rnew, hnew, Rold, Rconold);
V = Vf;
g = gammaw;
thetaMax = pi-g;
thetaboxMax = thetadet(thetaMax);
Rold = Rnew;
Rconold = Rcon;
hold = hnew;
/*N1 = Ns1det();
printf("H>Ns1, %d\t %d\t %d\n", SUM, Ns1, N1);*/
Ns1 -= (int) ((float) SUM/2.);
/*printf("H>Ns1, %d\t %d\t %d\n", SUM, Ns1, N1);*/
}
}
}


void geomch(double Rnew2, double hnew2, double Rold2, double Rconold2)
{
int index;
int ji;
double scal1, dtheta;
double hsphere2 = Rnew2*hnew2/Rold2;
double zlimit2;

zlimit2 = Rold2-hsphere2;
```

```
scal1 = (Rcon-Rconold2)/(zlimit2-(Rold2-hold));

if (gammaw > g){
double winkelmaxnew = pi-gammaw;
double winkelmaxold = acos(zlimit2/Rold2);

for (index=0; index < Lipidtotal1; index++){
if (spv[index][5] >= (zlimit2)) {
/* map spherical part onto new spherical part */
double arg =fabs(spv[index][5])/Rold2;
if ((arg > 1 && arg < 1.001) ){
spv[index][5] = spv[index][5]*Rold2/fabs(spv[index][5]);}

winkelold = acos(spv[index][5]/Rold2);
winkelnew = winkelold*winkelmaxnew/winkelmaxold;
winkeldiff = -(winkelnew-winkelold);
drehung(index, winkeldiff);
newbox(index, Rnew2, hnew2, Rcon);
}

if (spv[index][5] < (zlimit2) && spv[index][5] > (Rold2-hold)){
/* projection onto circle */
L = sqrt(spv[index][3]*spv[index][3]+spv[index][4]*spv[index][4]);
spv[index][3] = (Rconold2+scal1*(spv[index][5]-(Rold2-hold)))*spv[index][3]/L;
spv[index][4] = (Rconold2+scal1*(spv[index][5]-(Rold2-hold)))*spv[index][4]/L;
spv[index][5] = Rnew2-hnew2;
newbox(index, Rnew2, hnew2, Rcon);
}

if (spv[index][5] == (Rold2-hold)){
/* shifting from bottom to Rnew2-hnew2 */
spv[index][5] = Rnew2-hnew2;

newbox(index, Rnew2, hnew2, Rcon);
}

} /* end for */
} /* end gammaw */




if (gammaw < g){
winkelnew = acos((Rnew2-hold*Rold2/Rnew2)/Rnew2);
/*double winkelmin = atan(Rcon/(Rold2-hold));*/ /* theta old contact zone */
```

```
/*if (winkelmin < 0){
winkelmin = pi+winkelmin;}*/


for (ji=0; ji<Lipidtotal1; ji++){
L = sqrt(spv[ji][3]*spv[ji][3]+spv[ji][4]*spv[ji][4]);

if (spv[ji][5] == (Rold2-hold) && L <= Rcon) {
spv[ji][5] = Rnew2-hnew2;
}


if (spv[ji][5] > (Rold2-hold)) {
/* projection of spherical part on new spherical cap */
winkelold = acos(spv[ji][5]/Rold2);
double winkel = winkelold/(pi-g)*winkelnew;
winkeldiff = -(winkel-winkelold);
drehung(ji, winkeldiff);
}

if (spv[ji][5] == (Rold2-hold) && L > Rcon) {
/* projection of circle part on lower part of spherical cap */
double winkelneu = pi-gammaw-(pi-gammaw-winkelnew)*(L-Rcon)/(Rconold2-Rcon);

L = spv[ji][3]*spv[ji][3]+spv[ji][4]*spv[ji][4]+spv[ji][5]*spv[ji][5];
dtheta = -(winkelneu - acos(spv[ji][5]/sqrt(L)));
Lxy = sqrt(spv[ji][3]*spv[ji][3]+spv[ji][4]*spv[ji][4]);


/*fprintf(fpw,"%f\t %f\t %f\n", dtheta, Lxy, Rconold2);*/

cosw = cos(dtheta);
sinw = sin(dtheta);


/* perpendicular vector to r and u)*/
vp[0] = spv[ji][3]*spv[ji][5]/Lxy;
vp[1] = spv[ji][4]*spv[ji][5]/Lxy;
vp[2] = (spv[ji][3]*spv[ji][3]+spv[ji][4]*spv[ji][4])/Lxy;

L = sqrt(scalarproduct(vp,vp));

vp[0] = vp[0]/L;
vp[1] = vp[1]/L;
vp[2] = vp[2]/L;

L = sqrt(spv[ji][3]*spv[ji][3]+spv[ji][4]*spv[ji][4]+spv[ji][5]*spv[ji][5]);
```

```
spvR[0] = spv[ji][3]/L;
spvR[1] = spv[ji][4]/L;
spvR[2] = spv[ji][5]/L;

spv[ji][3] = cosw*spvR[0]-sinw*vp[0];
spv[ji][4] = cosw*spvR[1]-sinw*vp[1];
spv[ji][5] = cosw*spvR[2]+sinw*vp[2];

L = sqrt(spv[ji][3]*spv[ji][3]+spv[ji][4]*spv[ji][4]+spv[ji][5]*spv[ji][5]);

spv[ji][3] = Rnew2*spv[ji][3]/L;
spv[ji][4] = Rnew2*spv[ji][4]/L;
spv[ji][5] = Rnew2*spv[ji][5]/L;
}
newbox(ji, Rnew2, hnew2, Rcon);
} /* end for */
} /* end g <gammaw */
} /* end geomch */


void drehung(int spinindex, double winkeldiff)
{
double vpdreh[3];

cosw = cos(winkeldiff);
sinw = sin(winkeldiff);
L = sqrt(spv[spinindex][3]*spv[spinindex][3]+spv[spinindex][4]*spv[spinindex][4]);

/* perpendicular vector to r and u)*/
vpdreh[0] = spv[spinindex][3]*spv[spinindex][5]/L;
vpdreh[1] = spv[spinindex][4]*spv[spinindex][5]/L;
vpdreh[2] = (spv[spinindex][3]*spv[spinindex][3]+spv[spinindex][4]*spv[spinindex][4])/

L = sqrt(scalarproduct(vpdreh,vpdreh));

vpdreh[0] = Rold*vpdreh[0]/L;
vpdreh[1] = Rold*vpdreh[1]/L;
vpdreh[2] = Rold*vpdreh[2]/L;

spv[spinindex][3] = cosw*spv[spinindex][3]-sinw*vpdreh[0];
spv[spinindex][4] = cosw*spv[spinindex][4]-sinw*vpdreh[1];
spv[spinindex][5] = cosw*spv[spinindex][5]+sinw*vpdreh[2];

L = sqrt(spv[spinindex][3]*spv[spinindex][3]+spv[spinindex][4]*spv[spinindex][4]+spv[s

spv[spinindex][3] = Rnew*spv[spinindex][3]/L;
spv[spinindex][4] = Rnew*spv[spinindex][4]/L;
```

```
spv[spinindex][5] = Rnew*spv[spinindex][5]/L;
}



int Ns1det()
{
int Ns1number1=0;

for (i=51; i <= 101; i++){
for (k=1; k <= Lz[i][0]; k++){
float number1 = (float)(Lspin[Lz[i][k]][0]+1);
double number2 = number1/2.;
Ns1number1 += (int) (number2);}
}

return Ns1number1;
}
```

# Appendix F

# Explicit Calculations and Program Codes for Appendix B

## F.1 Explicit Calculations and Programs for the Model in B.1

### F.1.1 Calculation of the Steady state values for the model in B.1

From setting $\frac{dM}{dt} = 0$ we easily obtain the steady state value $C^*_{T0} = 0$. Using this in $\frac{dT}{dt} = 0$ we obtain $T_0 = \frac{\sigma}{\delta_T}$. Since $T_0 \neq 0$ and $C^*_{T0} = 0$ we need $C^*_0 = 0$. From $\frac{dC^*}{dt} = 0$ we then obtain $C_A = 0$ and from this with $\frac{dAg}{dt} = 0$ $Ag_0 = 0$. For the two remainig bits $B_0$ and $C_0$ Maple was used and program and results are given in the following:

```
> eqb:= B*(rho*Kb/(Kb+B)-db)-d*(B+C)*B=0;
```

$$eqb := B \left( \frac{rho\ Kb}{Kb + B} - db \right) - d\ (B + C)\ B = 0$$

```
> eqc:= d*(B+C)*rho*B-mu*C=0;
```

$$eqc := d\ (B + C)\ rho\ B - mu\ C = 0$$

```
> C:=solve(eqc,C);
```

$$C := -\frac{d\ B^2\ rho}{d\ B\ rho - mu}$$

```
> B:=solve(eqb,B);

                2                                                4   2  2
B := 0, 1/2 (rho  Kb d - db Kb d rho + db mu + d mu Kb + (rho  Kb  d

            3   2  2           2                    2   2  2
     - 2 rho  Kb  d  db - 2 rho  Kb d db mu + 2 rho  Kb  d  mu

         2   2  2    2       2                      2  2
     + db  Kb  d  rho  + 2 db  Kb d rho mu - 2 db Kb  d  rho mu

         2   2          2         2   2   2         2        1/2
     + db  mu  - 2 db mu  d Kb + d  mu  Kb  + 4 d mu  rho Kb)   )/(

                              2
    db d rho - d mu), 1/2 (rho  Kb d - db Kb d rho + db mu + d mu Kb

           4   2  2        3   2  2           2
     - (rho  Kb  d  - 2 rho  Kb  d  db - 2 rho  Kb d db mu

           2   2  2        2   2  2    2       2
     + 2 rho  Kb  d  mu + db  Kb  d  rho  + 2 db  Kb d rho mu

             2  2           2   2          2         2   2   2
     - 2 db Kb  d  rho mu + db  mu  - 2 db mu  d Kb + d  mu  Kb

             2        1/2
     + 4 d mu  rho Kb)   )/(db d rho - d mu)

>
```

### F.1.2 Program to the Numerical Solutions of the Model in B.1

```
% GC kinetic model with cell density dependent conversion factor


% parameters and variables
n = 10; % number of cycles before centrocyte conversion
dt = 0.1;

B = 3

pr = 0; % probability of recycling
Kb = 10^3; % density dependent centroblast proliferation
Kt = 100;  % density dependent T cell proliferation
Kt1 = 15;           % density dependent conversion of centroblasts to centrocyts
rho = 4*log(2); % maximum proliferation rate of centroblast (day^-1)
```

```
p   = 2 % maximum proliferation rate of GC T cells (day^-1)
db = 0.8; % Death rate of centroblasts (day^-1)
drt = 0.8; % Death rate of T cells (day^-1)
mu = 3; % maximum apoptosis rate for centrocytes (day^-1)
sigma = 50;  % influx of T cells to GC
z = 1/50 % 1/ average lifetime of Ag on FDC
u = 0.5 % consumption of Ag per centrocyte
sa = 500; % saturation constant for B cells binding FDCs
st = 50; % saturation constant for B cells binding T cells

M  = 0  % initial number of specific memory cells
T  = 0 % initial number of T cells in GC
F  = 100; % FDC per GC
Ag = 500; % antigen per FDC
C  = 0; % initial number of centrocytes
CAP = 0; % initial number of centrocytes that have been bound Ag
CA=C*Ag/(sa+Ag);
CTA=CAP*T/(st+CAP)  % centrocytes that have been selected by T cells

a = Kb/(Kb+B);
at = Kt/(Kt+T);



% Runge-Kutta method
for t=dt:dt:30
   d  = (B+C)/1000  % density dependent centroblast-centrocyte-conversion rate

   k1 = pr*CTA+(rho*a-d-db)*B;
   ck1 = rho*d*B-mu*C;
   cak1 = mu*(CA-CAP);
   ak1 = -z*Ag-u*CA;
   tk1 = sigma + p*at*CTA-drt*T;

k2 = pr*CTA+(rho*a-d-db)*(B+k1*dt/2);
ck2= rho*d*B-mu*(C+0.5*dt*ck1);
   cak2 = mu*(CA-(CAP+0.5*dt*cak1));
   ak2 = -z*(Ag+0.5*dt*ak1)-u*C*(Ag+0.5*dt*ak1)/(sa+(Ag+0.5*dt*ak1));
   tk2 = sigma + p*at*CAP*(T+0.5*dt*tk1)/(st+CAP)-drt*(T+0.5*dt*tk1);

   k3 = pr*CTA+(rho*a-d-db)*(B+k2*dt/2);
   ck3=rho*d*B-mu*(C+0.5*dt*ck2);
   cak3 = mu*(CA-(CAP+0.5*dt*cak2));
   ak3 = -z*(Ag+0.5*dt*ak2)-u*C*(Ag+0.5*dt*ak2)/(sa+(Ag+0.5*dt*ak2));
   tk3 = sigma + p*at*CAP*(T+0.5*dt*tk2)/(st+CAP)-drt*(T+0.5*dt*tk2);

   k4 = pr*CTA+(rho*a-d-db)*(B+k3*dt);
```

```
   ck4 = rho*d*B-mu*(C+dt*ck3);
   cak4 = mu*(CA-(CAP+dt*cak3));
   ak4 = -z*(Ag+dt*ak3)-u*C*(Ag+dt*ak3)/(sa+(Ag+dt*ak3));
   tk4 = sigma + p*at*CAP*(T+dt*tk3)/(st+CAP)-drt*(T+0.5*dt*tk3);


B = B + dt*(k1+2*k2+2*k3+k4)/6;
C=C+dt*(ck1+2*ck2+2*ck3+ck4)/6;          % dynamics of centrocytes
CAP=CAP+ dt*(cak1+2*cak2+2*cak3+cak4)/6; % dynamics of Ag-Centrocytes
M = M + dt*(1-pr)*mu*CTA; % dynamics of memory B cells
Ag = Ag + dt*(ak1+2*ak2+2*ak3+ak4)/6;          % dynamics of antigen
T = T+dt*(tk1+2*tk2+2*tk3+tk4)/6; % dynamics of T cells


% calculating new complexes
CA=C*Ag/(sa+Ag);
CTA=CAP*T/(st+CAP);  % centrocytes that have been selected by T cells
a = Kb/(Kb+B);
at = Kt/(Kt+T);


% plotting
hold on,
pause(0);

subplot(2,1,1),
hold on,
plot(t,Ag,'b+', t,B,'md', t,C, 'rd', t,(B+C), 'kd', t,CTA, 'm--', ...
   t,T, 'c*', t,M, 'gh');
title('Density dependent centroblast centrocyte conversion', ...
   'FontSize', 14);
legend('\bfAntigen', '\bfcentroblasts', '\bfcentrocytes', '\bftotal B cells',...
   '\bfselected centrocytes', '\bfT cells', '\bfmemory B cells');

subplot(2,1,2),
hold on,
plot(t,rho*a-db, 'kh-', t,d, 'gd');
title('conversion factor d (green) and {\rho}a_b-\delta_b (black)',...
   'FontSize', 14)
end
```

## F.2 Programs to the Numerical Solutions of the Model in B.2

### F.2.1 Program for the model in Chapter B.2.1

```
% model for the kintics of the true primary immune response
% with time dependent conversion factor (d(t)) and
% without explicit modelling of affinity maturation)



% starting values and parameters
dt = 0.1;

sa = 500; % saturation constant for B cells binding FDCs
st = 50; % saturation constant for B cells binding T cells

B = 3 % number of seeding B blasts
M  = 0  % initial number of specific memory cells
T  = 0 % initial number of T cells in GC
F  = 100; % FDC per GC
Ag = 500; % total number of antigen complexes on FDCs
C  = 0; % initial number of centrocytes
CAP = 0; % initial number of centrocytes that have been bound Ag
CA=C*Ag/(sa+Ag);
CTA=CAP*T/(st+CAP)  % centrocytes that have been selected by T cells

pr = 0.7; % probability of recycling
Kb = 1000; % density dependent centroblast proliferation
Kt = 100;  % density dependent T cell proliferation
a = Kb/(Kb+B);
at = Kt/(Kt+T)
Kt1 = 15;            % time dependent conversion of centroblasts to centrocyts
rho = 4*log(2); % maximum proliferation rate of centroblast (day^-1)
p   = 2; % maximum proliferation rate of GC T cells (day^-1)
db = 0.8; % Death rate of centroblasts (day^-1)
drt = 0.8; % Death rate of T cells (day^-1)
mu = 3; % maximum apoptosis rate for centrocytes (day^-1)
sigma = 50;  % influx of T cells to GC
z = 1/50 % 1/ average lifetime of Ag on FDC
u = 0.5 % consumption of Ag per centrocyte
n = 8;

figure
```

```
for t=3:dt:30
   d  = 2.5*t^n/(Kt1^n+t^n);    % time dependent rate at which centroblasts
    % differentiate to centrocytes (day^(-1))
   k1 = pr*mu*CTA+(rho*a-d-db)*B;
   ck1 = rho*d*B-mu*C;
   cak1 = mu*(CA-CAP);
   ak1 = -z*Ag-u*CA;
   tk1 = sigma + p*at*CTA-drt*T;

k2 = pr*mu*CTA+(rho*a-d-db)*(B+k1*dt/2);
ck2= rho*d*B-mu*(C+0.5*dt*ck1);
   cak2 = mu*(CA-(CAP+0.5*dt*cak1));
   ak2 = -z*(Ag+0.5*dt*ak1)-u*C*(Ag+0.5*dt*ak1)/(sa+(Ag+0.5*dt*ak1));
   tk2 = sigma + p*at*CAP*(T+0.5*dt*tk1)/(st+CAP)-drt*(T+0.5*dt*tk1);

   k3 = pr*mu*CTA+(rho*a-d-db)*(B+k2*dt/2);
   ck3=rho*d*B-mu*(C+0.5*dt*ck2);
   cak3 = mu*(CA-(CAP+0.5*dt*cak2));
   ak3 = -z*(Ag+0.5*dt*ak2)-u*C*(Ag+0.5*dt*ak2)/(sa+(Ag+0.5*dt*ak2));
   tk3 = sigma + p*at*CAP*(T+0.5*dt*tk2)/(st+CAP)-drt*(T+0.5*dt*tk2);

   k4 = pr*mu*CTA+(rho*a-d-db)*(B+k3*dt);
   ck4 = rho*d*B-mu*(C+dt*ck3);
   cak4 = mu*(CA-(CAP+dt*cak3));
   ak4 = -z*(Ag+dt*ak3)-u*C*(Ag+dt*ak3)/(sa+(Ag+dt*ak3));
   tk4 = sigma + p*at*CAP*(T+dt*tk3)/(st+CAP)-drt*(T+0.5*dt*tk3);


B = B + dt*(k1+2*k2+2*k3+k4)/6; % dynamics of centroblasts
C=C+dt*(ck1+2*ck2+2*ck3+ck4)/6;         % dynamics of centrocytes
CAP=CAP+ dt*(cak1+2*cak2+2*cak3+cak4)/6; % dynamics of Ag-Centrocytes
M = M + dt*(1-pr)*mu*CTA; % dynamics of memory B cells
Ag = Ag + dt*(ak1+2*ak2+2*ak3+ak4)/6;       % dynamics of antigen
T = T+dt*(tk1+2*tk2+2*tk3+tk4)/6; % dynamics of T cells

% calculating new complexes
CA=C*Ag/(sa+Ag);
CTA=CAP*T/(st+CAP);  % centrocytes that have been selected by T cells
a = Kb/(Kb+B);
at = Kt/(Kt+T);

% plotting
hold on,
pause(0);
subplot(2,1,1)
hold on,
plot(t,Ag,'b+', t,B,'md', t,C, 'rd', t,(B+C), 'kd', ...
```

```
   t,CTA, 'm--', t,T, 'c*', t,M, 'gh');
title('Time dependent centroblast centrocyte conversion', 'FontSize', 14);
legend('\bfAg', '\bfcentroblasts', '\bfcentrocytes', '\bftotal B cells', ...
   '\bfselected centrocytes', '\bfT cells', '\bfmemory B cells');

subplot(2,1,2),
hold on,
plot(t,rho*a-db, 'kh-', t,d, 'gd');
title('conversion factor (green) and \rho a_b-\delta_b (black)', 'FontSize', 14)
%legend('rho*a-db', 'conversion factor');
end
```

### F.2.2 Program for the model in Chapter B.2.2

```
% model for affinity maturation with Gaussian distribution of B cells into
% neighbouring affinity bins after mutation
% antigen density dependent B cell selection


% parameters
dt = 0.1;

B = 3

pr = 0; % probability of recycling
Kb = 10^3; % density dependent centroblast proliferation
Kt = 100;  % density dependent T cell proliferation
Kt1 = 15;         % time dependent conversion of centroblasts to centrocyts
rho = 4; % maximum proliferation rate of centroblast (day^-1)
p   = 2 % maximum proliferation rate of GC T cells (day^-1)
db = 0.8; % Death rate of centroblasts (day^-1)
drt = 0.8; % Death rate of T cells (day^-1)
mu = 3; % maximum apoptosis rate for centrocytes (day^-1)
sigma = 5;  % influx of T cells to GC
z = 1/50; % 1/ average lifetime of Ag on FDC
u = 0.5; % consumption of Ag per centrocyte
n = 10;

sa = 500; % saturation constant for B cells binding FDCs
st = 50; % saturation constant for B cells binding T cells


M  = 0;  % initial number of specific memory cells
T  = 0; % initial number of T cells in GC
F  = 100; % FDC per GC
Ag = 500; % antigen per FDC
```

```
C  = 0; % initial number of centrocytes
CAP = 0; % initial number of centrocytes that have been bound Ag
CA=C*Ag/(sa+Ag);
CTA=CAP*T/(st+CAP);  % centrocytes that have been selected by T cells
a = Kb/(Kb+B);
at = Kt/(Kt+T);



% construct initial affinity vector with all cells having affinity 3 (bin 30)
al = 100;          % number of bins for affintiy
for i=1:al
   aC(i,1) = 0;      % affinity vector with 100 bins
end

% Introduction of affintiy and density based selection
% construction of affinty distribution matrix (idea: approx. Gauss
% distribution). Matrix has size al*al.

A = -1 * speye(al);
% matrix A has exponential distribution over its bonds
for ib=0:(al-1)
  aa = exp(-(ib^2/100)) * ones(al, 1);
  A =  A + spdiags([aa aa], [ib -ib], al, al);
end

% column sum must be one -> divide by column sum
for j=1:al
   A(:,j)=A(:,j)/sum(A(:,j));
end


  aC((3*al/10),1) = B;

% 4th order Runge-Kutta method for solving the system of odes
for t=dt:dt:30
   n2 = round(t/dt);
   saC = sum(aC(:,n2));

   % time dependent rate at which centrocyte differentiate to centrocytes
   d  = 5*t^5/(Kt1^5+t^5);

   k1 = pr*mu*CTA+(rho*a-d-db)*B;
   ck1 = rho*d*B-mu*C;
   cak1 = mu*(CA-CAP);
   ak1 = -z*Ag-u*CA;
   tk1 = sigma + p*at*CTA;
```

```
k2 = pr*mu*CTA+(rho*a-d-db)*(B+k1*dt/2);
ck2= rho*d*B-mu*(C+0.5*dt*ck1);
   cak2 = mu*(CA-(CAP+0.5*dt*cak1));
   ak2 = -z*(Ag+0.5*dt*ak1)-u*C*(Ag+0.5*dt*ak1)/(sa+(Ag+0.5*dt*ak1));
   tk2 = sigma + p*at*CAP*(T+0.5*dt*tk1)/(st+CAP)-drt*(T+0.5*dt*tk1);

   k3 = pr*mu*CTA+(rho*a-d-db)*(B+k2*dt/2);
   ck3=rho*d*B-mu*(C+0.5*dt*ck2);
   cak3 = mu*(CA-(CAP+0.5*dt*cak2));
   ak3 = -z*(Ag+0.5*dt*ak2)-u*C*(Ag+0.5*dt*ak2)/(sa+(Ag+0.5*dt*ak2));
   tk3 = sigma + p*at*CAP*(T+0.5*dt*tk2)/(st+CAP)-drt*(T+0.5*dt*tk2);

   k4 = pr*mu*CTA+(rho*a-d-db)*(B+k3*dt);
   ck4 = rho*d*B-mu*(C+dt*ck3);
   cak4 = mu*(CA-(CAP+dt*cak3));
   ak4 = -z*(Ag+dt*ak3)-u*C*(Ag+dt*ak3)/(sa+(Ag+dt*ak3));
   tk4 = sigma + p*at*CAP*(T+dt*tk3)/(st+CAP)-drt*(T+0.5*dt*tk3);


B = B + dt*(k1+2*k2+2*k3+k4)/6; % dynamics of centroblasts
C=C+dt*(ck1+2*ck2+2*ck3+ck4)/6; % dynamics of centrocytes

% updating of aC vector in relation to their initial entries
if saC > 0
   aC(:,(n2+1)) = aC(:,n2)*(C/saC);
else
   aC(:,(n2+1)) = aC(:,n2);
end

% keep data points to monitor affinity development
if t > 4
   aC(:,(n2+1)) = A * aC(:,(n2+1));    % mutation of cells -> Gauss
end


% distribution of affinities in every bin
% Here selection needs to be introduced so that  antigen density sets the
% threshold. Selected cells become CAP. One can assume that CAP
% cells don't die but either recycle or become M cells. Therefore
% apoptosis of centrocytes with affinity below threshold

sb =100;
bc=33*2*round(sb^n/(sb^n+Ag^n));

if bc<=al
   for i=1:bc
```

```
      aC(i,(n2+1)) = 0;
   end
end

% into memory pool with very high affinity centrocytes
for i= (8*al/10): al
   M = M + aC(i,(n2+1));
   aC(i,(n2+1)) = 0;
end

% CAP = sum(ac(>threshold))
% Dependent on T cell help availability and affinity/density cells either
% recycle or become M cells. This yields a diminished vector aC of recycling
% B cells. Now need to calculate in a second round offsprings of parents in
% each bin.


CAP=CAP+ dt*(cak1+2*cak2+2*cak3+cak4)/6; % dynamics of Ag-Centrocytes
Ag = Ag + dt*(ak1+2*ak2+2*ak3+ak4)/6;          % dynamics of antigen
T = T+dt*(tk1+2*tk2+2*tk3+tk4)/6; % dynamics of T cells




% calculating new complexes
CA=C*Ag/(sa+Ag);
CTA=CAP*T/(st+CAP);  % centrocytes that have been selected by T cells
a = Kb/(Kb+B);
at = Kt/(Kt+T);


% plotting
plot(t,sum(B),'md', t,sum(C), 'r+', t,sum(B)+sum(C)+sum(CA)+sum(CAP)+sum(CTA),...
   'kd', t,sum(CTA), 'm--', t,sum(T), 'c-', t,sum(M), 'g-');
title('GC dynamics with time dependent centroblast centrocyte conversion (pr=0)');
legend('centroblasts', 'centrocytes', 'total B cells', 'selected centrocytes', ...
   'T cells', 'memory B cells');
hold on
end

x = linspace(1,al,al);
n1 = linspace(1,30, (30/dt+1));
figure
surfc(x,n1,aC'), title(['Affinity maturation with threshold for selection being lg(k
xlabel('affinity');
ylabel('time');
```

```
zlabel('number of cells');
hold off

figure
for i=1:100
   plot(i,A(50,i), 'kd')
   hold on
end
```

## F.3 Programs to the numerical solutions of the model in B.3

Program for the numerical solution for the affinity maturation model in Chapter B.3 with memory cell formation starting at day 7

```
% model for affinity maturation with generation dependent conversion
% discrete affinity shifts by mutations and
% selection dependent on antigen density and affinity
% memory cell compartment formation starts on day 7

% important parameter k(lb) -> gives kinetic

% parameters
%n = 10; % number of cycles before centrocyte conversion
dt = 0.25; % time step

pr = 0.2; % probability of recycling
Kb = 3* 10^3; % density dependent centroblast proliferation
KtT = 100;  % density dependent T cell proliferation
Kt1 = 15;       % density dependent conversion of centroblasts to centrocyts but descr

rho = 4*log(2); % maximum proliferation rate of centroblast (day^-1)
p   = 2 % maximum proliferation rate of GC T cells (day^-1)
db = 0; % Death rate of centroblasts (day^-1) just influenced by death through sh
drt = 0.8; % Death rate of T cells (day^-1)
mu = 0; % maximum apoptosis rate for centrocytes (day^-1) (influenced by outcome of se
d = 0;
sigma = 5;  % influx of T cells to GC
z = 0 % 1/ average lifetime of Ag on FDC
u = 100000 % consumption of Ag per centrocyte

sa = 10^9; % saturation constant for B cells binding FDCs
st = 50; % saturation constant for B cells binding T cells

B = 3
Mc  = sparse(100,1); % initial number of specific memory cells
```

```
AFC = sparse(16,1);
T  = 0 % initial number of T cells in GC
F  = 100; % FDC per GC
Ag = 10^7*F; % antigen per FDC
Cv  = zeros(100,1); % initial number of centrocytes in every affinity bin
C = 0;
cM = sparse(100,1);   % matrix of centrocytes inorder to let them die after one day
CAP = zeros(100,1); % initial number of centrocytes which present Ag
Cas = 0
CA = C*Ag/(sa+Ag); % initial number of centrocytes that have been bound Ag-FDC
CTAv= sparse(100,1);  % centrocytes that have been selected by T cells
CTA = 0;

at = KtT/(KtT+T)
a = Kb/(Kb+B);

% construct matrix which stores all affinities over time
bM(:,1) = zeros(100,1); % for centroblasts
ctaM = sparse(100,4); % for selected centrocytes
cM = zeros(100,1); % for centrocytes
bM(30,1) = B;

% Runge-Kutta method
% GC formation at day 4 post-immunisation (Jacob et al. (1993) J. Exp. Med. 178, 129
% onset of somatic hypermutation day 7 post immunisaton (Jacob et al. (1993) J. Exp.
% -> first 3 days only B and T cell proliferation
for t=4:dt:5-dt
   n2 = round(t-4+dt/dt); % counts time rounds for affinity matrix
k1 = (rho*a)*B;
k2 = (rho*a)*(B+k1*dt/2);
k3 = (rho*a)*(B+k2*dt/2);
   k4 = (rho*a)*(B+k3*dt);

B = B + dt*(k1+2*k2+2*k3+k4)/6;
bM(30, n2+1) = B;
ctaM(30,n2+1) = CTA;
cM(30,n2+1) = C;
T = T+dt*sigma;
hold on,
pause(0);
subplot(3,1,1),
hold on,
plot(t,B,'md', t,sum(C), 'rd', t,B+sum(C), 'kd', t,sum(CTA), 'm--', ...
t,T, 'c*', t,sum(Mc), 'gh');
title('GC dynamics with time dependent centroblast centrocyte conversion (pr=0)');
legend('centroblasts', 'centrocytes', 'total B cells', 'selected centrocytes', ...
'T cells', 'memory B cells');
```

```
subplot(3,1,2),
pause(0);
hold on,
%plot(t,Cas, 'gd');
plot(t,log10(Ag), 'b+');
%legend('rho*a-db', 'conversion factor');
g = 0

subplot(3,1,3),
hold on,
plot(t, g);
title('percentage of affinity enhancement')
end


C = B; % 100% conversion to centrocytes
B = 0;
cta = 0;

for t=5:dt:7-dt
   n2 = round(t-5+dt/dt);

   CA = C*Ag/(Ag+sa);
   Kt = C/20;

   %PROLIFERATION IN BINS%
   k1= (rho*a-d-db)*B;
   ctak1 = rho*cta;
   ck1= d*B-C*Ag*T/((sa+Ag)*(T+Kt));
   cak1 = CA*T/(T+Kt);
   ak1 = -z*Ag-u*C*Ag/(Ag+sa);
   tk1 = sigma + p*at*sum(CTA)-drt*T;

k2 = (rho*a-d-db)*(B+k1*dt/2);
ctak2 = rho*(cta+0.5*ctak1*dt);
ck2 = d*B-(C+0.5*ck1*dt)*Ag*T/((sa+Ag)*(T+Kt));
cak2 = CA*T/(T+Kt);
    ak2 = -z*(Ag+0.5*dt*ak1)-u*C*(Ag+0.5*ak1*dt)/(Ag+0.5*ak1*dt+sa);
tk2 = sigma + p*at*CTA*(T+0.5*dt*tk1)/(st+CTA)-drt*(T+0.5*dt*tk1);

k3 = (rho*a-d-db)*(B+k2*dt/2);
ctak3 = rho*(cta+0.5*ctak2*dt);
ck3 = d*B-(C+0.5*ck2*dt)*Ag*T/((sa+Ag)*(T+Kt));
    cak3 = CA*T/(T+Kt);
    ak3 = -z*(Ag+0.5*dt*ak2)-u*C*(Ag+0.5*ak2*dt)/(Ag+0.5*ak2*dt+sa);
tk3 = sigma + p*at*CTA*(T+0.5*dt*tk2)/(st+CTA)-drt*(T+0.5*dt*tk2);
```

```
k4 = (rho*a-d-db)*(B+k3*dt);
ctak4 = rho*(cta+ctak3*dt);
ck4 = d*B-(C+ck3*dt)*Ag*T/((sa+Ag)*(T+Kt));
   cak4 = CA*T/(T+Kt);
ak4 = -z*(Ag+dt*ak3)-u*C*(Ag+ak3*dt)/(Ag+ak3*dt+sa);
tk4 = sigma + p*at*CTA*(T+dt*tk3)/(st+CTA)-drt*(T+dt*tk3);


B = B + dt*(k1+2*k2+2*k3+k4)/6; % dynamics of B cells in affinity bins
C = C + dt*(ck1+2*ck2+2*ck3+ck4)/6 + cta(max(n2-10, 1)); % dynamics of centrocytes
CTA = CTA + 4.5*dt*(cak1+2*cak2+2*cak3+cak4)/6; % dynamics of Ag-Centrocytes-T
cta = cta + dt*(ctak1+2*ctak2+2*ctak3+ctak4)/6;
Ag = Ag + dt*(ak1+2*ak2+2*ak3+ak4)/6;        % dynamics of antigen
T = T+dt*(tk1+2*tk2+2*tk3+tk4)/6; % dynamics of T cells

cta(max(n2-10, 1)) = 0;
cta(n2+1) = 0.7*CTA;
Mc(30) = Mc(30)+0.3*CTA;
at = KtT/(KtT+T)

subplot(3,1,1),
hold on,
plot(t, B+sum(cta),'md', t,sum(C), 'r+', t,B+C+sum(cta), 'kd', t,Mc(30), 'gd', t,T,
title('GC dynamics with time dependent centroblast centrocyte conversion (pr=0)');
legend('centroblasts', 'centrocytes', 'total B cells', 'selected centrocytes', ...
'T cells', 'memory B cells');

subplot(3,1,2),
hold on,
%plot(t, log10(Ag), 'b+')
plot(t,log10(Ag), 'b+');
% legend('rho*a-db', 'conversion factor');

CTA = 0;
end

Cv(30) = C;
bv = sparse(100,1);
bv(30) = B;
ctaM(30, :) = cta;
McM = sparse(100, 10);


%%%%%%%%%%%%%%%% SOMATIC HYPERMUTATION STARTS %%%%%%%%%%%%%%%%%%%%%%%%%%%%

%%%%MUTATION MATRIX%%%%%%%%%%%
m = 2;
```

```
M = 0.57*speye(100,100);
M(30,1:29) = m *0.0171;
M(1,1) = 0.57+0.15-m*0.0171;

M(40,30) = m*0.0171/3;
M(30,40) = m*0.0171/3;
M(50,30) = m*0.0171/3;
M(30,50) = m*0.0171/3;
M(60,30) = m*0.0171/3;
M(30,60) = m*0.0171/3;

M(50,40) = m*0.0171/2;
M(60,40) = m*0.0171/2;
M(40,50) = m*0.0171/2;
M(40,60) = m*0.0171/2;


M(65,50) = m*0.0171;
M(50,65) = m*0.0171;

M(90,60) = m*0.0171;
M(80,65) = m*0.0171;

M(100,80) = m*0.0171;
M(100,90) = m*0.0171;

M(60,90) = m*0.0171;
M(65,80) = m*0.0171;

M(80,100) = 0.0171;
M(90,100) = 0.0171;

for j=2:100
   M(1,j) = 0.72-sum(M(2:100,j));
end


%%%%%%%%%%%%%%%%%%%%%%%%%%%%%%%

k = 20*ones(100,1);

cM(:,4) = Cv;
Cv = zeros(100,1);
ck1 = sparse(100,1);
ck2 = sparse(100,1);
ck3 = sparse(100,1);
```

```
ck4 = sparse(100,1);

for t=7:dt:30
   n2 = round((t-5.75)/dt);
   cM(:,n2) = ctaM(:,n2-4);
   ctaM(:,n2-4) = zeros(100,1); % recycling into centrocyte pool
   Cv = sum(cM(:,(n2-4):n2)')'
   CA = Cv*Ag/(Ag+sa);

   q=1;
   if u*sum(Cv)*2*Ag/(Ag+sa)>Ag
      q = 0;
   end

   Dbv = sparse(100,n2-1);
   Dbv(:,n2) = d*bv;

   %PROLIFERATION IN BINS%
   k1= (rho*a-d-db)*B;
   ctak1 = rho*ctaM;
   for i = 1:n2
      ck1(:,i)= Dbv(:,i)-k.*cM(:,i)*Ag*T/((sa+Ag)*(T+Kt));
   end
   cak1 = CA*T/(T+Kt);
   ak1 = -z*Ag-u*sum(Cv)*2*Ag/(Ag+sa)*q;
   tk1 = sigma + p*at*sum(ctaM(:,n2-1))*T/(st+sum(ctaM(:,n2-1)))-drt*T;

   k2 = (rho*a-d-db)*(B+k1*dt/2);
   ctak2 = rho*(ctaM+0.5*ctak1*dt);
   for i = 1:n2
      ck2(:,i) = Dbv(:,i)-k.*(cM(:,i)+0.5*ck1(:,i)*dt)*Ag*T/((sa+Ag)*(T+Kt));
   end
   cak2 = CA*T/(T+Kt);
   ak2 = -z*(Ag+0.5*dt*ak1)-q*u*2*sum(Cv)*(Ag+0.5*ak1*dt)/(Ag+0.5*ak1*dt+sa);
   tk2 = sigma + p*at*sum(ctaM(:,n2-1))*(T+0.5*dt*tk1)/(st+sum(ctaM(:,n2-1)))-drt*(T

   k3 = (rho*a-d-db)*(B+k2*dt/2);
   ctak3 = rho*(ctaM+0.5*ctak2*dt);
   for i= 1:n2
      ck3(:,i) = Dbv(:,i)-k.*(cM(:,i)+0.5*ck2(:,i)*dt)*Ag*T/((sa+Ag)*(T+Kt));
   end
   cak3 = CA*T/(T+Kt);
   ak3 = -z*(Ag+0.5*dt*ak2)-q*u*2*sum(Cv)*(Ag+0.5*ak2*dt)/(Ag+0.5*ak2*dt+sa);
   tk3 = sigma + p*at*sum(ctaM(:,n2-1))*(T+0.5*dt*tk2)/(st+sum(ctaM(:,n2-1)))-drt*(T

   k4 = (rho*a-d-db)*(B+k3*dt);
   ctak4 = rho*(ctaM+ctak3*dt);
```

```
   for i = 1:n2
      ck4(:,i) = Dbv(:,i)-k.*((cM(:,i)+ck3(:,i)*dt)*Ag*T)/((sa+Ag)*(T+Kt));
   end
   cak4 = CA*T/(T+Kt);
   ak4 = -z*(Ag+dt*ak3)-q*u*2*sum(Cv)*(Ag+ak3*dt)/(Ag+ak3*dt+sa);
   tk4 = sigma + p*at*sum(ctaM(:,n2-1))*(T+dt*tk3)/(st+sum(ctaM(:,n2-1)))-drt*(T+dt*tk


B = B + dt*(k1+2*k2+2*k3+k4)/6; % dynamics of B cells in affinity bins
cM = cM + dt*(ck1+2*ck2+2*ck3+ck4)/6 ;          % dynamics of centrocytes
CTAv = CTAv + dt*k.*(cak1+2*cak2+2*cak3+cak4)/6; % dynamics of Ag-Centrocytes-T
ctaM = ctaM + (dt/6)*(ctak1+2*ctak2+2*ctak3+ctak4);
Ag = Ag + dt*(ak1+2*ak2+2*ak3+ak4)/6;       % dynamics of antigen
T = T+dt*(tk1+2*tk2+2*tk3+tk4)/6; % dynamics of T cells

ctaM = M*ctaM; % mutation of recycled centroblasts
cM(:,(1:n2-4)) = 0.5*cM(:,(1:n2-4));   % centrocytes that do not get rescued die withi

% Selection rule in dependence of function f6
for i= 1: 100
   % distance function for selection of centrocytes
lb(i) = 0.5*(abs(log10(Ag)-uf6(i/10))+abs(i/10-f6(log10(Ag))));
   if (i/10)<f6(log10(Ag))
      CTAv(i)=0.5*CTAv(i);
      lb(i)=-1;
   end
   if lb(i)<1.2
      k(i)=(8/7)*lb(i)+8/7; % efficiency of antigen presentation...
   else
      k(i) = 2 * lb(i);
   end
end

McM(:,n2) = CTAv+Mc;

if t<14
   AFC = AFC + CTAv(85:100);
   CTAv(85:100) = 0;
end

ctaM(:,n2)=0.75*CTAv;
Mc = Mc +0.25*CTAv;

CTAv = 0.75*CTAv;

g = (sum(sum(cM(51:100,:)))+sum(CTAv(51:100))+sum(Mc(51:100)))/(sum(sum(cM))+sum(CTAv)
```

```
at = KtT/(KtT+T);

subplot(3,1,1),
pause(0);
hold on,
plot(t, B+sum(sum(ctaM)),'md', t,sum(sum(cM)), 'r+', ...
t,sum(bv)+sum(sum(cM))+sum(sum(ctaM))+sum(Mc)/2, 'kd', t,sum(CTAv), 'm--',...
t,T, 'c-', t,sum(Mc), 'gd');
title('GC dynamics with memory cell formation after 7 days; pr = 0.75');
legend('centroblasts', 'centrocytes', 'total B cells (half of memory B cells include
 'selected centrocytes', 'T cells', 'memory B cells');

subplot(3,1,2),
hold on,
plot(t, log10(Ag), 'b+')
title('Kinetic of antigen consumption')

subplot(3,1,3),
hold on,
plot(t,g*100, 'gd')
title('Affinity increase - percentage of affinity increase (log(Aff) >5)')



CTAv = sparse(100,1);
end



al = 100;
x = linspace(1,al,al);
n1 = linspace(7,30, (24/dt+1));
figure
surfc(x,n1,full(McM)'),
title(['Affinity maturation of C + CTA with threshold for selection being lg(K)=33']
xlabel('affinity');
ylabel('time');
zlabel('number of cells');
hold off
```

Program for the numerical solution for the affinity maturation model in Chapter B.1 with memory cell formation starting at day 10

```
% AFFINITY MATURATION %
```

```
% model for affinity maturation with generation dependent conversion
% discrete affinity shifts by mutations and
% selection dependent on antigen density and affinity
% memory cell compartment formation starts on day 10

% important parameter k(lb) -> gives kinetic

% parameters
dt = 0.25; % time step
Kb = 3* 10^3; % density dependent centroblast proliferation
KtT = 100;  % density dependent T cell proliferation
rho = 4*log(2); % maximum proliferation rate of centroblast (day^-1)
p   = 2 % maximum proliferation rate of GC T cells (day^-1)
db = 0; % Death rate of centroblasts (day^-1) just influenced by death through sh
drt = 0.8; % Death rate of T cells (day^-1)
d = 0;
sigma = 5;  % influx of T cells to GC
z = 0 % 1/ average lifetime of Ag on FDC
u = 100000 % consumption of Ag per centrocyte

sa = 10^9; % saturation constant for B cells binding FDCs
st = 50; % saturation constant for B cells binding T cells

B = 3
Mc  = sparse(100,1); % initial number of specific memory cells
AFC = sparse(16,1); % initial number of AFCs
T  = 0 % initial number of T cells in GC
F  = 100; % FDC per GC
Ag = 10^7*F; % total amount of antigen
Cv  = zeros(100,1); % initial number of centrocytes in every affinity bin
C = 0; % initial number of centrocytes
cM = sparse(100,1);   % matrix of centrocytes inorder to let them die after one day
CAP = zeros(100,1); % initial number of centrocytes which present Ag
CA = C*Ag/(sa+Ag); % initial number of centrocytes that have been bound Ag-FDC
CTAv= sparse(100,1);  % centrocytes that have been selected by T cells
CTA = 0;

at = KtT/(KtT+T)
a = Kb/(Kb+B);

% construct matrix which stores all affinities over time
bM(:,1) = zeros(100,1); % for centroblasts
ctaM = sparse(100,4); % for selected centrocytes
cM = zeros(100,1); % for centrocytes
bM(30,1) = B;

% Runge-Kutta method
```

```
% GC formation at day 4 post-immunisation
% (Jacob et al. (1993) J. Exp. Med. 178, 1293ff.)
% onset of somatic hypermutation day 7 post immunisaton
% (Jacob et al. (1993) J. Exp. Med. 178, 1293ff.)
% -> first 3 days only B and T cell proliferation
for t=4:dt:5-dt
   a = Kb/(Kb+B);
   n2 = round(t-4+dt/dt); % counts time rounds for affinity matrix

   k1 = (rho*a)*B;
k2 = (rho*a)*(B+k1*dt/2);
k3 = (rho*a)*(B+k2*dt/2);
   k4 = (rho*a)*(B+k3*dt);

B = B + dt*(k1+2*k2+2*k3+k4)/6;
bM(30, n2+1) = B;
ctaM(30,n2+1) = CTA;
cM(30,n2+1) = C;
T = T+dt*sigma;

hold on,
pause(0);
subplot(3,1,1),
hold on,
plot(t,B,'md', t,sum(C), 'rd', t,B+sum(C), 'kd', t,sum(CTA), 'm--', t,T, 'c*', t,sum
title('GC dynamics with time dependent centroblast centrocyte conversion (pr=0)');
legend('centroblasts', 'centrocytes', 'total B cells', 'selected centrocytes', ...
'T cells', 'memory B cells');

subplot(3,1,2),
pause(0);
hold on,
plot(t,log10(Ag), 'b+');
g = 0;

subplot(3,1,3),
hold on,
plot(t, g);
title('percentage of affinity enhancement')
end


C = B; % 100% conversion to centrocytes
B = 0;
cta = 0;
for t=5:dt:7-dt
   a = Kb/(Kb+B+sum(cta));
```

```
   n2 = round(t-5+dt/dt);

   CA = C*Ag/(Ag+sa);
   Kt = C/20;

   %PROLIFERATION IN BINS%
   k1= (rho*a-d-db)*B;
   ctak1 = rho*cta;
   ck1= d*B-C*Ag*T/((sa+Ag)*(T+Kt));
   cak1 = CA*T/(T+Kt);
   ak1 = -z*Ag-u*C*Ag/(Ag+sa);
   tk1 = sigma + p*at*sum(CTA)-drt*T;

   k2 = (rho*a-d-db)*(B+k1*dt/2);
   ctak2 = rho*(cta+0.5*ctak1*dt);
   ck2 = d*B-(C+0.5*ck1*dt)*Ag*T/((sa+Ag)*(T+Kt));
   cak2 = CA*T/(T+Kt);
   ak2 = -z*(Ag+0.5*dt*ak1)-u*C*(Ag+0.5*ak1*dt)/(Ag+0.5*ak1*dt+sa);
   tk2 = sigma + p*at*CTA*(T+0.5*dt*tk1)/(st+CTA)-drt*(T+0.5*dt*tk1);

k3 = (rho*a-d-db)*(B+k2*dt/2);
ctak3 = rho*(cta+0.5*ctak2*dt);
   ck3 = d*B-(C+0.5*ck2*dt)*Ag*T/((sa+Ag)*(T+Kt));
   cak3 = CA*T/(T+Kt);
   ak3 = -z*(Ag+0.5*dt*ak2)-u*C*(Ag+0.5*ak2*dt)/(Ag+0.5*ak2*dt+sa);
tk3 = sigma + p*at*CTA*(T+0.5*dt*tk2)/(st+CTA)-drt*(T+0.5*dt*tk2);

k4 = (rho*a-d-db)*(B+k3*dt);
ctak4 = rho*(cta+ctak3*dt);
ck4 = d*B-(C+ck3*dt)*Ag*T/((sa+Ag)*(T+Kt));
   cak4 = CA*T/(T+Kt);
   ak4 = -z*(Ag+dt*ak3)-u*C*(Ag+ak3*dt)/(Ag+ak3*dt+sa);
tk4 = sigma + p*at*CTA*(T+dt*tk3)/(st+CTA)-drt*(T+dt*tk3);


B = B + dt*(k1+2*k2+2*k3+k4)/6; % dynamics of B cells in affinity bins
C = C + dt*(ck1+2*ck2+2*ck3+ck4)/6 + cta(max(n2-10, 1)); % dynamics of centrocytes
CTA = CTA + 4.5*dt*(cak1+2*cak2+2*cak3+cak4)/6; % dynamics of Ag-Centrocytes-T
cta = cta + dt*(ctak1+2*ctak2+2*ctak3+ctak4)/6;
Ag = Ag + dt*(ak1+2*ak2+2*ak3+ak4)/6;        % dynamics of antigen
T = T+dt*(tk1+2*tk2+2*tk3+tk4)/6; % dynamics of T cells

cta(max(n2-10, 1)) = 0;
cta(n2+1) = 0.75*CTA;
Mc(30) = Mc(30)+0.25*CTA;
at = KtT/(KtT+T);
```

```
subplot(3,1,1),
hold on,
plot(t, B+sum(cta),'md', t,sum(C), 'r+', t,B+C+sum(cta), 'kd', t,Mc(30), 'gd', t,T,
title('GC dynamics with time dependent centroblast centrocyte conversion (pr=0)');
legend('centroblasts', 'centrocytes', 'total B cells', 'selected centrocytes', ...
'T cells', 'memory B cells');

subplot(3,1,2),
hold on,
%plot(t, log10(Ag), 'b+')
plot(t,log10(Ag), 'b+');
% legend('rho*a-db', 'conversion factor');

CTA = 0;
end

Cv(30) = C;
bv = sparse(100,1);
bv(30) = B;
ctaM(30, :) = cta;
McM = sparse(100, 10);


%%%%%%%%%%%%%%%% SOMATIC HYPERMUTATION STARTS %%%%%%%%%%%%%%%%%%%%%%%%%%%%

%%%%MUTATION MATRIX%%%%%%%%%%%
m = 1.5;

M = 0.57*speye(100,100);
M(30,1:29) = m *0.0171;
M(1,1) = 0.57+0.15-m*0.0171;

M(40,30) = m*0.0171/3;
M(30,40) = m*0.0171/3;
M(50,30) = m*0.0171/3;
M(30,50) = m*0.0171/3;
M(60,30) = m*0.0171/3;
M(30,60) = m*0.0171/3;

M(50,40) = m*0.0171/2;
M(60,40) = m*0.0171/2;
M(40,50) = m*0.0171/2;
M(40,60) = m*0.0171/2;


M(65,50) = m*0.0171;
```

```
M(50,65) = m*0.0171;

M(90,60) = m*0.0171;
M(80,65) = m*0.0171;

M(100,80) = m*0.0171;
M(100,90) = m*0.0171;

M(60,90) = m*0.0171;
M(65,80) = m*0.0171;

M(80,100) = 0.0171;
M(90,100) = 0.0171;

for j=2:100
   M(1,j) = 0.72-sum(M(2:100,j));
end

%%%%%%%%%%%%%%%%%%%%%%%%%%%%%

k = 20*ones(100,1);

cM(:,4) = Cv;
Cv = zeros(100,1);
ck1 = sparse(100,1);
ck2 = sparse(100,1);
ck3 = sparse(100,1);
ck4 = sparse(100,1);

rho = 0.85*rho

for t=7:dt:30


   % Selection rule in dependence of function f6
for i= 1: 100
   % distance function for selection of centrocytes
   lb(i) = 0.5*(abs(log10(Ag)-uf6(i/10))+abs(i/10-f6(log10(Ag))));
end


a = Kb/(Kb+B+sum(sum(ctaM)));

   n2 = round((t-5.75)/dt);
   cM(:,n2) = ctaM(:,n2-4);
   ctaM(:,n2-4) = zeros(100,1); % recycling into centrocyte pool
   Cv = sum(cM(:,(n2-4):n2)')';
```

```
CA = Cv*Ag/(Ag+sa);

q=1;
q1 = 1;
n5 = 1;
if u*sum(Cv)*2*Ag/(Ag+sa)>Ag
   n5 = u*sum(Cv)*2*Ag/(Ag*(Ag+sa))
   q = 0;
end

if log10(Ag) <= 5
   q1 = 0;
end

Dbv = sparse(100,n2-1);
Dbv(:,n2) = d*bv;

%PROLIFERATION IN BINS%
k1= (rho*a-d-db)*B;
ctak1 = rho*ctaM;
for i = 1:n2
   ck1(:,i)= Dbv(:,i)-k.*cM(:,i)*Ag*T/((sa+Ag)*(T+Kt));
end
cak1 = CA*T/(T+Kt);
ak1 = -z*Ag-q1*u*sum(Cv)*2*Ag/(n5*(Ag+sa));
tk1 = sigma + p*at*sum(ctaM(:,n2-1))*T/(st+sum(ctaM(:,n2-1)))-drt*T;

k2 = (rho*a-d-db)*(B+k1*dt/2);
ctak2 = rho*(ctaM+0.5*ctak1*dt);
for i = 1:n2
   ck2(:,i) = Dbv(:,i)-k.*(cM(:,i)+0.5*ck1(:,i)*dt)*Ag*T/((sa+Ag)*(T+Kt));
end
cak2 = CA*T/(T+Kt);
ak2 = -z*(Ag+0.5*dt*ak1)-q1/n5*u*2*sum(Cv)*(Ag+0.5*ak1*dt)/(Ag+0.5*ak1*dt+sa);
tk2 = sigma + p*at*sum(ctaM(:,n2-1))*(T+0.5*dt*tk1)/(st+sum(ctaM(:,n2-1)))-drt*(T

k3 = (rho*a-d-db)*(B+k2*dt/2);
ctak3 = rho*(ctaM+0.5*ctak2*dt);
for i= 1:n2
   ck3(:,i) = Dbv(:,i)-k.*(cM(:,i)+0.5*ck2(:,i)*dt)*Ag*T/((sa+Ag)*(T+Kt));
end
cak3 = CA*T/(T+Kt);
ak3 = -z*(Ag+0.5*dt*ak2)-q1/n5*u*2*sum(Cv)*(Ag+0.5*ak2*dt)/(Ag+0.5*ak2*dt+sa);
tk3 = sigma + p*at*sum(ctaM(:,n2-1))*(T+0.5*dt*tk2)/(st+sum(ctaM(:,n2-1)))-drt*(T

k4 = (rho*a-d-db)*(B+k3*dt);
ctak4 = rho*(ctaM+ctak3*dt);
```

```
   for i = 1:n2
      ck4(:,i) = Dbv(:,i)-k.*((cM(:,i)+ck3(:,i)*dt)*Ag*T)/((sa+Ag)*(T+Kt));
   end
   cak4 = CA*T/(T+Kt);
   ak4 = -z*(Ag+dt*ak3)-q1/n5*u*2*sum(Cv)*(Ag+ak3*dt)/(Ag+ak3*dt+sa);
   tk4 = sigma + p*at*sum(ctaM(:,n2-1))*(T+dt*tk3)/(st+sum(ctaM(:,n2-1)))-drt*(T+dt*tk


B = B + dt*(k1+2*k2+2*k3+k4)/6; % dynamics of B cells in affinity bins
cM = cM + dt*(ck1+2*ck2+2*ck3+ck4)/6 ;  % dynamics of centrocytes
CTAv = CTAv + dt*k.*(cak1+2*cak2+2*cak3+cak4)/6; % dynamics of Ag-Centrocytes-T
ctaM = ctaM + (dt/6)*(ctak1+2*ctak2+2*ctak3+ctak4);
Ag = Ag + dt*(ak1+2*ak2+2*ak3+ak4)/6;        % dynamics of antigen
T = T+dt*(tk1+2*tk2+2*tk3+tk4)/6; % dynamics of T cells

ctaM = M*ctaM; % mutation of recycled centroblasts
cM(:,(1:n2-4)) = 0.5*cM(:,(1:n2-4));   % centrocytes that do not get rescued die withi

% SELECTION %
for i = 1:100
   if (i/10)<f6(log10(Ag))
      CTAv(i)=0.5*CTAv(i);
      lb(i)=-1;
   end

   if lb(i)<1.2
      k(i)=1/n5*((8/7)*lb(i)+8/7); % efficiency of antigen presentation...
   else
      k(i) = 3.0*lb(i)/n5;
   end
end

McM(:,n2) = CTAv+Mc;



if t<12
   AFC = AFC + CTAv(85:100);
   CTAv(85:100) = 0;
else
   Mc(85:100) = Mc(85:100)+0.7*CTAv(85:100);
   CTAv(85:100) = 0.3*CTAv(85:100);
end


if t>10
ctaM(:,n2)=0.75*CTAv;
```

```
Mc = Mc +0.25*CTAv;
CTAv = 0.75*CTAv;
else
   ctaM(:,n2) = CTAv;
end



g = (sum(sum(cM(51:100,:)))+sum(CTAv(51:100))+sum(Mc(51:100)))/(sum(sum(cM))+sum(CTA


at = KtT/(KtT+T);

subplot(3,1,1),
pause(0);
hold on,
plot(t, B+sum(sum(ctaM)),'md', t,sum(sum(cM)), 'r+', t,sum(bv)+sum(sum(cM))+sum(sum(
 t,sum(CTAv), 'm--', t,T, 'c-', t,sum(Mc), 'gd');
title('GC dynamics with memory cell formation after 10 days; pr = 0.75');
legend('centroblasts', 'centrocytes', 'total B cells (half of memory B cells include
 'selected centrocytes', 'T cells', 'memory B cells');

subplot(3,1,2),
hold on,
plot(t, log10(Ag), 'b+')
title('kinetic of antigen consumption')

subplot(3,1,3),
hold on,
plot(t,g*100, 'gd')
title('Affinity increase - percentage of affinity increase (log(Aff) >5)')


CTAv = sparse(100,1);
end



al = 100;
x = linspace(1,al,al);
n1 = linspace(7,30, (24/dt+1));
figure
surfc(x,n1,full(McM)'), title(['Affinity maturation: selected B cells (CTA & Mc)'])
xlabel('affinity');
ylabel('time');
zlabel('number of cells');
hold off
```